Computer-guided drug discovery: application to the discovery of inhibitors targeting prolyl oligopeptidase and fibroblast activation protein α

by

Jessica Plescia

A thesis submitted to McGill University in partial fulfillment of the requirements for the degree of Doctor of Philosophy

Department of Chemistry,

McGill University

Montréal, QC, Canada

December 2019

Per i miei nonni, che non sono qui per vedere la loro nipotina diventare dottoressa

Copyright Statement

Parts of the material included in the following thesis is adapted from published papers and is under copyright.

Chapter 1 has been submitted to *Eur J Med Chem* and is currently under revision.

Chapter 2 has been published in

Plescia, J.;* De Cesco, S.;* Patrascu, M. B.;* Kurian, J.; Di Trani, J.; Dufresne, C.; Wahba, A. S.; Janmamode, N.; Mittermaier, A. K.; Moitessier, N., Integrated Synthetic, Biophysical, and Computational Investigations of Covalent Inhibitors of Prolyl Oligopeptidase and Fibroblast Activation Protein α. *J Med Chem* **2019,** *62* (17), 7874-7884

with permission from ACS. *These authors contributed equally.

Chapter 3 has been published in

Plescia, J.; Dufresne, C.; Janmamode, N.; Wahba, A. S.; Mittermaier, A. K.; Moitessier, N. Discovery of covalent prolyl oligopeptidase boronic ester inhibitors. *Eur J Med Chem* **2020**, 185, 111783.

with permission from Elsevier.

Chapters 4, 5, and 6 are drafts of manuscripts to be submitted for publication.

Not included in this thesis is my work on the confidential industrial collaborations

Abstract

Cancer will affect 50% of Canadians in their lifetimes. Although many biological targets have been linked to cancer, the focus of this dissertation is on two homologous serine proteases implicated in epithelial cancers: prolyl oligopeptidase (POP) and fibroblast activation protein alpha (FAP), associated with angiogenesis and tumour growth and expansion, respectively. The research outlined in this thesis consists of utilizing the computational platform FORECASTER, developed by the Moitessier research group, to conduct virtual screenings and docking-guided drug design of dual POP-FAP reversible covalent inhibitors.

In the past, our group focused on inhibitors of POP for its implication in neurodegenerative conditions, including Parkinson's and Alzheimer's diseases. Because of its more recent link to epithelial cancers, which make up approximately 90% of adult cancers, along with FAP, our group has shifted our focus to dual inhibition. Targeting both enzymes simultaneously has shown to hinder tumour growth and expansion and has even been suggested to have a synergistic effect *in vivo*.

In this dissertation, we explore several methodologies to obtain potent inhibitors. We begin with an integrative study among medicinal chemists, biophysicists, and computational chemists, in which we aim to determine the best electrophilic warhead for targeting POP and FAP. Our collaborative study led us to discover that boronic acids and esters are the optimal group in terms of reactivity and residence time. We further explore boronic acid drugs in this dissertation's introduction. Next, docking-guided virtual optimization of a known potent POP inhibitor, followed by a structure-activity relationship study, led to discovery of single-digit nanomolar potent POP inhibitors compounds with two-step syntheses. Further docking-guided peptidomimetics studies and synthetic development have led our group to our first bicyclic inhibitor that exhibits nanomolar POP-FAP potency and improves upon a drug that failed in Phase III trials. We are further developing this hit and hope to progress to pre-clinical studies. This study in particular led to the exploration of a complex mechanism required for its synthesis. Finally, a comprehensive virtual screening led to the discovery of a bicyclic borinic ester scaffold that yields very promising molecular docking predictions. We are currently in the late stages of the synthesis of this potential dual inhibitor.

Résumé

Le cancer est une maladie qui affectera 50% des canadiens au cours de leur vie. Bien que plusieurs cibles biologiques soient liées au cancer et à ses causes, le focus de cette dissertation sera deux sérine protéases liées aux cancers épithéliaux: la prolyl oligopeptidase (POP) et la protéine d'activation des fibroblastes (FAP), liées respectivement à l'angiogenèse et la croissance des tumeurs. Les recherches décrites dans cette thèse ont été conduites en utilisant la plateforme Forecaster développée par le groupe de recherche du Professeur Moitessier. Forecaster a permis la découverte d'inhibiteurs doubles réversibles et covalents ciblant POP et FAP par l'exécution de criblages virtuels et d'amarrage moléculaire.

Dans le passé, notre groupe de recherche s'est concentré sur les inhibiteurs sélectifs ciblant POP pour son rôle dans les maladies d'Alzheimer et de Parkinson. En raison des liens récents entre POP et FAP et les cancers épithéliaux, qui représentent 90% des cancers chez les adultes, notre vision a changé pour un mode d''inhibition double. Il a été démontrée que l'inhibition simultanée de POP et FAP empêchait la croissance et l'expansion tumorale et avait un effet synergétique *in vivo*.

Dans cette dissertation, nous explorerons plusieurs méthodologies pour l'obtention d'inhibiteurs puissants. Nous commencerons avec une étude qui intégrera des méthodes en chimie médicinale, biophysique et chimie informatique dont le but sera de déterminer le meilleur électrophile pour cibler POP et FAP simultanément. Notre étude collaborative nous a amené à la conclusion que les acides et les esters boroniques étaient les électrophiles idéaux en fonction de leur réactivité et de leur temps de résidence dans le site actif des protéines. Nous explorerons de plus près les acides et les esters boroniques dans l'introduction de cette thèse. Ensuite, l'optimisation virtuelle par amarrage moléculaire suivie d'une étude des relations structure-activité nous amenera à la découverte d'inhibiteurs sélectifs pour POP, exhibant une puissance nanomolaire et accessibles par une synthèse en seulement deux étapes. Une nouvelle étude utilisant l'amarrage moléculaire pour la conception d'inhibiteurs peptidomimétiques et du développement de leur synthèses a mené à notre premier inhibiteur double et bicyclique exhibant une puissance nanomolaire et qui démontre une amélioration par rapport à un composé ayant échoué à des essais cliniques en Phase III. Présentement, nous développons cette molécule avec l'espoir de commencer des tests précliniques. Cette étude en particulier nous a donné l'opportunité d'explorer un mécanisme réactionnel très complexe au cours de sa synthèse. Enfin, un criblage virtuel

compréhensif nous a amené à la découverte d'un squelette bicyclique muni d'un ester borinique avec des prédictions *in silico* très prometteuses. Nous complétons présentement la synthèse de cet inhibiteur double potentiel. Jusqu'ici, nos composés les plus prometteurs sont évalués dans des essais cellulaires par collaborateurs . Notre but actuel est de suivre ces composés et de continuer à appliquer nos méthodes efficaces pour la découverte de nouveaux composés prometteurs.

Acknowledgements

First and foremost, I would like to thank my supervisor, Professor Nicolas Moitessier, for all of his support and feedback over the years. I appreciated both the independence granted to me and the help and encouragement when I needed it.

To my summer interns Ben, Yufei, and Maud: thank you so much for all of your help. You guys all did so well, and I am so impressed with how quickly you picked up the skills and became autonomous. You will all excel in whatever it is you choose to do (I hope chemistry).

To my dear friend Paolo: your friendship, support, and advice, especially over the past couple of years, made this a lot easier. I don't think I would have made it through without you.

To my zii, cousins, brother, and sister-in-law: thanks for the emotional support and for putting up with me living under a rock for five years. You are sPecial.

To my computational chemist friend Stephen, and his successor, Wanlei: I'd like to thank you for and also apologize for your assuming the role of therapist when things became too much.

To the Auclair lab, namely Julie, Fabien, Jack, Dustin, Vanja, Justin, and Dan (and Kevin – honorary member), and Gleason lab, namely Adam: the late nights and shindigs made all of this a little less unbearable.

To my past lab mates: thanks to Gaëlle for both giving me all the training I needed and forcing me to be independent and learn on my own; Sylvain, Michelle, and Stéphane for the good times at Benelux; Josh for the advice and less-than-occasional ribbing.

To my present lab mates: thanks for your support and for putting up with me when things got really hectic (all the time). I'm looking forward to doing the same when it inevitably happens for you.

Table of Contents

Table of Figures

Table of Schemes

Table of Tables

List of Abbreviations

A.B.	activity buffer
AA	amino acid
abs	absorbance
Ac	acetyl
APCI	atmospheric pressure chemical ionization
Arg	arginine
Asn	asparagine
Asp	aspartic acid, aspartate
bipy	2,2′-Bipyridine
Bn	benzyl
Boc	*tert*-Butyloxycarbonyl
BOP	(benzotriazol-1-yloxy)tris(dimethylamino)phosphonium hexafluorophosphate
BSA	bovine serum albumin
CAM	ceric ammonium molybdate
Cbz	carboxybenzyl
CN	cyano-, nitrile, cyanide
d	doublet
d.r.	diastereomeric ratio
DCM	dichloromethane
DIPEA	diisopropylethylamine
DMAP	4-dimethylaminopyridine
DMF	dimethylformamide
DMSO	dimethyl sulfoxide
DPP	dipeptidyl peptidase
E	energy, enzyme
EDC	*N*-(3-Dimethylaminopropyl)-*N*′-ethylcarbodiimide
EDTA	ethylenediaminetetraacetic acid
E_{off}	calculated energy difference between product and transition state
E_{on}	calculated energy of activation

ESI	electrospray ionization
Et	ethyl
FAP	fibroblast activation protein alpha
FITTED	Flexibility Induced Through Targeted Evolutionary Description
FT-IR	Fourier-transform infrared spectroscopy
G	glycine
Glu	glutamic acid, glutamate
HATU	1-[Bis(dimethylamino)methylene]-1H-1,2,3-triazolo[4,5-b]pyridinium 3-oxid hexafluorophosphate
His	histidine
HPLC	high performance liquid chromatography
hPOP	human prolyl oligopeptidase
HRMS	high resolution mass spectroscopy
HSQC	heteronuclear single quantum coherence
I	inhibitor
IC_{50}	half maximal inhibitory concentration
*i*Pr	isopropyl
IR	infrared spectroscopy
J	coupling constant
k_{cat}	enzyme turnover rate
K_i	inhibition constant
K_m	Michaelis-Menten constant
k_{of}	off rate
k_{on}	on rate
m	multiplet
mCPBA	*meta*-chloroperoxybenzoic acid
Me	methyl
Me	methyl
MeCN	acetonitrile
mp	melting point
MS	mass spectroscopy

Ms	mesyl
NMR	nuclear magnetic resonance
OAc	acetate
P	proline
PES	potential energy surface
Ph	phenyl
Phe	phenylalanine
pin	pinacol
Piv	pivaloyl
pNA	*para*-nitroaniline
pnd	pinanediol
POP	prolyl oligopeptidase
Pro	proline
PyBOP	benzotriazol-1-yl-oxytripyrrolidinophosphonium hexafluorophosphate
q	quartet
QCCA	Quantum Chemical Cluster Approach
QM	quantum mechanics
R_f	retention factor
rt	room temperature
s	singlet
S	substrate
Ser	serine
t	triplet
TBS	*tert*-butyldimethylsilyl
*t*Bu	*tert*-butyl
Tf	triflate
TFA	trifluoroacetic acid
THF	tetrahydrofuran
Thr	threonine
TLC	thin layer chromatography
TME	tumour microenvironment

TMS	trimethylsilyl
t_R	residence time
Trp	tryptophan
TS	transition state
Ts	tosyl
Tyr	tyrosine
Z	carboxybenzyl
ΔG	free energy

Contribution(s) of authors

Professor Nicolas Moitessier, as my supervisor, is a co-author on and contributor of every chapter.

Chapter 1: I reviewed the field of boronic acid drugs and their respective discovery and design.

Chapter 2: I synthesized and characterized all molecules and conducted the molecular docking as well as the literature review of FAP-targeting electrophilic inhibitors. The assay designs, biophysical experiments, and kinetic characterizations are the work of Dr. Stephane De Cesco. The computational procedure development and all computational predictions apart from molecular docking are the work of Jerry Kurian and Mihai Burai Patrascu. The mass spectroscopy experiment was conducted by Alexander S. Wahba.

Chapter 3: I designed, synthesized, and characterized all molecules presented in this chapter and conducted 90% of the *in vitro* assays, the rest of which were conducted by Naëla Janmamode. Caroline Dufresne purified the POP enzyme. Alexander S. Wahba conducted the mass spectroscopy studies. I conducted the virtual screening and analysis with aide from Professor Nicolas Moitessier.

Chapter 4: I synthesized 95% of the compounds and intermediates presented in this chapter, the rest of which were synthesized by a summer intern student Maud Poussé. I characterized all compounds. Dr. Damien Hédou contributed to the optimization of the syntheses. I conducted all of the *in vitro* assays. Caroline Dufresne purified the POP enzyme. The docking studies were performed by myself and Dr. Damien Hédou.

Chapter 5: I synthesized and characterized all molecules presented in this chapter, with help in synthetic optimization from a summer intern student Benjamin Gerlovin. Dr. Damien Hédou contributed to the optimization of the syntheses. All computational work was done by Wanlei Wei.

Chapter 6: I designed, synthesized, and characterized all molecules presented in this chapter, with help in synthetic optimization from a summer intern student Yufei Wang, who also wrote the majority of this chapter's introduction. The virtual screening and analysis were conducted by myself and Dr. Stéphane De Cesco.

Chapter 7: I wrote the conclusion and future perspective

Chapter 1:

Design and Discovery of Boronic Acid Drugs

This chapter has been accepted and is reproduced from:

Plescia, J.; Moitessier, N. Design and discovery of boronic acid drugs. *Eur J Med Chem* **2020**, 112270.

Contribution(s) of authors: I reviewed the field of boronic acid drugs and their respective discovery and design.

1.1 Abstract

Research related to boronic acids, from synthetic development to materials to drug discovery, has skyrocketed in the past 20 years. In terms of drug discovery, the incorporation of boronic acids into medicinal chemistry endeavours has seen a steady increase in recent years. In fact, the FDA and Health Canada have thus far approved five boronic acid drugs, three of which were approved in the past four years, and several others are in clinical trials. Boronic acids have several desirable properties that has led to their increased use, including potentially enhancing potency of drugs and/or improving their pharmacokinetics profile. This review explores discovery processes of boronic acid drugs. It begins with a brief scope of boron in natural products and in current drugs, followed by an investigation into the various rationalizations for boronic acid incorporation and the synthetic developments that focused on facilitating their addition into organic compounds. We hope that the knowledge we have assembled in this literature review will encourage medicinal chemists to consider the potential benefits of incorporating boronic acids into their future drug discovery endeavours.

1.2 Introduction

Boron is ubiquitous in nature, from being an essential component of plant structural integrity[1] and metabolism[2] to being a regulator of mammalian vitamin D levels[3] and bone health.[4] In the form of boronic acids and esters, it is considered to be safe[5] for incorporation into pharmaceutical development.

In fact, instances of boron-based studies, whether for synthetic, biological, or pharmaceutical endeavours have skyrocketed since the late 1990's. Figure 1.1A illustrates the PubMed literature search results including "boron" in the publication title. More specifically, boron-related drug discovery endeavours have also made increasing appearances in scientific literature. Figure 1.1B illustrates the PubMed literature search results of "boron" in the publication title and "drug" in the text, showing a steep escalation in usage starting in the 1990's. Boronic acids as drugs are becoming increasingly relevant. In fact, four boron-containing drugs have been approved in the past five years, (Bortezomib as approved in 2005), with several others in clinical trials.

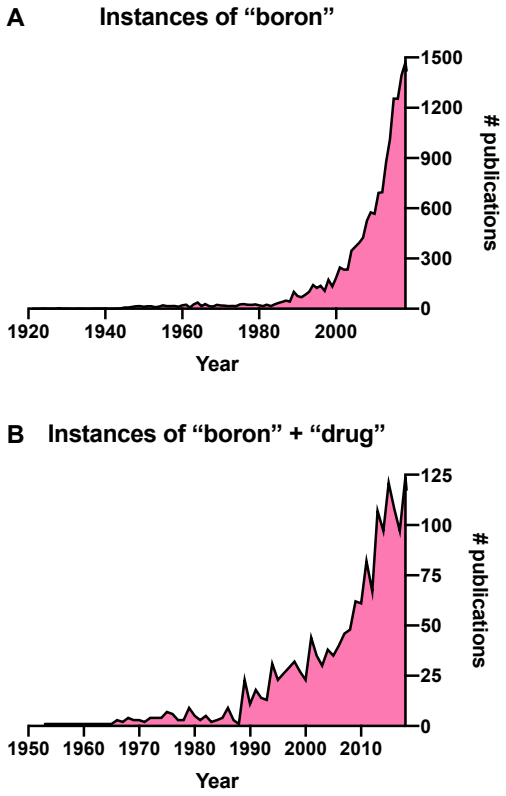

Figure 1.1. PubMed search results of the terms "boron" (A) and "boron" + "drug" (B)

Despite the use of boronic acids in diagnostic tools,[6-7] Boron Neutron Capture Therapy (BNCT) radiation treatment,[8-9] bioconjugation,[10] materials,[11] and catalysis,[12] among others, our focus in this review is on small molecule drugs and potential drugs containing boronic acids and esters and their associated design and therapeutic application. Reasons for incorporation of boronic acids into drug discovery endeavours vary, ranging from improvement of drug activity to enhancement of pharmacokinetic properties. The discovery process of boronic acids also depends on the approach, such as substrate mimicry or peptidomimetics design, rational design via computational methods, or use as bioisosteres to substitute for certain functional groups.

This chapter outlines the rationalization of boronic acid use and associated discovery processes, including incorporation of boronic acid moieties into bioactive compounds. While we do include a diverse scope of boron-based drug applications, this review in no means covers the vast span of boronic drug discovery (See Figure 1.1), but instead provides examples of progress made so far in pharmaceutical applications of boronic acids, along with a few examinations of the rationale behind inclusion of boronic acids.

1.3 Occurrence of boron in nature

1.3.1 Boron in bacteria

Boromycin (Figure 1.2), isolated from a *Streptomyces antibioticus* strain in African soil, was the first ever natural product found to contain boron.[13] Since then, this macrolide has been studied for its therapeutic properties. One study reported nanomolar potency against several HIV-infected cell lines.[14] Boromycin was also studied for its potent antibacterial activity against several strains, including *Mycobacterium tuberculosis*.[15] A related macrolide, Aplasmomycin, isolated from *Streptomyces griseus* and named for its antiplasmodial activity, was discovered about 10 years later and has a structure similar to that of Boromycin[16] (Figure 1.2). In these two natural products, boron has a structural role, inducing the folding of the polyols into compact structures.

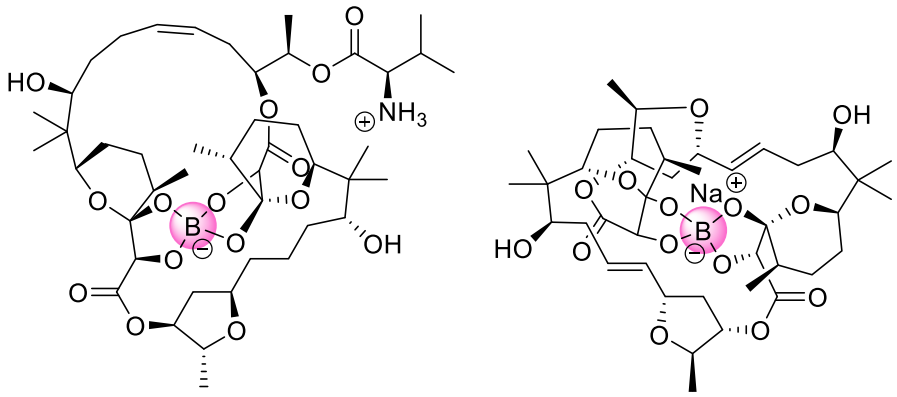

Figure 1.2. Boron in bacterial-derived antibacterials

These two bacterial compounds were both recently found to inhibit a biomolecular pathway in *Helicobacter pylori*, bacteria implicated in stomach cancer.[17] Derivatives of these two antibacterials (not shown), including Aplasmomycin B and C and *N*-acetylboromycin, also occur naturally and have also exhibited antibacterial activity. For a more comprehensive review of these natural boron-containing macrolides, see Dembitsky *et al.*[18]

1.3.2 Boron in plants

Boron is vital to plants and algae. In fact, boron deficiency in plants is detrimental to survival and often leads to plant death.[19] Similarly to the natural products described above, it is known to

form complexes with polysaccharide moieties – through interactions with diols – in the plant cell wall membrane and is therefore essential for structural integrity.[1] The mechanism is not fully understood, but one study of tobacco plants revealed that boron-deficient plants contained more reactive oxygen species (ROS) than control plants. The researchers hypothesize the ROS levels build up as a signalling mechanism when there is a disturbance in the structural integrity of the cell wall as a result of boron loss.[19] Although cell wall assembly seems to be its major role, boron is also known to be essential in several other plant biomechanisms, such as nitrogen fixation and plant metabolism.[2]

1.3.3 Importance in mammalian systems

Although the full extent of boron's roles in mammalian biological systems is not completely understood, several studies link boron to various mammalian biomechanisms. In fact, the World Health Organization (WHO) declares boron as a "probably essential element" for humans.[20]

Boron is suggested to be important in mammalian bone health and is present in higher concentrations in bones than in other tissues.[20] A study conducted by Gorustovich *et al.* aimed to determine the effect of boron-deficient diets on dental bone modelling and remodelling. It was found that boron-deficient diets inhibited bone formation when compared to boron-supplemented control diets, although the mechanism was not elucidated. These results were consistent with earlier discoveries that boron deprivation in rats led to decreased bone volume in vertebral development.[21] Another study employing mice with diabetes-induced osteoporosis showed that boron supplements improved bone strength and overall health in not only the diabetic mice, but also in the control group. These results were consistent with other animal studies, and suggest that boron supplementation may be beneficial for bone strength.[4] However, further studies would need to be conducted to demonstrate parallel effects in humans.

Boric acid treatment even advances wound healing. A preliminary study revealed that treatment with 3% boric acid solution on intensive care patients with deep wounds resulted in transfer to normal care three times as quickly as patients receiving standard treatments.[22] Another *in vivo* study of boron delivered in the form of a boric acid solution showed upregulation of synthesis of extracellular matrix proteins responsible for tissue reparation, although further studies are needed to determine the mechanisms of these observations.[23]

Several studies have shown that vitamin D deficiencies are compensated by boron supplementation. One study involved boron supplementation in the vitamin-D-adequate or -inadequate diets of chickens. It was found that addition of boron improved overall chicken health (mineral levels, body weight, food consumption, etc.) in both the vitamin-D-inadequate and control groups, though the increase was greater in the vitamin-D-inadequate group.[24] This study, along with other studies relating dietary boron to vitamin D levels, led to one group hypothesizing that boron's potential mechanism involves inhibition of an enzyme involved in metabolism of vitamin D to an inactive form.[3]

Even from the few above studies, it is clear that boron is implicated in several mammalian biomechanisms. For more comprehensive reviews on boron in biological systems, see Uluisik *et al.*[25]

1.4 Scope of boronic acid drugs

1.4.1 Approved boron-containing drugs

So far, five approved drugs exist on the market that contain boron (Figure 1.3). The first to be approved was Bortezomib, marketed under the name Velcade®, approved by the U.S. FDA in 2005[26] and by Health Canada in 2008[27] for the treatment of multiple myeloma. The structure was originally discovered through the study of substrate mimics in the form of peptidic aldehydes, which, through co-crystallization with the target were found to bind covalently to the nucleophilic threonine residue. However, as aldehydes are unsuitable for further drug development studies, boronic acid analogs were tested and showed high potency.[28-29] Although several proposed mechanisms of anti-cancer activities have been reported, its major mechanism of action involves the ubiquitination pathway of protein degradation; Bortezomib is a proteasome inhibitor, blocking the degradation of apoptotic proteins in tumour cells.[30] Through co-crystallization studies, it is suggested to act as a reversible covalent inhibitor, blocking the action of nucleophilic threonine residues in the active sites of the proteasome.[31]

Ninlaro®, or Ixazomib, similarly to Bortezomib, was approved by the FDA in 2015[32] and by Health Canada in 2016[33] for treatment of multiple myeloma[32] and is a second generation proteasome inhibitor.[34] It is the first oral proteasome inhibitor,[32] as Velcade® (Bortezomib) is currently administered as weekly injections.[26] Ixazomib was discovered from a screening of boron-containing proteasome inhibitors with improved pharmacokinetic properties over Bortezomib. Its

mechanism of action was found to be nearly identical to that of Bortezomib (See Section 1.5.2), yet it was found to be more potent, less prone to inducing adverse side effects (higher specificity), and even to treat certain patients whose tumours have developed resistance to Bortezomib.[34] Although approved, Ixazomib is also under clinical trials as part of combination therapies to treat multiple myeloma.[34-35]

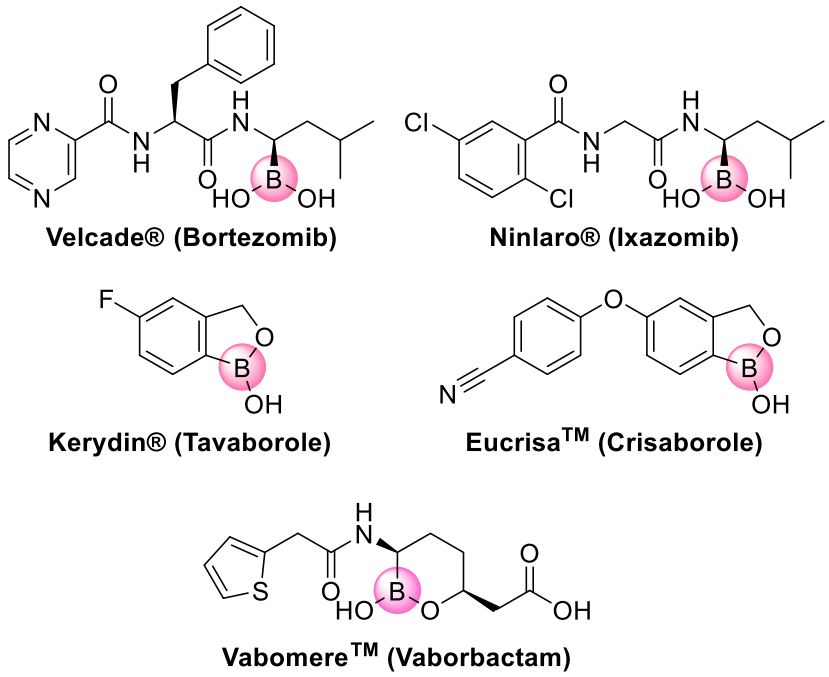

Figure 1.3. Approved boron-containing drugs

Kerydin®, or Tavaborole, received global approval[36] by the U.S. FDA in 2014 to treat onychomycosis, a fungal infection.[37] Its structure was originally discovered through structure-activity relationship (SAR) studies of a similar anti-bacterial borinic ester. Upon testing against several types of fungi, it was found to have broad-spectrum antifungal activity.[38-39] Tavaborole's mechanism of action is believed to involve the inhibition of fungal Leucyl-tRNA synthetase, preventing protein synthesis and thus fungal growth, and is three orders of magnitude more selective for fungal Leucyl-tRNA synthetase than the human equivalent. The necessity of the boron-containing moiety was confirmed by 50-fold loss of inhibitory activity upon testing analogues that substituted boron for carbon.[40]

Eucrisa™, or Crisaborole, was approved in 2016 by the U.S. FDA[41] and by Health Canada in 2018 to treat mild to moderate eczema.[42] It was discovered by the same research group as that who discovered Tavaborole through a screening of a boron-containing compound library against phosphodiesterase 4 (PDE4) and cytokine release factors, both implicated in anti-inflammatory response pathways.[43]

Vabomere™ is a combination drug (Figure 1.3 includes only the boronic acid component) approved by the U.S. FDA[44] and Health Canada in 2017[45] to treat bacterial infections.[46] It includes Vaborbactam, a β-lactamase inhibitor, and Meropenem, an inhibitor of bacterial cell-wall synthesis. Although Vaborbactam is not an antibacterial itself, it is administered in combination with the carbapenem Meropenem to prevent its hydrolysis by β-lactamases.[47] In terms of its discovery, boronic acids were already known to be potent β-lactamase inhibitors through their reversible covalent bond with catalytic serine residues.[48] Vaborbactam was therefore designed by structure-based modifications of various known active analogues. It was intended to be a reversible covalent inhibitor, and crystallography studies confirm its covalent complexation with the catalytic serine (pdb: 4XUZ).[49] Furthermore, the researchers successfully induced selectivity over other mammalian serine proteases through incorporation of a *cyclic* borinic acid, which would not fit in the smaller active sites of native serine proteases with more flexible substrates.[49]

1.4.2 Boron-containing drugs under investigation

Although not yet approved, there are several boronic acid drugs under investigation in clinical trials (Figure 1.4).

Dutogliptin[50] is a dipeptidyl peptidase 4 (DPP4) inhibitor. It failed in Phase II clinical trials for diabetes mellitus, but it is now under investigation in a combination therapy with granulocyte-colony stimulating factor (G-CSF) to treat myocardial infarctions. While implicated in diabetes, DPP4 is also responsible for degradation of factors responsible for recruiting stem cells for cardiac muscle repair. A Phase II trial of co-administration of Dutogliptin with G-CSF, a stem cell mobilizer,[51] is currently underway.[52]

Acoziborole, also referred to as SCYX-7158 or AN5568, is a parasite-inhibiting drug candidate to treat Human African Trypanosomiasis (HAT),[53] although neither its biological target nor its mechanism of action is known.[54] Current available HAT treatments are unfortunately quite

cytotoxic and lack efficacy. Acoziborole, on the other hand, is safe, orally bioavailable, and has the potential to be administered in one sole dose.[53] It is currently in Phase III trials.[55]

GSK3036656, another benzoxaborole compound, is a leucyl-tRNA synthetase inhibitor for treatment of Tuberculosis infections;[56] it was designed to be a reversibly covalent inhibitor that binds to Ade76 of tRNA and prevents RNA synthesis.[57] It's structure is a modified version of GSK2251052, or AN3365, which failed in Phase II due to development of resistance.[58] An SAR study produced GSK3036656, a potent inhibitor with favorable pharmacokinetic properties that shows selectivity for bacterial leucyl-tRNA synthetase over the human homologue.[57] This compound is currently in Phase II studies for Tuberculosis.[59]

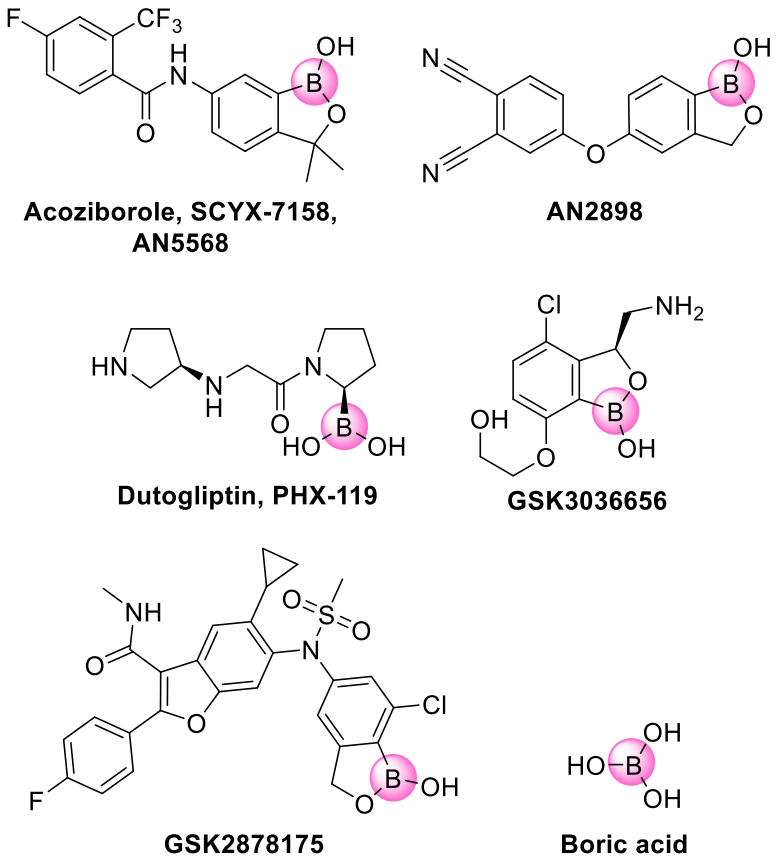

Figure 1.4. Boron-containing drugs in clinical trials

Similar to the already-approved Crisaborole is AN2898, another phosphodiesterase 4 inhibitor for the treatment of atopic dermatitis.[60] Clinical trials are ongoing, but in a Phase II study, it was

deemed to be safe and effective for treatment.[61] As can be seen in Figure 1.3 and Figure 1.4, the structures are nearly identical, save for one extra nitrile in AN2898's side chain.

An antiviral compound, **GSK2878175**, has completed Phase 2 clinical trials[62] as a combination therapy targeting the Hepatitis C virus RNA polymerase NS5B enzyme. Its design stemmed from optimizations of the metabolic profile of a failed clinical candidate. After several rounds of structural modification, *in vitro* and *in cellulo* assays confirmed potent activity of **GSK2878175**, and *in vivo* studies confirmed its superior pharmacokinetic profile.[63]

Although not a synthetic drug, boric acid itself is currently in Phase II/III clinical trials as BASIC (Boric Acid, Alternate Solution for Intravaginal Colonization), formulated as a cream to treat bacterial vaginosis (BV).[64] Separate Phase IV clinical trials are also ongoing, testing a boric acid in combination with probiotics – as a combination capsule – to treat BV and candidiasis, or yeast infection.[65]

While there are only a handful of boron-containing drugs currently in clinical trials, several have been halted for various reasons. One example is AN3365, mentioned above. Currently, however, studies of analogs are underway which have produced compounds that appear to evade this resistance.[66] Others include Talabostat (PT-100), a multi-target anti-cancer drug which failed in Phase III;[67] PHX1766, an HCV protease inhibitor that failed in accelerated Phase I trials;[68] and Delanzomib, a proteasome inhibitor similar to Bortezomib and Ixazomib that failed in Phase I/II trials due to limited efficacy.[69]

Based on the frequency of boron drugs reaching Phase II clinical trials, it is likely there will be further developments and more approvals in coming years.

1.4.3 Over-the-counter boron-containing drugs and supplements

As discussed earlier, elemental boron supplements have been used in many animal studies to investigate the role of boron in mammalian systems. Although not approved by the Food and Drug Administration, general safety has led to the sale of boron supplements as long as they are not labeled as a treatment for any disease.[70]

Although it is undergoing clinical trials as a cream to treat BV,[48] boric acid solutions and powders have been available over-the-counter for many years, such as for ophthalmic[71] or vaginal[72] use, though its effectiveness is questionable.

Calcium fructoborate (CF), sold under FruiteX-B®, is found naturally in fruits and vegetables and is a complex of fructose with boronic acids (intracellular) or esters (extracellular).[73] It is sold as a supplement whose claims include improvement of bone and cardiovascular health. Although these claims are not fully substantiated, a double-blind study on middle-aged adults with osteoarthritis did conclude that CF led to improvement in quality of life of patients in the short-term with a favourable prognosis for inflammation. The mechanism of action for this result is not fully known, although *in vitro* studies reveal that CF is responsible for inhibiting the release of proteins responsible for inflammation response (e.g. interleukins).[74] The claim of improvement in cardiovascular health is still preliminary, although early clinical studies indicate that CF significantly reduces levels of low-density lipoprotein and triglycerides while raising levels of high-density lipoprotein, suggesting that CF may improve cardiovascular health.[75] Despite these results, long-term studies and larger cohorts are necessary for more conclusive results.

1.4.4 Boron-containing compounds in drug discovery

Though they have yet to lead to approved drugs, there have been countless drug discovery endeavours that have incorporated boron into the target molecules for a variety of therapeutic purposes. The following sections highlight some medicinal chemistry applications of boronic acids so far.

1.4.4.1 Anti-cancer boron-containing compounds

As described earlier, Bortezomib, or Velcade® (Figure 1.3), was the first boronic acid drug to be approved by the U.S. FDA for the treatment of multiple myeloma,[26] followed several years later by Ixazomib, or Ninlaro® (Figure 1.3).[32] These approvals have led to a surge of boronic acid drug discovery. Furthermore, due to off-target effects and resistance development against Bortezomib,[29] research continues into proteasome inhibitors, especially after the clinical failure of Delanzomib (Figure 1.5).[69] Han *et al.* recently conducted an SAR relationship study of urea-containing peptidic compounds as proteasome inhibitors. From this study, they discovered compound **1.1** (Figure 1.5). In *in vitro* assays, **1.1** exhibited sub-picomolar activity against the human 20S proteasome. Furthermore, its activity against eleven human cancer cells lines was consistently in the nanomolar range, and *in vivo* mice assays revealed that not only was its anti-tumour activity similar to that of Bortezomib, but it also exhibited lower toxicity and more promising pharmacokinetic properties.

Based on these promising results, this compound is currently in pre-clinical studies.[76] More recently, Lei *et al.* have focused on the discovery of a proteasome inhibitor that would not only be effective for multiple myeloma, but also triple-negative breast cancer. Through an SAR study of Bortezomib and Ixazomib analogues, they discovered compound **1.2** (Figure 1.5), an unusual eight-membered ring boronic ester pro-drug, which exhibited low nanomolar activities *in vitro* and *in cellulo* similar to those of the two approved drugs. *In vivo* assays against triple negative breast cancer in mice also yielded promising results, including tumour necrosis. However, the pharmacokinetics of **1.2** require lead optimization, as *in vivo* bioavailability is low.[77]

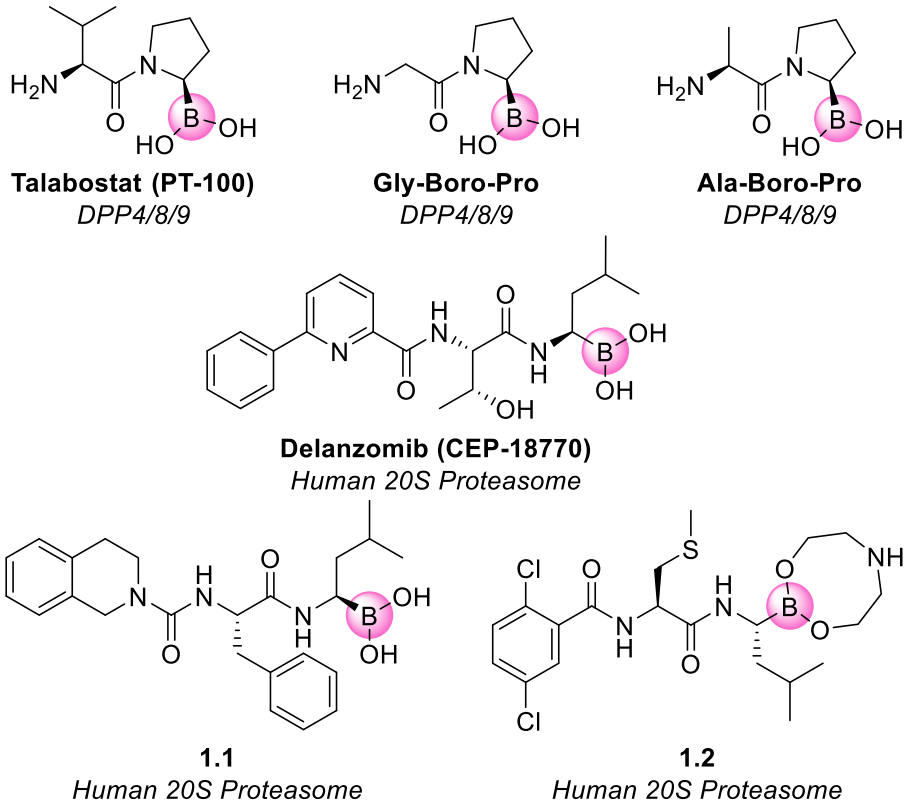

Figure 1.5. Examples of boronic acid compounds as anti-cancer therapeutics

In much more recent context, the dipeptidyl peptidase (DPP) family of serine proteases, including DPP8 and DPP9, have been discovered to be involved in various biomechanisms in cancer and associated immune response.[78] Studies utilizing DPP8/9 inhibitor Talabostat (Figure 1.5), a drug that failed in Phase III as a non-selective DPP/FAP/POP inhibitor,[67] show that inhibition leads to induction of cell death through several immune response mechanisms.[79]

However, results are still inconclusive, as Talabostat is non-selective and the extent of its mechanisms of action is not fully known.[78] DPP8 and DPP9 are very structurally similar to a widely-studied homologous enzyme, DPP4, and many studies focused on inhibitors, mainly on nitriles[80] but some boronic acids (Gly-Boro-Pro and Ala-Boro-Pro, Figure 1.5),[81] targeting DPP4 for diabetes treatment were tested on both DPP8 and DPP9 to determine selectivity. Similarly, while there exist several FDA-approved DPP4 inhibitors (e.g. sitagliptin, saxagliptin),[82] DPP4 has more recently been discovered to be implicated in certain epithelial cancers. In fact, preliminary studies have demonstrated that in patients with diabetes and colorectal or lung cancer, DPP4 inhibition is associated with greater overall survival,[83] though further studies are required. Additionally, recent accounts associate DPP4 inhibitor use with increased risk for pancreatic cancer, although results so far are inconclusive, as longer-term studies are required.[84]

Apart from the proteasome or DPP family, boronic acids in anti-cancer pursuits include modifications of failed drug Combretastatin A-4 targeting tubulin assembly by Kong *et al.*,[85] and design of epidermal growth factor receptor (EGFR) tyrosine kinase (TK) inhibitors by Ban *et al.*, both design rationales explored in more detail later.[86]

1.4.4.2 Anti-viral boron-containing compounds

Viral proteases are also common biological targets of boron-based inhibitors, such as the NS3 protease of the hepatitis C virus (HCV). Though there exist approved drugs for the HCV NS3 serine protease,[87] research has gone into discovery of inhibitors that replace the α-ketoamide moiety of approved drugs with boronic acid moieties, taking advantage of the catalytic serine in the active site. For example, one group based at Anacor Pharmaceuticals has studied on modifying telaprevir and boceprevir, both linear hexapeptides, with cyclic boronic acids (**1.3**, Figure 1.6),[88] but eventually improvements in structure and a few additional HCV NS3 approved drugs danoprevir and vaniprevir[87] led to studies of macrocylic drug structures (**1.4**, Figure 1.6).[89] More recent examples of viral NS3 protease inhibition with boronic acids include that of flaviviruses such as dengue fever virus (DV) and Zika. One group in particular discovered modified dipeptides (Phe-Arg) containing boronic acids as reversible covalent groups (**1.5**, Figure 1.6) that were over one hundred times more active than the carboxylic acid derivatives.[90]

On a separate note, the human immunodeficiency virus (HIV) aspartic acid protease was recently targeted with an aromatic boronic acid exhibiting subpicomolar activity (**1.6**, Figure 1.6),

two orders of magnitude more potent than its previously-published carboxylic acid derivative (Figure 1.11) and current HIV approved protease inhibitor, Darunavir.[91] In a follow-up SAR study, Ghosh *et al*.[92] studied a set of analogues of Darunavir and this compound. Their study design and rationale are discussed on more detail later, with similar studies.

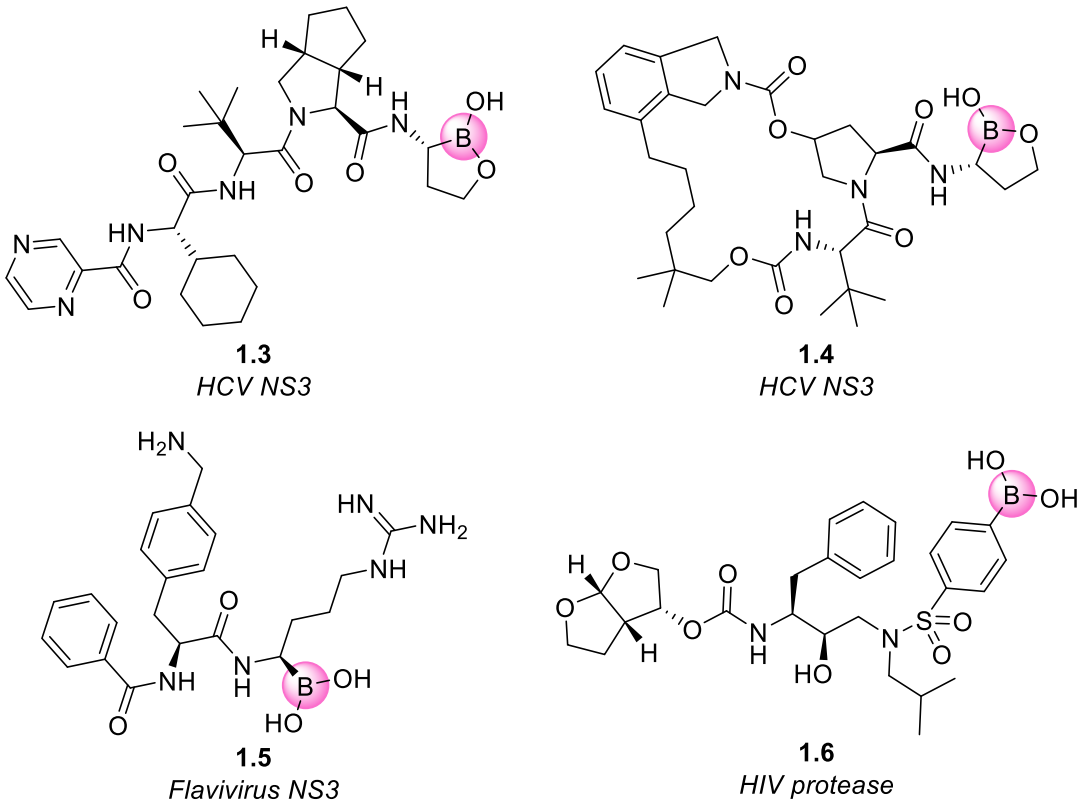

Figure 1.6. Examples of boronic acid compounds as antivirals

1.4.4.3 Other anti-infective boron-containing compounds

Boronic acids have been used quite widely in drug discovery studies targeting fungal, bacterial, and parasitic infections. As discussed earlier, some boronic acid drugs have either been approved (Figure 1.3) or are currently in clinical trials (Figure 1.4) for anti-fungal or anti-parasitic therapeutics, all of which contain the boronic acid benzoxaborole structure. This scaffold was also recently applied, again by Anacor Pharmaceuticals, to studies of the parasitic infection cryptosporidiosis, yielding compound AN7973 (Figure 1.7A). This compound exhibited potent *in vitro* and *in vivo* activities against infected mice and showed favourable pharmacokinetics. It is currently in pre-clinical studies.

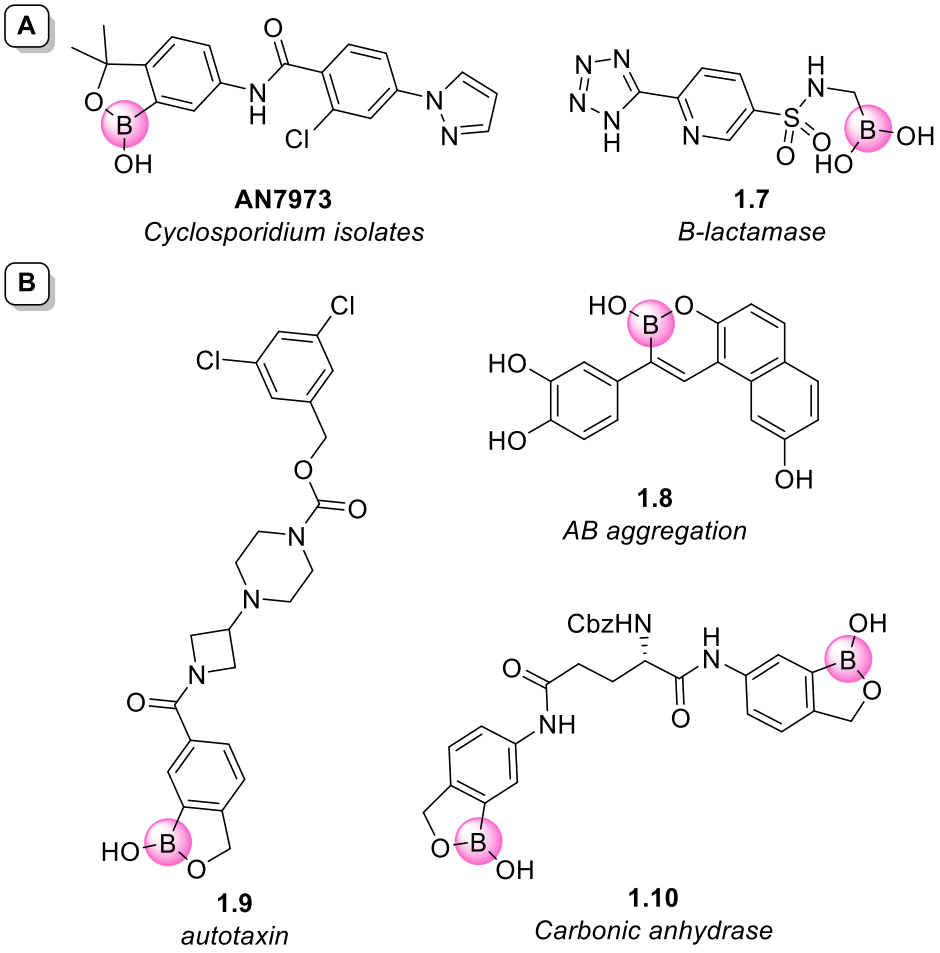

Figure 1.7. Examples of bioactive boronic acid compounds (A) targeting non-viral infections and (B) for other therapeutic applications

The bacterial enzyme β-lactamase has also been a target in boronic acid drug discovery, and is the target of approved drug Vaborbactam (Figure 1.3).[93] One of the most potent β-lactamase inhibitors reported to date was discovered through a fragment-guided *in silico* design (**1.7**, Figure 1.7A) and exhibited sub-nanomolar activity *in vitro* and promising results *in vivo*, though pharmacokinetics need improvement.[94] Nevertheless, drug discovery studies targeting β-lactamase have continued due to increasing need to combat anti-bacterial resistance.[93]

1.4.4.4 Other therapeutic applications of boron-containing compounds

Besides as anti-cancer and anti-infective therapeutics, boron drugs have a number of other applications. In fact, one recent study discovered anti-Alzheimer's compounds from modifying

curcumin, a known amyloid-beta (AB) aggregation inhibitor, to contain a borinic acid moiety (**1.8**, Figure 1.7B). After an SAR study, compound was found to not only be a potent AB aggregation inhibitor on the same order as curcumin, but also exhibited good antioxidant activity, as oxidative stress is associated with neurodegeneration.[95]

As previously discussed, the benzoxaborole scaffold has been applied over a large scope of enzymes, including the phosphodiesterase 4 (PDE4) inhibitor[43] Crisaborole, to treat mild to moderate eczema.[41] Autotaxin, a target also implicated in inflammation, as well as fibrosis and cancer, has been targeted with boronic acid drugs, including the benzoxaborole scaffold[96] and aromatic boronic acids.[97-98] Kraljić *et al.* have designed benzoxazole analogues (**1.9**, Figure 1.7B) of recently-discovered hits that not only exhibited submicromolar potency against autotaxin, but also very favourable pharmacokinetic properties,[96] though further biological studies are needed to confirm potency.

Recently, Larcher *et al.* discovered a series of *bis*-benzoxaboroles targeting carbonic anhydrase, an enzyme implicated in several diseases, though isoform selectivity is difficult.[99] They found their linked *bis*-benzoxaborole inhibitors to be potent against the disease-implicated carbonic anhydrases, while remaining selective over the human cytosolic form. Their most promising compound, **1.10** (Figure 1.7B), contains two benzoxaboroles connected by an almost-symmetrical seven-atom linker containing one stereocenter.[100]

1.5 Design of boron in drugs

Reasons and rationalizations for inclusion of boron, namely in the form of boronic acids, varies, as covered in Section 1.4 highlighting approved drugs and drugs in clinical trials. This section focuses in more detail on the design and rationalization leading to incorporation of boronic acids into drug discovery endeavours.

1.5.1 Boronic acids as bioisosteres

Boronic acids are ionically stable in physiological pH,[101] making them promising unionized alternatives for ionized bioisosteres (Figure 1.8).

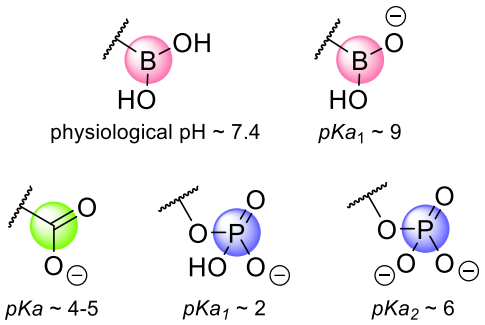

Figure 1.8. pKa of boronic acid, carboxylic acid, and phosphate protons[101-103]

As a more specific example, boronic acids have been studied as bioisosteres of carboxylic acids. Their structures are similar, but the boronic acid's higher pKa allows it to be unionized at physiological pH.[102] Examples of this bioisostere application include studies by Albers *et al.*[97-98] and Ghosh *et al.*[92] A discussion detailing their design rationale follows.

Phosphates, while not as similar in structure to boronic acids as carboxylic acids, have also been replaced with boronic acids to study nucleosides.[103] For example, the Vasseur research group has synthesized analogues of DNA nucleotides, replacing the phosphate group with a boronic acid (Figure 1.9, A). Computational studies revealed that these boronucleotides were structurally very similar to their native analogues.[104] Furthermore, reaction with native ribonucleoside uridine gave the corresponding dinucleotide through reaction of the boronic acid with diol of the RNA nucleoside (Figure 1.9, B).[105]

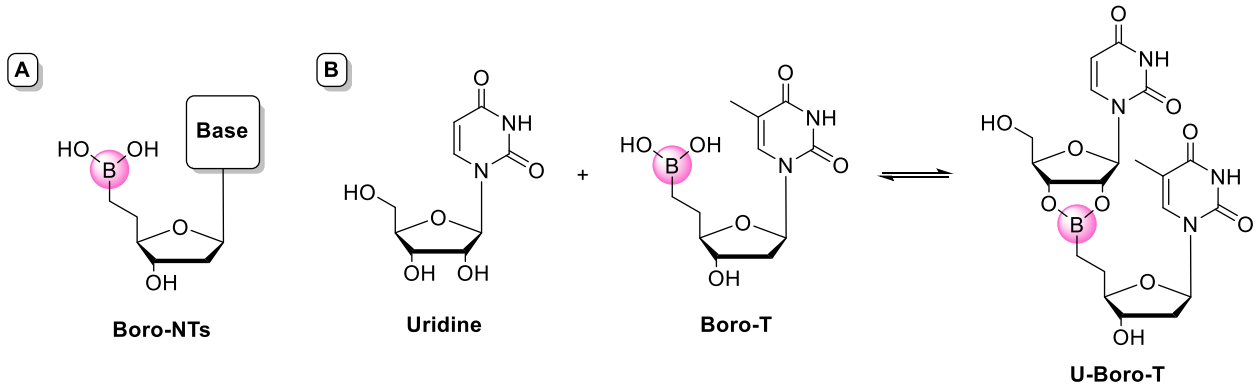

Figure 1.9. Vasseur's boronucleotide analogues. (A) structure of the boronucleotide, replacing the phosphate with a boronic acid;[104] (B) reversible reaction of RNA's uridine with the boronucleotide thymidine analogue[105]

For a more comprehensive review of boronic acids in nucleic acid chemistry, see a review from the Vasseur research group.[106]

1.5.1.1 Utilizing boronic acids for improvement of pharmacokinetic properties

Addition of boron or replacement of certain functional groups with a boron-containing group affects the octanol-water partition coefficient (logP) and distribution coefficient (logD), which, in turn, affects several pharmacokinetic properties.[107]

One example of utilizing a boronic acid as an isostere for a phenol group to improve solubility was investigated by Kong *et al.*[85] In their study of analogs of Combretastatin A-4, an anti-cancer agent halted in Phase II clinical trials,[108] they aimed to improve both the activity and solubility of the compound without the use of a phosphate prodrug. Their replacement of an aromatic phenol with an aromatic boronic acid (Figure 1.10) led to not only improved bioactivity, but a nearly two-fold improvement in solubility in acidic media, suggesting the enhanced stability and solubility upon oral administration.[85]

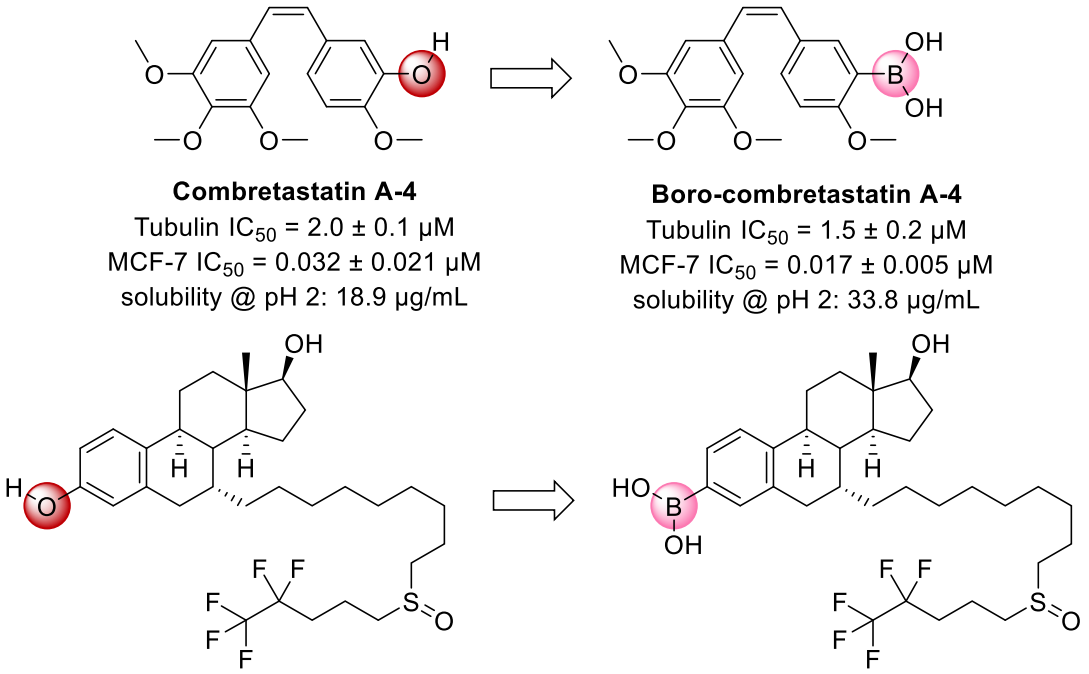

Figure 1.10. Improved properties of upon utilizing the boronic acid group as an isostere for (A) Combretastatin A-4[85] and (B) Fulvestrant[109]

Another example of utilizing boron for improved bioavailability comes from Liu *et al.* and their research in the discovery of breast cancer selective estrogen receptor downregulators (SERDs). The researchers aimed to improve the compound Fulvestrant,[109] the only FDA-approved SERD (Figure 1.10).[110] Wanting to overcome rapid glucuronidation of its phenol, the researchers replaced the phenol group with an aromatic boronic acid. Not only did the activity of the boron analogue remain nearly equipotent as Fulvestrant *in cellulo* against breast cancer cells, but it displayed superior pharmacokinetic properties and was therefore more potent *in vivo*.[109] More specifically, incorporation of a boronic acid slowed down the clearance rate of Fulvestrant, allowing for a slow release upon slower metabolic oxidation of the boronic acid to the phenol. ZB716 is currently in pre-clinical development.[111] The same research group, continuing their studies of SERDs, has since utilized the boronic acid moiety as an orally available bioisostere for phenols in their discovery and development of other anti-breast cancer drugs.[110]

1.5.1.2 Utilizing boronic acids for improvement of drug activity

Boronic acids have been utilized as bioisosteres for several different functional groups, including carboxylic acids as mentioned above. One example from Albers *et al.* involves a study in which the researchers replace a carboxylic acid with a boronic acid in aims to improve potency of their hit autotaxin inhibitor.[97-98] Their rationale included knowledge of a threonine nucleophilic residue; they realized that, while the carboxylic acid moiety could hydrogen bond to the nucleophilic threonine, a boronic acid could act as an electrophile to block the enzyme's activity reversibly.[97]

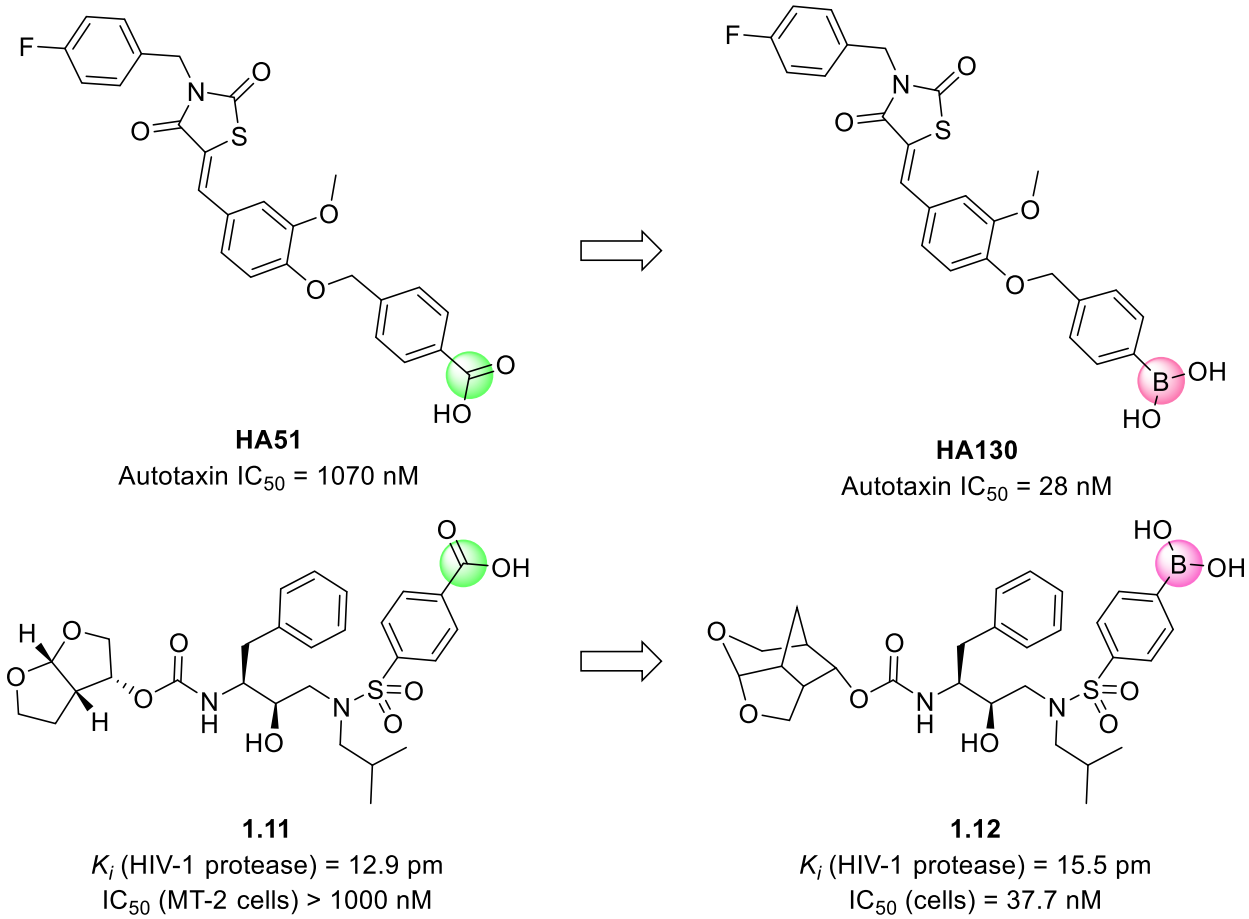

Figure 1.11. Use of a boronic acid as an isostere for a carboxylic acid to improve anti-autotaxin activity[97-98] and anti-HIV activity.[92]

In their studies of HIV protease inhibitors, Ghosh *et al*. discovered analogues of Darunavir containing either carboxylic acids or boronic acids (Figure 1.11). Upon testing the inhibitors against the enzyme itself, both series of compounds exhibited low-nanomolar potencies. When tested against MT-2 cells, however, the boronic acids retained their potency, while the carboxylic acids potency decreased by at least 2 orders of magnitude. This inactivity was attributed to the inhibitors' presumed inability to cross the cell membranes, as their binding mode was very similar by X-ray crystallography (aside from their differing bicyclic side chains).[92]

1.5.2 Boronic acids as reversible covalent inhibitors

When used as an isostere for a carboxylic acid, boronic acids can be used in peptide mimics as a reversible covalent group. In fact, most drug discovery studies depend on boron's ability to react with a serine or cysteine residue in the active site of various protease enzymes. (For a much more comprehensive review of boronic acids as inhibitors of proteases, see Smoum *et al.*[112] For a review on covalent inhibitors, see De Cesco *et al.*[113]) Figure 1.12 outlines the general reaction of three reversibly covalent warheads in a serine protease, as compared to the natural peptide substrate. Unlike the weakly electrophilic nitrile **C**, the aldehyde and boronic acid reactions **B** and **D** result in a tetrahedral intermediate that mimics that of the substrate reaction **A**, which likely explains their higher potencies and longer residence time in the active sites serine proteases.[114]

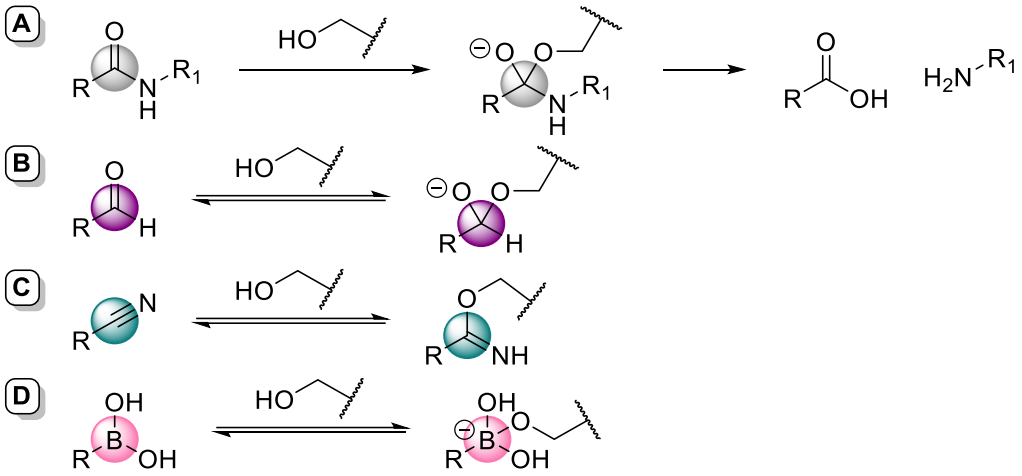

Figure 1.12. Comparison of various reversibly covalent warheads (B-C) to a peptidase-substrate reaction (A), using the example of serine proteases.[114] The serine proton is either transferred to the electrophile or the basic residue of the catalytic triad, depending on the enzyme's mechanism. Figure adapted from Plescia *et al.*[114]

Nevertheless, although aldehydes are ubiquitous in nature, their high reactivities cause oxidative stress in humans and lead to cytotoxic, mutagenic, and carcinogenic effects, among others.[115] Boronic acids, on the other hand, are generally considered safe[5] and are therefore preferred over aldehydes for drug development.

Figure 1.13 shows the mechanism of the reversible covalent bond formation between a catalytic nucleophilic residue and the electrophilic boronic acid.

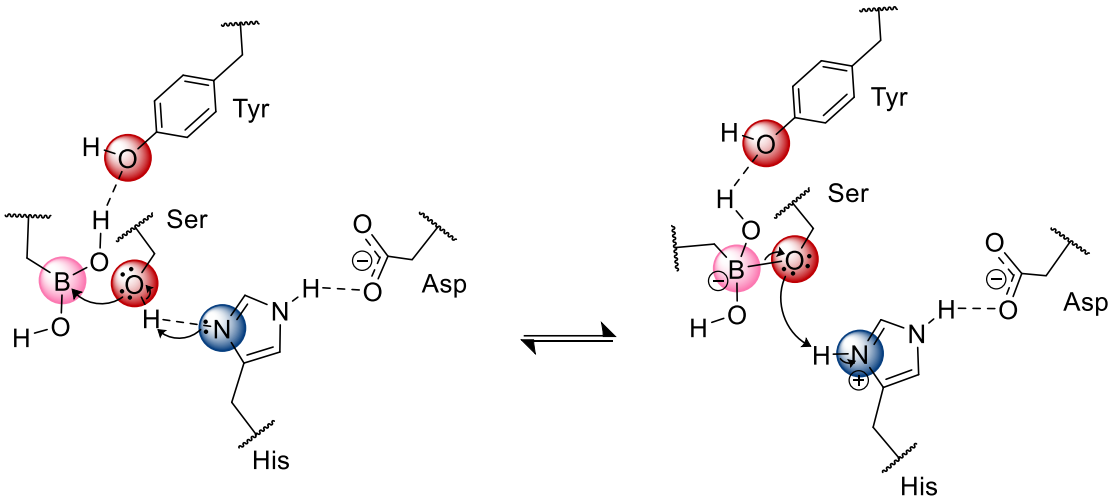

Figure 1.13. Generic reversible mechanism of a catalytic serine residue attacking an electrophilic boronic acid, including stabilization by a tyrosine residue.

One study takes advantage of this transition state mimic in their SAR studies to target β-lactamases. Instead of the irreversibly-binding β-lactam group, the researchers incorporated a reversibly covalent boronic acid (Figure 1.14), achieving submicromolar and nanomolar potencies.[116]

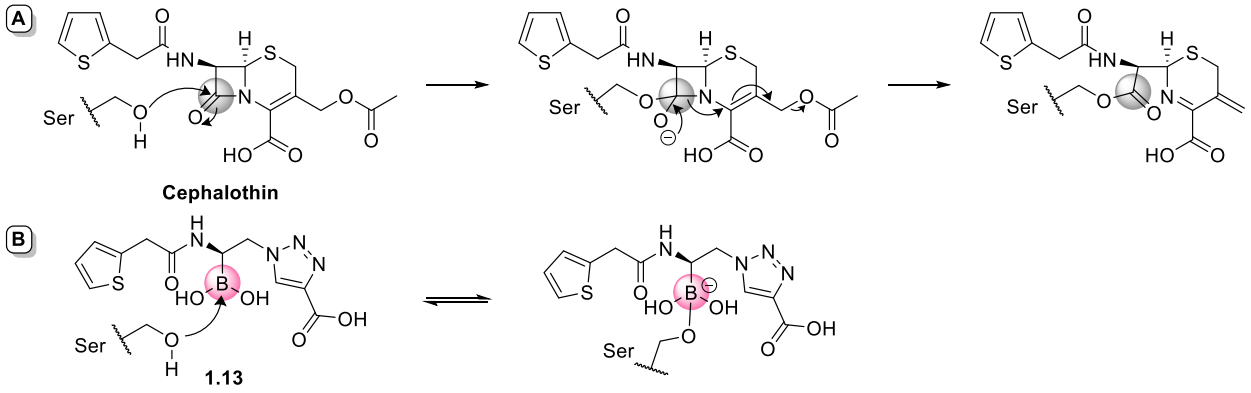

Figure 1.14. Transition-state mimics in the discovery of β-lactamase inhibitors. (A) irreversible reaction of β-lactamase cleaving cephalothin; (B) reversible reaction of boronic acid inhibitor **1.13**. Figure adapted from Rojas *et al.*[116]

Vaborbactam (Figure 1.3), as discussed earlier, was designed to be a serine protease inhibitor of β-lactamases to complex with the catalytic serine residue.[49] Figure 1.15 shows the crystal structure of β-lactamase CTX-M-15 covalently complexed with Vaborbactam.

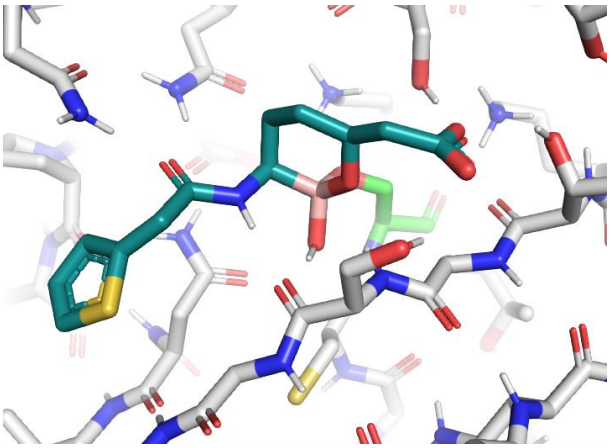

Figure 1.15. Vaborbactam complexed into the active site of β-lactamase CTX-M-15. Vaborbactam in teal; CTX-M-15 in gray; nucleophilic serine highlighted (green) (pdb: 4XUZ).[49]

In another study by Ban *et al.*,[86] mentioned earlier, the researchers designed several boronic acid analogues of EGFR TK inhibitors that originally contained Michael acceptors acting as irreversible inhibitors. A few are featured in Figure 1.16, but boronic ester analogues of each were also synthesized.

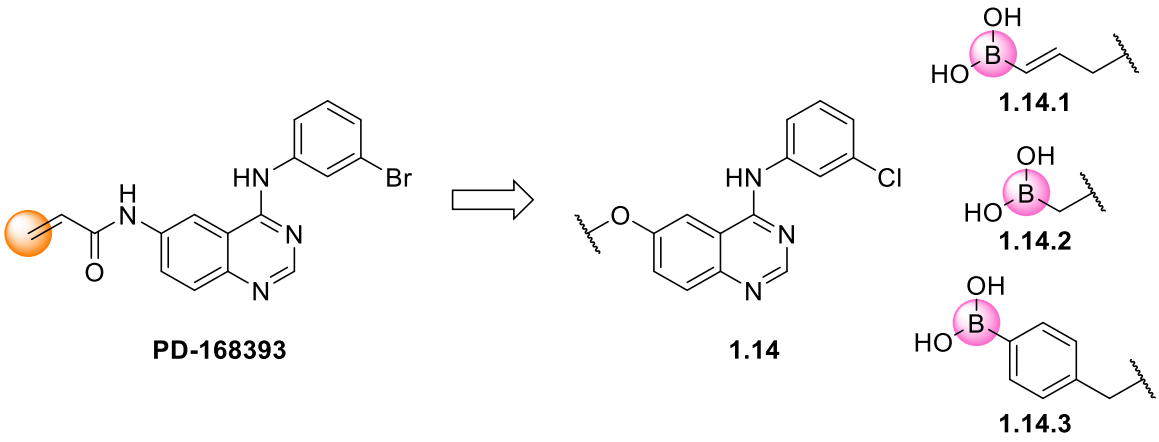

Figure 1.16. Modification of EGFR TK inhibitor to replace the acrylamide Michael acceptor group with the boronic acid moiety.[86]

The intention was to target the active site's cysteine residue without needing an irreversible inhibitor. Upon *in vitro* and *in cellulo* testing, it was found that (1) the boronic acids were slightly more potent than their boronic ester derivatives; (2) the boronic acids **1.14.1** and **1.14.3** exhibited submicromolar activity against EGFR TK without inhibiting other human kinases (**1.14.2**'s linker was deemed too short upon low inhibitory activity); and (3) **1.14.3** continued to inhibit EGFR activity even after five-hour incubation.[86] The boronic acid therefore remained bound to the cysteine residue in a pseudo-irreversible manner without the risks of suicide inhibitors.

In our research, we have found that the replacement of nitriles in our compounds have increased both potency[117] and residence time in the active site of the enzyme prolyl oligopeptidase (POP).[114] Figure 1.17A shows two of our inhibitors differing only in their electrophiles. The boronic ester derivative exhibits nanomolar activity, while the nitrile it replaced exhibited double digit micromolar activity. Figure 1.17B shows two other compounds by Jansen *et al.*[118] exhibiting inhibition against POP and an homologous enzyme fibroblast activation protein α (FAP). Potency increased by an order of magnitude upon replacement of the nitrile with the boronic acid.

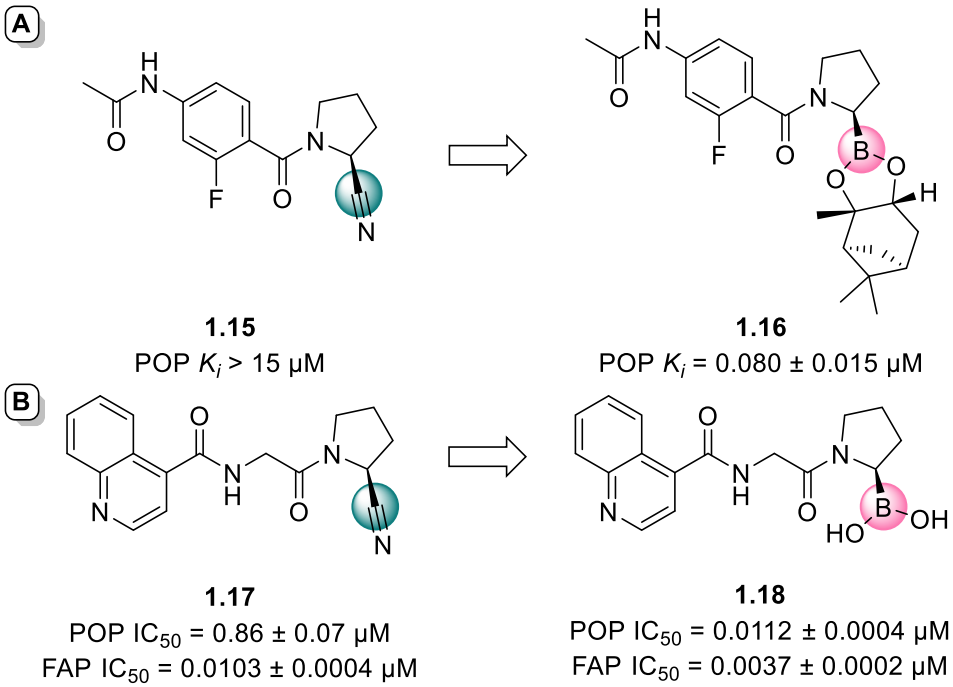

Figure 1.17. Inhibitors showing increased potency by replacing the nitrile electrophile with a boronic ester/acid. (A) Our group's designed POP inhibitors[117] (B) Two POP-FAP inhibitors by Jansen *et al.*[118]

Unfortunately, as discussed in a recent review from our group, current docking programs do not account for reactivity of an electrophile nor for the kinetics of the binding/dissociation (residence time).[113] For example, our own covalent docking program, FITTED,[119-121] gives identical predicted poses for both **1.15** and **1.16** (Figure 1.18), yet the *in vitro* activities of these compounds differ by three orders of magnitude.

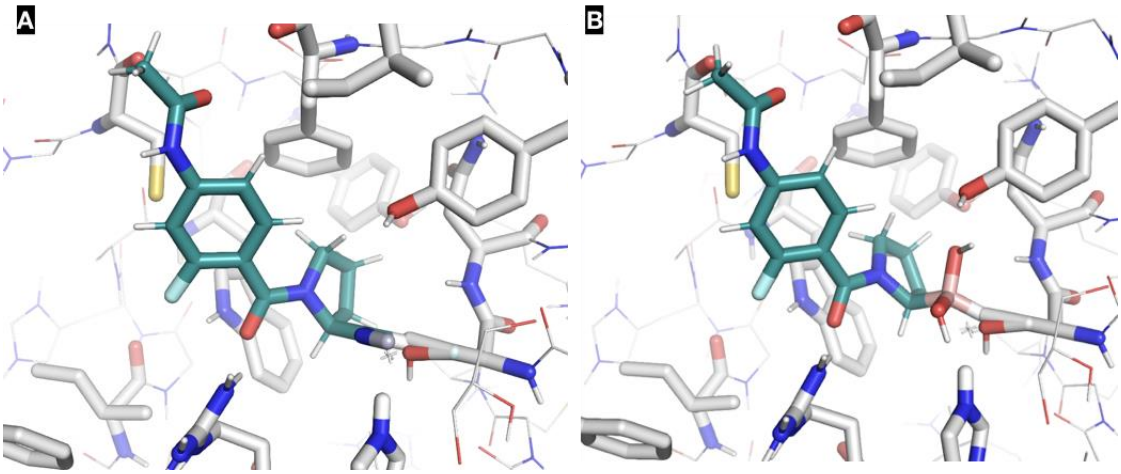

Figure 1.18. Boronic acid and nitrile inhibitors displaying identical docking poses. (A) **1.15** (teal) docked to POP (gray); (B) **1.16** (teal), hydrolyzed, docked to POP (gray). Compounds from Plescia *et al.*[117] and are docked using FITTED.[119-121]

Bortezomib (Figure 1.3), as previously discussed, was designed to be a reversible covalent inhibitor. Several peptide analogs containing various covalent groups, including aldehydes, were probed against the tumour proteasome, though boronic acids were the only functional group that were suitable for further pre-clinical studies. Figure 1.19A shows Bortezomib co-crystallized to the human 20S proteasome complex (pdb code 5LF3).[122]

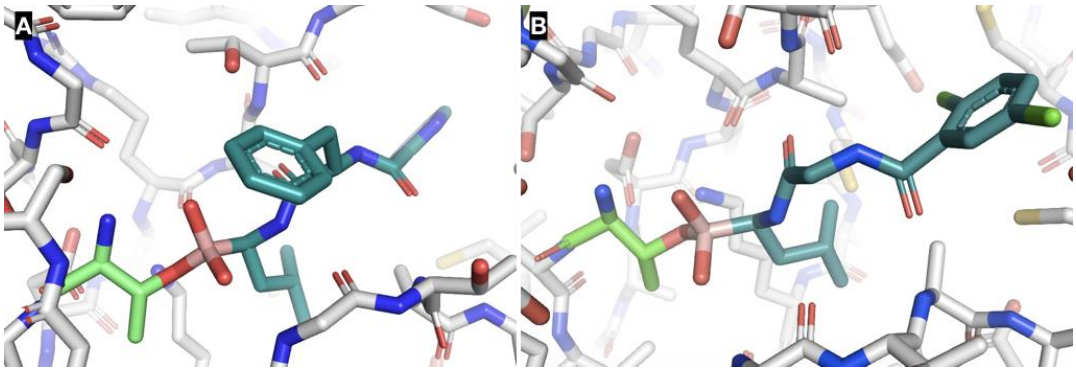

Figure 1.19. Bortezomib and Ixazomib co-crystallized with the human 20S proteasome complex. (A) Bortezomib (teal) (pdb code 5LF3) and (B) Ixazomib (teal) (pdb code 5LF7) complexed to the protein (gray), with the nucleophilic threonine highlighted (green)[122]

Ixazomib (Figure 1.3), whose structure is very similar to Bortezomib, was discovered several years after Bortezomib's approval, as discussed earlier. It's mechanism of action is similar to that of Bortezomib: it inhibits the catalytic threonine in the active site of the 20S proteasome. Figure 1.19B shows Ixazomib crystallized in the active site.

Talabostat, or Val-Boro-Pro (Figure 1.20), is a dipeptidic boronic acid dipeptidyl peptidase (DPP) inhibitor.[123] It was marketed as a multi-target drug that inhibited cancer-implicated homologous serine proteases FAP, DPP4, DPP8, and DPP9. Its mechanism of action involved activation of innate immune response against tumours through its dipeptidyl peptidase inhibition.[124] Talabostat was discovered during a study of DPP family inhibition. Because DPP enzymes cleave terminal dipeptides with Xaa-Pro (i.e. any amino acid adjacent to proline) sequences from their substrates, the researchers tested a number of Xaa-Pro analogs in which the proline was substituted with boroPro, or a boronic acid in place of the carboxylic acid[125] to bind to the catalytic serine.[123]

Ultimately, inefficacy lead to its failure at Phase III.[101] Although not confirmed, it is believed to have failed due to *in vivo* cyclization to its inactive form via the free amine reacting intramolecularly with the boronic acid moiety[126] (Figure 1.20).

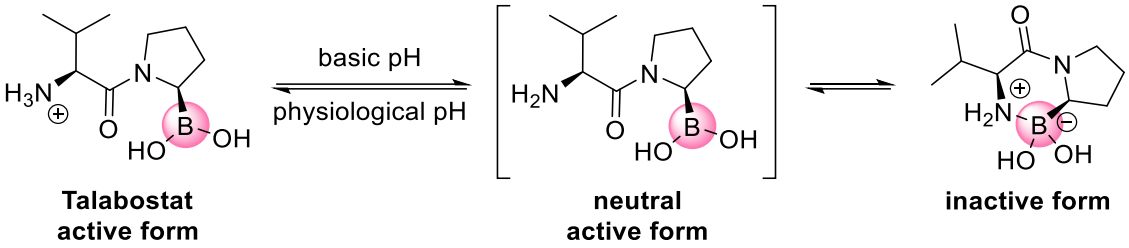

Figure 1.20. Cyclization of Talabostat at physiological and basic pH. Adapted from Kelly *et al.*[126]

It is speculated that Talabostat failure was also due to lack of patient tolerance at doses high enough for anti-tumoral activity, due to partial toxicity.[127] This compound continues to be studied, however, and more recently, it was used to crystallize DPP8[128] and is the first ligand-bound crystal structure of this enzyme available on the Protein Data Bank. Figure 1.21 shows this crystal structure with Talabostat bound to the catalytic serine in the active site, confirming its covalent inhibition.

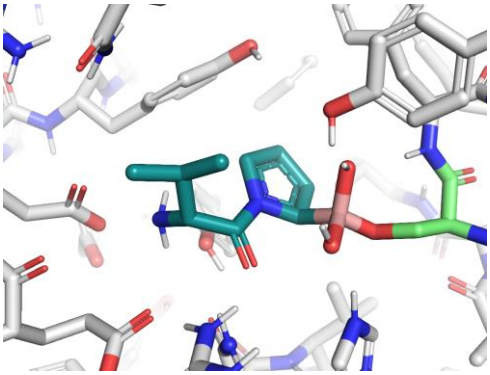

Figure 1.21. Talabostat co-crystallized with DPP 8. Talabostat in teal, DPP8 in gray, with the nucleophilic serine highlighted in green. (pdb: 6HP8)[128]

In general, reversible covalent inhibition is a promising approach in drug discovery, as outlined in a recent review out of our group.[113] Its use in medicinal chemistry endeavours is on the rise, as seen in Figure 1.22.

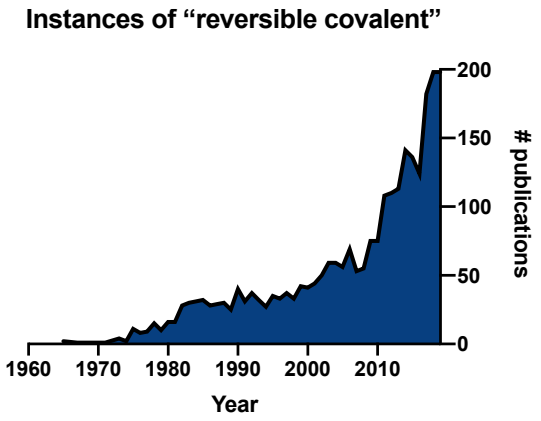

Figure 1.22. PubMed search results of the terms "reversible covalent."

Following the approval of Bortezomib and Ixazomib, discovery and development of reversible covalent boronic acid drugs has become more commonplace and is expected to lead to more approved drugs in coming years.

1.5.3 Boronic acids and esters as prodrugs

Boronic acids have been used as anti-cancer pro-drugs. Several groups have taken advantage of elevated levels of reactive oxygen species (e.g. H_2O_2) in certain cancer cells and resultant drug oxidation to synthesize prodrugs that release the active species upon oxidation. Lin *et al.* studied boronic acid substituted Camptothecin **B1** as a prodrug for neoplastic drug **SN-38**.[129] Taking advantage of elevated levels of reactive oxygen species (ROS) hydrogen peroxide in cancer cells,[130] the group used a boronic acid that would be oxidized to the hydroxylated **SN-38** (Figure 1.23).

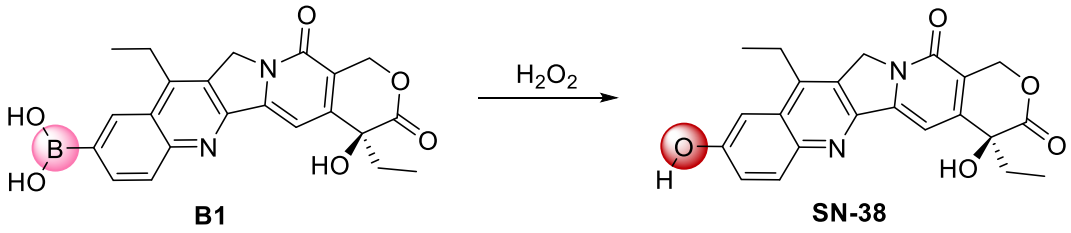

Figure 1.23. Oxidation of pro-drug **B1** to **SN-38** by intracellular reactive oxygen species hydrogen peroxide [129]

Upon adding to cell media, the researchers measured that nearly 60% of **B1** was converted to **SN-38** after 48 hour incubation. Upon testing against several cancer cell lines, they found that even with this structural change, **B1** exhibited comparable or greater cytotoxicity than **SN-38** and was actually a greater inhibitor of their target enzyme, DNA Topoisomerase I.[129] Using a boronic acid analogue, they were able to successfully design a prodrug that is not only active on its own, but releases its chemotherapeutic drug *in vivo*.

Another example utilizes a boronic acid-containing extension to active drug **Belinostat** and involves a more complex prodrug release. In their quest to improve bioavailability and biocompatibility of **Belinostat** , they included boronic acid moieties, giving prodrugs **1.19** and **1.20** (Figure 1.24). Upon *in cellulo* testing of the active compound and both prodrugs, it was found that prodrug **1.19** exhibited activity three to five times less than that of **Belinostat**, but, more surprisingly, that prodrug **1.20** was weaker than prodrug **1.19** by an order of magnitude, and in one case, was 30 times less potent.[131]

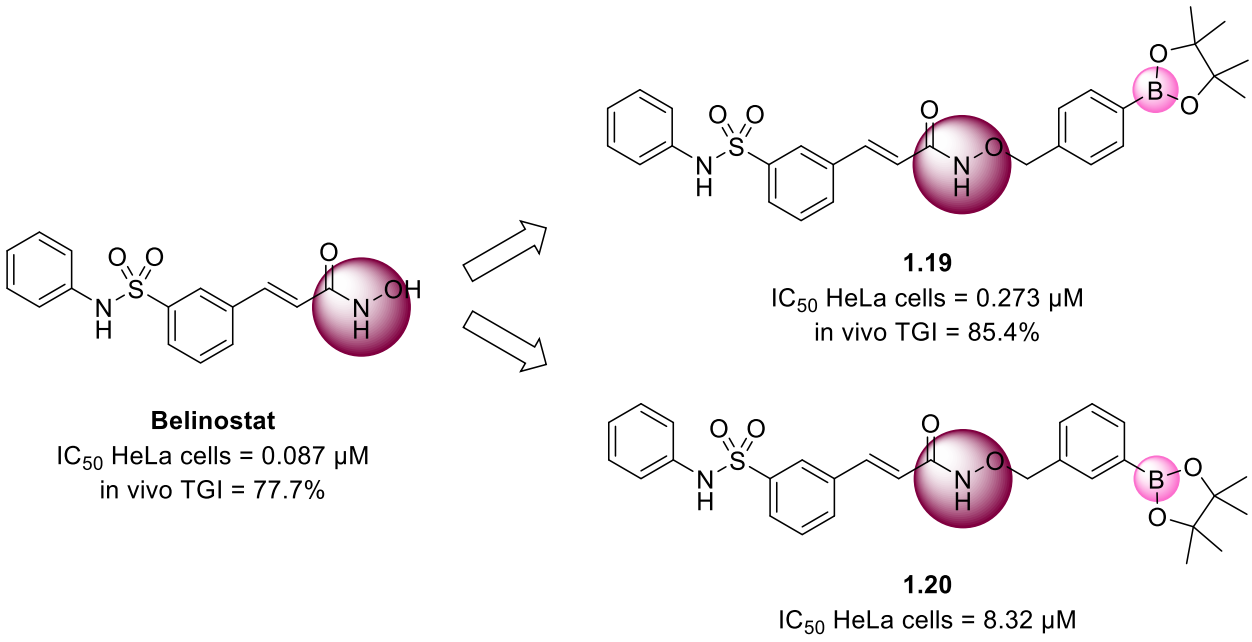

Figure 1.24. Comparison of drug and boronic prodrug activities. TGI = tumour growth inhibition. Figure adapted from Zheng *et al.*[131]

To explain this large difference in activity between the prodrugs **1.19** and **1.20**, the authors proposed a mechanism to determine the means by which the active compound **Belinostat** is released (Figure 1.25). Upon assumed oxidation by H_2O_2 present in the cells, only prodrug **1.19** is

able to undergo a mechanism to release the resultant phenolic moiety and a *para*-quinone; prodrug **1.20** rests as a phenolic intermediate. The inability of prodrug **1.20** to release the active form of the drug likely explains its decreased activity *in cellulo*. When **Belinostat** and prodrug **1.19** were tested in mice, however, the *in vivo* efficacy of tumour growth inhibition (TGI) of **1.19** was significantly greater, contradicting *in cellulo* data. Tissue analysis found that **1.19** released **Belinostat** , but amounts of boronic acid **1.21** remained, potentially contributing to slower release and therefore higher efficacy.[131]

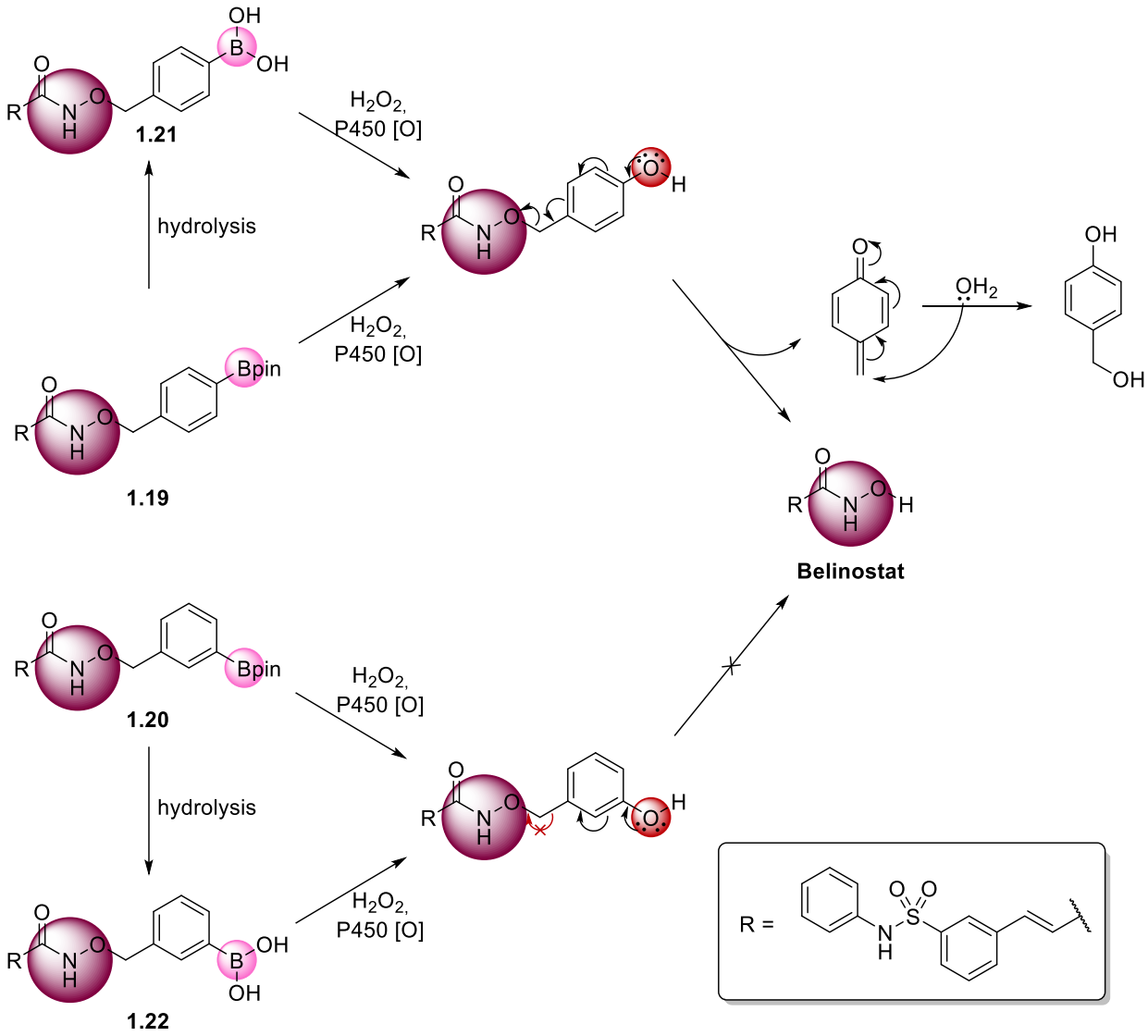

Figure 1.25. Proposed mechanism of oxidation of boronic ester prodrug and subsequent release of drug. Figure from Zheng *et al.*[131] pin refers to the pinacol protecting group

Our group has used boronic esters as prodrugs for their corresponding boronic acids. The basic buffer used in our assays hydrolyzed the (+)-pinanediol-protected boronic ester **1.23** (Figure 1.26A) to the respective free boronic acid within 20 minutes based on mass spectroscopy analysis (Figure 1.26B).[114, 117] This study's results allow for a much more diverse scope of potential drugs in future medicinal chemistry endeavours: harsh conditions normally used to cleave boronic esters to free boronic acids (strong acid, BBr_3/BCl_3, fluoride, etc.) normally affect other sensitive functional groups, such as methoxy esters or Boc- or Cbz-protected amines. Using a buffer-sensitive boronic ester allows for inclusion of many more functional groups that contribute to potency of potential drugs.

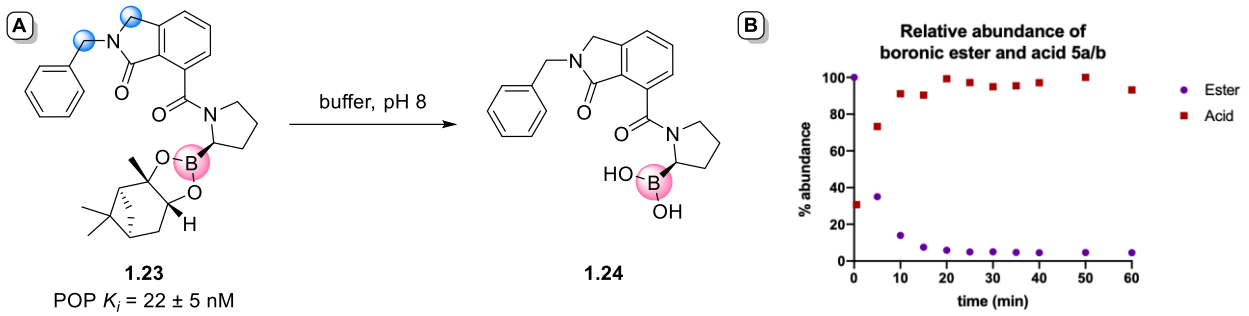

Figure 1.26. Hydrolysis of a boronic ester prodrug (A) Buffer-mediated hydrolysis of compound **1.23** to the active species **1.24**; BCl_3-sensitive carbons highlighted in blue; (B) Mass spectroscopy study of the boronic ester hydrolysis. Figure adapted from Plescia *et al.*[114]

In fact, in our own synthetic efforts, the harsh conditions attempted to hydrolyze **1.23** resulted in (1) premature precipitation of the starting material in strongly acidic media during attempted transesterification of the (+)-pinanediol auxiliary and (2) mixtures of debenzylated products upon utilizing BCl_3 to remove the (+)-pinanediol protecting group. Testing the boronic ester directly allowed us to obtain a very potent compound without having to sacrifice the study of a boron-based drug.[114]

Ninlaro®, or Ixazomib, is formulated as a prodrug so as to ensure oral bioavailability. The boronic acid is complexed with a citrate molecule to form a citrate ester, which is cleaved under aqueous physiological conditions to give the active form Ixazomib (Figure 1.27).[34]

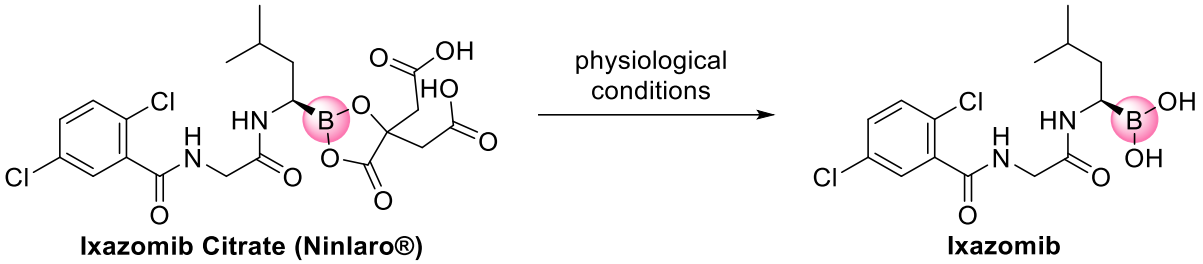

Figure 1.27. Hydrolysis of prodrug Ixazomib Citrate to Ixazomib

From these examples, it is clear that not only can a boronic acid or ester be a prodrug to release the desired chemical species *in vivo*, but a boronic ester can also be utilized to release the desired boronic acid drug. For a more comprehensive review of boronic acids and esters as prodrugs, see Cadahía *et al.*[132]

1.5.4 Using computational methods

Certain discoveries of bioactive boronic acid compounds originated with predictive computational methods. In one case, the Shoichet and Taunton research groups designed a virtual screening protocol to discover boronic acid inhibitors of AmpC β-lactamase. The researchers screened a virtual library of 23,000 commercially available boronic acids. They then selected several ligands that scored in the top two percent and tested them both *in vitro* and against several cell lines. Several hits were obtained, and one in particular (**7**, Figure 1.28A, B) exhibited *in vitro* potency of 10 nM and was potent against cells when administered with Cefotaxime.[133]

A different approach to the discovery of AmpC β-lactamase inhibitors was taken by Eidam *et al.* and used fragment-based *in silico* hit optimization.[94] Following previous studies of the Shoichet lab which used molecular docking to determine the best fragments for the enzyme active site,[134] Eidam *et al.* superposed docked fragments with their hit molecule to determine the most promising side chain modifications. Through several rounds, they were able to modify their hit to improve the *in vitro* activity by two orders of magnitude into sub-nanomolar potency (Figure 1.28C, D) and achieve potency *in cellulo* and *in vivo* upon testing in combination with Ceftazidime.[94]

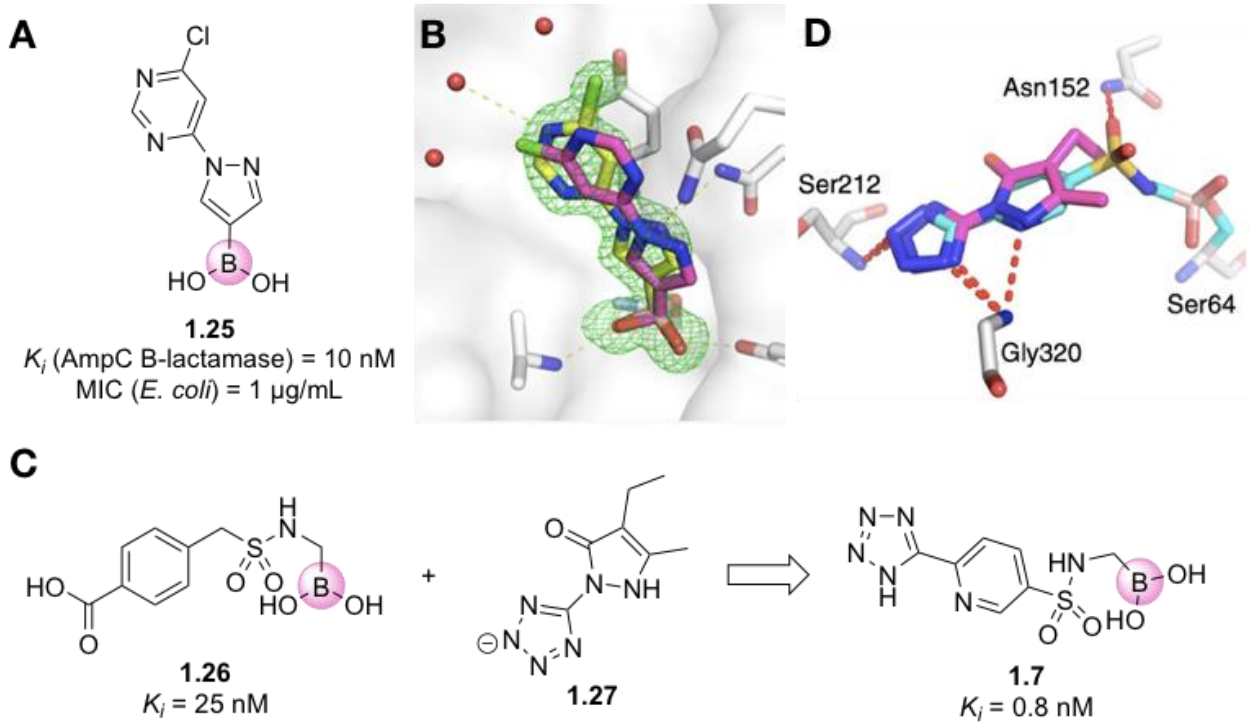

Figure 1.28. Computational methods for boronic acid drug discovery. (A) boronic acid hit **1.25** discovered by virtual screening; (B) crystal structure of hit **1.25** (yellow, green electron map) superposed over its predicted binding pose (magenta) to AmpC β-lactamase; (A and B from London *et al.*[133]) (C) hit **1.26** for optimization with one fragment **1.27** used in the *in silico* design, giving resultant hit **1.7**;[94] (D) docking prediction of fragment **1.27** superposed to docking prediction of **1.17** (D from Eidam *et al.*[94])

Although many research groups do not use computational methods to design their target compounds, countless studies involve using molecular docking to rationalize differences in inhibitor activity to improve their compounds for future work.

1.6 Boronic acids in delivery systems

Apart from inclusion of boronic acids in bioactive compounds, boronic acids' ability to bind to diols (e.g. sugars) on the extracellular domain has been exploited in studies aiming to improve cellular uptake of liposomes and macromolecules; boronic and borinic acids have been conjugated to more complex molecular systems for the purpose of macromolecule delivery, such as increased uptake of gene-delivery complexes,[135] transport of proteins,[136] and cellular uptake of liposomes.[137]

In one example, Yadav *et al.* observed uptake issues of genetic material containing terminal polyethylenimines (PEIs). Reaction of these PEIs with 4-bromobutylboronic acid yielded tertiary amines with terminal boronic acids (Scheme 1.1). These modifications increased uptake of the plasmids without compromising structural integrity of the carrier nor cell viability,[135] as the boronic acids' high pKa allows for uncharged interaction with the membrane.

Scheme 1.1. Reaction of polyethylenimines with 4-bromobutylboronic acid, from Yadav *et al.*[135]

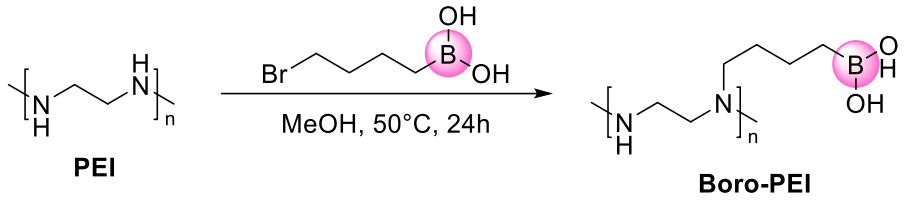

Another research group aimed to facilitate cell entry of liposomes by incorporating boronic acids on the surface. They began with the design of an aminoglycerolipid conjugated to an aromatic boronic acid (Figure 1.29, A and B). Through a series of fluorescent experiments using rhodamine-labeled phosphatidylethanolamine (Rd-PE), they determined that liposomes with 10% boronic acid-conjugated lipid content entered the cells, while control liposomes did not.[137]

One group has incorporated benzoxaboroles into delivery vehicles for the transport of proteins over mammalian bilayers (Figure 1.29, C and D). They designed a delivery vehicle with benzoxaborole conjugated to *o*-hydroxydihydrocinnamic acid derivative trimethyl lock (TML), which would in turn be conjugated to green fluorescent protein (GFP), a fluorescent protein unable to traverse the lipid bilayer. A series of experiments and control experiments led to the conclusions that (1) benzoxaborole was aiding in the uptake of the GFP; (2) the uptake was proceeding through an endosomal pathway; and (3) the labeling was stable but ultimately reversible, leading to the release of the delivered target protein in the cells.[136]

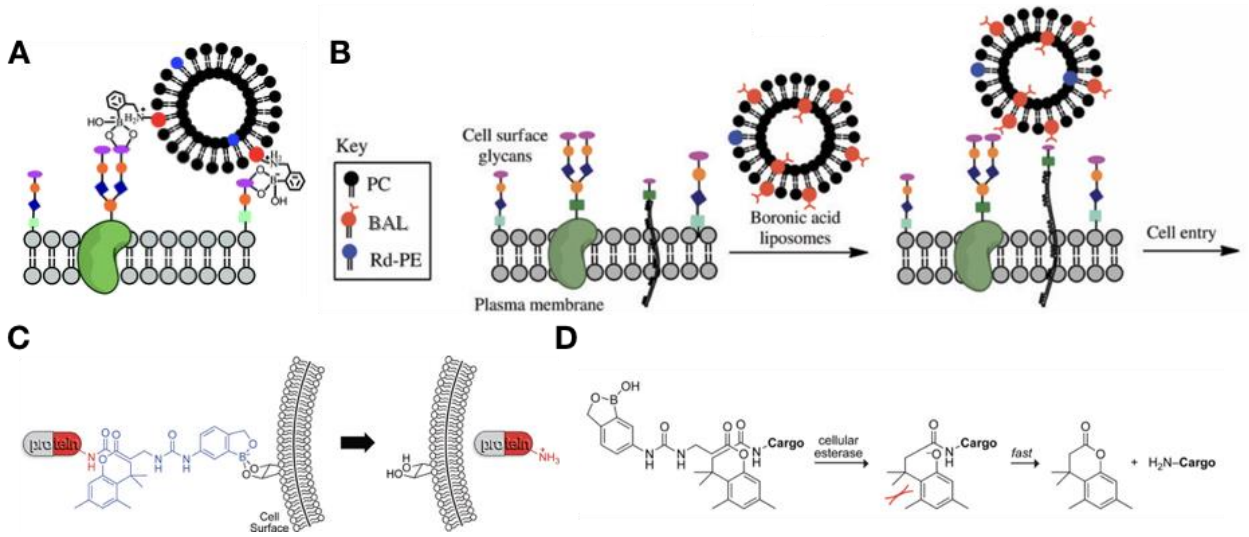

Figure 1.29. Boronic acids in delivery systems. (A) Close-up schematic diagram of a liposome's terminal boronic acids interacting with carbohydrates on the extracellular domain of the cellular membrane lipid bilayer; (B) Schematic diagram depicting uptake of boronic acid-coated liposomes; PC = phosphatidylcholine, BAL = boronic acid-coated liposomes, Rd-PE = rhodamine-labeled phosphatidylethanolamine; (C) (D); Figures A and B from Zhang *et al.*;[137] Figures C and D from Andersen *et al.*[136]

Although there exist many other applications of boron in delivery systems, such as advanced nanomaterials and usage in radiation therapy, they are beyond the scope of this review.

1.7 Synthesis of boronic acid drugs

Access to all of these drugs and potential drugs would not be possible without efficient synthetic methodologies. To obtain the final boronic acids, prodrugs are usually synthesized first, as boronic acids are difficult to purify and to carry through multiple steps. Boronic acid synthesis varies depending on surrounding functional groups, whether it is to be aromatic or aliphatic, and if applicable, the desired stereochemistry of the final product. Furthermore, in the synthesis of boropeptides, such as Delanzomib, the process synthesis is not so different from the discovery synthesis.[138] Similar methodologies allow for more efficient development.

1.7.1 Synthesis of α-aminoboronates

One of the more popular α-aminoboronic ester derivatives is the proline-derived analog. As discussed earlier, medicinal chemistry endeavours targeting certain families of peptidases have relied heavily on the use of this chiral boronic analogue of proline (Figure 1.30, **1.29**).

The increased use of α-amino boronic acids in the discovery of inhibitors of this family of serine proteases has led to the increased commercial availability of prepared and enantiopure (+)-pinanediol-protected α-amino boronic ester analogs of many amino acids, such as the very commonly used isoleucine, used in the synthesis of Bortezomib[139] and Ixazomib, and proline, used in the synthesis of Talabostat.[140]

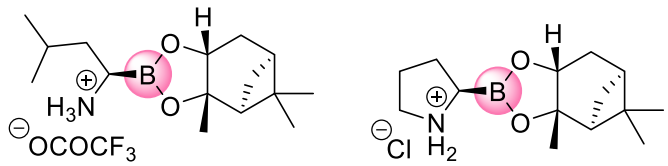

1.28
iso-Leucine boronic ester

1.29
Proline boronic ester

Figure 1.30. Commercially available enantiopure boronic (+)-pinanediol esters.[140]

The Ellman group at Yale has developed syntheses of highly enantiopure α-amino boronic esters using their own Ellman chiral auxiliary to synthesize diastereopure (*R*)- or (*S*)-*tert*-butyl-sulfinylimines.[141-142]

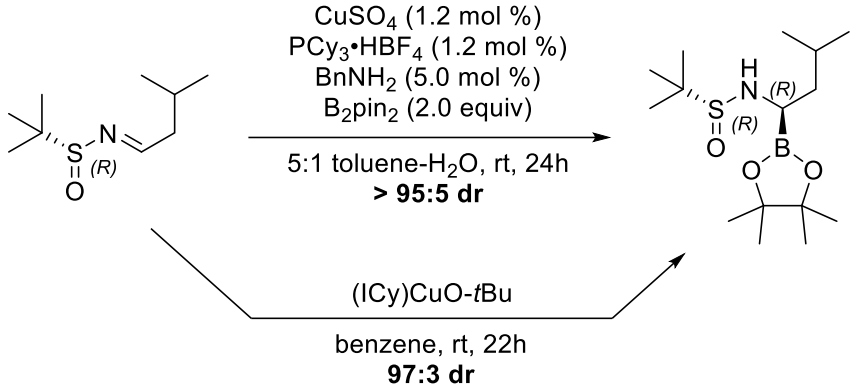

Figure 1.31. Ellman syntheses of diastereopure sulfinylimines[141-142]

In fact, the Ellman group's research sparked interest in synthetic development of chiral **1.29** for the synthesis of boro-peptide inhibitors (Scheme 1.2), as performed by Chen *et al.*[143]

Scheme 1.2. Synthesis of enantiopure **1.29** via the Ellman borylation.[a]

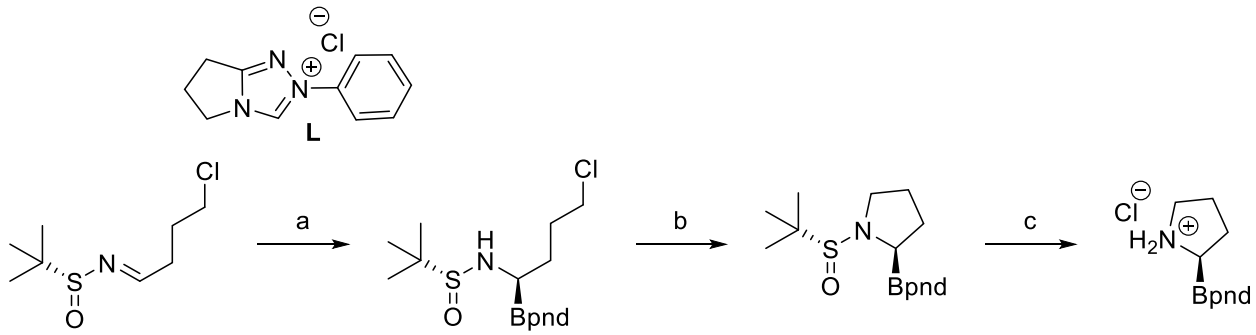

[a]a) CuI (10 mol%), Cs_2CO_3 (10 mol%), **L** (10 mol%), B_2pnd_2* (1 eq), benzene, rt, 48h; b) NaO*t*Bu, DMF, rt, 6h; c) HCl, dioxane-MeOH, rt, 30 mins. *pnd refers to (+)-pinanediol protecting group[143]

In our own chemistry, we have found that the α-amino boronic pinacol esters are very difficult to purify and consequently difficult to carry through multiple steps, as they react with SiO_2 in flash chromatography columns and therefore require used of H_2O-deactivated SiO_2, as reported by the Ellman group.[141] However, application of a transesterification with (+)- or (-)-pinanediol as reported by the Matteson group[144] (Figure 1.32) gives diastereopure boronic esters that are more easily purified on a silica gel column.

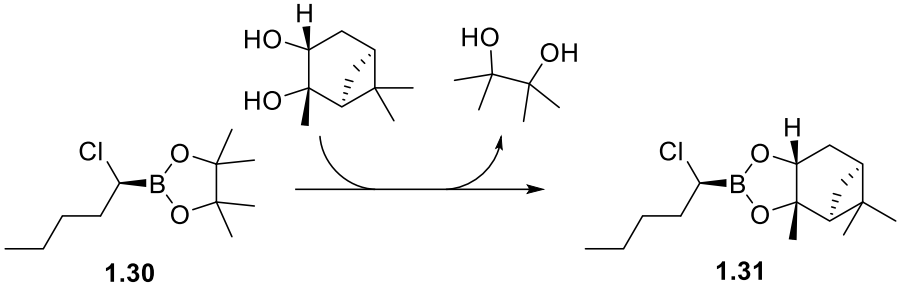

Figure 1.32. Matteson conversion of boronic pinacol ester to (+)-pinanediol ester via transesterification

1.7.2 Aromatic boronic esters and acids

The synthesis of aryl boronic esters and acids is well-established, such as in synthesis of starting material for the Suzuki cross-coupling reaction, one of the most widely used coupling reactions in medicinal chemistry. The Miyaura reaction allows for the facile synthesis of these boronic esters (Figure 1.33).[145] Furthermore, purification is much simpler than that of the α-aminoboronic ester derivatives, as they can be purified by flash chromatography on normal phase silica.

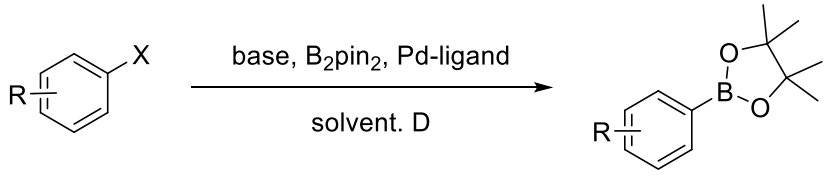

Figure 1.33. The Miyaura reaction[145]

Many aromatic boronic acids are available commercially (e.g. from Sigma-Aldrich,[146] BoroChem,[147] or Combi-Blocks[140]) either as building blocks or as known bioactive compounds for testing.

With this chemistry, the discovery of drugs containing this aromatic boronic ester group can be facilitated with *in silico* combinatorial chemistry studies; aryl halides can be virtually converted to aryl boronic acids to generate large libraries for virtual screening.[133]

1.7.3 Other aliphatic boronic acids

Already well known and studied is the addition of bis(pinacolato)diboron, or B_2pin_2 to α,β-unsaturated compounds (Figure 1.34). Usually, reactions involve a metal catalyst for activation of the boron and a base for assisting in heterolytic cleavage of the B–B bond. For a comprehensive review of various conditions and associated mechanisms of addition, see Lillo *et al.*[148]

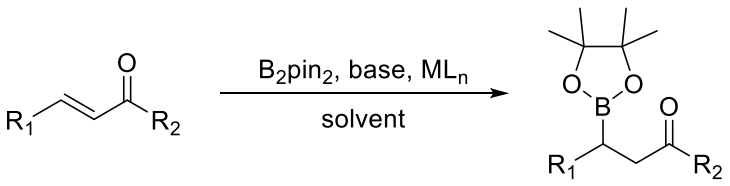

Figure 1.34. Addition of boron to α,β-unsaturated compounds

The Baran lab recently discovered a nickel-catalyzed decarboxylative borylation method applicable to a variety of aliphatic carboxylic acids. Their method involves simple preparation of metal- and ligand-containing suspensions, quick reaction times, and high yields. Although not completely stereo-selective, diastereoselectivity can be improved with lower reaction temperatures and steric control.[149] Their research sparked several other decarboxylative-borylation procedures, including a modified, transition metal-free procedure using blue light as a radical initiator,[150] an iridium- and visible light catalyzed procedure,[151] and another Baran procedure copper-catalyzed reaction.[152] A summary of these decarboxylative borylations can be found in Figure 1.35.

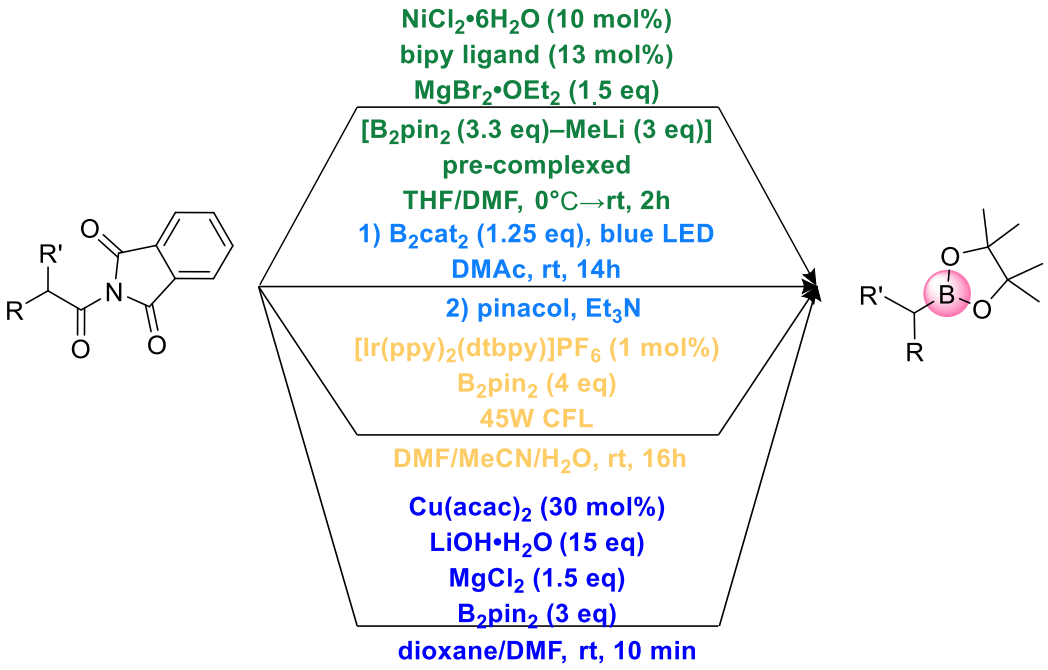

Figure 1.35. Decarboxylative borylations[149-152]

Baran's nickel chloride method was applied to a small library of various aliphatic carboxylic acids, including several natural products and known bioactive compounds. In fact, decarboxylative borylation was conducted to obtain known compounds **1.32** and **1.33**, bioactive against human neutrophil elastase (HNE) implicated in cystic fibrosis (CF) (Figure 1.36). This new synthesis, including a deprotection step, allowed for efficient preparation and gave a single diastereomer. Furthermore, the boronic acid analog of the original trifluoromethyl ketone hit exhibited a potency increase of three orders of magnitude.[149]

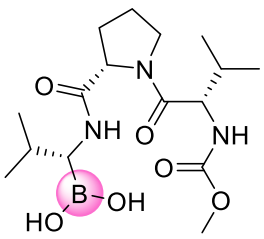

1.32
NHE IC_{50} = 0.27 ± 0.02 nM
CF sputum IC_{50} = 0.51 ± 0.04 nM

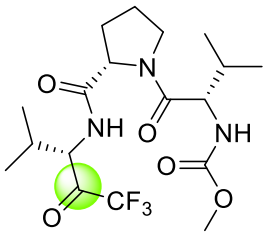

1.33
NHE IC_{50} = 135 ± 12 nM
CF sputum IC_{50} = 358 ± 55 nM

Figure 1.36. Compounds active against human neutrophil elastase (HNE) implicated in cystic fibrosis (CF); Compound **1.32** synthesized with Baran's decarboxylative deborylation.[149]

While we have highlighted here only a few of the more common synthetic procedures for boronic acid incorporation, many others have been developed over the years. For a more comprehensive review of synthesis of bioactive boronic acids, see Yang *et al.*[153]

1.7.4 Deprotection of boronic ester pro-drugs

Boronic ester prodrugs are often deprotected before initial *in vitro* testing to their bioactive boronic acid analogues. Various methods exist for this deprotection step. The choice of conditions depends on stability of the starting compound and compatibility of the comprising functional groups.

Some research groups opt to perform simultaneous cleavage of *tert*-Butyloxycarbonyl (Boc) or carboxybenzyl (Cbz) protecting groups and boronic ester using BCl_3 or BBr_3 (Figure 1.37).[154-155] Unfortunately, these highly reactive Lewis acids affect certain other functional groups, such as benzyl ethers/amines or methoxy groups. In the synthesis of Bortezomib, the final boronic ester is deprotected via a transesterification with isobutylboronic acid.[156] Again, with reaction conditions that require strong acid, certain functional groups are not compatible. Other methods for deprotection include a telescoped method reacting the boronic ester first with potassium hydrogen difluoride (KHF_2) to give the boron trifluoride potassium salt, followed by hydrolysis in the presence of TMSCl or LiOH to give the free boronic acid,[157] or oxidative cleavage via sodium periodate.[158-159] A summary of these methods is provided in Figure 1.37. Furthermore, boronic acids at the β-position of an electron withdrawing group were discovered to be susceptible to deprotection by forming an ionic bicyclic structure with diethanolamine, followed by acidic

hydrolysis (Figure 1.37).[160] Interestingly, this cage-like bicyclic intermediate was used in the process chemistry synthesis of a Delanzomib pro-drug for clinical trials, as it improved purity and stability.[138]

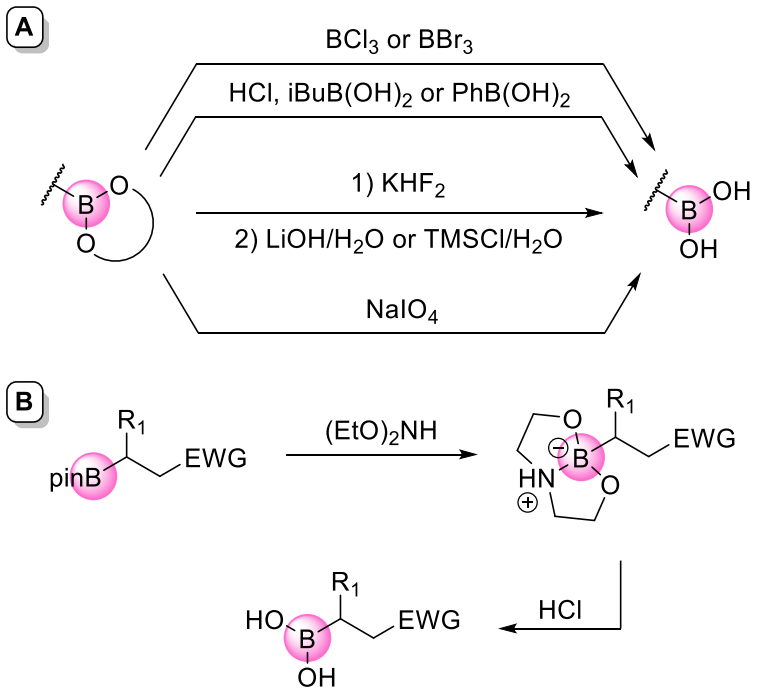

Figure 1.37. Summary of boronic ester deprotection methods via (A) various cleaving reagents[154-159] (B) conversion of β boronic esters to boronic acids via diethanolamine cages.[160] pin refers to the pinacol protecting group.

In our own studies, we have found that the deprotection of our boronic esters was not necessary, as our basic buffer mediated the hydrolysis of (+)-pinanediol boronic esters. Figure 1.38 displays two compounds and mass spectroscopy studies monitoring the relative abundance of the ester and acid species. Even for two compounds with different expected intrinsic reactivities (di-*ortho*-fluoro vs. unsubstituted), the hydrolysis rate was very similar; both esters were cleaved within twenty minutes, i.e. during the sample preparation step before the enzyme was even added.

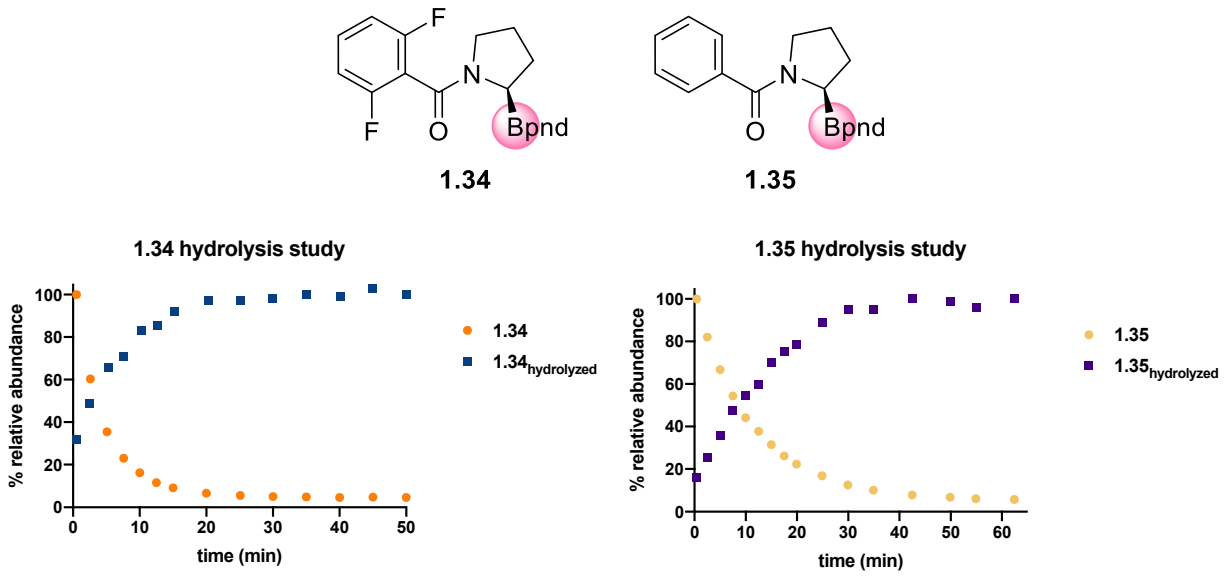

Figure 1.38. Hydrolysis studies of boronic esters **1.34** and **1.35** in POP assay buffer. The graphs display relative abundance of each ionic species at intervals over 50-63 minutes. Figure from Plescia *et al.*[117] pnd refers to the (+)-pinanediol protecting group.

In the case of the protecting group not being labile enough to hydrolyze in buffer, they would need to be deprotected under the discussed conditions. Purification of the resultant boronic acids is unfortunately not so straight-forward, as they are not suited for normal phase silica gel column chromatography, and require reverse-phase conditions, often by semi-preparative or preparative HPLC.[118, 154]

1.8 Conclusion and Perspectives

The abundance of boron in natural products and its general safety as a mineral make it an attractive synthetic target in drug discovery endeavours. Following the approval of Bortezomib, there have been many medicinal chemistry endeavours aimed at discovering boronic acid drugs.

As we have seen in this review, several approaches have been taken in the discovery of boron-containing drugs. Because of its reversible electrophilicity, it is commonly used as a reversible covalent group to incorporate into peptides to inhibit proteases, whether that was the original intention or the result of medicinal chemistry hit optimizations. We have also seen that boronic acids or esters, stable and uncharged at physiological pH, have been incorporated as bioisosteres of ionized groups, such as carboxylic esters or phosphate groups, for either activity or pharmacokinetic improvement or for structural purposes. Boron-containing groups have additionally been used as prodrugs, either boronic esters for their corresponding acids, such as FDA-approved Ixazomib, or boronic acids and esters for their ability to be oxidized *in vivo* to their active analogue by tumour environments abundant in reactive oxygen species. Finally, we have described boron-based drugs designed by computational methods, including virtual screening and *de novo* design.

Along with drug design came the associated synthetic efforts aimed at synthesizing boronic acids. Since the approval of Bortezomib, much focus has been on the design of diastereopure aliphatic boronic esters/acids, especially α-amino boronic esters/acids. In turn, many groups have taken advantage of these discoveries to incorporate boronic acids into their drug discovery programs.

Lastly, we saw several examples of boronic acids facilitating drug and macromolecule delivery, either through incorporation into lipid bilayer for entry via liposomes or through reversible conjugation to a protein.

These explorations into boron-based drug discovery will hopefully shed light on the benefits of boron incorporation and encourage medicinal and pharmaceutical chemists to consider boronic acids and esters as possibilities and solutions in their drug discovery programs.

1.9 Thesis Outline

The themes around and knowledge of boronic acids presented in this introduction will be further explored in terms of discovery of inhibitors targeting prolyl oligopeptidase (POP), a serine protease implicated in neurodegenerative diseases and cancer, and homologous enzyme fibroblast activation protein α (FAP), implicated in tumour growth and metastases.

In line with the discovery of boronic ester inhibitors, several different approaches were taken to reach the final hit compounds. Chapter 2 is a study of various covalent groups used to target both POP and FAP. Chapter 3 outlines a docking-guided optimization of a known POP hit, which was re-designed with a boronic ester warhead to increase activity. Chapter 4 involves the design of constrained peptidomimetic boron-containing electrophilic analogues of proline substrates and the development of the complex syntheses to reach these final compounds. Chapter 5, although not focused on boron, elaborates on the complex syntheses discovered during the synthesis of these peptidomimetic bicycles. Chapter 6 outlines a virtual screening of several covalent groups, the virtual hits of which were virtually optimized to bicyclic borinic esters.

To conclude, Chapter 7 outlines future perspectives of the boron-derived compounds discovered with these various approaches and their potential applications across the various endeavours pursued in our research group.

1.10 References

(1) Dembitsky, V. M.; Smoum, R.; Al-Quntar, A. A.; Ali, H. A.; Pergament, I.; Srebnik, M., Natural occurrence of boron-containing compounds in plants, algae and microorganisms. *Plant Sci* **2002,** *163* (5), 931-942.

(2) Camacho-Cristobal, J. J.; Rexach, J.; Gonzalez-Fontes, A., Boron in plants: deficiency and toxicity. *J Integr Plant Biol* **2008,** *50* (10), 1247-55.

(3) Miljkovic, D.; Miljkovic, N.; McCarty, M. F., Up-regulatory impact of boron on vitamin D function -- does it reflect inhibition of 24-hydroxylase? *Med Hypotheses* **2004,** *63* (6), 1054-6.

(4) Dessordi, R.; Spirlandeli, A. L.; Zamarioli, A.; Volpon, J. B.; Navarro, A. M., Boron supplementation improves bone health of non-obese diabetic mice. *J Trace Elem Med Biol* **2017,** *39*, 169-175.

(5) Hall, D. G., *Boronic Acids: Preparation and Applications in Organic Synthesis and Medicine*. Wiley-VGH: Weinheim, Germany, 2005; p 565.

(6) Zielonka, J.; Sikora, A.; Hardy, M.; Joseph, J.; Dranka, B. P.; Kalyanaraman, B., Boronate probes as diagnostic tools for real time monitoring of peroxynitrite and hydroperoxides. *Chem Res Toxicol* **2012,** *25* (9), 1793-9.

(7) Sanjoh, M.; Miyahara, Y.; Kataoka, K.; Matsumoto, A., Phenylboronic Acids-based Diagnostic and Therapeutic Applications. *Anal Sci* **2014,** *30*, 111-117.

(8) Barth, R. F.; Mi, P.; Yang, W., Boron delivery agents for neutron capture therapy of cancer. *Cancer Commun (Lond)* **2018,** *38* (1), 35.

(9) Barth, R. F.; Zhang, Z.; Liu, T., A realistic appraisal of boron neutron capture therapy as a cancer treatment modality. *Cancer Commun (Lond)* **2018,** *38* (1), 36.

(10) Antonio, J. P. M.; Russo, R.; Carvalho, C. P.; Cal, P.; Gois, P. M. P., Boronic acids as building blocks for the construction of therapeutically useful bioconjugates. *Chem Soc Rev* **2019,** *48* (13), 3513-3536.

(11) Brooks, W. L.; Sumerlin, B. S., Synthesis and Applications of Boronic Acid-Containing Polymers: From Materials to Medicine. *Chem Rev* **2016,** *116* (3), 1375-97.

(12) Hall, D. G., Boronic acid catalysis. *Chem Soc Rev* **2019,** *48* (13), 3475-3496.

(13) Chen, T. S. S.; Chang, C.-J.; Floss, H. G., On the Biosynthesis of Boromycin. *J Org Chem* **1981,** *46*, 2661-2665.

(14) Kohno, J.; Kawahata, T.; Otake, T.; Morimoto, M.; Mori, H.; Ueba, N.; Nishio, M.; Kinumaki, A.; Komatsubara, S.; Kawashima, K., Boromycin, an anti-HIV antibiotic. *Biosci Biotechnol Biochem* **1996,** *60* (6), 1036-7.

(15) Moreira, W.; Aziz, D. B.; Dick, T., Boromycin Kills Mycobacterial Persisters without Detectable Resistance. *Front Microbiol* **2016,** *7*, 199.

(16) Nakamura, H.; Iitaka, Y., Structure of aplasmomycin. *J Antibiot* **1977,** *30* (9), 714-719.

(17) Shimizu, Y.; Ogasawara, Y.; Matsumoto, A.; Dairi, T., Aplasmomycin and boromycin are specific inhibitors of the futalosine pathway. *J Antibiot* **2018,** *71* (11), 968-970.

(18) Dembitsky, V. M.; Quntar, A. A. A. A.; Srebnik, M., Natural and Synthetic Small Boron-Containing Molecules as Potential Inhibitors of Bacterial and Fungal Quorum Sensing. *Chem Rev* **2011,** *111*, 209–237.

(19) Koshiba, T.; Kobayashi, M.; Matoh, T., Boron deficiency. *Plant Signal Behav* **2014,** *4* (6), 557-558.

(20) Organization, W. H., *Trace elements in human nutrition and health*. Geneva, 1996.

(21) Gorustovich, A. A.; Steimetz, T.; Nielsen, F. H.; Guglielmotti, M. B., A histomorphometric study of alveolar bone modelling and remodelling in mice fed a boron-deficient diet. *Arch Oral Biol* **2008,** *53* (7), 677-82.

(22) Blech, M. F.; Martin, C.; Borrelly, J.; Hartemann, P., Treatment of deep wounds with loss of tissue. Value of a 3 percent boric acid solution. [Article in French]. *Presse Med* **1990,** *19* (22), 1050-1052.

(23) Nzietchueng, R. M.; Dousset, B.; Franck, P.; Benderdour, M.; Nabet, P.; Hes, K., Mechanisms implicated in the effects of boron on wound healing. *J Trace Elem Med Biol* **2002,** *16*, 239-244.

(24) Kurtoglu, V.; Kurtoglu, F.; Coskun, B., Effects of boron supplementation of adequate and inadequate vitamin D3-containing diet on performance and serum biochemical characters of broiler chickens. *Res Vet Sci* **2001,** *71* (3), 183-7.

(25) Uluisik, I.; Karakaya, H. C.; Koc, A., The importance of boron in biological systems. *J Trace Elem Med Biol* **2018,** *45*, 156-162.

(26) Kane, R. C.; Farrell, A. T.; Sridhara, R.; Pazdur, R., United States Food and Drug Administration approval summary: bortezomib for the treatment of progressive multiple myeloma after one prior therapy. *Clin Cancer Res* **2006,** *12* (10), 2955-60.

(27) VELCADE* for multiple myeloma receives front-line approval in Canada. https://johnsonandjohnson.gcs-web.com/news-releases/news-release-details/velcade-multiple-myeloma-receives-front-line-approval-canada (accessed 1 Dec 2019).

(28) Adams, J., The development of proteasome inhibitors as anticancer drugs. *Cancer Cell* **2003,** *5*, 417-421.

(29) Arkwright, R.; Pham, T. M.; Zonder, J. A.; Dou, Q. P., The preclinical discovery and development of bortezomib for the treatment of mantle cell lymphoma. *Expert Opin Drug Discov* **2017,** *12* (2), 225-235.

(30) Chen, D.; Frezza, M.; Schmitt, J.; Kanwar, J.; Dou, Q. P., Bortezomib as the First Proteasome Inhibitor Anticancer Drug: Current Status and Future Perspectives. *Curr Cancer Drug Targets* **2011,** *11*, 239-253.

(31) Groll, M.; Berkers, C. R.; Ploegh, H. L.; Ovaa, H., Crystal structure of the boronic acid-based proteasome inhibitor bortezomib in complex with the yeast 20S proteasome. *Structure* **2006,** *14* (3), 451-6.

(32) Shirley, M., Ixazomib: First Global Approval. *Drugs* **2016,** *76* (3), 405-11.

(33) Health Canada Approves Ninlaro (ixazomib) for Use in Relapsed/Refractory Multiple Myeloma. https://www.myeloma.org/article/health-canada-approves-ninlaro-ixazomib-use-relapsedrefractory-multiple-myeloma (accessed 2 Dec 2019).

(34) Muz, B.; Ghazarian, R. N.; Ou, M.; Luderer, M. J.; Kusdono, H. D.; Azab, A. K., Spotlight on ixazomib: potential in the treatment of multiple myeloma. *Drug Des Devel Ther* **2016,** *10*, 217-26.

(35) Ludwig, H.; Poenisch, W.; Knop, S.; Egle, A.; Schreder, M.; Lechner, D.; Hajek, R.; Gunsilius, E.; Krenosz, K. J.; Petzer, A.; Weisel, K.; Niederwieser, D.; Einsele, H.; Willenbacher, W.; Melchardt, T.; Greil, R.; Zojer, N., Ixazomib-Thalidomide-Dexamethasone for induction therapy followed by Ixazomib maintenance treatment in patients with relapsed/refractory multiple myeloma. *Br J Cancer* **2019,** *121* (9), 751-757.

(36) Markham, A., Tavaborole: first global approval. *Drugs* **2014,** *74* (13), 1555-8.

(37) Jinna, S.; Finch, J., Spotlight on tavaborole for the treatment of onychomycosis. *Drug Des Devel Ther* **2015,** *9*, 6185-90.

(38) Baker, S. J.; Zhang, Y.-K.; Akama, T.; Lau, A.; Zhou, H.; Hernandez, V.; Mao, W.; Alley, M. R. K.; Sanders, V.; Plattner, J. J., Discovery of a New Boron-Containing Antifungal Agent, 5-Fluoro-1,3-dihydro-1-hydroxy-2,1benzoxaborole (AN2690), for the Potential Treatment of Onychomycosis. *J Med Chem* **2006,** *49* (15), 4447-4450.

(39) Benkovic, S. J.; Baker, S. J.; Alley, M. R. K.; Woo, Y.-H.; Zhang, Y.-K.; Akama, T.; Mao, W.; Baboval, J.; Rajagopalan, P. T. R.; Wall, M.; Kahng, L. S.; Tavassoli, A.; Shapiro, L., Identification of Borinic Esters as Inhibitors of Bacterial Cell Growth and Bacterial Methyltransferases, CcrM and MenH. *J Med Chem* **2005,** *48*, 7468-7476.

(40) Markinson, B.; Ghannoum, M.; Winter, T.; Rycerz, A.; Rock, F.; Gupta, A. K., Examining the Benefits of the Boron-Based Mechanism of Action and Physicochemical Properties of Tavaborole in the Treatment of Onychomycosis. *J Am Podiatr Med Assoc* **2018,** *108* (1), 12-19.

(41) Fischer, A., FDA approves Eucrisa for eczema. FDA.gov, 2016.

(42) Eucrisa™ (Crisaborole) Now Available in Canada. https://www.pfizer.ca/eucrisa™-crisaborole-now-available-canada (accessed 2 Dec 2019).

(43) Akama, T.; Baker, S. J.; Zhang, Y. K.; Hernandez, V.; Zhou, H.; Sanders, V.; Freund, Y.; Kimura, R.; Maples, K. R.; Plattner, J. J., Discovery and structure-activity study of a novel benzoxaborole anti-inflammatory agent (AN2728) for the potential topical treatment of psoriasis and atopic dermatitis. *Bioorg Med Chem Lett* **2009,** *19* (8), 2129-32.

(44) FDA approves new antibacterial drug. https://www.fda.gov/news-events/press-announcements/fda-approves-new-antibacterial-drug (accessed 2 Dec 2019).

(45) Meds Entry Watch. New Medicines Approved in 2017. http://www.pmprb-cepmb.gc.ca/view.asp?ccid=1430&lang=en (accessed 2 Dec 2019).

(46) Livermore, D. M.; Mushtaq, S., Activity of biapenem (RPX2003) combined with the boronate beta-lactamase inhibitor RPX7009 against carbapenem-resistant Enterobacteriaceae. *J Antimicrob Chemother* **2013,** *68* (8), 1825-31.

(47) Lee, Y.; Kim, J.; Trinh, S., Meropenem–Vaborbactam (VabomereTM): Another Option for Carbapenem-Resistant Enterobacteriaceae. *P T* **2019,** *44* (3).

(48) Beesley, T.; Gascoyne, N.; Knott-Hunziker, V.; Petursson, S.; Waley, S. G.; Jaurint, B.; Grundstromt, T., The inhibition of class C β-lactamases by boronic acids. *Biochem J* **1983,** *209*, 229-233.

(49) Hecker, S. J.; Reddy, K. R.; Totrov, M.; Hirst, G. C.; Lomovskaya, O.; Griffith, D. C.; King, P.; Tsivkovski, R.; Sun, D.; Sabet, M.; Tarazi, Z.; Clifton, M. C.; Atkins, K.; Raymond, A.; Potts, K. T.; Abendroth, J.; Boyer, S. H.; Loutit, J. S.; Morgan, E. E.; Durso, S.; Dudley, M. N., Discovery of a Cyclic Boronic Acid beta-Lactamase Inhibitor (RPX7009) with Utility vs Class A Serine Carbapenemases. *J Med Chem* **2015,** *58* (9), 3682-92.

(50) Schenk, R.; Nix, D., TCT-180 Impact of the novel DPP-IV-inhibitor Dutogliptin in combination with G-CSF on survival rates and cardiac remodelling after acute myocardial infarction. *J Am Coll Cardiol* **2016,** *68* (18).

(51) Nix, D.; Jilma, B.; Schenk, R., Evaluation of the pharmacokinetics and pharmacodynamics of subcutaneously administered dutogliptin for daily injection with granulocyte colony stimulating factor (G-CSF) for AMI. *Eur Heart J* **2018,** *39* (1), 49.

(52) Recardio, Study of Dutogliptin in Combination With Filgrastim in Post-Myocardial Infarction. https://ClinicalTrials.gov/show/NCT03486080: 2018.

(53) Baker, C. H.; Welburn, S. C., The Long Wait for a New Drug for Human African Trypanosomiasis. *Trends Parasitol* **2018,** *34* (10), 818-827.

(54) Wall, R. J.; Rico, E.; Lukac, I.; Zuccotto, F.; Elg, S.; Gilbert, I. H.; Freund, Y.; Alley, M. R. K.; Field, M. C.; Wyllie, S.; Horn, D., Clinical and veterinary trypanocidal benzoxaboroles target CPSF3. *Proc Natl Acad Sci U S A* **2018,** *115* (38), 9616-9621.

(55) Prospective Study on Efficacy and Safety of SCYX-7158 in Patients Infected by Human African Trypanosomiasis Due to T.b. Gambiense. https://ClinicalTrials.gov/show/NCT03087955.

(56) Tenero, D.; Derimanov, G.; Carlton, A.; Tonkyn, J.; Davies, M.; Cozens, S.; Gresham, S.; Gaudion, A.; Puri, A.; Muliaditan, M.; Rullas-Trincado, J.; Mendoza-Losana, A.; Skingsley, A.; Barros-Aguirre, D., First-Time-in-Human Study and Prediction of Early Bactericidal Activity for GSK3036656, a Potent Leucyl-tRNA Synthetase Inhibitor for Tuberculosis Treatment. *Antimicrob Agents Chemother* **2019,** *63* (8).

(57) Li, X.; Hernandez, V.; Rock, F. L.; Choi, W.; Mak, Y. S. L.; Mohan, M.; Mao, W.; Zhou, Y.; Easom, E. E.; Plattner, J. J.; Zou, W.; Perez-Herran, E.; Giordano, I.; Mendoza-Losana,

A.; Alemparte, C.; Rullas, J.; Angulo-Barturen, I.; Crouch, S.; Ortega, F.; Barros, D.; Alley, M. R. K., Discovery of a Potent and Specific M. tuberculosis Leucyl-tRNA Synthetase Inhibitor: (S)-3-(Aminomethyl)-4-chloro-7-(2-hydroxyethoxy)benzo[c][1,2]oxaborol-1(3H)-ol (GSK656). *J Med Chem* **2017,** *60* (19), 8011-8026.

(58) Monteferrante, C. G.; Jirgensons, A.; Varik, V.; Hauryliuk, V.; Goessens, W. H.; Hays, J. P., Evaluation of the characteristics of leucyl-tRNA synthetase (LeuRS) inhibitor AN3365 in combination with different antibiotic classes. *Eur J Clin Microbiol Infect Dis* **2016,** *35* (11), 1857-1864.

(59) An Early Bactericidal Activity, Safety and Tolerability of GSK3036656 in Subjects With Drug-sensitive Pulmonary Tuberculosis. https://ClinicalTrials.gov/show/NCT03557281.

(60) Zane, L.; Gogoleva, T.; Heerinckx, F.; Jermano, J., AN2728 and AN2898 Ointments Demonstrate Safety and Efficacy in a Bilateral Study of Atopic Dermatitis. *J Dermatol Sci* **2013,** *69* (2).

(61) Yang, H.; Wang, J.; Zhang, X.; Zhang, Y.; Qin, Z. L.; Wang, H.; Luo, X. Y., Application of Topical Phosphodiesterase 4 Inhibitors in Mild to Moderate Atopic Dermatitis: A Systematic Review and Meta-analysis. *JAMA Dermatol* **2019,** *155* (5), 585-593.

(62) EU Clinical Trials Register: Greece. EudraCT Number: 2015-004702-42. A Multi-Center, Parallel Group, Open-Label, Phase 2 Study to Evaluate the Efficacy and Safety of a Single Subcutaneous Injection of RG-101 Combined with Oral GSK2878175 Taken Once Daily for 6, 9, or 12 Weeks in Treatment Naïve, Genotype 1 and 3, Chronic Hepatitis C Patients. 2016.

(63) Chong, P. Y.; Shotwell, J. B.; Miller, J.; Price, D. J.; Maynard, A.; Voitenleitner, C.; Mathis, A.; Williams, S.; Pouliot, J. J.; Creech, K.; Wang, F.; Fang, J.; Zhang, H.; Tai, V. W.; Turner, E.; Kahler, K. M.; Crosby, R.; Peat, A. J., Design of N-Benzoxaborole Benzofuran GSK8175-Optimization of Human Pharmacokinetics Inspired by Metabolites of a Failed Clinical HCV Inhibitor. *J Med Chem* **2019,** *62* (7), 3254-3267.

(64) BASIC (Boric Acid, Alternate Solution for Intravaginal Colonization) Study. https://ClinicalTrials.gov/show/NCT00799214.

(65) Use of Boric Acid in Combination With Probiotics for the Treatment of Vaginal Infections. https://ClinicalTrials.gov/show/NCT02860845.

(66) Zhang, P.; Ma, S., Recent development of leucyl-tRNA synthetase inhibitors as antimicrobial agents. *MedChemComm* **2019,** *10* (8), 1329-1341.

(67) Study of Talabostat + Docetaxel Versus Docetaxel in Stage IIIB/IV Non-Small Cell Lung Cancer (NSCLC) After Failure of Platinum-Based Chemotherapy. https://ClinicalTrials.gov/show/NCT00243204.

(68) Hotho, D. M.; de Bruijne, J.; O'Farrell, A. M.; Boyea, T.; Li, J.; Bracken, M.; Li, X.; Campbell, D.; Guler, H. P.; Weegink, C. J.; Schinkel, J.; Molenkamp, R.; van de Wetering de Rooij, J.; van Vliet, A.; Janssen, H. L.; de Knegt, R. J.; Reesink, H. W., Pharmacokinetics and antiviral activity of PHX1766, a novel HCV protease inhibitor, using an accelerated Phase I study design. *Antivir Ther* **2012,** *17* (2), 365-75.

(69) Vogl, D. T.; Martin, T. G.; Vij, R.; Hari, P.; Mikhael, J. R.; Siegel, D.; Wu, K. L.; Delforge, M.; Gasparetto, C., Phase I/II study of the novel proteasome inhibitor delanzomib (CEP-18770) for relapsed and refractory multiple myeloma. *Leuk Lymphoma* **2017,** *58* (8), 1872-1879.

(70) Dietary Supplement Health and Education Act of 1994, Public Law 103-417. Food and Drug Administration: 1994.

(71) Pucker, A. D.; Ng, S. M.; Nichols, J. J., Over the counter (OTC) artificial tear drops for dry eye syndrome. *Cochrane Database Syst Rev* **2016,** *2*, CD009729-CD009729.

(72) Angotti, L. B.; Lambert, L. C.; Soper, D. E., Vaginitis: making sense of over-the-counter treatment options. *Infect Dis Obstet Gynecol* **2007,** *2007*, 97424.

(73) Mogosanu, G. D.; Bita, A.; Bejenaru, L. E.; Bejenaru, C.; Croitoru, O.; Rau, G.; Rogoveanu, O. C.; Florescu, D. N.; Neamtu, J.; Scorei, I. D.; Scorei, R. I., Calcium Fructoborate for Bone and Cardiovascular Health. *Biol Trace Elem Res* **2016,** *172* (2), 277-81.

(74) Scorei, R.; Mitrut, P.; Petrisor, I.; Scorei, I., A double-blind, placebo-controlled pilot study to evaluate the effect of calcium fructoborate on systemic inflammation and dyslipidemia markers for middle-aged people with primary osteoarthritis. *Biol Trace Elem Res* **2011,** *144* (1-3), 253-63.

(75) Rogoveanu, O. C.; Mogosanu, G. D.; Bejenaru, C.; Bejenaru, L. E.; Croitoru, O.; Neamtu, J.; Pietrzkowski, Z.; Reyes-Izquierdo, T.; Bita, A.; Scorei, I. D.; Scorei, R. I., Effects of Calcium Fructoborate on Levels of C-Reactive Protein, Total Cholesterol, Low-Density Lipoprotein, Triglycerides, IL-1beta, IL-6, and MCP-1: a Double-blind, Placebo-controlled Clinical Study. *Biol Trace Elem Res* **2015,** *163* (1-2), 124-31.

(76) Han, L. Q.; Yuan, X.; Wu, X. Y.; Li, R. D.; Xu, B.; Cheng, Q.; Liu, Z. M.; Zhou, T. Y.; An, H. Y.; Wang, X.; Cheng, T. M.; Ge, Z. M.; Cui, J. R.; Li, R. T., Urea-containing peptide boronic acids as potent proteasome inhibitors. *Eur J Med Chem* **2017,** *125*, 925-939.

(77) Lei, M.; Feng, H.; Bai, E.; Zhou, H.; Wang, J.; Qin, Y.; Zhang, H.; Wang, X.; Liu, Z.; Hai, O.; Liu, J.; Zhu, Y., Discovery of a novel dipeptidyl boronic acid proteasome inhibitor for the treatment of multiple myeloma and triple-negative breast cancer. *Org Biomol Chem* **2019,** *17* (3), 683-691.

(78) Okondo, M. C.; Johnson, D. C.; Sridharan, R.; Go, E. B.; Chui, A. J.; Wang, M. S.; Poplawski, S. E.; Wu, W.; Liu, Y.; Lai, J. H.; Sanford, D. G.; Arciprete, M. O.; Golub, T. R.; Bachovchin, W. W.; Bachovchin, D. A., DPP8 and DPP9 inhibition induces pro-caspase-1-dependent monocyte and macrophage pyroptosis. *Nat Chem Biol* **2017,** *13* (1), 46-53.

(79) Okondo, M. C.; Rao, S. D.; Taabazuing, C. Y.; Chui, A. J.; Poplawski, S. E.; Johnson, D. C.; Bachovchin, D. A., Inhibition of Dpp8/9 Activates the Nlrp1b Inflammasome. *Cell Chem Biol* **2018,** *25* (3), 262-267 e5.

(80) Ji, X.; Xia, C.; Wang, J.; Su, M.; Zhang, L.; Dong, T.; Li, Z.; Wan, X.; Li, J.; Li, J.; Zhao, L.; Gao, Z.; Jiang, H.; Liu, H., Design, synthesis and biological evaluation of 4-fluoropyrrolidine-2-carbonitrile and octahydrocyclopenta[b]pyrrole-2-carbonitrile derivatives as dipeptidyl peptidase IV inhibitors. *Eur J Med Chem* **2014,** *86*, 242-56.

(81) Connolly, B. A.; Sanford, D. G.; Chiluwal, A. K.; Healey, S. E.; Peters, D. E.; Dimare, M. T.; Wu, W.; Liu, Y.; Maw, H.; Zhou, Y.; Li, Y.; Jin, Z.; Sudmeier, J. L.; Lai, J. H.; Bachovchin, W. W., Dipeptide Boronic Acid Inhibitors of Dipeptidyl Peptidase IV: Determinants of Potency and in Vivo Efficacy and Safety. *J Med Chem* **2008,** *51* (19), 6005-6013.

(82) Gourgari, E.; Wilhelm, E. E.; Hassanzadeh, H.; Aroda, V. R.; Shoulson, I., A comprehensive review of the FDA-approved labels of diabetes drugs: Indications, safety, and emerging cardiovascular safety data. *J Diabetes Complicat* **2017,** *31* (12), 1719-1727.

(83) Bishnoi, R.; Hong, Y. R.; Shah, C.; Ali, A.; Skelton, W. P. t.; Huo, J.; Dang, N. H.; Dang, L. H., Dipeptidyl peptidase 4 inhibitors as novel agents in improving survival in diabetic patients with colorectal cancer and lung cancer: A Surveillance Epidemiology and Endpoint Research Medicare study. *Cancer Med* **2019,** *8* (8), 3918-3927.

(84) Overbeek, J. A.; Bakker, M.; van der Heijden, A.; van Herk-Sukel, M. P. P.; Herings, R. M. C.; Nijpels, G., Risk of dipeptidyl peptidase-4 (DPP-4) inhibitors on site-specific cancer: A systematic review and meta-analysis. *Diabetes Metab Res Rev* **2018,** *34* (5), e3004.

(85) Kong, Y.; Grembecka, J.; Edler, M. C.; Hamel, E.; Mooberry, S. L.; Sabat, M.; Rieger, J.; Brown, M. L., Structure-based discovery of a boronic acid bioisostere of combretastatin A-4. *Chem Biol* **2005,** *12* (9), 1007-14.

(86) Ban, H. S.; Usui, T.; Nabeyama, W.; Morita, H.; Fukuzawa, K.; Nakamura, H., Discovery of boron-conjugated 4-anilinoquinazoline as a prolonged inhibitor of EGFR tyrosine kinase. *Org Biomol Chem* **2009,** *7* (21), 4415-27.

(87) Hepatitis B and C Treatments. https://www.fda.gov/patients/hepatitis-b-c/hepatitis-b-and-c-treatments (accessed 29 November 2019).

(88) Li, X.; Zhang, Y. K.; Liu, Y.; Ding, C. Z.; Li, Q.; Zhou, Y.; Plattner, J. J.; Baker, S. J.; Qian, X.; Fan, D.; Liao, L.; Ni, Z. J.; White, G. V.; Mordaunt, J. E.; Lazarides, L. X.; Slater, M. J.; Jarvest, R. L.; Thommes, P.; Ellis, M.; Edge, C. M.; Hubbard, J. A.; Somers, D.; Rowland, P.; Nassau, P.; McDowell, B.; Skarzynski, T. J.; Kazmierski, W. M.; Grimes, R. M.; Wright, L. L.; Smith, G. K.; Zou, W.; Wright, J.; Pennicott, L. E., Synthesis and evaluation of novel alpha-amino cyclic boronates as inhibitors of HCV NS3 protease. *Bioorg Med Chem Lett* **2010,** *20* (12), 3550-6.

(89) Li, X.; Zhang, Y. K.; Liu, Y.; Ding, C. Z.; Zhou, Y.; Li, Q.; Plattner, J. J.; Baker, S. J.; Zhang, S.; Kazmierski, W. M.; Wright, L. L.; Smith, G. K.; Grimes, R. M.; Crosby, R. M.; Creech, K. L.; Carballo, L. H.; Slater, M. J.; Jarvest, R. L.; Thommes, P.; Hubbard, J. A.; Convery, M. A.; Nassau, P. M.; McDowell, W.; Skarzynski, T. J.; Qian, X.; Fan, D.; Liao, L.; Ni, Z. J.; Pennicott, L. E.; Zou, W.; Wright, J., Novel macrocyclic HCV NS3 protease inhibitors derived from alpha-amino cyclic boronates. *Bioorg Med Chem Lett* **2010,** *20* (19), 5695-700.

(90) Nitsche, C.; Zhang, L.; Weigel, L. F.; Schilz, J.; Graf, D.; Bartenschlager, R.; Hilgenfeld, R.; Klein, C. D., Peptide-Boronic Acid Inhibitors of Flaviviral Proteases: Medicinal Chemistry and Structural Biology. *J Med Chem* **2017,** *60* (1), 511-516.

(91) Windsor, I. W.; Palte, M. J.; Lukesh, J. C., 3rd; Gold, B.; Forest, K. T.; Raines, R. T., Sub-picomolar Inhibition of HIV-1 Protease with a Boronic Acid. *J Am Chem Soc* **2018,** *140* (43), 14015-14018.

(92) Ghosh, A. K.; Xia, Z.; Kovela, S.; Robinson, W. L.; Johnson, M. E.; Kneller, D. W.; Wang, Y. F.; Aoki, M.; Takamatsu, Y.; Weber, I. T.; Mitsuya, H., Potent HIV-1 Protease Inhibitors Containing Carboxylic and Boronic Acids: Effect on Enzyme Inhibition and Antiviral Activity and Protein-Ligand X-ray Structural Studies. *ChemMedChem* **2019,** *14* (21), 1863-1872.

(93) Zhou, J.; Stapleton, P.; Haider, S.; Healy, J., Boronic acid inhibitors of the class A beta-lactamase KPC-2. *Bioorg Med Chem* **2018,** *26* (11), 2921-2927.

(94) Eidam, O.; Romagnoli, C.; Dalmasso, G.; Barelier, S.; Caselli, E.; Bonnet, R.; Shoichet, B. K.; Prati, F., Fragment-guided design of subnanomolar beta-lactamase inhibitors active in vivo. *Proc Natl Acad Sci U S A* **2012,** *109* (43), 17448-53.

(95) Lu, C. J.; Hu, J.; Wang, Z.; Xie, S.; Pan, T.; Huang, L.; Li, X., Discovery of boron-containing compounds as Abeta aggregation inhibitors and antioxidants for the treatment of Alzheimer's disease. *MedChemComm* **2018,** *9* (11), 1862-1870.

(96) Kraljic, K.; Jelic, D.; Ziher, D.; Cvrtila, A.; Dragojevic, S.; Sinkovic, V.; Mesic, M., Benzoxaboroles-Novel Autotaxin Inhibitors. *Molecules* **2019,** *24* (19).

(97) Albers, H. M.; van Meeteren, L. A.; Egan, D. A.; van Tilburg, E. W.; Moolenaar, W. H.; Ovaa, H., Discovery and optimization of boronic acid based inhibitors of autotaxin. *J Med Chem* **2010,** *53* (13), 4958-67.

(98) Albers, H. M.; Dong, A.; van Meeteren, L. A.; Egan, D. A.; Sunkara, M.; van Tilburg, E. W.; Schuurman, K.; van Tellingen, O.; Morris, A. J.; Smyth, S. S.; Moolenaar, W. H.; Ovaa, H., Boronic acid-based inhibitor of autotaxin reveals rapid turnover of LPA in the circulation. *Proc Natl Acad Sci U S A* **2010,** *107* (16), 7257-62.

(99) Winum, J. Y.; Innocenti, A.; Scozzafava, A.; Montero, J. L.; Supuran, C. T., Carbonic anhydrase inhibitors. Inhibition of the human cytosolic isoforms I and II and transmembrane, tumor-associated isoforms IX and XII with boronic acids. *Bioorg Med Chem* **2009,** *17* (10), 3649-52.

(100) Larcher, A.; Nocentini, A.; Supuran, C. T.; Winum, J. Y.; van der Lee, A.; Vasseur, J. J.; Laurencin, D.; Smietana, M., Bis-benzoxaboroles: Design, Synthesis, and Biological Evaluation as Carbonic Anhydrase Inhibitors. *ACS Med Chem Lett* **2019,** *10* (8), 1205-1210.

(101) Westmark, P. R.; Gardiner, S. J.; Smith, B. D., Selective Monosaccharide Transport through Lipid Bilayers Using Boronic Acid Carriers. *J Am Chem Soc* **1996,** *118* (45), 11093-11100.

(102) Ballatore, C.; Huryn, D. M.; Smith, A. B., 3rd, Carboxylic acid (bio)isosteres in drug design. *ChemMedChem* **2013,** *8* (3), 385-95.

(103) Elliott, T. S.; Slowey, A.; Ye, Y.; Conway, S. J., The use of phosphate bioisosteres in medicinal chemistry and chemical biology. *MedChemComm* **2012,** *3* (7).

(104) Martin, A. R.; Mohanan, K.; Luvino, D.; Floquet, N.; Baraguey, C.; Smietana, M.; Vasseur, J. J., Expanding the borononucleotide family: synthesis of borono-analogues of dCMP, dGMP and dAMP. *Org Biomol Chem* **2009,** *7* (21), 4369-77.

(105) Luvino, D.; Baraguey, C.; Smietana, M.; Vasseur, J. J., Borononucleotides: synthesis, and formation of a new reversible boronate internucleosidic linkage. *Chem Commun (Camb)* **2008,** (20), 2352-4.

(106) Martin, A. R.; Vasseur, J. J.; Smietana, M., Boron and nucleic acid chemistries: merging the best of both worlds. *Chem Soc Rev* **2013,** *42* (13), 5684-713.

(107) Gleeson, M. P., Generation of a Set of Simple, Interpretable ADMET Rules of Thumb. *J Med Chem* **2008,** *51*, 817-834.

(108) Libutti, S. K.; Anthony, L. B.; Chaplin, D. J.; Sosa, J. A., A phase II study of combretastatin A4-phosphate (CA4P) in the treatment of well-differentiated, low- to intermediate-grade, unresectable, recurrent, or metastatic pancreatic, or GI neuroendocrine tumors/carcinoid (GI-NETs/PNETs) with elevated biomarkers. *J Clin Oncol* **2017,** *35* (4_suppl), 432-432.

(109) Liu, J.; Zheng, S.; Akerstrom, V. L.; Yuan, C.; Ma, Y.; Zhong, Q.; Zhang, C.; Zhang, Q.; Guo, S.; Ma, P.; Skripnikova, E. V.; Bratton, M. R.; Pannuti, A.; Miele, L.; Wiese, T. E.; Wang, G., Fulvestrant-3 Boronic Acid (ZB716): An Orally Bioavailable Selective Estrogen Receptor Downregulator (SERD). *J Med Chem* **2016,** *59* (17), 8134-40.

(110) Liu, J.; Zheng, S.; Guo, S.; Zhang, C.; Zhong, Q.; Zhang, Q.; Ma, P.; Skripnikova, E. V.; Bratton, M. R.; Wiese, T. E.; Wang, G., Rational Design of a Boron-Modified Triphenylethylene (GLL398) as an Oral Selective Estrogen Receptor Downregulator. *ACS Med Chem Lett* **2017,** *8* (1), 102-106.

(111) Zhang, C.; Guo, S.; Yang, L.; Liu, J.; Zheng, S.; Zhong, Q.; Zhang, Q.; Wang, G., Metabolism, pharmacokinetics, and bioavailability of ZB716, a Steroidal Selective Estrogen Receptor Downregulator (SERD). *Oncotarget* **2017,** *8* (61), 103874-103889.

(112) Smoum, R.; Rubinstein, A.; Dembitsky, V. M.; Srebnik, M., Boron containing compounds as protease inhibitors. *Chem Rev* **2012,** *112* (7), 4156-220.

(113) De Cesco, S.; Kurian, J.; Dufresne, C.; Mittermaier, A. K.; Moitessier, N., Covalent inhibitors design and discovery. *Eur J Med Chem* **2017,** *138*, 96-114.

(114) Plescia, J.; De Cesco, S.; Patrascu, M. B.; Kurian, J.; Di Trani, J.; Dufresne, C.; Wahba, A. S.; Janmamode, N.; Mittermaier, A. K.; Moitessier, N., Integrated Synthetic, Biophysical, and Computational Investigations of Covalent Inhibitors of Prolyl Oligopeptidase and Fibroblast Activation Protein alpha. *J Med Chem* **2019,** *62* (17), 7874−7884.

(115) Ahmed Laskar, A.; Younus, H., Aldehyde toxicity and metabolism: the role of aldehyde dehydrogenases in detoxification, drug resistance and carcinogenesis. *Drug Metab Rev* **2019,** *51* (1), 42-64.

(116) Rojas, L. J.; Taracila, M. A.; Papp-Wallace, K. M.; Bethel, C. R.; Caselli, E.; Romagnoli, C.; Winkler, M. L.; Spellberg, B.; Prati, F.; Bonomo, R. A., Boronic Acid Transition State Inhibitors Active against KPC and Other Class A beta-Lactamases: Structure-Activity Relationships as a Guide to Inhibitor Design. *Antimicrob Agents Chemother* **2016,** *60* (3), 1751-9.

(117) Plescia, J.; Dufresne, C.; Janmamode, N.; Wahba, A. S.; Mittermaier, A. K.; Moitessier, N., Discovery of covalent prolyl oligopeptidase boron ester inhibitors. *Eur J Med Chem* **2019**.

(118) Jansen, K.; Heirbaut, L.; Verkerk, R.; Cheng, J. D.; Joossens, J.; Cos, P.; Maes, L.; Lambeir, A. M.; De Meester, I.; Augustyns, K.; Van der Veken, P., Extended structure-activity relationship and pharmacokinetic investigation of (4-quinolinoyl)glycyl-2-cyanopyrrolidine inhibitors of fibroblast activation protein (FAP). *J Med Chem* **2014,** *57* (7), 3053-74.

(119) Corbeil, C. R.; Englebienne, P.; Moitessier, N., Docking Ligands into Flexible and Solvated Macromolecules. 1. Development and Validation of FITTED 1.0. *J Chem Inf Model* **2007,** *47*, 435-449.

(120) Moitessier, N.; Pottel, J.; Therrien, E.; Englebienne, P.; Liu, Z.; Tomberg, A.; Corbeil, C. R., Medicinal Chemistry Projects Requiring Imaginative Structure-Based Drug Design Methods. *Acc Chem Res* **2016,** *49* (9), 1646-57.

(121) Corbeil, C. R.; Moitessier, N., Docking Ligands into Flexible and Solvated Macromolecules. 3. Impact of Input Ligand Conformation, Protein Flexibility, and Water Molecules on the Accuracy of Docking Programs. *J Chem Inf Model* **2009,** *49*, 997-1009.

(122) Schrader, J., Henneberg, F., Mata, R.A., Tittmann, K., Schneider, T.R., Stark, H., Bourenkov, G., Chari, A., The inhibition mechanism of human 20S proteasomes enables next-generation inhibitor design. *Science* **2016,** *353*, 594-598.

(123) Adams, S.; Miller, G. T.; Jesson, M. I.; Watanabe, T.; Jones, B.; Wallner, B. P., PT-100, a Small Molecule Dipeptidyl Peptidase Inhibitor, Has Potent Antitumor Effects and Augments Antibody-Mediated Cytotoxicity via a Novel Immune Mechanism. *Cancer Res* **2004,** *64*, 5471–5480.

(124) Cunningham, C. C., Talabostat. *Expert Opin Investig Drugs* **2007,** *16* (9), 1459-1465.

(125) Flentke, G. R.; Munozt, E.; Hubert, B. T.; Plautt, A. G.; Kettner, C. A.; Bachovchin, W. W., Inhibition of dipeptidyl aminopeptidase IV (DP-IV) by Xaa-boroPro dipeptides and use of these inhibitors to examine the role of DP-IV in T-cell function. *Proc Natl Acad Sci U S A* **1991,** *88*, 1556-1559.

(126) Kelly, T. A.; Adams, J.; Bachovchin, W. W.; Barton, R. W.; Campbell, S. J.; Coutts, S. J.; Kennedy, C. A.; Snow, R. J., Immunosuppressive Boronic Acid Dipeptides: Correlation between Conformation and Activity. *J Am Chem Soc* **1993,** *115*, 12637-12638.

(127) Poplawski, S. E.; Lai, J. H.; Sanford, D. G.; Sudmeier, J. L.; Wu, W.; Bachovchin, W. W., Pro-soft Val-boroPro: a strategy for enhancing in vivo performance of boronic acid inhibitors of serine proteases. *J Med Chem* **2011,** *54* (7), 2022-8.

(128) Diaz, B. H. R. Improvement of Protein Crystal Diffraction Using Post-Crystallization Methods: Infrared Laser Radiation Controls Crystal Order. University of Hamburg, 2018.

(129) Wang, L.; Xie, S.; Ma, L.; Chen, Y.; Lu, W., 10-Boronic acid substituted camptothecin as prodrug of SN-38. *Eur J Med Chem* **2016,** *116*, 84-89.

(130) Lin, B.; Chen, H.; Liang, D.; Lin, W.; Qi, X.; Liu, H.; Deng, X., Acidic pH and High-H2O2 Dual Tumor Microenvironment-Responsive Nanocatalytic Graphene Oxide for Cancer Selective Therapy and Recognition. *ACS Appl Mater Interfaces* **2019,** *11* (12), 11157-11166.

(131) Zheng, S.; Guo, S.; Zhong, Q.; Zhang, C.; Liu, J.; Yang, L.; Zhang, Q.; Wang, G., Biocompatible Boron-Containing Prodrugs of Belinostat for the Potential Treatment of Solid Tumors. *ACS Med Chem Lett* **2018,** *9* (2), 149-154.

(132) Peiro Cadahia, J.; Previtali, V.; Troelsen, N. S.; Clausen, M. H., Prodrug strategies for targeted therapy triggered by reactive oxygen species. *MedChemComm* **2019,** *10* (9), 1531-1549.

(133) London, N.; Miller, R. M.; Krishnan, S.; Uchida, K.; Irwin, J. J.; Eidam, O.; Gibold, L.; Cimermancic, P.; Bonnet, R.; Shoichet, B. K.; Taunton, J., Covalent docking of large libraries for the discovery of chemical probes. *Nat Chem Biol* **2014,** *10* (12), 1066-72.

(134) Teotico, D. G.; Babaoglu, K.; Rocklin, G. J.; Ferreira, R. S.; Giannetti, A. M.; Shoichet, B. K., Docking for fragment inhibitors of AmpC beta-lactamase. *Proc Natl Acad Sci U S A* **2009,** *106* (18), 7455-60.

(135) Yadav, S.; Kumar, P., Enhanced uptake of plasmid at boronic acid decorated linear polyethylenimines results in higher transfection efficiency. *Biointerphases* **2018,** *13* (6), 061003.

(136) Andersen, K. A.; Smith, T. P.; Lomax, J. E.; Raines, R. T., Boronic Acid for the Traceless Delivery of Proteins into Cells. *ACS Chem Biol* **2016,** *11* (2), 319-23.

(137) Zhang, X.; Alves, D. S.; Lou, J.; Hill, S. D.; Barrera, F. N.; Best, M. D., Boronic acid liposomes for cellular delivery and content release driven by carbohydrate binding. *Chem Commun (Camb)* **2018,** *54* (48), 6169-6172.

(138) Roemmele, R. C.; Christie, M. A., Development and Scale-Up of an Optimized Route to the Peptide Boronic Acid, CEP-18770. *Org Process Res Dev* **2013,** *17* (3), 422-426.

(139) Ivanov, A. S.; Zhalnina, A. A.; Shishkov, S. V., A convergent approach to synthesis of bortezomib: the use of TBTU suppresses racemization in the fragment condensation. *Tetrahedron* **2009,** *65* (34), 7105-7108.

(140) Combi-Blocks, Inc. https://www.combi-blocks.com (accessed 2 Dec 2019).

(141) Buesking, A. W.; Bacauanu, V.; Cai, I.; Ellman, J. A., Asymmetric synthesis of protected alpha-amino boronic acid derivatives with an air- and moisture-stable Cu(II) catalyst. *J Org Chem* **2014,** *79* (8), 3671-7.

(142) Beenen, M. A.; An, C.; Ellman, J. A., Asymmetric Copper-Catalyzed Synthesis of α-Amino Boronate Esters from N-tert-Butanesulfinyl Aldimines. *J Am Chem Soc* **2008,** *130*, 6910-6911.

(143) Chen, J.; Chen, L.-y.; Zheng, Y.; Sun, Z., Asymmetric synthesis of stable α-aminoboronic esters catalyzed by N-heterocylic carbene and copper(i) chloride. *RSC Advances* **2014,** *4* (40).

(144) Kim, B. J.; Matteson, D. S., Conversion of alkyltrifluoroborates into alkyldichloroboranes with tetrachlorosilane in coordinating solvents. *Angew Chem Int Ed Engl* **2004,** *43* (23), 3056-8.

(145) Ishiyama, T.; Murata, M.; Miyaura, N., Palladium(0)-Catalyzed Cross-Coupling Reaction of Alkoxydiboron with Haloarenes: A Direct Procedure for Arylboronic Esters. *J Org Chem* **1995,** *60*, 7508-7510.

(146) MilliporeSigma https://www.sigmaaldrich.com/ (accessed 2 Dec 2019).

(147) BoroChem PBO. http://borochem.fr/en (accessed 2 Dec 2019).

(148) Lillo, V.; Bonet, A.; Fernandez, E., Asymmetric induction on beta-boration of alpha,beta-unsaturated compounds: an inexpensive approach. *Dalton Trans* **2009,** (16), 2899-908.

(149) Li, C.; Wang, J.; Barton, L. M.; Yu, S.; Tian, M.; Peters, D. S.; Kumar, M.; Yu, A. W.; Johnson, K. A.; Chatterjee, A. K.; Yan, M.; Baran, P. S., Decarboxylative borylation. *Science* **2017,** *356* (6342), 1-8.

(150) Fawcett, A.; Pradeilles, J.; Wang, Y.; Mutsuga, T.; Myers, E. L.; Aggarwal, V. K., Photoinduced decarboxylative borylation of carboxylic acids. *Science* **2017,** *357* (6348), 283-286.

(151) Hu, D.; Wang, L.; Li, P., Decarboxylative Borylation of Aliphatic Esters under Visible-Light Photoredox Conditions. *Org Lett* **2017,** *19* (10), 2770-2773.

(152) Wang, J.; Shang, M.; Lundberg, H.; Feu, K. S.; Hecker, S. J.; Qin, T.; Blackmond, D. G.; Baran, P. S., Cu-Catalyzed Decarboxylative Borylation. *ACS Catal* **2018,** *8* (10), 9537-9542.

(153) Yang, F.; Zhu, M.; Zhang, J.; Zhou, H., Synthesis of biologically active boron-containing compounds. *MedChemComm* **2018,** *9* (2), 201-211.

(154) Poplawski, S. E.; Lai, J. H.; Li, Y.; Jin, Z.; Liu, Y.; Wu, W.; Wu, Y.; Zhou, Y.; Sudmeier, J. L.; Sanford, D. G.; Bachovchin, W. W., Identification of selective and potent inhibitors of fibroblast activation protein and prolyl oligopeptidase. *J Med Chem* **2013,** *56* (9), 3467-77.

(155) Wu, W.; Liu, Y.; Milo, L. J., Jr.; Shu, Y.; Zhao, P.; Li, Y.; Woznica, I.; Yu, G.; Sanford, D. G.; Zhou, Y.; Poplawski, S. E.; Connolly, B. A.; Sudmeier, J. L.; Bachovchin, W. W.; Lai, J. H., 4-Substituted boro-proline dipeptides: synthesis, characterization, and dipeptidyl peptidase IV, 8, and 9 activities. *Bioorg Med Chem Lett* **2012,** *22* (17), 5536-40.

(156) Pickersgill, F.; Bishop, J.; Lo, Y.; Chiu, F.-T.; Kulkarni, V. R. Synthesis of Bortezomib. EP11167263A, 2004.

(157) Yuen, A. K. L.; Hutton, C. A., Deprotection of pinacolyl boronate esters via hydrolysis of intermediate potassium trifluoroborates. *Tet Lett* **2005,** *46* (46), 7899-7903.

(158) Coutts, S. J.; Adams, J.; Krolikowski, D.; Snow, R. J., Two efficient methods for the cleavage of pinanediol boronate esters yielding the free boronic acids. *Tet Lett* **1994,** *35* (29), 5109-5112.

(159) Murphy, J. M.; Tzschucke, C. C.; Hartwig, J. F., One-pot synthesis of arylboronic acids and aryl trifluoroborates by Ir-catalyzed borylation of arenes. *Org Lett* **2007,** *9* (5), 757-760.

(160) Sun, J.; Perfetti, M. T.; Santos, W. L., A method for the deprotection of alkylpinacolyl boronate esters. *J Org Chem* **2011,** *76* (9), 3571-5.

Chapter 2:

Integrated Synthetic, Biophysical, and Computational Investigations of Covalent Inhibitors of Prolyl Oligopeptidase and Fibroblast Activation Protein α

This chapter has been published and is reproduced from:

Plescia, J.;* De Cesco, S.;* Patrascu, M. B.;* Kurian, J.; Di Trani, J.; Dufresne, C.; Wahba, A. S.; Janmamode, N.; Mittermaier, A. K.; Moitessier, N., Integrated Synthetic, Biophysical, and Computational Investigations of Covalent Inhibitors of Prolyl Oligopeptidase and Fibroblast Activation Protein α. *J Med Chem* **2019,** 62(17), 7874-7884.

**These authors contributed equally*

Chapter 1 provided many examples of boronic acid drugs and their versatility in drug design. We have used this information in our own research of our target enzymes, prolyl oligopeptidase and fibroblast activation protein α to design reversible covalent inhibitors. Herein we describe a collaborative study of synthetic, biophysical, and computational pursuits to determine the optimal electrophilic warheads for POP and FAP.

Contribution(s) of authors: I synthesized and characterized all molecules and conducted the molecular docking as well as the literature review of FAP-targeting electrophilic inhibitors. The assay designs, biophysical experiments, and kinetic characterizations are the work of Dr. Stephane De Cesco. The computational procedure development and all computational predictions apart from molecular docking are the work of Jerry Kurian and Mihai Burai Patrascu. The mass spectroscopy experiment was conducted by Alexander S. Wahba.

2.1 Abstract

Over the past decade, there has been increasing interest in covalent inhibition as a drug design strategy. Our own interest in the development of prolyl oligopeptidase (POP) and fibroblast activation protein α (FAP) covalent inhibitors has led us to question whether these two serine proteases were equal in terms of their reactivity toward electrophilic warheads. To streamline such investigations, we exploited both computational and experimental methods to investigate the influence of different reactive groups on both potency and binding kinetics using both our own series of POP inhibitors and others' discovered hits. A direct correlation between inhibitor reactivity and residence time was demonstrated through quantum mechanics methods and further supported by experimental studies. This computational method was also successfully applied to FAP, as an overview of known FAP inhibitors confirmed our computational predictions that more reactive warheads (e.g., boronic acids) must be employed to inhibit FAP than for POP.

2.2 Introduction

Following the resurgence of covalent inhibition in the last decade,[1-3] kinases and serine proteases have been targeted with numerous covalent inhibitors,[4] and covalent inhibitors have reached the market (Figure 2.1). Among these targets are prolyl oligopeptidase (POP), initially associated with neurodegenerative diseases,[5-8] and fibroblast activation protein α (FAP), a promising target for anti-cancer therapies.[9-12] In the past, our group and others have reported a number of potent covalent POP inhibitors,[8] including Cbz-Pro-Prolinal (**2.1**), JTP-4819 (**2.2**), KYP-2047 (**2.3**), and bicyclic derivative **2.5**,[13] as well as FAP covalent inhibitors such as compounds **2.6**, **2.8**, and Talabostat (Figure 2.2). Although these two druggable targets have been inhibited by many covalent inhibitors, the major differences lie in the chemical nature of the warheads, or electrophilic functional groups that form covalent bonds with protein residues.

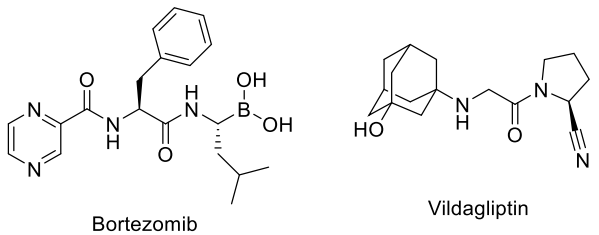

Figure 2.1. Selected marketed covalent inhibitors.

Non-covalent inhibitors often bind and dissociate very quickly and exhibit short residence times and are therefore often largely under thermodynamic control. In contrast, covalent inhibitors are believed to often bind in a two-step process (Figure 2.3a): a fast, non-covalent initial binding followed by a slower covalent bond formation. As a result, kinetic factors and residence time cannot be ignored and could indeed be critical for inhibitor efficacy.[3] Recently the reactivity of the warheads used in covalent inhibition has been increasingly investigated either experimentally[14-15] or computationally[16] as reactivity often dictates whether the inhibitor will bind reversibly or irreversibly.[17] Similarly, the reactivity of the protein's catalytic residues in covalent inhibition has been investigated with focus on cysteines.[18-22] A very interesting method based on free energy perturbation (FEP) has recently been reported which computes binding free energies including both covalent and non-covalent contribution to binding.[23-24]

However, although these methods proved effective, the focus has been primarily on cysteine residues and acrylamides as warheads, as kinase cysteines have likely been the major targets for covalent inhibitors (often acrylamides) in the recent years.[25] A number of research groups are nowadays searching for alternative warheads and residues to bind to (marketed covalent drugs are binding to catalytic residues) and computational methods must be assessed.[26]

Prior to designing covalent inhibitors, the biological target must be first identified as covalently druggable (i.e., can be targeted with covalent inhibitors). Unfortunately, there are very few tools currently available, experimental or computational, to accomplish this. We report herein a developed computational protocol using POP and FAP that could eventually be used to (1) predict whether an enzyme is covalently druggable and (2) identify potentially potent warheads. To illustrate the potential application of such a protocol, it took our team months to optimally express and purify POP and to optimize the *in vitro* activity assays, which was followed by months of synthesis until we found potent inhibitors. With our current computational protocol in hand, requiring only 2-3 weeks of calculations, we would have been able to make a more informed decision on whether to initiate our hit-discovery endeavor. Similarly, until this protocol was available, our efforts focused on the unsuccessful development of nitrile-containing FAP inhibitors. Running reactivity predictions before synthesis would have allowed us to opt for the appropriate warheads much earlier.

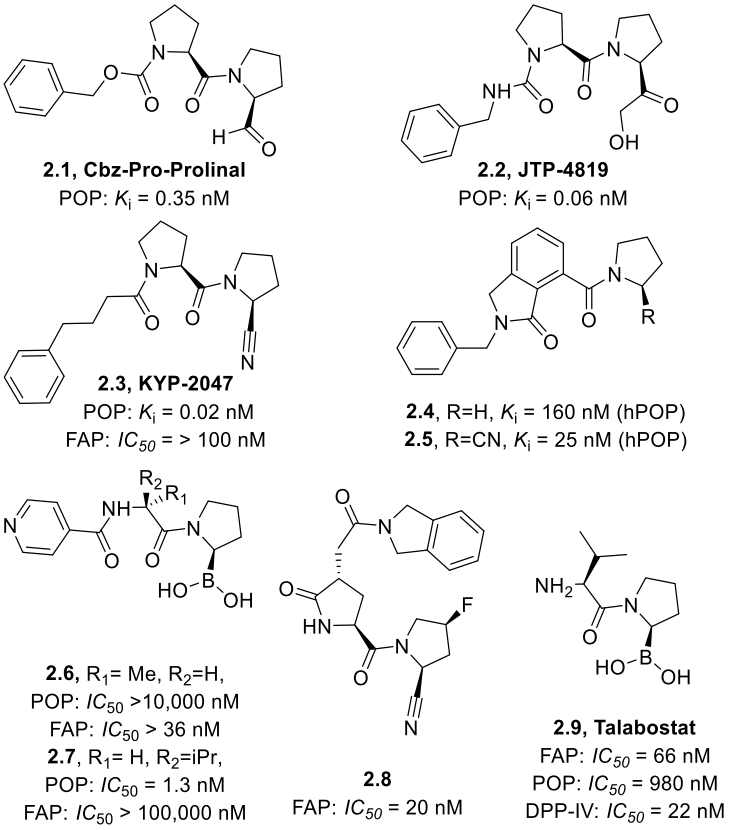

Figure 2.2. Selected POP and FAP inhibitors.

As demonstrated via co-crystallization,[27-28] POP inhibition can be achieved through covalent bond formation between the reactive group of a ligand and the catalytic serine in the active site (Ser554). The reaction of Ser554 with aldehyde **2.1** leads to the formation of a hemiacetal, which favorably mimics the tetrahedral intermediate of the endogenous catalytic reaction, stabilizing its presence in the active site (Figure 2.3b and c). In contrast, reaction with a nitrile group leads to a trigonal planar iminoether, an intermediate which less favorably mimics the amide group of the peptide substrates (Figure 2.3d). While maintaining favorable non-covalent interactions (e.g. via the scaffold) is essential for both potency and selectivity, modification of the covalent warhead is also expected to have a significant impact on the binding affinity and kinetics via its influence on the second step of the binding event (Figure 2.3a).

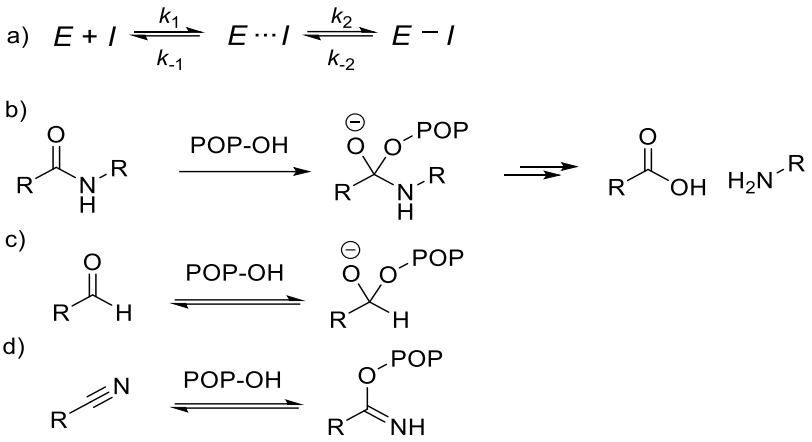

Figure 2.3. Reactions of POP with the substrate and various inhibitors a) Two-step process for covalent inhibition. E: enzyme; I: inhibitor; E···I: non-covalent complex; k_1: association rate constant; k_{-1}: dissociation rate constant. b) cleavage of a substrate; c) aldehyde inhibitor covalent binding; d) nitrile inhibitor covalent binding.

Herein, we describe our collaborative approach, including computational predictions and experimental evaluations, to the investigation of the relative reactivities of FAP and POP and the nature of the covalent warheads that are more likely to lead to potent inhibitors.

2.3 Results

2.3.1 Strategy

We sought to develop a computational protocol which would first be tested against experimental data collected on POP and then validated on a homologous enzyme, FAP (Figure 2.4).

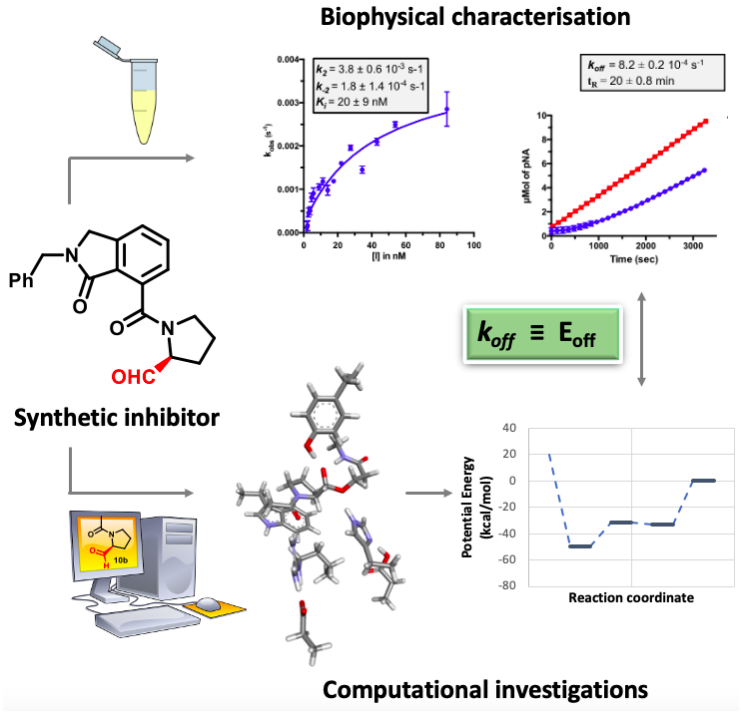

Figure 2.4. Computational model and experimental data collection. The residence times of various inhibitors depends on kinetics factors ($t_R = 1/k_{off}$), which are measured using biophysical methods. These kinetic parameters are related to the energy required for the inhibitors to break the covalent bond and leave the enzyme (E_{off}). Advantageously, E_{off} can be computed, ultimately demonstrating that computations can substitute complex, time-consuming, and expensive experiments for initial assessments as to whether a newly discovered target is covalently druggable.

In order to probe the impact of the intrinsic reactivity of the warhead on the overall binding process, we designed a series of inhibitors **2.5a**, **2.10a-2.17a** which complement previously reported inhibitors **2.5c**, **2.11c**, **2.13c-2.15c**[29] (Figure 2.5). Two strategies were envisioned: (1) substitution of the warhead – the nitrile, aldehyde, and boronic acid were selected, as these are

known to form covalent bonds with nucleophilic protein residues;[30-31] and (2) modification of the electronic environment of a given warhead – electron withdrawing fluorine atoms could be introduced on the nitrile analogue, a strategy exploited to prepare FAP inhibitors (Figure 2.2).

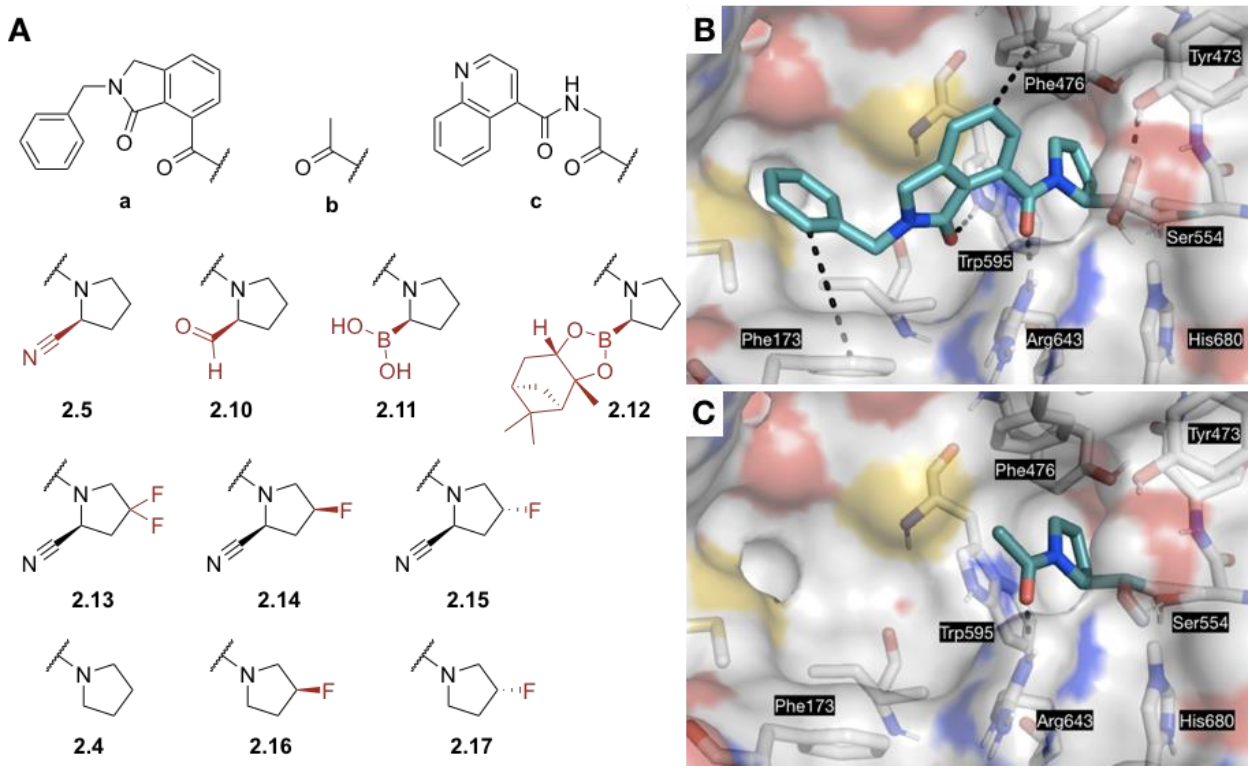

Figure 2.5. Inhibitors featured in this study. a) selected inhibitor structures;i) different reactive groups; ii) modulated nitrile reactivity; iii) effects of fluorine atoms alone. b) Docked binding mode of boronic acid **2.11a** into the POP active site. c) Snapshot of the POP active site and with **2.10b** bound to Ser554 and the residues kept for the Quantum Chemical Cluster Approach (QCCA) study.

2.3.2 Chemistry.

The synthesis of bicyclic scaffold **a** was optimized and previously published by our group.[13] Bicyclic precursor **2.18** (Scheme 2.1), previously discovered through a virtual screening/virtual optimization strategy, was selected because of its straightforward and efficient synthesis. More specifically, this core was readily available in only three synthetic steps and an overall yield of 74% with no flash chromatography purification, offering the unprotected carboxylic acid **2.18** as a diversity point.

The individual proline analogs were then coupled to the scaffold **2.18** to afford the desired inhibitors. Because the proline analogues were either commercially or readily available, expedient and efficient synthesis of potential POP inhibitors was achieved in only 1-2 steps. The synthesis of these selected analogues (**2.4a**, **2.5a** and **2.10a**-**2.17a**) is outlined in Scheme 2.1 and Scheme 2.2.

The boron-containing analogue **2.12a** was obtained by coupling scaffold **2.18** with the commercially available proline analog **2.19** to yield product **2.12a** in moderate yield (Scheme 2.1). Attempts at hydrolysis of boronic ester **2.12a** to obtain boronic acid **2.11a** were unsuccessful, exhibiting solubility issues and yielding complex mixtures, so **2.12a** was utilized instead. Our own mass spectrometry experiment revealed that the boronic ester **2.12a** is nearly quantitatively hydrolyzed to boronic acid **2.11a** in the assay buffer (ca. 90% after 10 minutes, Figure 2.6), and can therefore be tested as a pro-drug cleaved in the assay. Furthermore, our own *in vitro* assay controls show that the cleaved pinanediol exhibits no inhibitory activity against POP (data not shown).

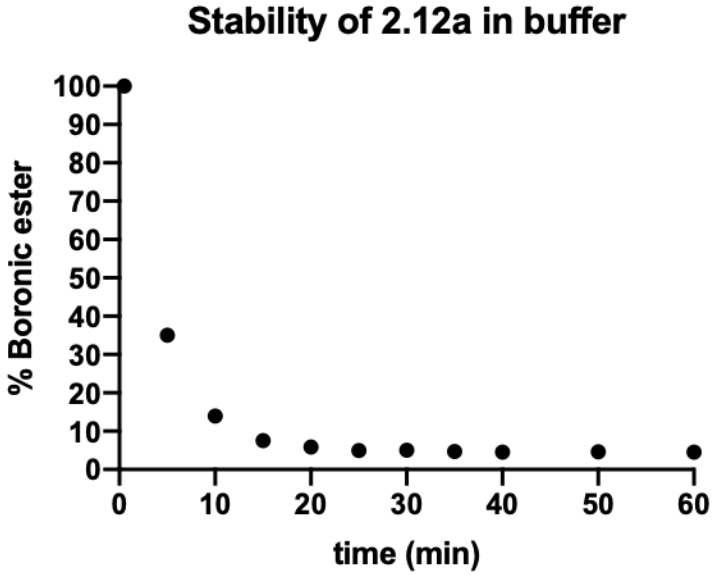

Figure 2.6. Mass spectroscopy study of boronic ester cleavage in the POP buffer. The relative abundance of the boronic ester **2.12a** was recorded over one hour, plateauing at approximately 5% abundance.

Synthesis of the potential inhibitor **2.10a** bearing an aldehyde as the warhead started with the coupling of commercially available L-prolinol with scaffold **2.18**, to afford the primary alcohol **2.20** in excellent yield. Further oxidation under Swern conditions led to the desired aldehyde **2.10a**. Synthesis of the non-covalent analog **2.4a** was accomplished by coupling scaffold **2.18** to pyrrolidine. The nitrile analog **2.5a** was obtained by coupling **2.18** with readily available (*S*)-pyrrolidine-2-carbonitrile (Scheme 2.1).

Scheme 2.1. Synthesis of diversely functionalized inhibitors.[a]

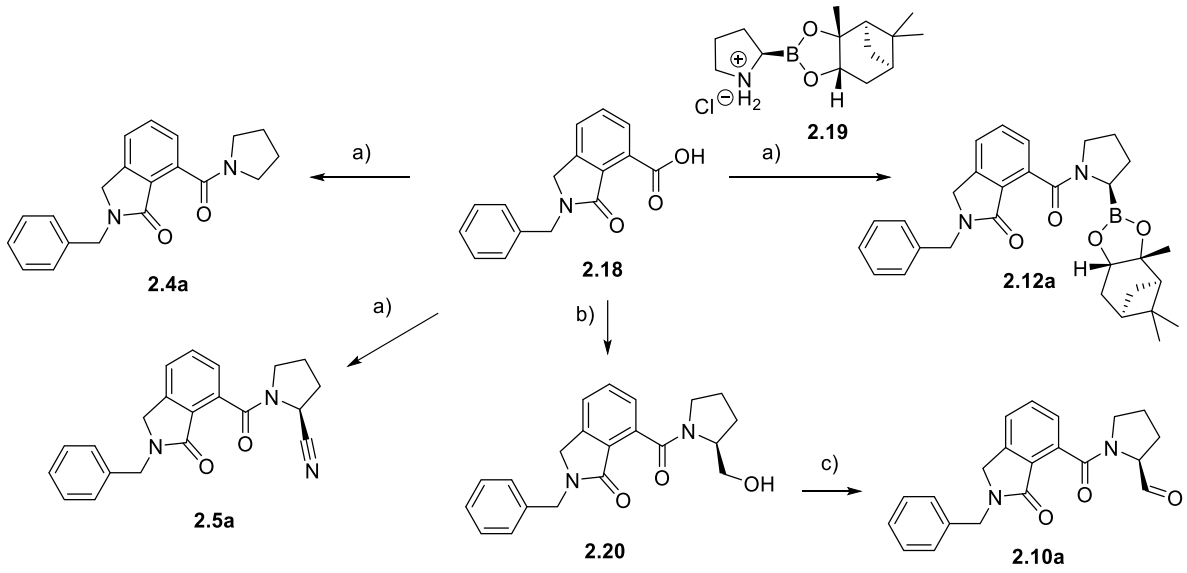

[a]a) i. PivCl, Et_3N, DCM, 0°C; ii. amine (see Experimental Section), rt, 18 h (**2.4a**, 40%, **2.5a**, 92%, **2.12a**, 43%); b) i. PivCl, Et_3N, DCM, 0°C; ii. Prolinol, 18 h, rt (87%); c) DMSO, Oxalylchloride, Et_3N, DCM, −78°C (40%).

Synthesis of the selected fluorocyanopyrrolidine analogues began from readily available starting materials.[32] Coupling of **2.18** with nitrile **2.21** led to the corresponding inhibitor **2.13**. Reaction of readily available free amines **2.22** and **2.23** with the bicycle core **2.18** under standard coupling conditions afforded the intended inhibitors **2.14a** and **2.15a**, respectively. The non-covalent inhibitors **2.16a** and **2.17a** were prepared through coupling of carboxylic acid **2.18** with **2.24** and **2.25**, respectively.

Scheme 2.2. Synthesis of the fluorine-containing compounds.[a]

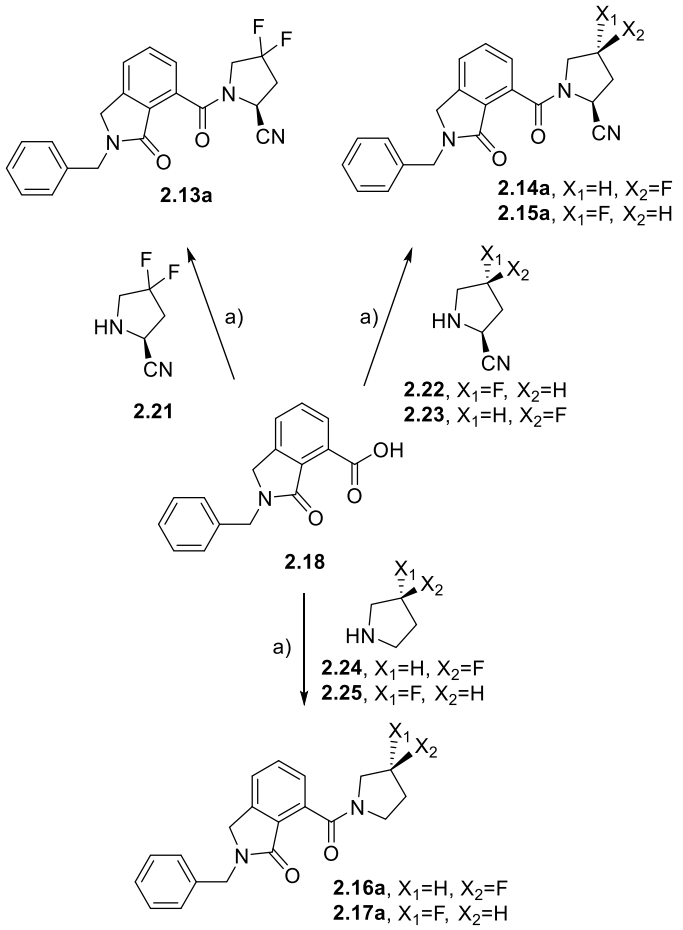

[a]Reagents: a) i. PivCl, Et_3N, DCM, 0°C; ii. amine (see Experimental Section), rt, 18h (**2.13a**, 35%; **2.14a**, 30%; **2.15a**, 32%; **2.16a**; 90%; **2.17a**, 88%)

2.3.3 Biophysical characterization.

Next, these selected molecules were first evaluated for their inhibitory potency against recombinant human POP (Table 2.1). Figure 2.7 shows the dose-response curves for covalent inhibitors **2.10a** and **12a**. As expected, while non-functionalized pyrrolidine derivative **2.4a** exhibited a potency of 160 nM, the measured K_i values for the nitrile (**2.5a**), aldehyde (**2.10a**) and boronic ester (**2.12a**) derivatives were significantly lower. The high reactivity of aldehydes as electrophiles has often been a major issue for developing safe drugs, even in the discovery of Bortezomib (boronic acid proteasome inhibitor, Figure 2.1).[33-34] In contrast, the lower reactivity of nitriles allowed medicinal chemists to use them as warhead in drugs such as Vildagliptin (nitrile-

containing covalent DPP-IV inhibitor, Figure 2.1). The reactivity of these warheads is further discussed below.

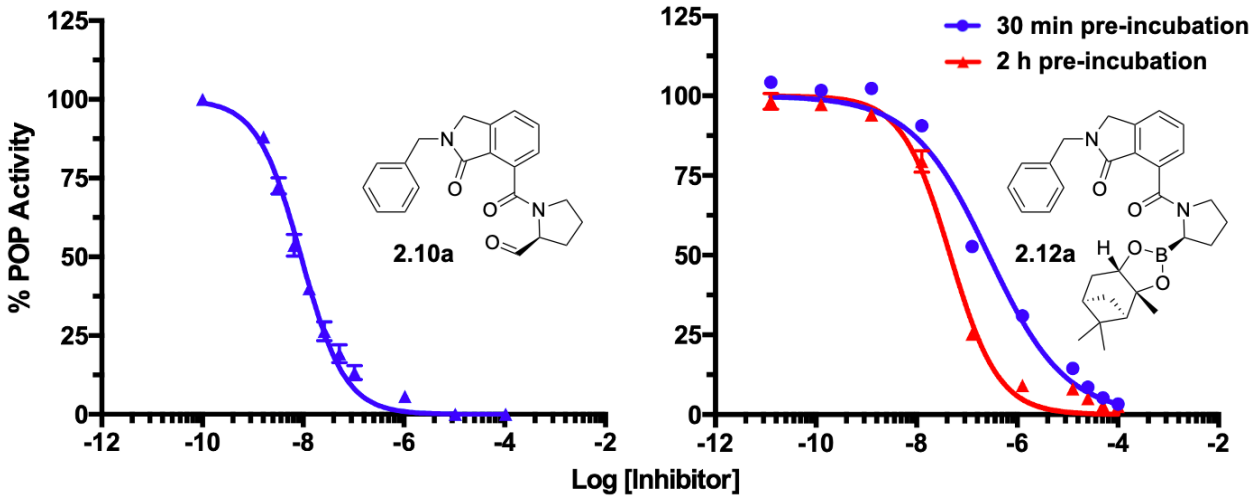

Figure 2.7. Dose-response curves of inhibitors **2.10a** (left) and **2.12a** (right) against human recombinant POP after 30-minute pre-incubation periods (blue). Boronic ester **2.12a** was additionally tested with a two-hour pre-incubation (red) period to allow for *in situ* hydrolysis of the (-)-pinanediol protecting group

As an observed effect of kinetic factors, the K_i decreases over time until equilibrium is reached. While the nitrile and aldehyde derivatives reached equilibrium after 30 minutes of pre-incubation, the boronic ester **2.12a** required a longer incubation period. This was most likely due to the rate of hydrolysis of the boronic ester to the boronic acid **2.11a**, which is required for enzyme binding. Residence time is largely controlled by binding kinetics of the covalent ligand, illustrating the importance of this property.[2, 35-36] Introduction of fluorine atoms onto the pyrrolidine ring of our lead compound **2.5a** led to complete loss (**2.15a**) or a decrease (**2.13a**, **2.14a**) in potency. A similar decrease in affinity was also observed for the non-covalent inhibitors bearing a fluorine atom on the pyrrolidine ring (**2.4a** vs. **2.16a** and **2.17a**), suggesting that factors other than the nitrile reactivity modulate potency.

Additional biophysical characterization experiments were performed for select inhibitors **2.10a**, **2.12a**, and control **2.1**. To extract kinetic parameters, progress curve experiments were conducted at various inhibitor concentrations. Data from these curves were then used to extract the respective k_{obs} values, which were further plotted against inhibitor concentration; the resultant data

was subsequently fitted to the corresponding equations in order to retrieve the inhibitors' kinetic parameters. Finally, rapid dilution experiments were performed to obtain residence time t_R. Kinetic parameters of each compound are provided in Table 2.1. Unfortunately, any attempts to obtain kinetic parameters for the non-covalent, the prolinonitrile, and the fluorinated prolinonitrile derivatives proved unsuccessful, as the off rates were too quick to measure experimentally.

Table 2.1. Summary of the kinetic parameters measured experimentally.*

Cpd	K_i (nM)[a]	K_i (nM)[b]	K_i*(nM)[c]	k_{on} (10^5 M^1 s^{-1})	k_{off} (10^{-4} s^{-1})	t_R (min)	FAP[d]
2.1	1 ± 0.1	8 ± 1	0.4 ± 0.02	7.8 ± 2.2	3.9 ± 0.5	42 ± 5	< 5%[37]
2.4a	160 ± 40	-	-	-	-	< 1	<5%
2.5a	25 ± 4	-	25 ± 4	-	-	< 1	20%
2.10a	4.0 ± 0.4	20 ± 9	3.5 ± 0.2	1.86 ± 0.7	8.2 ± 0.2	20 ± 0.8	80% (11%)
2.12a	110 ± 40[e] 22 ± 5[f]	60 ± 10	29 ± 2	0.04 ± 0.01	2.3 ± 0.3	73 ± 10	<5%
2.13a	3,300 ± 780	-	-	-	-	-	<5%
2.14a	170 ± 40	-	-	-	-	-	<5%
2.15a	> 100 μM	-	-	-	-	-	<5%
2.16a	290 ± 50	-	-	-	-	-	<5%
2.17a	620 ± 90	-	-	-	-	-	<5%

[a]Affinity constant, measured by absorbance assay. [b]Affinity constant of the first step of the binding event, measured by dilution experiments. [c]Affinity constant of the second step of inhibition. [d]inhibition at 100 μM (at 1 μM). [e]30 minute E—I pre-incubation time. [f]2 hour E—I pre-incubation time. *missing parameters (-) indicate that the kinetics of the reaction were too quick to measure experimentally

2.3.4 Computational study.

To study these kinetic parameters and provide insight into the development of effective prediction methods for covalent inhibitors, the quantum chemical cluster approach (QCCA)[38] was employed. Starting geometries were taken from crystal structures. The ligands were truncated to focus on energetics of covalent bond formation/breakage while maintaining the electronics of the electrophile (e.g., **2.10b** as a model for **2.10a**).

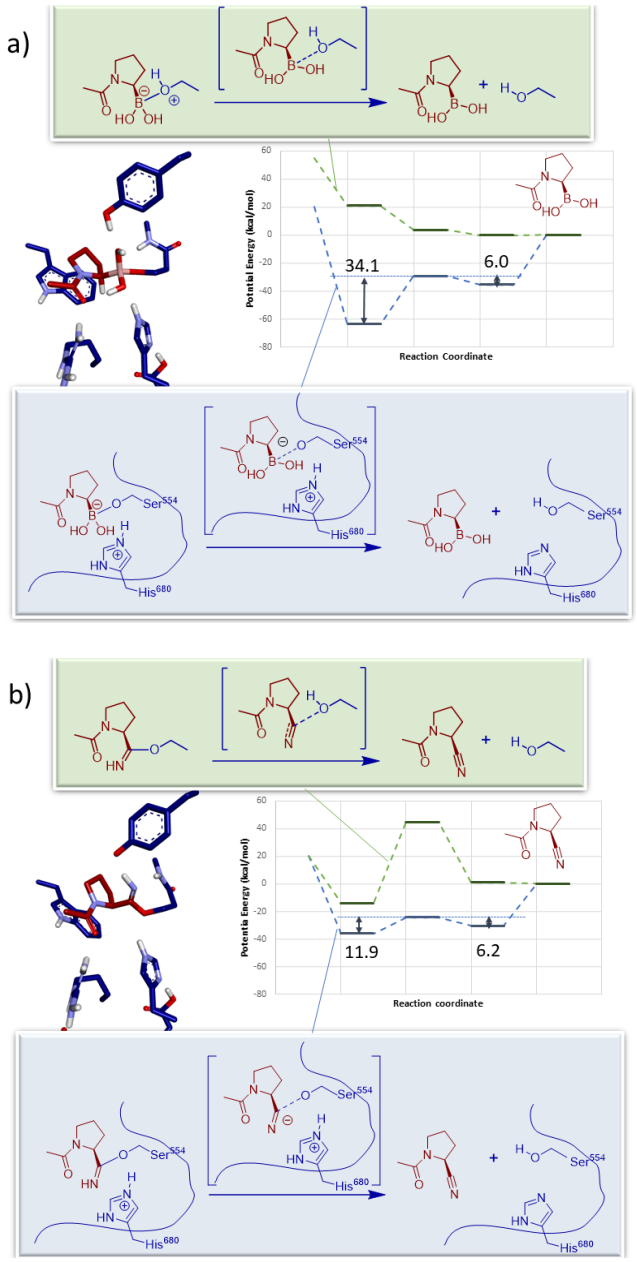

Figure 2.8. Data collected for boronic acid (a) and nitrile (b) as warheads. In blue is the energy of the enzyme-catalyzed reaction and in green the same reaction with no enzyme. Non-polar hydrogens are omitted for clarity. Numbers refer to the differences in energy between the transition states and starting or product conformations. Similar data has been collected for all the probes and both proteins (not shown).

As per the QCCA protocol, the binding site was restricted to the catalytic triad residues along with other key residues, such as the backbone of residues contributing to the oxy-anion hole (Figure 2.5c). The second step of the binding process was then simulated to acquire several thermodynamic and kinetic parameters, such as binding energies and activation energies for binding and unbinding, which together with enzyme mobility and non-bonded interactions contribute to k_{on} and k_{off} (Table 2.2, Figure 2.8). In order to develop a protocol that would minimize calculation time, we decided to compute the energy at evenly distributed distances only. As a result, the "ideal" distance or transition state distances were not necessarily assessed, only close-to-minima structures. Although the search for the energy at the optimal distances is expected to improve accuracy, it is also expected to significantly increase computational time and hence decrease efficiency, as locating a transition state is not a simple task. Rather, our method is expected to provide us with trends which would be accurate enough to make informed decisions on whether a target is covalently druggable. Considering this approximation, we also considered different levels of theory, from semiempirical (AM1) to higher levels (PBE0/def2-TZVP/D3BJ).

Table 2.2. Summary of the parameters obtained computationally (all values are in kcal/mol).

	E_{off}		E_{on}		ΔG (cov. – non-cov.)		Binding Energy	
Cpd.	POP	FAP	POP	FAP	POP	FAP	POP	FAP
2.5b	11.9	6.2	6.2	7.5	-5.7	1.3	-36.0	-27.0
2.10b	18.8	16.9	1.8	3.9	-17.0	-13.0	-49.9	-42.9
2.11b	34.1	26.0	6.0	<1.0 [a]	-28.1	-26.0	-63.5	-55.8
2.13b	14.2	12.6	8.4	5.9	-5.8	-6.7	-37.3	-29.1
2.14b	9.8	5.7	8.5	10.6	-1.3	4.9	-34.4	-25.4
2.15b[b]	13.7	10.9	6.6	10.2	-7.1	-0.7	-39.2	-32.8

[a] The compound forms a covalent bond without an energy barrier. [b] computed with the pseudo axial conformation (see text).

2.4 Discussion

The computational data suggests that the warhead does in fact have a direct influence on the kinetics and thus activity of the second step in ligand binding. According to this data, the aldehyde and boronic acid are predicted to have longer residence times than any of the nitrile derivatives, represented by significantly larger E_{off} values. This is consistent with the in-depth intrinsic

electrophilicity analysis at the HF/def2-TZVP level of theory we have conducted on compounds **2.5b**, **2.10b** and **2.11b** (not shown), using our own QM package QUEMIST. This analysis is based on computing the LUMO energies of the three compounds, alongside intrinsic atomic orbital (IAO) atomic charges[39] for the reactive atoms (boron, carbonyl carbon and nitrile carbon) and total atomic nucleophilic superdelocalizabilities (TANS) for the reactive atoms.[40] The TANS is a measure of interaction with a nucleophile by an electrophile, and can be reliably used to compare two or more sites for this specific interaction. A high value of TANS is representative of a larger capacity of an atom to interact with a nucleophile through their LUMO orbital. According to this data, the boronic acid **2.11b** has the lowest LUMO energy (7.4 kcal/mol lower than the aldehyde and 5.3 kcal/mol lower than the nitrile) along with a higher IAO atomic charge for the reactive atom (0.74 vs. 0.33 for **2.10b** and 0.15 for **2.5b**) and a higher TANS for the reactive atom (9.84 vs. 1.24 for **2.10b** and 1.06 for **2.5b**). This analysis is also consistent with the binding energies presented in Table 2.2, which suggests the boronic acid is the strongest binder/more intrinsically reactive.

The data also suggested that the nitriles had a slightly higher activation energy (E_{on}) in FAP than in POP. More surprisingly, the conversion of the aldehyde to the hemi-acetal and the boronic acid to the boronate in the active site appear to possess a very low energy barrier. This would imply that covalent bond formation is rapid, only limited by diffusion of the ligand into the active site and reorientation of the electrophilic warhead to allow covalent bond formation. This low energy barrier is attributed to two observations: (1) the ligands appear to be pre-activated by Tyr473 as they approach the nucleophilic serine, and (2) the transition states of these reactions resemble the transition state adopted by the natural substrates and are highly stabilized through hydrogen bonding. Interestingly, in the case of nitriles, the proximal Tyr473 hydroxyl group is properly positioned to transfer a proton to the forming imine despite the sp^2 character of this intermediate. While ligand-enzyme kinetics were the focus of these computations, we also observed that in the case of the nitrile, energy of the covalently bound state was not necessarily significantly lower than that of the non-covalent complexes, keeping in agreement with low residence time. We next investigated whether computing the full binding process was required. First, we computed the correlation between the binding energies and E_{off} for POP (Table 2.2), according to the Bell-Evans-Polanyi principle.[41] This principle establishes a linear relationship between the activation energy and the enthalpy of reaction in the same family of reactions. The R^2 coefficient of 0.96 confirms a

significant correlation between the binding energies and E_{off}, and suggest that future investigations should simply focus on ground states, thus streamlining the process. We next computed theoretical half-lives $t_{1/2}$ of both the initial bond formation as well as the bond breakage (not shown), which are significantly lower than the residence times (Table 2.2). The bond formation/breaking was significantly faster than the experimental residence time, suggesting that the inhibition process is under thermodynamic control. Thus, the binding energies should also correlate with the experimentally determined K_i values. We plotted the relevant graph, and we observed no correlation between the binding energies and K_i values ($R^2 = 0.17$). Several factors are responsible for this apparent lack of correlation: first, we computed the binding energies of truncated fragments, while the K_i values were determined using the full molecules. While we tried to obtain K_i values for the fragments alone, they showed no activity in POP or FAP (data not shown), revealing the critical contribution of the rest of the molecules to the binding affinity. Secondly, the K_i values were computed in solution, while our computations were performed exclusively in the gas phase. We believe that for accurate solvent effects an explicit solvent should be used,[42] which can be reliably done using molecular dynamics simulations. However, this is beyond the scope of our computations, which intend to offer a qualitative analysis and trends with respect to reactive warheads. In addition, the use of small fragments assumes that the warheads are properly positioned to form a reversible covalent bond. Adding groups to these fragments certainly modulates these optimal alignments hence the K_i. Finally, we observed that association rate of **2.10a** showed a significant temperature dependence, which we attribute to the large conformational rearrangement of POP that accompanies ligand binding,[43] a motion not considered when computationally binding fragments.

It should be noted that the objective of this research is to define whether a covalent bond is possible (covalent druggability) and which warhead would be optimal but not whether a given molecule is to be a strong inhibitor.

Although the computational trends match the experimental trends, the computed low energy barriers for the aldehyde and boronic acid contrast with the commonly reported slow covalent binding step (Figure 2.3a). One such disagreement between computations and experiment exists for compound **2.15a/b**. A closer look at the models revealed that the preferred conformation (pseudo-axial fluorine) cannot geometrically form the covalent bond and must rearrange into the less energetically favored pseudo-equatorial conformation. We and others have previously found

that fluorine atoms have major control on five-membered ring conformations.[42] This phenomenon was also observed in FAP by Jansen *et al*., with inhibitors bearing the *cis*-fluorine as in **2.14c** exhibiting potency two orders of magnitude greater than those bearing the *trans*-fluorine as in **2.15c**.[29] Computations of binding energies (from dissociated complexes to covalently bound complexes) suggests that POP binds these fluorinated proline mimics more tightly than FAP. As discussed above, this apparent discrepancy between experimental and computational results stems from the use of ideally positioned fragments used in the computational investigations of the covalent bond formation which experimentally do not inhibit the enzymes vs. the larger molecules used in the *in vitro* assays.

By means of progress curve analyses and rapid dilution experiments, relevant parameters such as the K_i (affinity constant of the non-covalent component of binding), the K_i* (affinity of the second step of inhibition), k_{on} (association rate) and k_{off} (dissociation rate) were experimentally determined (Table 2.1). As a control experiment, Cbz-Pro-prolinal (**2.1**) was first investigated, and the data obtained was in agreement with a previous report.[31] The results for our designed inhibitors confirmed that the intrinsic reactivity of the warhead of the covalent inhibitor greatly influenced the on- and off-rates of ligand binding. The boronic ester inhibitor (**2.12a**) displayed the slowest on-rate of inhibition (k_{on}). As discussed above, hydrolysis of the boronic ester was an additional factor in the on-rate of inhibition.[44-45] Similarly, aldehyde **2.10a**, although displaying significantly faster on-rates than boronic ester **2.12a**, interacted relatively slowly compared to nitrile **2.5a**, where no slow-binding was detected. The relatively slow binding of the aldehyde-containing inhibitor was attributed to the presence of a pre-existing equilibrium in aqueous solution of an active aldehyde form and an inactive hydrate form of the ligand, while no such equilibrium exists with nitriles. While fast binding was predicted when covalent bond formation was computed (k_2 in Figure 2.3a), k_{on} measures the entire two-step process.

In agreement with the computations, aldehydes and boronic acids have the longest residence times. Experimentally, our aldehyde compound **2.10a** has a residence time 20 minutes shorter than that of Cbz-Pro-prolinal (**2.1**). In contrast, boronic ester **2.12a** displayed nearly a four-fold longer residence time, rationalized by the additional stabilizing interactions of the resultant boronic acid hydroxyl groups with residues in the active site of POP, as proposed by docking and QM studies (Figure 2.5b, c). Nitrile inhibitor **2.5a** displayed a very short residence time, despite bearing the same scaffold as **2.12a** and **2.10a**, correlating with the low E_{off} computed in POP. These short

residence times may also result from **2.5a** binding non-covalently as suggested by the small difference in energy between covalently bound and non-covalently bound complexes (Table 2.2). From the experimental data, we can conclude that the nitrile does not provide a strong enough covalent adduct needed to maintain a longer-bound time in POP, which is in agreement with the computations. As discussed above, covalent ligand-protein complexes of both **2.12a** and **2.10a** with POP exhibit a tetrahedral geometry, resembling that of the transition state geometry formed by the enzyme while carrying out its peptidase activity. In contrast, the covalent complex resulting from reaction with nitrile **2.5a** exhibits a trigonal planar geometry (Figure 2.3d).

The computations suggested that the pre-orientation of the ligand by the tyrosine facilitates rapid bond formation and, coupled to the small activation barrier, that the covalent binding step may be very fast (**Figure 2.8**). This prediction is supported by kinetic results we recently obtained for a related scaffold in which addition of a nitrile warhead actually led to a moderate increase in the binding rate compared to the equivalent non-covalent inhibitor.[46] In contrast, the association rate for the covalent inhibitor would be lower than that of the non-covalent analogue if bond formation were indeed rate-limiting.

The correlation between computations and experiments provides validation for the QCCA method's ability to predict the overall trends in binding kinetics in POP for covalent ligands and gave us confidence in the data for FAP, an enzyme which is extremely difficult to express and handle experimentally. Our computations indicate that the binding of our truncated nitrile ligands to FAP should have greater E_{on} and smaller E_{off} likely rendering it less active, while the aldehyde and boronic acid remain reactive enough to inhibit the enzyme. This prediction is consistent with our literature survey, which revealed that although many POP inhibitors feature a nitrile, most potent FAP inhibitors feature a boronic acid or an activated nitrile (Figure 2.1). The computations were also in agreement with our experimental data on FAP inhibitory activity of compound **2.5a** (20% inhibition at 100 μM) and compound **2.10a** (80% inhibition at 100 μM), although the large bicyclic core of our inhibitor may also hinder binding to FAP.

2.5 Conclusion

In conclusion, this study aimed to streamline the investigation of two covalently druggable targets using computational methods to provide a better understanding of experimentally-obtained thermodynamic and kinetic factors involved in their covalent inhibition and to further study the factors controlling general covalent drug potency. With POP, an enzyme which can easily be expressed and purified, experimental and computational data were in excellent agreement and revealed that the commonly held belief that covalent bond formation is rate limiting for covalent inhibitors does not necessarily stand when highly reactive enzyme residues and/or inhibitors are involved. Our validated computational protocol then rationalized the wide use of boronic acids in FAP inhibition versus the more commonly used nitrile in POP inhibition. The results presented here are a first step towards using computational methods to complete a larger study of covalent binding kinetics, a concept which is entirely unaccounted for in current computational prediction tools such as molecular docking. The ability to integrate kinetic data into prediction tools will improve the ability to rank ligands shown to be active.

Our collaborative approach to this model system aims to facilitate future covalent drug discovery endeavors. By applying our computational methods to predict the relative reactivity of a newly-discovered target's catalytic residue, biologists and chemists can determine whether the target is covalently druggable and therefore more efficiently design the most promising drug candidates. These predictions will, in the long run, save valuable time and resources in the very costly drug discovery and development processes.

2.6 Experimental

2.6.1 Chemistry

2.6.1.1 General information.

All commercially available reagents were used without further purification unless otherwise stated. The 4 Å molecular sieves were dried at 100°C prior to use. FTIR spectra were recorded using a Perkin-Elmer Spectrum One FT-IR. ^{1}H and ^{13}C NMR spectra were recorded on Varian Mercury 400 MHz, Varian 300 MHz, Unity 500 MHz, Bruker 400 MHz, or Bruker 500 MHz spectrometers. Chemical shifts are reported in ppm using the residual of deuterated solvents as internal standard. Thin layer chromatography visualization was performed by UV or by development using $KMnO_4$, H_2SO4/MeOH, Mo/Ce, or CAM solutions. Chromatography was performed on silica gel 60 (230-40 mesh) or using Biotage Isolera One purification system with ZIP cartridges. Low resolution mass spectrometry was performed by ESI using a Thermoquest Finnigan LCQ Duo. High resolution mass spectrometry was performed by EI peak matching (70 eV) on a Kratos MS25 RFA double focusing mass spectrometer or by ESI on a Ion Spec 7.0 T FTMS at McGill University.

2.6.1.2 Purity determination by High Performance Liquid Chromatography (HPLC)

Prior to biological testing, reverse-phase HPLC was used to verify the purity of compounds on an Agilent 1100 series instrument, equipped with VWD-detector, using a C18 reverse column (Agilent, Eclipse C18 150 mm Å~ 4.6 mm, 5 μm) with UV detection at 254 nm. All biologically tested compounds were determined to be > 95% pure. The solvents used were H_2O (A) and either MeCN or MeOH (B) in a gradient. Retention times and purities are provided for each compound.

Method A: H_2O (A) and MeOH (B); t = 0 mins, 95% A / 5% B; t = 3 to 20 mins, gradually to 5% A / 95% B; t = 20 to 25 mins, 5% A / 95% B; t = 25 to 28 mins, gradually to 95% A / 5% B; t = 28 to 30 mins, 95% A / 5% B.

Method B: H_2O (A) and MeCN (B); t = 0 mins, 95% A / 5% B; t = 5 to 15 mins, gradually to 5% A / 95% B; t = 15 to 20 mins, 5% A / 95% B; t = 20 to 28 mins, gradually to 95% A / 5% B; t = 28 to 30 mins, 95% A / 5% B.

2.6.1.3 Synthesis

General Procedure for peptidic coupling. The carboxylic acid **2.18** (1 eq) was suspended in anhydrous DCM (0.1 M) under argon atmosphere, and Et_3N (5 eq) was added. The resultant solution was cooled to 0°C, and pivaloyl chloride (1.1 eq) was added. After 1 h of stirring at 0°C,

the amine (1.1 eq) was added, and the reaction stirred at room temperature overnight. Water was added, and the product was extracted with EtOAc or with DCM (depending on the amount of original DCM solvent). The combined organic layers were washed with 1 M HCl, saturated $NaHCO_3$, and brine, dried over Na_2SO_4, filtered, and concentrated *in vacuo*. The crude residue was purified by flash chromatography on a silica gel column to give the product. Residues were triturated in hexanes and/or Et_2O and filtered under vacuum to give solids.

2-benzyl-7-(pyrrolidine-1-carbonyl)isoindolin-1-one (2.4a) Compound **2.4a** was synthesized following the general procedure for peptidic coupling, using pyrrolidine as the corresponding amine (40%). ^{1}H NMR (500 MHz, Chloroform-*d*) δ 7.52 (t, *J* = 7.6 Hz, 1H), 7.37 (dd, *J* = 7.5, 1.7 Hz, 2H), 7.34 – 7.25 (m, 5H), 4.97 – 4.80 (m, 1H), 4.73 – 4.50 (m, 1H), 4.24 (s, 2H), 3.92 – 3.75 (m, 1H), 3.75 – 3.59 (m, 1H), 3.42 – 3.20 (m, 1H), 3.17 – 2.99 (m, 1H), 2.06 – 1.73 (m, 4H); ^{13}C NMR (126 MHz, Chloroform-*d*) δ 24.61, 26.01, 45.70, 46.48, 48.25, 49.33, 123.34, 126.22, 127.85, 128.28, 128.39 (2C), 128.91 (2C), 131.80, 135.51, 136.94, 141.76, 166.88, 167.02. Spectral and experimental data previously published by our group.[13] HPLC (Method B) t_R = 12.7 min, 99.5%.

1-(2-benzyl-3-oxoisoindoline-4-carbonyl)pyrrolidine-2-carbonitrile (2.5a) Compound **2.5a** was synthesized following the general procedure for peptidic coupling, using (*S*)-pyrrolidine-2-carbonitrile pTsOH salt as the corresponding amine (92%). ^{1}H NMR (400 MHz, Acetone-d_6) δ 7.70 – 7.48 (m, 2H), 7.47 – 7.38 (m, 1H), 7.37 – 7.13 (m, 5H), 5.03 – 4.54 (m, 3H), 4.41 (s, 2H), 3.79 – 3.66 (m, 0.5H), 3.38 – 3.17 (m, 1.5H), 2.48 – 2.34 (m, 1H), 2.34 – 2.21 (m, 1H), 2.21 – 2.07 (m, 1H), 2.04 – 1.96 (m, 1H); ^{13}C NMR (101 MHz, Acetone-d_6) δ 25.75, 29.84, 31.25, 46.56, 47.04, 48.58, 50.05, 119.70, 125.15, 126.83, 128.31, 128.84 (2C), 129.11, 129.55 (2C), 132.54, 134.47, 138.48, 143.32, 167.22, 167.88. Spectral and experimental data previously published by our group.[13] HPLC (Method A) t_R = 16.7 min, 99.7%.

***(S)*-1-(2-benzyl-3-oxoisoindoline-4-carbonyl)pyrrolidine-2-carbaldehyde (2.10a)**. Oxalyl chloride (108 mg, 1.2 eq) was dissolved in DCM (3 mL), and the solution was cooled to –78°C. DMSO (139 mg, 2.5 eq, in DCM, 2 mL) was added dropwise, and the solution stirred for 2 minutes. **2.20** (250 mg, 1 eq, in 2 mL DCM) was added dropwise, and the solution stirred for 15 minutes. Et_3N (361 mg, 5 eq) was added, and the solution stirred for 15 minutes. Water was added, and the mixture was warmed to room temperature. The product was extracted with EtOAc, and the combined organic layers were washed with brine, dried over Na_2SO_4, filtered, and concentrated in

vacuo to give an orange oil, which was purified by flash chromatography on a silica gel column (eluent 100% EtOAc) to give the product as a white solid (100 mg, 40%). R_f 0.30 (100% EtOAc); IR (film) ν_{max} (cm^{-1}) 3387, 3006, 1675, 1626, 1601, 1434; ^1H NMR (500 MHz, Acetone-d_6) δ 10.13 – 9.17 (m, 1H), 7.76 – 7.20 (m, 8H), 4.94 – 4.58 (m, 2H), 4.56 – 4.18 (m, 3H), 3.91 – 3.11 (m, 2H), 2.29 – 2.09 (m, 1H), 2.02 – 1.76 (m, 3H); ^{13}C NMR (126 MHz, Acetone-d_6) δ 26.05, 27.59, 46.56, 49.28, 50.01, 65.74, 124.86, 126.43, 128.31, 128.83 (2C), 129.54, 129.56 (2C), 132.49, 135.22, 138.54, 143.36, 167.38, 167.98, 202.63; HRMS (ESI+): calculated for $[C_{21}H_{20}N_2O_3 + H]^+$, 349.15467; found, 349.15418; HPLC (Method B) t_R = 12.7 min, 73.4%; t_R = 1.5 min, 23.4%.

2-benzyl-7-((*R*)-2-((3a*R*,4*R*,6*R*,7a*S*)-3a,5,5-trimethylhexahydro-4,6-methanobenzo[*d*][1,3,2] dioxaborol-2-yl)pyrrolidine-1-carbonyl)isoindolin-1-one (2.12a). Compound **2.12** was synthesized following the general procedure for peptidic coupling, using **2.19** as the corresponding amine. The crude residue was purified using (1:1 EtOAc/hexanes) as the eluent system (43%, white foam); IR (film) ν_{max} (cm^{-1}) 3225, 2922, 1686, 1606, 1451; ^1H NMR (500 MHz, Chloroform-*d*) δ 7.52 (t, *J* = 7.6 Hz, 1H), 7.42 (d, *J* = 7.5 Hz, 1H), 7.37 (d, *J* = 7.6 Hz, 1H), 7.35 – 7.26 (m, 5H), 4.84 (d, *J* = 14.8 Hz, 1H), 4.68 (d, *J* = 14.8 Hz, 1H), 4.39 (dd, *J* = 8.9, 2.2 Hz, 1H), 4.25 – 4.19 (m, 2H), 3.47 (dt, *J* = 9.2, 6.3 Hz, 1H), 3.42 – 3.31 (m, 1H), 3.22 (dd, *J* = 17.3, 7.9 Hz, 1H), 2.41 – 2.12 (m, 3H), 2.09 (t, *J* = 5.5 Hz, 1H), 2.01 – 1.85 (m, 5H), 1.61 (d, *J* = 10.9 Hz, 1H), 1.45 (s, 3H), 1.29 (s, 3H), 0.86 (s, 3H); ^{13}C NMR (126 MHz, Chloroform-*d*) δ 24.28, 26.43, 27.29, 27.30, 27.33, 28.92, 35.82, 38.39, 39.79, 44.60, 46.53, 48.15, 49.31, 51.57, 78.08, 86.04, 123.60, 127.03, 127.84, 128.42 (2C), 128.67, 128.92 (2C), 128.95, 131.65, 137.08, 141.75, 166.58, 166.69; ^{11}B NMR (161 MHz, Chloroform-*d*) δ 32.45; HRMS (ESI+): calculated for $[C_{30}H_{35}B_1N_2O_4 + H]^+$, 499.27736; found, 499.27634; HPLC (Method A) t_R = 1.5 min, 94.5%.

(*S*)-1-(2-benzyl-3-oxoisoindoline-4-carbonyl)-4,4-difluoropyrrolidine-2-carbonitrile (2.13a) Compound **2.13a** was synthesized following the general procedure for peptidic coupling, using **2.21** as the corresponding amine. The crude residue was purified using 3:1 EtOAc/hexanes as the eluent system (35%, white solid); (R_f = 0.53; 3:1 EtOAc/hexanes); IR (film) ν_{max} (cm^{-1}) 2918, 2850, 1666, 1604, 1411, 1108; ^1H NMR (400 MHz, Acetone-d_6) δ 7.80 – 7.60 (m, 2H), 7.63 – 7.40 (m, 1H), 7.38 – 7.21 (m, 5H), 5.37 (dd, *J* = 9.4, 3.1 Hz, 1H), 4.91 – 4.66 (m, 2H), 4.44 (s, 2H), 4.30 – 3.97 (m, 0.5H), 3.88 – 3.57 (m, 1.5H), 3.23 – 2.98 (m, 1H), 2.98 – 2.83 (m, 1H); ^{13}C NMR (101 MHz, Acetone-d_6) δ 167.86, 167.21, 143.51, 138.43, 132.97, 132.82, 129.58 (2C),

128.95, 128.87 (2C), 128.37, 127.16, 125.83, 118.09, 54.33 (t, *J* = 31.8 Hz), 50.22, 46.65, 45.09, 38.47 (t, *J* = 27.7 Hz); HRMS (ESI+): calculated for $[C_{21}H_{17}F_2N_3O_2 + H]^+$, 382.13616; found, 382.13599; HPLC (Method B) t_R = 14.0 min, 99.1%.

(2*S*,4*S*)-1-(2-benzyl-3-oxoisoindoline-4-carbonyl)-4-fluoropyrrolidine-2-carbonitrile (14a) Compound **14a** was synthesized following the general procedure for peptidic coupling, using **2.22** as the corresponding amine. The crude residue was purified using 100% EtOAc as the eluent system (30%, white solid); *R_f*: 0.18 (100% EtOAc); IR (film) ν_{max} (cm^{-1}) 3012, 2920, 1682, 1653, 1605, 1409, 1212; ^{1}H NMR (500 MHz, Chloroform-*d*) δ 7.72 – 7.41 (m, 3H), 7.40 – 7.20 (m, 5H), 5.58 – 5.18 (m, 1.6H), 4.87 (dd, *J* = 18.8, 14.9 Hz, 1H), 4.70 – 4.52 (m, 1.4H), 4.40 – 4.20 (m, 2H), 4.20 – 4.02 (m, 1H), 3.79 – 3.45 (m, 1H), 2.78 – 2.49 (m, 2H); *Carbon peaks reported for both rotamers*. ^{13}C NMR (126 MHz, $CDCl_3$) δ ^{13}C NMR (126 MHz, $CDCl_3$) δ 167.66, 167.64, 166.91, 166.89, 141.77 (2C), 136.47, 136.38, 132.69, 132.66, 132.49, 132.38, 129.10 (2C), 129.07 (2C), 128.33 (2C), 128.27 (2C), 128.15, 128.10, 127.53 (2), 126.89 (2C), 124.74, 124.53, 117.93 (2C), 92.32 (d, *J* = 111.2 Hz), 90.83 (d, *J* = 122.6 Hz), 54.23 (d, *J* = 23.5 Hz), 53.27 (d, *J* = 23.7 , 49.77, 49.63, 47.12, 46.67, 46.60, 44.97, 38.40, 38.32 (d, *J* = 20.3 Hz), 36.59 (d, *J* = 21.2 Hz); HRMS (ESI+): calculated for $[C_{21}H_{18}FN_3O_2 + H]^+$, 364.14558; found, 364.14500; HPLC (Method A) t_R = 16.0 min, 96.3%.

(2*S*,4*R*)-1-(2-benzyl-3-oxoisoindoline-4-carbonyl)-4-fluoropyrrolidine-2-carbonitrile (2.15) Compound **2.15a** was synthesized following the general procedure for peptidic coupling, using **2.23** as the corresponding amine. The crude residue was purified using 1:1 EtOAc/hexanes as the eluent system (30%, white solid); (*R_f* = 0.1; 1:1 EtOAc/hexanes); IR (film) ν_{max} (cm^{-1}) 3008, 2920, 1686, 1648, 1603, 1413, 1205; ^{1}H NMR (400 MHz, Acetone-d_6) δ 8.38 – 7.55 (m, 2H), 7.52 – 7.24 (m, 6H), 5.36 (dt, *J* = 52.2, 3.7 Hz, 1H), 5.15 – 4.65 (m, 3H), 4.55 – 4.17 (m, 2H), 3.96 – 3.43 (m, 2H), 2.99 – 2.83 (m, 1H), 2.75 – 2.52 (m, 1H); ^{13}C NMR (101 MHz, Acetone) δ 167.78, 166.90, 143.46, 138.53 (2C), 133.90, 132.52, 129.56 (2C), 128.87 (2C), 128.31, 127.79, 125.61, 118.79, 92.22 (d, *J* = 178.0 Hz), 54.93 (d, *J* = 22.1 Hz), 49.99, 46.59, 45.40, 37.61 (d, *J* = 22.3 Hz); HRMS (ESI+): calculated for $[C_{21}H_{18}F_1N_3O_2 + H]^+$, 364.14558; HPLC (Method B) t_R = 13.2 min, 95.1%.

(*S*)-2-benzyl-7-(3-fluoropyrrolidine-1-carbonyl)isoindolin-1-one (2.16a) / (*R*)-2-benzyl-7-(3-fluoropyrrolidine-1-carbonyl)isoindolin-1-one (2.17a) Compounds **2.16a/2.17a** were synthesized following the general procedure for peptidic coupling, using **2.14/2.25** as the

corresponding amines. The crude residues were purified using 100% EtOAc as the eluent system (90%/90%, white solids); *As they are enantiomers, they gave identical spectral properties*. R_f: 0.18 (100% EtOAc); IR (film) νmax (cm^{-1}) 3005, 1682, 1627, 1607, 1433, 1206; ^{1}H NMR (500 MHz, Chloroform-*d*) δ 7.54 (td, *J* = 7.5, 2.6 Hz, 1H), 7.40 (t, *J* = 7.5 Hz, 2H), 7.34 – 7.22 (m, 5H), 5.26 (ddt, *J* = 82.8, 52.9, 3.9 Hz, 1H), 4.87 – 4.56 (m, 2H), 4.32 – 4.19 (m, 2H), 4.15 – 3.75 (m, 2H), 3.63 – 3.32 (m, 2H), 2.46 – 2.03 (m, 2H); *Carbon peaks reported for both rotamers*. ^{13}C NMR (126 MHz, $CDCl_3$) δ 167.31, 167.27, 166.83, 166.79, 141.82, 141.76, 136.81, 136.75, 134.59, 134.57, 131.99, 131.87, 128.92 (2C), 128.90 (2C), 128.34 (2C), 128.31 (2C) 128.20 (2C), 127.89, 127.86, 126.55 (2C), 126.28 (2C), 123.75, 123.68, 92.80 (d, *J* = 177.7 Hz), 92.06 (d, *J* = 175.3 Hz), 54.31 (d, *J* = 23.1 Hz), 52.50 (d, *J* = 23.7 Hz), 49.37, 46.47, 45.90, 43.60, 32.83 (d, *J* = 21.6 Hz), 31.28 (d, *J* = 21.5 Hz); HRMS (ESI+): calculated for $[C_{20}H_{19}FN_2O_2 + Na]^+$, 361.1323; found, 361.132; HPLC **2.16a** (Method B) t_R = 12.6 min, 97.8%; **2.17a** (Method B) t_R = 12.7 min, 96.5%.

(*S*)-2-benzyl-7-(2-(hydroxymethyl)pyrrolidine-1-carbonyl)isoindolin-1-one (2.20). Compound **2.20** was synthesized following the general procedure for peptidic coupling, using L-prolinol as the corresponding amine. The crude residue was purified using 100% EtOAc as the eluent system (87%, white solid); (R_f = 0.15; 100% EtOAc); IR (film) ν_{max} (cm^{-1}) 3434, 2943, 1671, 1624, 1602, 1432; ^{1}H NMR (500 MHz, Chloroform-*d*) δ 7.56 (t, *J* = 7.6 Hz, 1H), 7.42 (t, *J* = 8.0 Hz, 2H), 7.36 – 7.31 (m, 2H), 7.31 – 7.25 (m, 3H), 4.91 – 4.76 (m, 2H), 4.74 – 4.59 (m, 2H), 4.35 (t, *J* = 7.7 Hz, 1H), 4.33 – 4.22 (m, 2H), 3.50 (t, *J* = 11.2 Hz, 1H), 3.29 (td, *J* = 9.7, 6.8 Hz, 1H), 3.13 (ddd, *J* = 10.7, 7.8, 3.5 Hz, 1H), 2.26 – 2.15 (m, 1H), 2.16 – 2.08 (m, 1H), 2.04 – 1.93 (m, 1H), 1.82 – 1.69 (m, 1H); ^{13}C NMR (126 MHz, Chloroform-*d*) δ 25.09, 27.56, 46.56, 49.30, 50.08, 59.46, 62.21, 77.16, 123.61, 125.90, 127.78, 127.91, 128.36 (2C), 128.93 (2C), 132.07, 135.46, 136.57, 141.90, 166.51, 167.01; HRMS (ESI+): calculated for $[C_{21}H_{22}N_2O_3 + Na]^+$, 373.15226; found, 373.15174; HPLC (Method B) t_R = 11.5 min, 19.7%; t_R = 12.5 min, 80.2%.

2.6.2 Mass Spectroscopy study of the hydrolysis of the boronic ester

The stability of boronic ester **2.12a** in buffer was assessed by mass spectroscopy using a Dionex Ultimate 3000 UHPLC coupled to a Bruker Maxis Impact QTOF in positive ESI mode. A 0.1 mL sample of **2.12a** in DMSO (100 mM stock) was added to 0.9 mL of buffer in a septum capped vial and placed in the Ultimate 3000 autosampler. At 5 minute intervals, a 1 µL aliquot of the mixture was injected into the QTOF by loop injection at a flow rate of 0.1 mL/min in a mobile

phase consisting of a 1:1 mixture of water and acetonitrile and 0.1% formic acid. The data was processed using the Bruker DataAnalysis software version 4.2.

2.6.3 Biological assays and biophysical characterization.

2.6.3.1 FAP Assay.

The FAP assay was performed using the FAP Assay Kit from BPS BioScience.[47]

2.6.3.2 POP Protein Expression

POP was expressed and purified according to a procedure previously described.[48]

2.6.3.3 POP Activity Assays

The colorimetric substrate ZGP-pNA was obtained from Bachem (Bubendorf, Switzerland). IC_{50} / K_i measurements were carried out as follows. The reactions were performed in micro titer plates of 96 wells. For each reaction, activity buffer (A.B.) (140 µL, sodium phosphate 20 mM, NaCl 150 mM, β-mercaptoethanol 5 mM, EDTA 2 mM, 10% glycerol, 0.5 mg/mL BSA, pH=8) was pre-incubated for 30 min at 30°C with hPOP (20 µL, 10 nM in A.B., final concentration of 1 nM) and with the corresponding inhibitor solution (20 µL) or A.B. (controls). Stock inhibitors were prepared in DMSO (100 mM); dilutions for inhibitor evaluation were prepared from the stock in A.B. A control experiment with the same DMSO concentration was performed. After pre-incubation, ZGP-pNA (20 µL, 0.8 mM in A.B., final concentration of 80 µM) was added and formation of the product was followed by absorbance at 405 nm every 30 sec. Initial velocity was measured for each concentration of inhibitor and compared to the initial velocity of reactions that did not contain inhibitor. The IC_{50} value was defined as the inhibitor concentration causing a 50 % decrease in activity. The K_i was defined as $IC_{50}/(1+([S]/K_m))$. K_m of the substrate has been measured by monitoring the initial velocity of the enzymatic reaction of 1 nM of hPOP with various concentrations of substrate. Data obtained were: K_m = 74.6 µM; k_{cat} = 20.56 s^{-1}.

2.6.3.4 Progress curves

The reactions were performed in micro titer plates of 96 wells. For each reaction, 140 µL of A.B. was added, followed by 20 µL of hPOP (10 nM in A.B.). After 15 min of equilibration at 30°C, 20 µL of inhibitor solution was added (different concentrations were prepared by serial dilution from an original 0.1 M stock in DMSO that was kept at -80°C). Directly afterwards, 20 µL of a 800 µM substrate solution (30% MeCN in A.B.). Once substrate was added, the absorbance at 405 nm was recorded every 30 sec. during a period of time ranging from 2 h to 5 h depending on the inhibitor. Data were then fitted to the corresponding in order to extract k_{obs}. These values

were further plotted against inhibitor concentration used and the data fitted to the corresponding equations in order to retrieve kinetic parameters.

2.6.3.5 Dilution experiment

Inhibitor at a concentration of 100xK_i was pre-incubated with 200 nM of hPOP in A.B. for 2 h at 30°C. Rapid serial dilutions (two times 40-fold dilution for a total of 1600-fold) were made with a substrate-containing buffer (Substrate concentration = 80 μM) pre-equilibrated at 30°C. Final concentrations of inhibitor were 0.06xK_i and the concentration of enzyme was 0.125 nM. The absorbance at 405 nm was immediately recorded every 30 sec for the first 60 minutes followed by every 2 minutes for the next 5 h. Data were then fitted to the corresponding equations in order to extract k_{off}.

2.6.4 Computational Chemistry.

2.6.4.1 Preparation of the initial systems.

The crystal structures for POP and FAP - 2xdw (POP bound to an aldehyde-containing inhibitor), 4an0 (POP bound to a nitrile-containing inhibitor), 4bcb (POP bound to a nitrile-containing inhibitor) and 1z68 (FAP unbound) were downloaded from the PDB. The six ligands (**2.5b**, **2.10b**, **2.11b**, **2.13b**-**2.15b**) were docked covalently to 2xdw and 1z68 using our docking program Fitted.[49] These crystal structures and docked poses were used to build starting structures. For example, docked poses in POP are similar to the crystal structure with the proline ring properly positioned. However, the stereochemistry of the acetal (from **2.10b**) and the orientation of the iminoether (from **2.5b**) are inexact and are repositioned to generate starting structures. Then the FAP structure (1z68) was superposed onto POP (2xdw) and the ligands added to FAP as docked in POP. Considering the rigidity of the aldehyde-containing small molecule and the similarity between the FAP and POP catalytic triad and oxy-anion hole, the binding mode is very likely similar.

The proteins were next truncated; the starting structures are provided as xyz coordinates (mol2 format). For POP the following residues were kept: Asp149, Tyr473, Ser554, Asn555 (backbone NH), Trp595, Asp641, Arg643 and His680; for FAP: Arg123, Glu203, Tyr541, Ser624, Tyr625 (backbone NH), Tyr656, Asp702 and His734. To ensure that all the hot spots are removed, the systems were relaxed according to the following procedure:

- Hydrogens were optimized (AM1) with all heavy atoms frozen.
- The inhibitors were optimized (AM1) with all the protein heavy atoms frozen.

- The complexes were optimized (PBE0/def2-SVP) with only the α and β carbons of the amino acids frozen (quantum chemical cluster approach).

2.6.4.2 Potential energy surface scans.

One dimensional potential energy surface (PES) scans were performed in ORCA v.4.0.1.2[50] at the PBE0/def2-SVP level of theory on the optimized structures obtained as described above. The coordinate for the scans was the Ser(O)-warhead(C) distance – 13 points were recorded for each scan. For each system the α and β carbons of the amino acids were frozen, while the remaining atoms were allowed to move freely. For each system the bound minima, the maxima (if applicable) and the unbound minima were subjected to single point energy calculations at the PBE0/D3BJ/def2-TZVP level of theory. To simulate the unbound states, optimizations were carried on the separate partners (truncated proteins and ligands) at the PBE0/def2-SVP level of theory. Single point energies calculations were then performed on the separated partners in gas phase at the PBE0/def2-TZVP/D3BJ level of theory.

2.7 References

(1) Bauer, R. A., Covalent inhibitors in drug discovery: from accidental discoveries to avoided liabilities and designed therapies. *Drug Discov Today* **2015,** *20* (9), 1061-1073.

(2) Singh, J.; Petter, R. C.; Baillie, T. A.; Whitty, A., The resurgence of covalent drugs. *Nat Rev Drug Discov* **2011,** *10* (4), 307-317.

(3) De Cesco, S.; Kurian, J.; Dufresne, C.; Mittermaier, A. K.; Moitessier, N., Covalent inhibitors design and discovery. *Eur J Med Chem* **2017,** *138*, 96-114.

(4) Powers, J. C.; Asgian, J. L.; Ekici, Ö. D.; James, K. E., Irreversible Inhibitors of Serine, Cysteine, and Threonine Proteases. *Chem Rev* **2002,** *102* (12), 4639-4750.

(5) Szeltner, Z.; Polgar, L., Structure, function and biological relevance of prolyl oligopeptidase. *Curr Protein Pept Sci* **2008,** *9* (1), 96-107

(6) Mannisto, P. T.; Vanalainen, J.; Jalkanen, A.; Garcia-Horsman, J. A., Prolyl oligopeptidase: A potential target for the treatment of cognitive disorders. *Drug News Perspect* **2007,** *20* (5), 293-305.

(7) Brandt, I.; Scharpe, S.; Lambeir, A. M., Suggested functions for prolyl oligopeptidase: A puzzling paradox. *Clin. Chim. Acta* **2007,** *377* (1-2), 50-61.

(8) Lawandi, J.; Gerber-Lemaire, S.; Juillerat-Jeanneret, L.; Moitessier, N., Inhibitors of prolyl oligopeptidases for the therapy of human diseases: Defining diseases and inhibitors. *J Med Chem* **2010,** *53* (9), 3423-3438

(9) Santos, A. M.; Jung, J.; Aziz, N.; Kissil, J. L.; Puré, E., Targeting fibroblast activation protein inhibits tumor stromagenesis and growth in mice. *J Clin Invest* **2009,** *119* (12), 3613-3625.

(10) Liao, D.; Luo, Y.; Markowitz, D.; Xiang, R.; Reisfeld, R. A., Cancer associated fibroblasts promote tumor growth and metastasis by modulating the tumor immune microenvironment in a 4T1 murine breast cancer model. *PLoS ONE* **2009,** *4* (11).

(11) Hamson, E. J.; Keane, F. M.; Tholen, S.; Schilling, O.; Gorrell, M. D., Understanding fibroblast activation protein (FAP): Substrates, activities, expression and targeting for cancer therapy. *Proteomics Clin Appl* **2014,** *8* (5-6), 454-463.

(12) Teichgra, V.; Monasterio, C.; Chaitanya, K.; Boger, R.; Gordon, K.; Dieterle, T.; Jager, D.; Bauer, S., Specific inhibition of fibroblast activation protein (FAP)-alpha prevents tumor progression in vitro. *Adv Med Sci* **2015,** *60*, 264-272.

(13) De Cesco, S.; Deslandes, S.; Therrien, E.; Levan, D.; Cueto, M.; Schmidt, R.; Cantin, L. D.; Mittermaier, A.; Juillerat-Jeanneret, L.; Moitessier, N., Virtual screening and computational optimization for the discovery of covalent prolyl oligopeptidase inhibitors with activity in human cells. *J Med Chem* **2012,** *55* (14), 6306-6315.

(14) Jöst, C.; Nitsche, C.; Scholz, T.; Roux, L.; Klein, C. D., Promiscuity and selectivity in covalent enzyme inhibition: a systematic study of electrophilic fragments. *J Med Chem* **2014,** *57* (18), 7590-7599.

(15) Potashman, M. H.; Duggan, M. E., Covalent modifiers: an orthogonal approach to drug design. *J Med Chem* **2009,** *52* (5), 1231-1246.

(16) Flanagan, M. E.; Abramite, J. A.; Anderson, D. P.; Aulabaugh, A.; Dahal, U. P.; Gilbert, A. M.; Li, C.; Montgomery, J.; Oppenheimer, S. R.; Ryder, T.; Schuff, B. P.; Uccello, D. P.; Walker, G. S.; Wu, Y.; Brown, M. F.; Chen, J. M.; Hayward, M. M.; Noe, M. C.; Obach, R. S.; Philippe, L.; Shanmugasundaram, V.; Shapiro, M. J.; Starr, J.; Stroh, J.; Che, Y., Chemical and computational methods for the characterization of covalent reactive groups for the prospective design of irreversible inhibitors. *J Med Chem* **2014,** *57* (23), 10072-10079.

(17) Palazzesi, F.; Grundl, M. A.; Pautsch, A.; Weber, A.; Tautermann, C. S., A fast ab initio predictor tool for covalent reactivity estimation of acrylamides. *J Chem Inf Model* **2019**.

(18) Zhao, Z.; Liu, Q.; Bliven, S.; Xie, L.; Bourne, P. E., Determining Cysteines Available for Covalent Inhibition Across the Human Kinome. *J Med Chem* **2017,** *60* (7), 2879-2889.

(19) Weerapana, E.; Wang, C.; Simon, G. M.; Richter, F.; Khare, S.; Dillon, M. B.; Bachovchin, D. A.; Mowen, K.; Baker, D.; Cravatt, B. F., Quantitative reactivity profiling predicts functional cysteines in proteomes. *Nature* **2010,** *468* (7325), 790-5.

(20) Awoonor-Williams, E.; Rowley, C. N., How reactive are druggable cysteines in protein kinases? *J Chem Inf Model* **2018,** *58* (9), 1935-1946.

(21) Wang, H.; Chen, X.; Li, C.; Liu, Y.; Yang, F.; Wang, C., Sequence-based prediction of cysteine reactivity using machine learning. *Biochemistry* **2018,** *57* (4), 451-460.

(22) Soylu, İ.; Marino, S. M., Cy-preds: an algorithm and a web service for the analysis and prediction of cysteine reactivity. *Prot Struct Funct Bioinf* **2016,** *84* (2), 278-291.

(23) Chatterjee, P.; Botello-Smith, W. M.; Zhang, H.; Qian, L.; Alsamarah, A.; Kent, D.; Lacroix, J. J.; Baudry, M.; Luo, Y., Can relative binding free energy predict selectivity of reversible covalent inhibitors? *J Am Chem Soc* **2017,** *139* (49), 17945-17952.

(24) Zhang, H.; Jiang, W.; Chatterjee, P.; Luo, Y., Ranking reversible covalent drugs: from free energy perturbation to fragment docking. *J Chem Inf Model* **2019,** *59* (5), 2093-2102.

(25) Zhao, Z.; Bourne, P. E., Progress with covalent small-molecule kinase inhibitors. *Drug Discov Today* **2018,** *23* (3), 727-735.

(26) Gehringer, M.; Laufer, S. A., Emerging and re-emerging warheads for targeted covalent inhibitors: applications in medicinal chemistry and chemical biology. *J Med Chem* **2019,** *62* (12), 5673-5724.

(27) Szeltner, Z.; Rea, D.; Renner, V.; Fulop, V.; Polgar, L., Electrostatic effects and binding determinants in the catalysis of prolyl oligopeptidase. Site specific mutagenesis at the oxyanion binding site. *J Biol Chem* **2002,** *277* (45), 42613-22.

(28) Kaszuba, K.; Rog, T.; Danne, R.; Canning, P.; Fulop, V.; Juhasz, T.; Szeltner, Z.; St Pierre, J. F.; Garcia-Horsman, A.; Mannisto, P. T.; Karttunen, M.; Hokkanen, J.; Bunker, A., Molecular dynamics, crystallography and mutagenesis studies on the substrate gating mechanism of prolyl oligopeptidase. *Biochimie* **2012,** *94* (6), 1398-411.

(29) Jansen, K.; Heirbaut, L.; Verkerk, R.; Cheng, J. D.; Joossens, J.; Cos, P.; Maes, L.; Lambeir, A. M.; De Meester, I.; Augustyns, K.; Van der Veken, P., Extended structure-activity relationship and pharmacokinetic investigation of (4-quinolinoyl)glycyl-2-cyanopyrrolidine inhibitors of fibroblast activation protein (FAP). *J Med Chem* **2014,** *57* (7), 3053-74.

(30) Smoum, R.; Rubinstein, A.; Dembitsky, V. M.; Srebnik, M., Boron containing compounds as protease inhibitors. *Chem Rev* **2012,** *112* (7), 4156-4220.

(31) Bakker, A. V.; Jung, S.; Spencer, R. W.; Vinick, F. J.; Faraci, W. S., Slow tight-binding inhibition of prolyl endopeptidase by benzyloxycarbonyl-prolyl-prolinal. *Biochem J* **1990,** *271* (2), 559-62.

(32) Fukushima, H.; Hiratate, A.; Takahashi, M.; Saito, M.; Munetomo, E.; Kitano, K.; Saito, H.; Takaoka, Y.; Yamamoto, K., Synthesis and structure-activity relationships of potent 3- or 4-substituted-2-cyanopyrrolidine dipeptidyl peptidase IV inhibitors. *Bioorg Med Chem* **2004,** *12* (23), 6053-61.

(33) Nelson, M.-A. M.; Baba, S. P.; Anderson, E. J., Biogenic Aldehydes as Therapeutic Targets for Cardiovascular Disease. *Curr Opin Pharmacol* **2017,** *33*, 56-63.

(34) Adams, J., The development of proteasome inhibitors as anticancer drugs. *Cancer Cell* **2003,** *5*, 417-421.

(35) Copeland, R. A., The drug-target residence time model: a 10-year retrospective. *Nat Rev Drug Discov* **2016,** *15* (2), 87-95.

(36) Copeland, R. A.; Pompliano, D. L.; Meek, T. D., Drug-target residence time and its implications for lead optimization. *Nat Rev Drug Discov* **2006,** *5* (9), 730-739.

(37) Jambunathan, K.; Watson, D. S.; Endsley, A. N.; Kodukula, K.; Galande, A. K., Comparative analysis of the substrate preferences of two post-proline cleaving endopeptidases, prolyl oligopeptidase and fibroblast activation protein α. *FEBS Lett* **2012,** *586* (16), 2507-2512.

(38) Siegbahn, P. E. M.; Himo, F., The quantum chemical cluster approach for modeling enzyme reactions. *Wiley Interdiscip Rev Comput Mol Sci* **2011,** *1* (3), 323-336.

(39) Knizia, G., Intrinsic Atomic Orbitals: An Unbiased Bridge between Quantum Theory and Chemical Concepts. *J Chem Theory Comput* **2013,** *9* (11), 4834-4843.

(40) Gomez-Jeria, J. S., A New Set of Local Reactivity Indices within the Hartree - Fock - Roothaan and Density Functional Theory Frameworks. *Can Chem Trans* **2013,** *1* (1), 25-55.

(41) Evans, M. G.; Polanyi, M., Further considerations on the thermodynamics of chemical equilibria and reaction rates. *J Chem Soc Trans Faraday Soc* **1936,** *32* (0), 1333-1360.

(42) Burai Patrascu, M.; Malek-Adamian, E.; Damha, M. J.; Moitessier, N., Accurately modeling the conformational preferences of nucleosides. *J Am Chem Soc* **2017,** *139*, 13620-13623.

(43) López, A.; Herranz-Trillo, F.; Kotev, M.; Gairí, M.; Guallar, V.; Bernadó, P.; Millet, O.; Tarragó, T.; Giralt, E., Active-Site-Directed Inhibitors of Prolyl Oligopeptidase Abolish Its Conformational Dynamics. *ChemBioChem* **2016,** *17* (10), 913-917.

(44) Kettner, C. A.; Shenvi, A. B., Inhibition of the serine proteases leukocyte elastase, pancreatic elastase, cathepsin G, and chymotrypsin by peptide boronic acids. *J Biol Chem* **1984,** *259* (24), 15106-14.

(45) Snow, R. J.; Bachovchin, W. W.; Barton, R. W.; Campbell, S. J.; Coutts, S. J.; Freeman, D. M.; Gutheil, W. G.; Kelly, T. A.; Kennedy, C. A., Studies on proline boronic acid dipeptide inhibitors of dipeptidyl peptidase IV: identification of a cyclic species containing a B-N bond. *J Am Chem Soc* **1994,** *116* (24), 10860-10869.

(46) Di Trani, J. M.; De Cesco, S.; O'Leary, R.; Plescia, J.; do Nascimento, C. J.; Moitessier, N.; Mittermaier, A. K., Rapid measurement of inhibitor binding kinetics by isothermal titration calorimetry. *Nat Commun* **2018,** *9* (1), 893.

(47) BPS Bioscience, I. FAP Assay Kit. http://bpsbioscience.com/fluorogenic-fap-assay-kit-80210 (accessed 29 Aug).

(48) Mariaule, G.; De Cesco, S.; Airaghi, F.; Kurian, J.; Schiavini, P.; Rocheleau, S.; Huskic, I.; Auclair, K.; Mittermaier, A.; Moitessier, N., 3-Oxo-hexahydro-1H-isoindole-4-carboxylic Acid as a Drug Chiral Bicyclic Scaffold: Structure-Based Design and Preparation of Conformationally Constrained Covalent and Noncovalent Prolyl Oligopeptidase Inhibitors. *J Med Chem* **2016,** *59* (9), 4221-34.

(49) Moitessier, N.; Pottel, J.; Therrien, E.; Englebienne, P.; Liu, Z.; Tomberg, A.; Corbeil, C. R., Medicinal chemistry projects requiring imaginative structure-based drug design methods. *Acc Chem Res* **2016,** *49* (9), 1646-1657.

(50) Neese, F., Software update: the ORCA program system, version 4.0. *Wiley Interdiscip Rev Comput Mol Sci* **2018,** *8* (1), e1327.

Chapter 3:

Discovery of covalent prolyl oligopeptidase boronic ester inhibitors

This chapter has been published and is reproduced from:

Plescia, J. *et al.* Discovery of covalent prolyl oligopeptidase boronic ester inhibitors. *Eur J Med Chem* **2020**, 185, 111783.

While Chapter 1 reviewed the field of boronic acid/ester drugs, Chapter 2 focused more narrowly on our two enzymes of interest, prolyl oligopeptidase and fibroblast activation protein α, to determine the optimal electrophilic groups for targeting the two enzymes simultaneously; it was found that boronic acids are the optimal group. Herein we prepare peptidomimetic boronic *esters* as POP inhibitor pro-drugs, an electrophilic group that has largely been unexplored in targeting POP. Using docking-guided hit optimization, we conducted a structure-activity relationship study to further explore the scope of active POP inhibitors.

Contribution(s) of authors: I designed, synthesized, and characterized all molecules presented in this chapter and conducted 90% of the *in vitro* assays, the rest of which were conducted by Naëla Janmamode. Caroline Dufresne purified the POP enzyme. Alexander S. Wahba conducted the mass spectroscopy studies. I conducted the virtual screening and analysis with aide from Professor Nicolas Moitessier.

3.1 Abstract

Over the past decade, many drug discovery endeavors have been invested in targeting the serine proteases prolyl oligopeptidase (POP) for the treatment of Alzheimer's and Parkinson's disease and, more recently, epithelial cancers. Our research group has focused on the discovery of reversible covalent inhibitors, namely nitriles, to target the catalytic serine residue in this enzyme. While there have been many inhibitors discovered containing a nitrile to covalently bind to the catalytic serine, we have been investigating others, particularly boronic acids and boronic esters, the latter of which have been largely unexplored as covalent warheads. Herein we report a series of computationally-designed POP boronic ester pro-drug inhibitors exhibiting nanomolar-potencies *in vitro* as their active boronic acid species. These easily-accessible (1-2 step syntheses) compounds could facilitate future biochemical and biological studies of this enzyme's role in neurodegenerative diseases and cancer progression.

3.2 Introduction

Despite significant improvement in cancer therapies, survival rate remains low for several forms, such as lung cancer.[1] The tumor microenvironment (TME) – which includes malignant cells and the surrounding structures – is suggested to contribute to the metastasis and progression of tumors.[2-4] Many studies have been conducted to identify the structural targets implicated in tumors and the TME and to develop drugs blocking the action of these targets.[5-11] Our focus is on prolyl oligopeptidase (POP), a serine protease of the S9 protein family[12-13] While initially linked to neurodegenerative diseases[14-16] POP has now been established as a viable candidate for cancer therapies and is suggested to be involved in angiogenesis through its proline-specific peptidase activity.[12-13, 17] More specifically, POP inhibition has been shown to strongly inhibit the growth and proliferation of tumor cells *in vivo*,[12-13, 17-20]

Thus far, the majority of POP inhibitors have heavily resembled its peptide substrates, with most structures consisting of modified dipeptides (or pseudopeptides) with a reversibly electrophilic group (e.g., aldehyde, nitrile, fluorine-activated nitrile, or boronic acid)[17, 21-23] or irreversible ketone or Michael acceptor.[24] Research into drug-like inhibitors is a very promising strategy, as currently, there exist no inhibitors of POP on the market. S-17092, a potential POP selective inhibitor was stopped at Phase I trials.[25-26]

Over the past few years, our group has reported three chemical series investigating POP covalent inhibition *in vitro*, both against recombinant protein and in cancer cell lines,[27-29] but the long and complex syntheses – including difficult separations of stereoisomers and hazardous reaction conditions – prove to be inefficient for gram-scale synthesis and pharmaceutical development. Furthermore, each series focuses on the same 1,4-dicarbonyl molecular scaffold (**3.1**, **3.3**, **3.4**, **3.4**, and **3.6** in Figure 3.1), and one series (**3.4, MCMG01-2009** and analogues) was terminated due to metabolic instability and potential toxicity of the lead compound.[30]

These previous chemical series were discovered by docking-guided design of constrained peptidomimetics,[27] virtual screening,[28] and docking-guided optimization,[29] using our in-house computational platform.[31-33] The first-of-their-kind covalent inhibitors showed high activity *in vitro* against recombinant protein, inhibitor **3.6** being one of the most potent compounds reported to date.

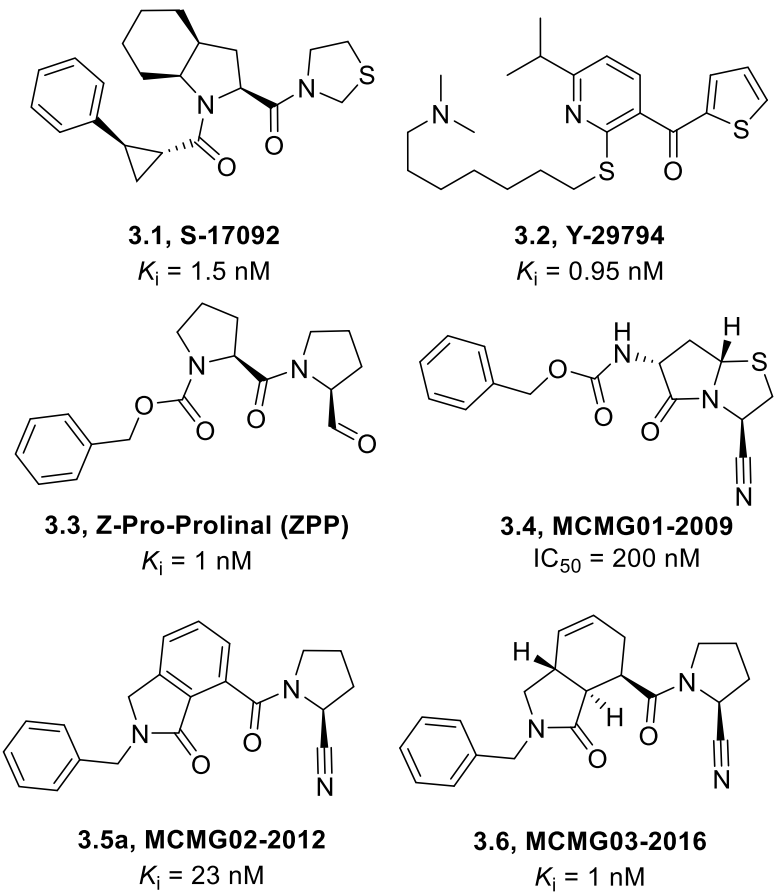

Figure 3.1. Previously-reported POP inhibitors

While reviewing the field of covalent enzyme inhibition, we concluded that, with the proper kinetics-structure relationship experiments, covalent inhibition could be a promising avenue in the discovery of anticancer therapeutics.[34] Our team has since developed the necessary kinetics experiments to study covalent inhibition in the context of POP inhibition.[35-37]

In this work, we use our combined expertise in computational, medicinal, and biological chemistry to design synthetically accessible POP inhibitors in a focused structure activity relationship study.

3.3 Results

3.3.1 Docking-based investigations of the POP active site

It is now well established that docking-guided drug discovery endeavors are significantly more effective if knowledge of the target (e.g., key interacting residues) is available.[38] In order to obtain more insights into the optimal structural requirements for inhibition, we docked known active POP inhibitors (including those shown in Figure 3.1) and investigated the interactions between the inhibitors and the residues in the active sites, using the latest version of our docking program.[32-33] Our comprehensive review on POP inhibitors previously outlined the necessary interactions between inhibitors and the enzyme.[17] The results of this docking study supported our original findings that three residues participate in necessary interactions for high inhibitor activity: Phe173 for aromatic interactions and Trp595 and Arg643 for hydrogen bonding with potent POP inhibitors (Figure 3.2).

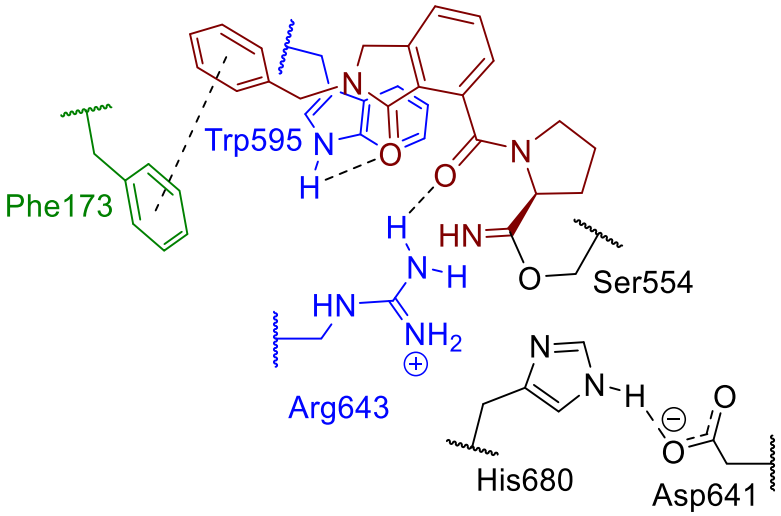

Figure 3.2. Our previously published hit **3.5a** docked into the active site of POP. Hydrogen bonding interactions between **3.5a** (maroon) can be observed between the 1,4-carbonyl moiety and residues Trp595 and Arg643 (blue). An additional aromatic interaction can be observed between the benzyl group and Phe173 (green).

3.3.2 Docking-guided optimizations.

Once the necessary enzyme-inhibitor interactions were established, this information was converted into interaction sites to improve the docking predictions.[32] Next, we carried out docking-guided optimizations. Of the known POP inhibitor structures, including those in Figure 3.1, compound **3.2**[39-40] was particularly interesting. It is one of the only known active POP inhibitors that does not contain the aforementioned 1,4-dicarbonyl moiety that is presumed to offer hydrogen bonding to the arginine and tryptophan residues in the active site. Instead of a second carbonyl group, the scaffold contains a thioether as a hydrogen bond acceptor. In addition, it includes an aromatic core shared by one of our leads (**3.5a**, Figure 3.3). To the best of our knowledge, the mode of binding (competitive binding, allosteric, etc.) of inhibitor **3.2** remains unknown. However, computational studies revealed that binding in the catalytic site is possible.[41] Assuming that this compound binds to the active site, upon docking-guided optimizations of **3.2**, compounds **3.7a-j** were designed, varying in heteroatoms on the scaffold and covalent electrophilic warhead (Figure 3.3).

The docking pose of compound **3.2** was not optimal, so several modifications were made following information from our lead molecules **3.5a**[28] and **3.5b**[42] (Figure 3.3). The long chain of

the thioether was removed, as it contained many rotatable bonds, subtracting from its viability as a drug candidate.[43] Unfortunately, the thioether analogue was not commercially available, and the synthesis was too complex for the purposes of this study. To address this issue, the thioether was replaced with a readily available methoxy group. Next, the distal isopropyl, pyridinyl, and amine moieties were combined into an *N*-acetyl group placed in the same position as the isopropyl group in **3.2**; the *N*-acetyl group contains the hydrogen bond acceptor (pyridine vs. carbonyl), hydrogen bond donor (protonated amine vs. amide) and steric bulk (isopropyl vs. *N*-acetyl). To determine the effect of the ether on inhibitor potency, an analog was synthesized containing a fluorine atom in place of the methoxy group. Interestingly, the docked pose of the fluorinated compound, like that of the methoxy-containing compound, orients the fluorine atom almost directly between Arg643 and Trp595, potentially interacting with both as a weak hydrogen bond acceptor (Figure 3.4). Series **3.7** was thus selected as the synthetic target. Interestingly, our review of the literature revealed that a similar scaffold was previously used although in irreversible inhibitors.[24]

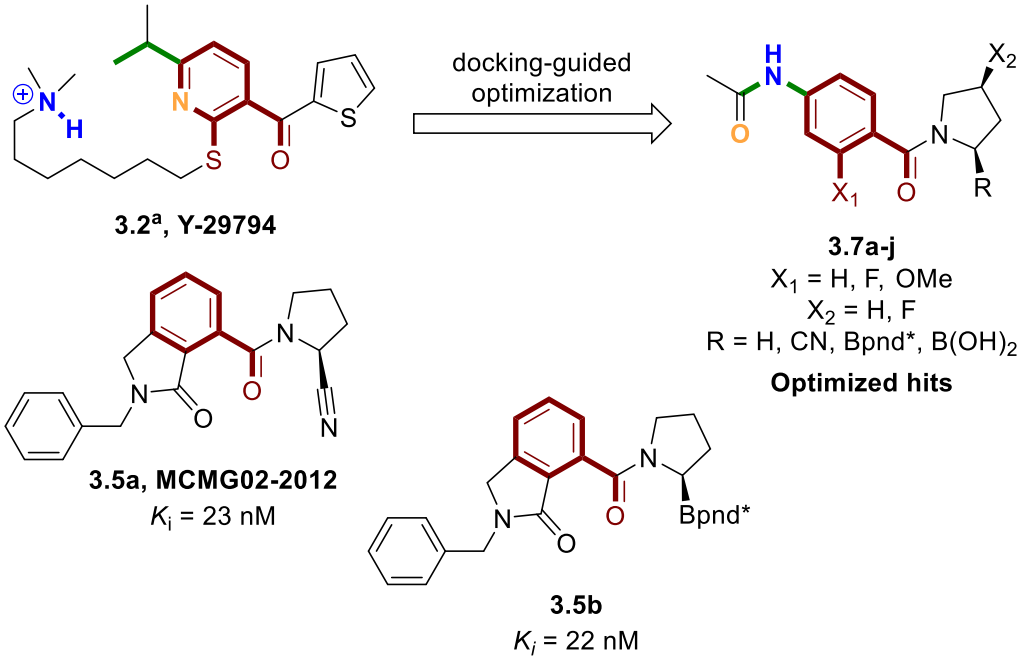

Figure 3.3. The docking guided optimization process to obtain our new hits: from compound **3.2**, **3.5a**[28] and **3.5b**[42] to compounds **3.7a-j**. Red: main scaffold; orange: hydrogen bond acceptor; blue: hydrogen bond donor. Structural similarities highlighted in corresponding colours. *pnd refers to (+)-pinanediol; [a]protonated at physiological pH.

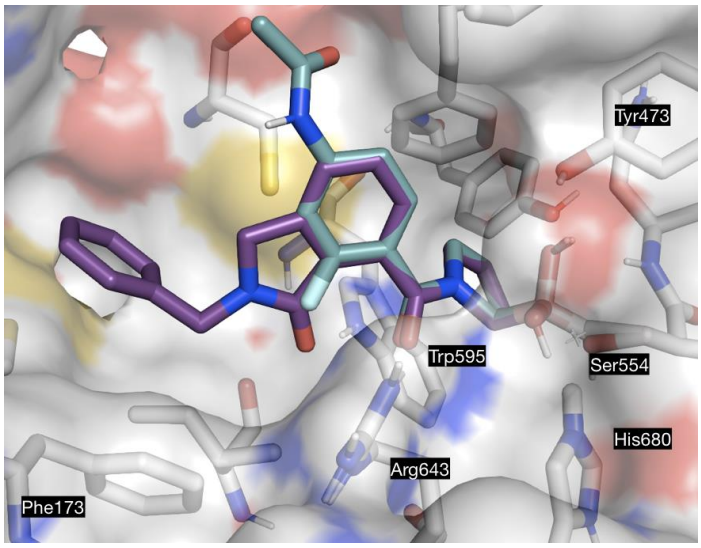

Figure 3.4. Our newly designed virtual hit and past POP inhibitor docked to POP: compounds **3.7j** (teal) and **3.5b** (purple; hydrolyzed to the boronic acid).

3.3.3 Synthesis.

Analogues both with and without the aromatic fluorine or methoxy group were synthesized to determine their effect on activity. The efficient synthesis was optimized to 1-2 steps, 3 including deprotection of the boronic ester to the corresponding boronic acid (Scheme 3.1). The first *N*-acetylation step for the synthesis of the fluorine-containing series was adapted from a procedure by Veera Reddy *et al.*[44] This reaction was carried out under sonication and proceeded smoothly, producing the benzoic acid derivative **3.10** in quantitative yields. The subsequent coupling step leading to **3.7a**-**3.7k** gave varied yields. The amine salts were readily available proline analogues.[45-46] The potentially non-covalent inhibitor analogues **3.7a** and **3.7f** were included to determine the effect of a covalent group on the activity of the inhibitor. The boronic acid analogues were initially synthesized as boronic esters and required one further deprotection step to attain compounds **3.7e**/**3.7j**.

Scheme 3.1 Synthesis of POP inhibitors[a]

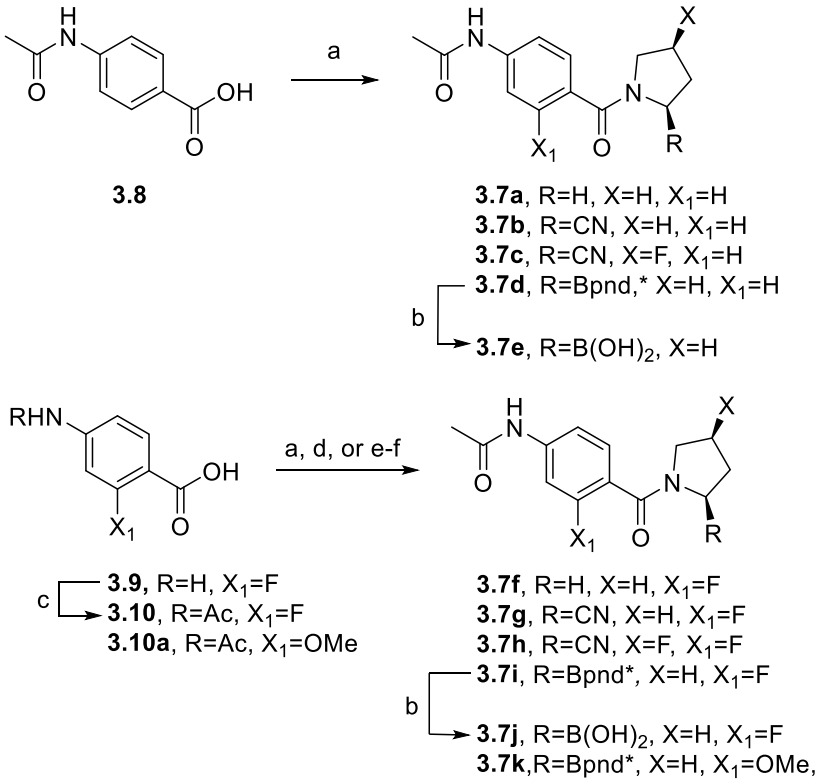

Reagents[a]: (a) Et_3N, Piv-Cl, modified proline salt, 0°C→rt, 18 h; 56% (**3.7a**), 25% (**3.7b**), 24% (**3.7c**), 39% (**3.7f**), 67% (**3.7g**), 21% (**3.7h**); (b) BCl_3, DCM, –78°C, 1h; 91% (**3.7e**), 71% (**3.7j**); (c) Ac_2O, H_2O, sonication, rt, 15 mins, quant.; (d) BOP, Et_3N, modified proline salt, 18 h; 82% (**3.7d**), 63% (**3.7i**); (e) EDC•HCl, HOSu, DCM, rt, 18 h; (f) Et_3N, modified proline salt, 0°C→rt, 18 h; 45% over two steps (**3.7k**); *pnd refers to (+)-pinanediol.

Several analogues were next synthesized to explore the effect of fluorine and various combinations of functional groups on the activity of this new chemical series. The synthesis remained 1-2 steps as shown in Scheme 3.2.

Scheme 3.2. Synthesis of second-generation analogues[a]

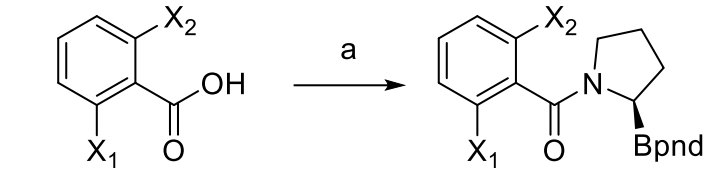

3.11a, X_1=F, X_2=NH_2
3.11b, X_1=H, X_2=NH_2
3.11c, X_1=F, X_2=H
3.11d, X_1=X_2=F
3.11e, X_1=X_2=H
3.11f, X_1=F, X_2=OMe
3.11g, X_1=H, X_2=OMe
3.11h, X_1=H, X_2=SMe

3.12a, X_1=F, X_2=NH_2
3.12b, X_1=H, X_2=NH_2
3.12c, X_1=F, X_2=H
3.12d, X_1=X_2=F
3.12e, X_1=X_2=H
3.12f, X_1=F, X_2=OMe
3.12g, X_1=H, X_2=OMe
3.12h, X_1=H, X_2=SMe

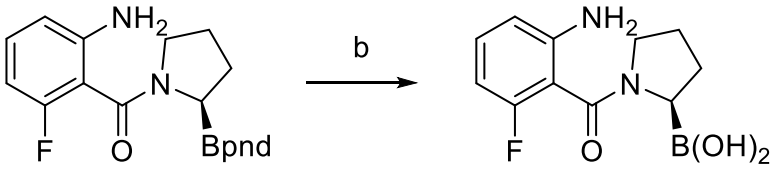

3.12a **3.12i**

[a]Reagents: (a) PyBOP, DIPEA, modified proline salt, DMF, rt, 18 h; 92% (**3.12a**), 89% (**3.12b**), 89% (**3.12c**), 94% (**3.12d**), 77% (**3.12e**), 75% (**3.12f**), 75% (**3.12g**), 97% (**3.12h**); b) BCl_3, DCM, –78°C→rt, 18 h, 57%; *pnd refers to (+)-pinanediol.

3.4 Discussion

3.4.1 Inhibitory potency of the first series.

Table 3.1 summarizes the results from the *in vitro* assays of our inhibitor series on POP. As expected, the increase in activity from pyrrolidine (**3.7a**/**3.7f**) and cyanoproline (**3.7b**/**3.7g)** analogues in POP supports our argument that covalent inhibitors exhibit higher potencies than their non-covalent analogues. The boron-containing inhibitors were the most potent, however. While we have no direct evidence that these boronic acid inhibitors are binding covalently, our previous work revealed long residence time (ca. 70 min) for a similar boronic acid derivative, together with high calculated energy stabilization when covalently bound supporting a reversible covalent binding mode.[42] The complete loss of inhibitory potency observed with **3.7a** and **3.7f** further support a covalent binding mode.

Interestingly, addition of a fluorine to the aromatic ring, while having little to no effect on the inhibitory activity of compounds containing the weakly-reactive nitrile group, shows a significant increase in activity of boronic ester compounds **3.7d** and **3.7i**. Even without the understood requirement of aromatic interactions with Phe173, both compounds showed submicromolar activity, with fluorinated **3.7i** showing nearly a 3-fold increase in potency from non-fluorinated **3.7d**. This contradicts our previous knowledge that the pharmacophore of POP inhibitors requires a phenyl ring to participate in aromatic interactions with Phe173 in the active site.[17] It appears as though fluorine, as predicted by our docking software, is oriented in such as a way as to compensate for the loss of these specific stabilizing interactions (Figure 3.4). To determine the significance of the fluorine, a boronic ester analogue replacing the fluorine for a methoxy group (**3.7k**) was also tested. Interestingly, this compound increased in potency by an order of magnitude, indicating that while fluorine must be participating in supplemental interactions or simply increasing the reactivity of the distal boronic ester, a true hydrogen bond acceptor renders the inhibitor much more potent. While the scaffold does not seem to significantly contribute to activity of the weakly reactive nitrile-containing compounds, it appears to highly enhance the activity of the boronic ester analogues **3.7d**, **3.7i**, and **3.7k**, depending upon the aromatic substituents.

Table 3.1. *In vitro* inhibitory potency against. POP.

Entry	Compound #	X	X_1	R	POP *Ki* (μM)
1	**3.7a**	H	H	H	> 30
2	**3.7b**	H	H	CN	2.2 ± 0.7
3	**3.7c**	F	H	CN	11.4 ± 3.4
4	**3.7d**	H	H	Bpnd*	0.27 ± 0.03
5	**3.7e**	H	H	$B(OH)_2$	0.95 ± 0.04
6	**3.7f**	H	F	H	> 30
7	**3.7g**	H	F	CN	> 15
8	**3.7h**	F	F	CN	> 15
9	**3.7i**	H	F	Bpnd*	0.08 ± 0.015
10	**3.7j**	H	F	$B(OH)_2$	0.21 ± 0.03
11	**3.7k**	H	OMe	Bpnd*	0.006 ± 0.0015

*Bpnd refers to the (+)-pinanediol protecting group

Figure 3.5 displays the dose response curve of compounds **3.7i** and **3.7k**.

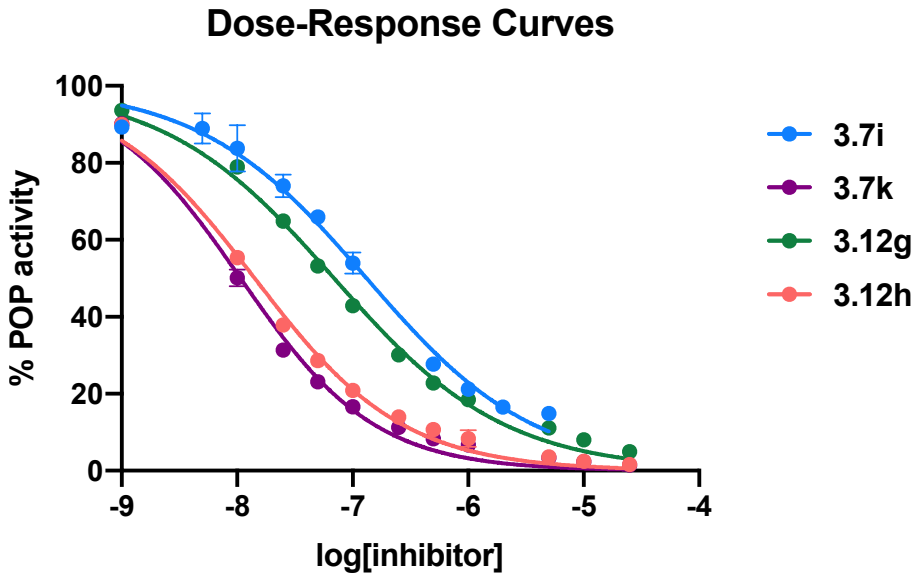

Figure 3.5. Dose-response curves for inhibitors **3.7i** (blue), **3.7k** (purple), **3.12g** (green), and **3.12h** (orange).

3.4.2 Hit optimization.

The promising activity of compound **3.7i** and **3.7k** led to further virtual derivatization of our hits. We hypothesized that if we moved the *N*-acetyl group to the ortho position, retaining the fluorine in the other ortho position, the activity would increase even further, as the hydrogen bond acceptor acetyl would be closer to the arginine and tryptophan residues. Upon docking, however, it appeared the *N*-acetyl group was repelled from the active site. To decrease its size, the acetyl group (hydrogen bond acceptor) was removed to leave the aniline group (hydrogen bond donor), leading to compound **3.12a**. With the removal of the hydrogen bond acceptor group, docking this new modification (**Figure 3.6**b and c) gave two proposed binding modes. In the first (**Figure 3.6**b), the fluorine was no longer interacting with two key residues. The aniline was instead predicted to hydrogen bond intramolecularly with the neighboring carbonyl. This interaction polarizes the carbonyl and may affect the reactivity of the boronic ester. Currently, the reactivity of the electrophilic warhead is not considered by any docking program including routines for covalent docking.[34] In an alternative proposed binding mode (**Figure 3.6**c), the position of the fluorine in **3.12a** is similar to that of **3.7i**, further supporting our hypothesis that the fluorine may compensate for the missing key interactions. Furthermore, the aniline would hydrogen bond with a proximal tyrosine (not shown), adding an additional stabilizing ligand-protein interaction. This molecule was thus selected as our new synthetic target.

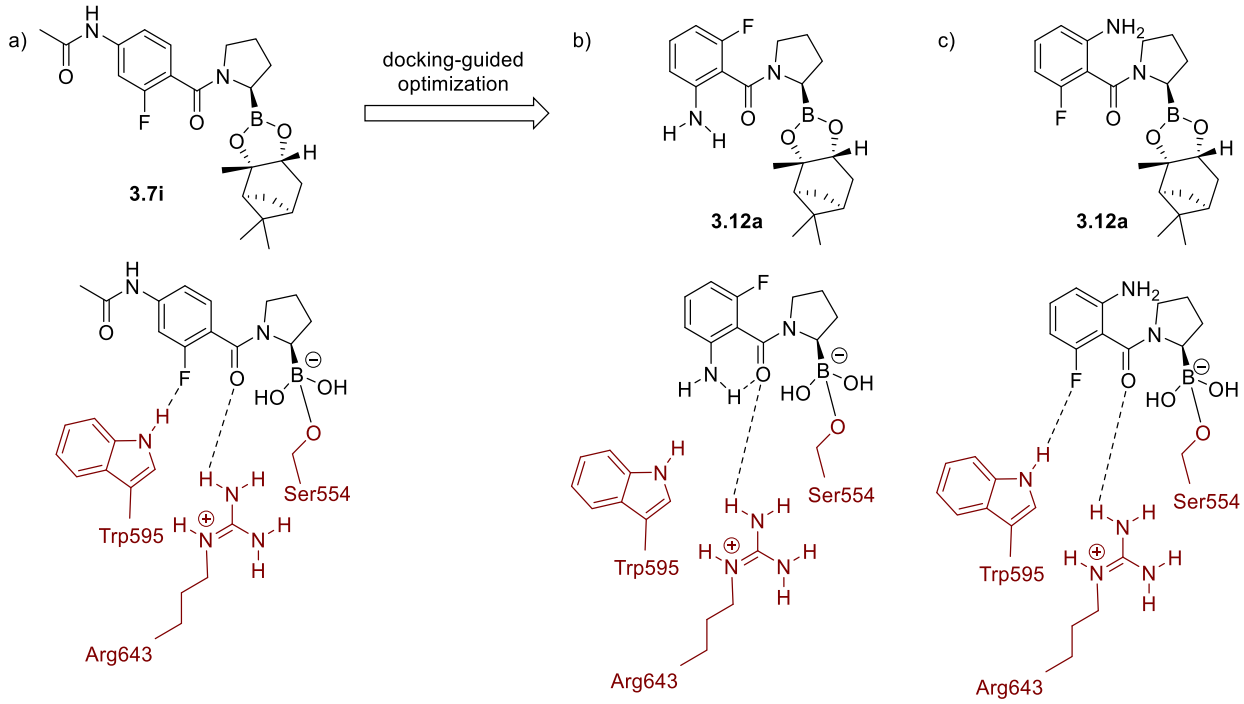

Figure 3.6. Docking-guided optimization of compound **3.7i.** a) Compound **3.7j** docked to the active site of POP; b) Hydrolyzed ester **3.12a** docked to the active site of POP; c) alternative binding mode of hydrolyzed **3.12a** docked to the active site of POP

In order to further probe the impact of the electronics on the inhibitory potency, a set of molecules with various electron donating and withdrawing groups was designed and synthesized (Scheme 3.2). The synthesis was similar to that of the first series; commercially available benzoic acid analogues were coupled to a proline analog to give the resultant boronic esters. One boronic ester was deprotected to the boronic acid. Upon *in vitro* testing against POP, we obtained several interesting results. Our optimized hit **3.12a** showed low micromolar potency against POP (Table 3.2), yet it was still not nearly as active as our original hits **3.7i** and **3.7k**. As discussed above, it is possible that after having removed the acetyl group and moved the resultant aniline to the *ortho* position, the aniline is hydrogen bonding intramolecularly to the carbonyl of the amide, thereby preventing the fluorine atom from assuming its predicted advantageous position in the active site. Removal of the aniline restored some of the activity (**3.12c**) while addition of a hydrogen bond acceptor (**3.12f**) led to further increase in potency by an order of magnitude. In contrast, removal of this fluorine (giving **3.12b**) decreases the inhibitor potency six-fold, further suggesting that fluorine is contributing to the stabilization of the ligand in the active site or to the reactivity of the

boronic ester acting as the electrophile. These data indicated that (1) the aniline is potentially hindering activity of this new inhibitor and/or (2) fluorine on its own can lead to sub-micromolar inhibitory potency. This last observation may also suggest potentially quicker hydrolysis of the boronic ester in the buffer, as electronegative fluorine atoms are expected to increase the reactivity of boronic esters. This hydrolysis mechanism was investigated more closely (see below). Upon addition of a second *ortho*-fluorine (**3.12d**), a significant increase in potency is observed from the mono-fluorine analogue. Once more, two likely explanations exist for this activity: the di-fluoro system is inductively increasing the electrophilicity of the boronic ester (and its hydrolysis to the likely active species), and/or the two fluorine atoms are participating in supplementary stabilizing interactions that allow the inhibitor to interact with the active site more strongly than any of the other tested compounds. Another analogue featuring a methoxy group as a hydrogen bond acceptor (**3.12g**) displayed nanomolar activity in an even higher potency than **3.7i**. Interestingly, replacement of the methoxy with a thioether (**3.12h**) increased potency further. This analogue more closely resembles active compound **3.2**, the original scaffold from which this series was designed. It seems as though a thioether increases stability of the inhibitor in the active site more so than its methoxy counterpart. A control inhibitor with no *ortho*- substituents (**3.12e**) exhibited much lower potency, two orders of magnitude lower than the thioether or methoxy analogues. These results indicate that there does exist a substituent requirement for inhibitory potency, whether it be to stabilize the inhibitor in the active site, to increase the reactivity of the boronic ester towards hydrolysis, or to form a stronger covalent bond in the binding site.

Table 3.2. *In vitro* on POP inhibition for second chemical series.

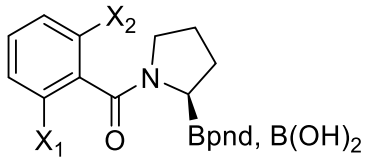

Entry	Compound #	X_1	X_2	K_i (μM)
1	**3.12a**	F	NH_2	1.1 ± 0.1
2	**3.12b**[a]	H	NH_2	6.3 ± 0.5
3	**3.12c**	F	H	1.0 ± 0.1
4	**3.12d**	F	F	0.355 ± 0.054
7	**3.12e**	H	H	0.767 ± 0.1
8	**3.12f**	F	OMe	0.049 ± 0.008
9	**3.12g**	H	OMe	0.044 ± 0.004
10	**3.12h**	H	SMe	0.009 ± 0.001
11	**3.12i**[a]	F	NH_2	3.0 ± 0.4

[a]boronic acid analogues

3.4.3 Mechanism of action.

A close look at the collected data reveals that the activity of the boronic esters is most likely resulting from minor modifications of the scaffold. On one side, electron-withdrawing fluorine atoms are believed to increase the Lewis acidity of the boronic ester, hence its potency (IC_{50}(**3.12c**) > IC_{50}(**3.12d**)). The introduction of true hydrogen bond acceptors (OMe, SMe) is expected to increase the potency (IC_{50}(**3.12e**) > IC_{50}(**3.12g**) > IC_{50}(**3.12h**)).

In order to determine the full effect of the boronic ester prodrug, the (+)-pinanediol group was removed under Lewis acidic conditions from two selected esters to give the corresponding boronic acids **3.7e** and **3.7j**. Upon *in vitro* testing against recombinant POP, it was surprisingly found that the boronic acid analogues were slightly less active than their corresponding esters **3.7d** and **3.7i**. This data appears inconsistent with the design strategy that relies upon the formation of a covalent bond between the boronic acid group and the catalytic serine. Based on these results, we hypothesized that the boronic pinanediol ester might be either (1) hydrolyzed in the buffer as we

recently observed[42] or (2) a substrate of POP, hence the boronic acid, product of this hydrolysis, does not leave the binding site, inhibiting the enzymatic activity.

To distinguish between these two alternative boronic acid release pathways, we investigated the stability of the boronic ester in neutral aqueous solution and did not observe significant hydrolysis over a period of several hours. In fact, strongly acidic conditions are usually required to cleave alkyl boronic esters; 6N HCl was used by Lebarbier *et al.*,[47] and boronic pinanediol esters were also found to be stable under acidic conditions used to remove a Boc group.[48] We were hence skeptical that hydrolysis would occur readily in the slightly basic buffer used in our assays. However, mass spectrometry studies revealed that under the slightly basic conditions of the assay (pH 8 buffer), the esters were hydrolyzed very quickly even in the absence of enzyme. This data confirmed that the enzyme is not involved in the hydrolysis process. As a result, the boronic esters act as pro-drugs releasing the boronic acids, in turn acting as POP inhibitors. To confirm that the active species are stable boronic acids, MS experiments were carried out. **Figure 3.7** details the hydrolysis of boronic ester **3.12d** and **3.12e** to their respective boronic acid species. Despite the expected higher intrinsic reactivity of **3.12d**, its hydrolysis occurred on approximately the same time scale as both the unsubstituted **3.12e** and our previously published **3.5b**[42] which contains an entirely different scaffold. This evidence indicates that the boronic ester inhibitors are hydrolyzed during the serial dilution and 96-well plate preparation, i.e. well before the enzyme is added. The active species participating in the enzymatic reaction are therefore the boronic acids.

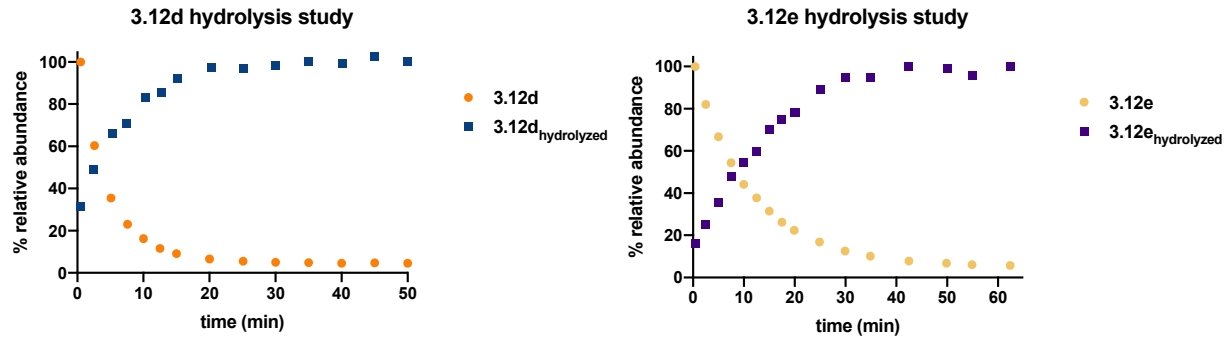

Figure 3.7. Hydrolysis studies of boronic esters **3.12d** and **3.12e** in POP assay buffer. The graphs display relative abundance of each ionic species at intervals over 50-63 minutes.

3.5 Conclusion

In summary, by introducing various combinations of amines/amides, hydrogen bond donors and acceptors, and fluorines, to a very simple molecular scaffold, we were able to achieve potent POP inhibition with compounds that move away from the pseudopeptide scaffold of previously-discovered inhibitors[18, 22-23] and the use of irreversibly covalent electrophiles.[24] Furthermore, our study has led to the synthesis of inhibitors that are available in just one or two steps, facilitating future kinetic or biological studies of this enzyme or cancer cell lines.

More unexpectedly, the boronic esters, initially seen as synthetic intermediates, exhibited strong inhibitory potency. We confirmed that the activity of these bulky boronic esters is the result of their buffer-mediated hydrolysis into the active boronic acids, the latter being less active (when tested directly); the boronic esters act as pro-drugs, while the boronic acids are the active species. This finding also facilitates future medicinal chemistry endeavors, as (1) boronic esters are much easier to synthesize and handle, and (2) many substituents are unstable to boronic ester cleavage conditions. The removal of this formerly necessary synthetic step allows for a broader spectrum of inhibitors to be studied. Based on these promising results of our boronic ester compounds, we are currently exploring more complex, non-peptidic boronic ester drugs.

3.6 Experimental Section.

3.6.1 *In Vitro* Assays

POP expression, purification, and testing were performed as previously described by our group.[28] The enzyme batch tested in this study exhibited a K_m of 141.2 μM and k_{cat} of 21.2 s^{-1}.

3.6.2 Chemistry

3.6.2.1 General information.

All commercially available reagents were used without further purification. All reactions, unless otherwise indicated, were carried out in flame-dried flasks under argon atmosphere with anhydrous solvents. FTIR spectra were recorded using a Perkin-Elmer Spectrum One FT-IR or Bruker ALPHA FTIR-ATR. ^{1}H and ^{13}C NMR spectra were recorded on Bruker 400 or 500 MHz or Varian 400 or 500 MHz spectrometers. Chemical shifts are reported in ppm using the residual of deuterated solvents as an internal standard. Thin layer chromatography visualization was performed by UV or by development using ninhydrin, *para*-anisaldehyde, vanillin, ceric ammonium molybdate, or $KMnO_4$. Chromatography was performed on silica gel 60 (230−40 mesh) or using the Biotage One Isolera with ZIP cartridges. High resolution mass spectrometry was performed by ESI on a Bruker Maxis Impact API QqTOF or by ESI or APCI on a ThermoFisher Exactive Plus Orbitrap-API at McGill University. All tested compounds were at least 95% pure. All compounds were stored at –20°C.

3.6.2.2 Mass Spectroscopy study of boronic ester hydrolysis

This study was performed as previously published by our group[42].

3.6.2.3 Purity determination by High Performance Liquid Chromatography (HPLC)

Prior to biological testing, reverse-phase HPLC was used to verify the purity of compounds on an Agilent 1100 series instrument, equipped with VWD-detector, using a C18 reverse column (Agilent, Eclipse C18 150 mm Å~ 4.6 mm, 5 μm) with UV detection at 254 nm. All biologically tested compounds were determined to be > 95% pure. The solvents used were H_2O (A) and either MeOH or MeCN (B) in a gradient. Retention times and purities are provided for each compound.

Method A: H_2O (A) and MeOH (B); t = 0 mins, 95% A / 5% B; t = 3 to 20 mins, gradually to 5% A / 95% B; t = 20 to 25 mins, 5% A / 95% B; t = 25 to 28 mins, gradually to 95% A / 5% B; t = 28 to 30 mins, 95% A / 5% B.

Method B: H_2O (A) and MeCN (B); t = 0 mins, 95% A / 5% B; t = 5 to 15 mins, gradually to 5% A / 95% B; t = 15 to 20 mins, 5% A / 95% B; t = 20 to 28 mins, gradually to 95% A / 5% B; t = 28 to 30 mins, 95% A / 5% B.

3.6.2.4 Synthesis

4-Acetamido-2-fluorobenzoic acid (3.10) 4-amino-2-fluorobenzoic acid benzoic acid (500 mg, 3.22 mmol, 1 eq) was suspended in H_2O (3.2 mL, 1 M) in a static-free round-bottom flask, and acetic anhydride (0.65 mL, 658 mg, 6.45 mmol, 2 eq) was added. An empty balloon was inserted into the septum to trap AcOH vapors and prevent pressure build-up, and the mixture was sonicated for 5 minutes. The reaction was incomplete (TLC 90:10 EtOAc-MeOH, ninhydrin stain). Acetic anhydride (2 eq) was added again, and the mixture was sonicated for 5 minutes. This was repeated a third time (totaling 6 eq of Ac_2O, 15 minutes). The mixture was concentrated *in vacuo* to give a beige powder, which was taken to the next step without purification (635 mg, quant.) R_f = 0.46 (90:10 EtOAc-MeOH); mp = 247–252°C; IR (neat) cm^{-1} 3329, 3043, 2924, 2853, 1687, 1645, 1603, 1544, 866; ^1H NMR (500 MHz, DMSO-d_6) δ 12.93 (s, 1H), 10.45 (s, 1H), 7.82 (t, *J* = 8.6 Hz, 1H), 7.66 (dd, *J* = 13.8, 1.9 Hz, 1H), 7.34 (dd, *J* = 8.6, 1.9 Hz, 1H), 2.09 (s, 3H); ^{13}C NMR (126 MHz, DMSO-d_6) δ 169.24, 164.56 (d, *J* = 3.7 Hz), 161.76 (d, *J* = 255.4 Hz), 144.76 (d, *J* = 11.9 Hz), 132.74 (d, *J* = 2.4 Hz), 114.05 (d, *J* = 2.9 Hz), 112.84 (d, *J* = 10.1 Hz), 106.08 (d, *J* = 27.7 Hz), 24.19; ^{19}F NMR (471 MHz, Methanol-d_4) δ -109.19 (dd, *J* = 13.5, 8.4 Hz); HRMS (ESI+) *m/z* calcd for $[C_9H_8O_3NF + Na]^+$ 220.03804, found 220.03742.

General Coupling Procedure A: The carboxylic acid starting material was suspended in DCM (0.1 M), and Et_3N (5 eq) was added. The resultant solution was cooled to 0°C, and pivaloyl chloride (1.1 eq) was added. After 30 minutes at 0°C, the corresponding amine (1.5 eq) was added, and the reaction stirred at room temperature overnight. The reaction was quenched with H_2O (or 3 M HCl if a precipitate formed), and the product was extracted with DCM (or EtOAc for **3.4c** and **3.7h**). The combined organic layers were washed with 1 M HCl, saturated $NaHCO_3$, and brine, dried over Na_2SO_4, filtered, and concentrated *in vacuo*. The crude product was purified by flash chromatography on a silica gel column to give the product as a solid. Trace impurities could be removed by trituration in hexanes or Et_2O and subsequent vacuum filtration.

General Coupling Procedure B: The carboxylic acid starting material was dissolved in DMF (1 M), and BOP (1.2 eq) was added, followed by by *rac*-*N*-Boro-Pro pinanediol ester hydrochloride (prepared as described in the literature[45]) (1.2 eq) and Et_3N (3 eq). The reaction

stirred at room temperature overnight. The reaction was quenched with 3 M HCl, and the product was extracted with EtOAc. The combined organic layers were washed with 1 M HCl, saturated $NaHCO_3$, and brine, dried over Na_2SO_4, filtered, and concentrated *in vacuo*. The crude product was purified by flash chromatography on a silica gel column to give the product as an oil, which was precipitated in hexanes and vacuum filtered to give the product as a solid as a mixture of diastereomers.

General Coupling Procedure C: The carboxylic acid starting material was dissolved in DMF (1 M), and PyBOP (1.2 eq) was added, followed by *rac*-*N*-Boro-Pro pinanediol ester hydrochloride (prepared as described in the literature[45]) (1 eq), and DIPEA (4 eq). The reaction stirred at room temperature overnight. The reaction was quenched with H_2O, and the product was extracted with EtOAc. The combined organic layers were washed with saturated $NaHCO_3$ and brine, dried over Na_2SO_4, filtered, and concentrated *in vacuo*. The crude product was purified by flash chromatography on a silica gel column to give the product as a mixture of diastereomers.

General Coupling Procedure D: The carboxylic acid starting material was dissolved/suspended in DCM (0.8 M), and the solution/mixture was cooled to 0°C. *N*-hydroxysuccinimide (1 eq) was added, followed by EDC•HCl (1 eq). The resultant solution was stirred at room temperature overnight. The activated esters were isolated via vacuum filtration. The activated ester was dissolved in DMF (0.2 M), and the solution was cooled to 0°C. The *rac*-*N*-Boro-Pro pinanediol ester hydrochloride (prepared as described in the literature[45]) (1.5 eq) was added, followed by Et_3N (5 eq). The reaction stirred at room temperature until completion (1–18 h). The reaction was quenched with H_2O, and the product was extracted with EtOAc. The combined organic layers were washed with saturated $NaHCO_3$ and brine, dried over Na_2SO_4, filtered, and concentrated *in vacuo*. The crude product was purified by flash chromatography on a silica gel column to give the product as a mixture of diastereomers.

***N*-(4-(pyrrolidine-1-carbonyl)phenyl)acetamide (3.7a)** The product was synthesized following General Coupling Procedure A, using pyrrolidine as the corresponding amine. The crude product was purified by flash chromatography on a silica gel column (eluent 90:10 EtOAc-MeOH) to give a white solid (56%). R_f = 0.29 (90:10 EtOAc-MeOH); mp = 201–205°C; IR (neat) cm^{-1} 3244, 3039, 2975, 1697, 1603, 759; ^1H NMR (500 MHz, Chloroform-*d*) δ 9.16 (s, 1H), 7.50 (d, *J* = 8.7 Hz, 2H), 7.36 (d, *J* = 8.7 Hz, 2H), 3.60 (t, *J* = 7.0 Hz, 2H), 3.41 (t, *J* = 6.7 Hz, 2H), 2.09 (s, 4H), 1.93 (p, *J* = 6.9 Hz, 2H), 1.85 (p, *J* = 6.7 Hz, 2H); ^{13}C NMR (126 MHz, $CDCl_3$) δ 169.75,

169.52, 140.40, 131.75, 127.97 (2C), 119.35 (2C), 49.88, 46.48, 26.47, 24.49, 24.43; HRMS (ESI+) *m/z* calcd for $[C_{13}H_{16}O_2N_2 + H]^+$ 233.1285, found 233.1294; HPLC (Method A) t_R = 14.8 min, 97.7%.

(*S*)-*N*-(4-(2-cyanopyrrolidine-1-carbonyl)phenyl)acetamide (3.7b) The product was synthesized following General Coupling Procedure A, using (*S*)-pyrrolidine-2-carbonitrile pTsOH salt (prepared as described in the literature[46]) as the corresponding amine. The crude product was purified by flash chromatography on a silica gel column (eluent 90:10 EtOAc-MeOH) to give a white solid (25%). R_f = 0.60 (90:10 EtOAc-MeOH); mp = 171–174°C; IR (neat) cm^{-1} 3325, 3110, 2986, 2244, 1693, 1606, 1596, 1526, 853.; ^{1}H NMR (500 MHz, Chloroform-*d*) δ 8.86 (s, 1H), 7.55 (d, *J* = 8.3 Hz, 2H), 7.44 (d, *J* = 8.4 Hz, 2H), 4.81 (m, 1H), 3.68 – 3.57 (m, 1H), 3.57 – 3.44 (m, 1H), 2.36 – 2.23 (m, 2H), 2.18 – 2.14 (m, 1H), 2.12 (s, 3H), 2.11 – 2.07 (m, 1H), 2.05 – 1.93 (m, 1H); ^{13}C NMR (126 MHz, $CDCl_3$) δ 24.49, 25.67, 30.27, 47.10, 49.77, 118.77, 119.37 (2C), 128.50 (2C), 129.60, 141.13, 169.58, 169.80; HRMS (ESI+) *m/z* calcd for $[C_{14}H_{15}O_2N_3 + H]^+$ 258.1237, found 258.1241; HPLC (Method A) t_R = 13.5 min, 97.0%.

***N*-(4-((2*S*,4*S*)-2-cyano-4-fluoropyrrolidine-1-carbonyl)phenyl)acetamide (3.7c)** The product was synthesized following General Coupling Procedure A, using 2-(*S*)-cyano-4-(*S*)-fluoropyrrolidine hydrochloride (prepared as described in the literature[46]) as the corresponding amine. The crude product was purified by flash chromatography on a silica gel column (eluent 90:10 EtOAc-MeOH + 1.5% Et_3N) to give a yellow solid. The solid was triturated in diethyl ether and vacuum filtered to give the final product as a yellow solid (10%). R_f = 0.45 (90:10 EtOAc-MeOH); mp = 111–114°C; IR (neat) cm^{-1} 3308, 3189, 2987, 1665, 1626, 1607, 1542, 839; ^{1}H NMR (500 MHz, Methanol-d_4) δ 7.69 (d, *J* = 8.5 Hz, 2H), 7.56 (d, *J* = 8.6 Hz, 2H), 5.38 (d, *J* = 51.7 Hz, 1H), 5.19 – 4.96 (m, 1H), 4.10 – 3.61 (m, 2H), 2.76 – 2.38 (m, 2H), 2.15 (s, 3H); ^{13}C NMR (126 MHz, Methanol-d_4) δ 171.86 (2C), 142.65, 131.01, 129.32 (2C), 120.43 (2C), 119.30, 93.83 (d, *J* = 172.0 Hz), 56.66 (d, *J* = 23.1 Hz), 46.81, 37.18 (d, *J* = 21.7 Hz), 23.97; ^{19}F NMR (471 MHz, MeOD) δ -76.94; HRMS (ESI+) *m/z* calcd for $[C_{14}H_{14}FO_2N_3 + Na]^+$ 298.0962, found 298.0976; HPLC (Method A) t_R = 12.6 min, 99.1%.

***N*-(4-(2-((3a*S*,4*S*,6*S*,7a*R*)-3a,5,5-trimethylhexahydro-4,6-methanobenzo[*d*][1,3,2]dioxaborol-2-yl)pyrrolidine-1-carbonyl) phenyl)acetamide (3.7d)** The product was synthesized following General Coupling Procedure B. The crude residue was purified by flash chromatography on a silica gel column (eluent 80→100% EtOAc in hexanes,

then 10% MeOH in EtOAc) to give a white solid as a mixture of diastereomers (75%). R_f = 0.26 (100% EtOAc); mp = 159–162°C; IR (in $CDCl_3$) cm^{-1} 3266, 3190, 2921, 1699, 1679, 1602, 1514, 1457, 1385, 1372, 1124; ^1H NMR (500 MHz, Chloroform-*d*) δ 8.94 (s, 1H), 8.80 (s, 1H), 7.53 (dd, *J* = 8.5, 2.7 Hz, 4H), 7.45 (d, *J* = 8.4 Hz, 2H), 7.41 (d, *J* = 8.4 Hz, 2H), 4.30 (ddd, *J* = 20.0, 8.8, 2.2 Hz, 2H), 3.60 (tt, *J* = 9.1, 4.0 Hz, 2H), 3.41 (p, *J* = 8.6 Hz, 2H), 3.04 (ddd, *J* = 15.4, 11.2, 6.8 Hz, 2H), 2.36 (ddt, *J* = 14.6, 8.9, 3.0 Hz, 2H), 2.19 (s, 3H), 2.18 (s, 3H), 2.17 – 2.08 (m, 4H), 2.08 – 2.00 (m, 4H), 1.99 – 1.92 (m, 2H), 1.92 – 1.87 (m, 3H), 1.87 – 1.83 (m, 1H), 1.76 – 1.66 (m, 2H), 1.52 (dd, *J* = 10.5, 7.6 Hz, 2H), 1.49 (s, 3H), 1.48 (s, 3H), 1.29 (s, 6H), 0.88 (s, 6H); ^{13}C NMR (126 MHz, $CDCl_3$) δ 24.36 (2C), 24.60, 24.66, 25.77, 26.08, 26.67, 26.77, 27.51, 27.54, 28.80, 28.87, 29.53, 29.66, 36.94 (2C), 38.31, 38.33, 40.25, 40.29, 48.56, 48.62, 51.93 (2C), 52.58, 52.61, 76.72, 76.82, 83.85, 83.98, 119.66 (2C), 119.69 (2C), 124.32, 124.53, 130.00 (2C), 130.22 (2C), 141.89, 141.98, 169.37, 169.42, 170.45, 170.64; ^{11}B NMR (161 MHz, $CDCl_3$) δ 19.26; HRMS (ESI+) *m/z* calcd for $[C_{23}H_{31}O_4N_2B+ H]^+$ 411.2450, found 411.2450; HPLC (Method B) t_R = 17.6 min, 96.9%.

***N*-(3-fluoro-4-(pyrrolidine-1-carbonyl)phenyl)acetamide (3.7f)** The product was synthesized following General Coupling Procedure A, using pyrrolidine as the corresponding amine. The crude product was purified by flash chromatography on a silica gel column (eluent 90:10 EtOAc-MeOH) to give a yellow solid (39%). R_f = 0.50 (90:10 EtOAc-MeOH); mp = 187–190°C; IR (neat) cm^{-1} 3252, 3095, 2965, 1597, 828, 867; ^1H NMR (500 MHz, Chloroform-*d*) δ 9.65 (s, 1H), 7.54 (dd, *J* = 12.2, 1.9 Hz, 1H), 7.18 – 7.13 (m, 1H), 7.09 (dd, *J* = 8.4, 1.9 Hz, 1H), 3.58 (t, *J* = 7.0 Hz, 2H), 3.29 (t, *J* = 6.7 Hz, 2H), 2.05 (s, 3H), 1.93 (p, *J* = 6.4 Hz, 2H), 1.86 (p, *J* = 6.1 Hz, 2H); ^{13}C NMR (126 MHz, Chloroform-*d*) δ 169.79, 165.59, 158.41 (d, *J* = 246.2 Hz), 141.96 (d, *J* = 11.1 Hz), 128.57 (d, *J* = 5.1 Hz), 119.65 (d, *J* = 17.8 Hz), 115.28 (d, *J* = 2.8 Hz), 107.19 (d, *J* = 27.0 Hz), 48.13 (d, *J* = 4.1 Hz), 46.12, 25.85, 24.48, 24.23; ^{19}F NMR (471 MHz, Chloroform-*d*) δ -112.73 (dd, *J* = 12.0, 7.5 Hz); HRMS (ESI+) *m/z* calcd for $[C_{13}H_{15}FO_2N_2 + H]^+$ z251.1190, found 251.1189; HPLC (Method A) t_R = 15.5 min, 98.9%.

(*S*)-*N*-(4-(2-cyanopyrrolidine-1-carbonyl)-3-fluorophenyl)acetamide (3.7g) The product was synthesized following General Coupling Procedure A, using (*S*)-pyrrolidine-2-carbonitrile pTsOH salt (prepared as described in the literature[46]) as the corresponding amine. The crude product was purified by flash chromatography on a silica gel column (eluent 90:10 EtOAc-MeOH) to give a yellow solid (74%). R_f = 0.53 (90:10 EtOAc-MeOH); mp = 157–161°C; IR (neat) cm^{-1}

3267, 3106, 2984, 2237, 1693, 1615, 1597, 881, 825.; ^{1}H NMR (500 MHz, Chloroform-*d*) δ 9.02 (s, 1H), 7.61 (dd, *J* = 12.3, 1.9 Hz, 1H), 7.25 (t, *J* = 8.0 Hz, 1H), 7.11 (dd, *J* = 8.4, 1.9 Hz, 1H), 4.81 (dd, *J* = 7.1, 5.1 Hz, 1H), 3.51 (ddd, *J* = 10.5, 7.4, 5.2 Hz, 1H), 3.41 (dt, *J* = 10.4, 7.1 Hz, 1H), 2.39 – 2.30 (m, 2H), 2.19 – 2.13 (m, 1H), 2.11 (s, 3H), 2.08 – 1.96 (m, 1H); ^{13}C NMR (126 MHz, Chloroform-*d*) δ 169.71, 166.01, 158.78 (d, *J* = 247.8 Hz), 142.58 (d, *J* = 11.3 Hz), 129.26 (d, *J* = 4.5 Hz), 118.36, 117.97 (d, *J* = 17.0 Hz), 115.38, 107.27 (d, *J* = 27.0 Hz), 47.97 (d, *J* = 5.0 Hz), 46.73, 30.43, 25.12, 24.45; ^{19}F NMR (471 MHz, Chloroform-*d*) δ -111.90 (dd, *J* = 12.5, 7.6 Hz); HRMS (ESI+) *m/z* calcd for $[C_{14}H_{14}FO_2N_3 + H]^+$ 276.1143, found 276.1140; HPLC (Method A) t_R = 13.7 min, 99.2%.

N*-(4-((2*S*,4*S*)-2-cyano-4-fluoropyrrolidine-1-carbonyl)-3-fluorophenyl)acetamide (3.7h)** The product was synthesized following General Coupling Procedure A, using 2-(S***)-cyano-4-(*S*)-fluoropyrrolidine hydrochloride (prepared as described in the literature[46]) as the corresponding amine. The crude product was purified by flash chromatography on a silica gel column (eluent 90:10 EtOAc-MeOH) to give a yellow solid. The solid was triturated in diethyl ether and vacuum filtered to give the final product as a pink solid (10%). R_f = 0.53 (90:10 EtOAc-MeOH); mp = 112–116°C; IR (neat) cm^{-1} 3309, 3124, 2985, 2244, 1664, 1624, 1604, 1543, 911, 800; 1H), 4.16 – 3.57 (m, 2H), 2.79 – 2.45 (m, 2H), 2.15 (s, 3H); ^{13}C NMR (126 MHz, Methanol-d_4) δ 171.95, 167.50, 159.92 (d, *J* = 246.1 Hz), 144.20 (d, *J* = 11.4 Hz), 130.33 (d, *J* = 4.5 Hz), 119.18 (d, *J* = 17.3 Hz), 118.94, 116.47 (d, *J* = 2.9 Hz), 107.87 (d, *J* = 26.9 Hz), 93.60 (d, *J* = 177.9 Hz), 55.43 (d, *J* = 4.6 Hz), 55.24 (d, *J* = 4.5 Hz), 37.38 (d, *J* = 20.9 Hz), 24.00; ^{19}F NMR (471 MHz, Methanol-d_4) δ -114.60 – -114.88 (m); HRMS (ESI+) *m/z* calcd for $[C_{14}H_{13}F_2O_2N_3 + Na]^+$ 316.0868, found 316.0868; HPLC (Method A) t_R =12.6 min, 95.4%.

***N*-(3-fluoro-4-(2-((3a*S*,4*S*,6*S*,7a*R*)-3a,5,5-trimethylhexahydro-4,6-methanobenzo[*d*][1,3,2]dioxaborol-2-yl)pyrrolidine-1-carbonyl)phenyl) acetamide (3.7i)** The product was synthesized following General Coupling Procedure B. The crude residue was purified by flash chromatography on a silica gel column (eluent 80→100% EtOAc in hexanes) to give a white solid as a mixture of diastereomers (63%). R_f = 0.36 (100% EtOAc); mp = 142-146°C; IR (in $CDCl_3$) cm^{-1} 3270, 3111, 2968, 2921, 1699, 1683, 1606, 1455, 1389, 1376, 1249; ^{1}H NMR (400 MHz, Chloroform-*d*) δ 8.78 (s, 1H), 7.50 (dd, *J* = 11.9, 2.0 Hz, 1H), 7.33 – 7.21 (m, 1H), 7.07 (dt, *J* = 8.4, 1.8 Hz, 1H), 4.32 (td, *J* = 8.6, 8.1, 1.9 Hz, 1H), 3.48 – 3.36 (m, 1H), 3.40 – 3.23 (m, 2H), 2.39 – 2.26 (m, 1H), 2.23 – 2.12 (m, 1H), 2.12 (s, 3H), 2.12 – 1.98 (m, 3H), 1.99 – 1.90

(m, 1H), 1.93 – 1.81 (m, 3H), 1.50 – 1.33 (m, 4H), 1.30 – 1.25 (m, 3H), 0.87 – 0.72 (m, 3H); ^{13}C NMR (126 MHz, Chloroform-*d*) δ 169.43, 169.42, 165.66, 165.39, 158.99 (d, *J* = 248.5 Hz), 159.07 (d, *J* = 248.9 Hz), 142.17 (d, *J* = 11.3 Hz), 141.97 (d, *J* = 11.5 Hz), 129.81 (d, *J* = 4.5 Hz), 129.53 (d, *J* = 4.6 Hz), 118.19 (d, *J* = 17.0 Hz), 117.62 (d, *J* = 16.7 Hz), 115.36, 115.34, 107.57 (d, *J* = 6.6 Hz), 107.36 (d, *J* = 6.8 Hz), 85.63, 85.51, 77.89, 77.66, 51.75, 51.70, 48.01 (d, *J* = 4.5 Hz), 47.89 (d, *J* = 5.0 Hz), 46.51, 46.07, 39.83, 39.77, 38.36 (2C), 36.02, 35.96, 28.97, 28.85, 27.36, 27.31, 27.29 (2C), 27.20, 27.02, 26.53, 26.42, 24.53, 24.51, 24.23 (2C); *^{19}F NMR taken with ^{1}H decoupling.* ^{19}F NMR (471 MHz, $CDCl_3$) -111.34, -110.81; ^{11}B NMR (161 MHz, $CDCl_3$) δ 29.96; HRMS (ESI-) *m/z* calcd for $[C_{23}H_{30}O_4N_2BF- H]^-$ 427.2210, found 427.2213; HPLC (Method B) t_R = 17.6 min, 99.5%.

***N*-(3-methoxy-4-(2-((3a*S*,4*S*,6*S*,7a*R*)-3a,5,5-trimethylhexahydro-4,6-methanobenzo[*d*][1,3,2]dioxaborol-2-yl)pyrrolidine-1-carbonyl)phenyl) acetamide (3.7k)** The product was synthesized following General Coupling Procedure D. The crude residue was purified by flash chromatography on a silica gel column (eluent 90:10 EtOAc-MeOH) to give a white solid as a mixture of diastereomers (63%); R_f = 0.55 (90:10 EtOAc-MeOH); mp = 107-111°C; IR (neat) cm^{-1} 3258, 3187, 2929, 1683, 1598, 1534, 1449, 1399, 1372, 906; ^{1}H NMR (500 MHz, Acetone-d_6) δ 9.42 (s, 1H), 7.61 (t, J = 2.2 Hz, 1H), 7.27 – 7.21 (m, 1H), 7.16 (ddd, J = 8.3, 4.1, 1.9 Hz, 1H), 4.24 (ddd, J = 14.7, 8.7, 2.1 Hz, 1H), 3.86 – 3.80 (m, 3H), 3.46 – 3.37 (m, 1H), 3.23 – 3.15 (m, 1H), 3.10 – 2.99 (m, 1H), 2.36 – 2.18 (m, 1H), 2.17 – 2.10 (m, 1H), 2.09 (s, 3H), 2.03 – 1.87 (m, 4H), 1.86 – 1.80 (m, 2H), 1.80 – 1.66 (m, 1H), 1.55 (dd, J = 18.6, 10.4 Hz, 1H), 1.38 – 1.32 (m, 3H), 1.27 (s, 3H), 0.87 (s, 3H); ^{13}C NMR (126 MHz, Acetone-d_6) δ 24.37 (2C), 24.40 (2C), 26.87, 27.00, 27.27, 27.51, 27.62, 27.66, 28.03, 28.06, 29.36 (2C), 36.91, 36.98, 38.82, 38.83, 40.68, 40.74, 47.37 (2C), 47.75, 47.84, 52.87, 52.90, 55.99, 56.01, 77.65, 77.88, 84.83, 84.96, 103.13, 103.18, 111.56 (2C), 118.81, 119.52, 130.29, 130.53, 143.66, 143.88, 157.69, 157.82, 168.20, 168.51, 169.26, 169.30; ^{11}B NMR (161 MHz, Acetone) δ 26.62; HRMS (ESI+) *m/z* calcd for $[C_{24}H_{33}O_5N_2B + Na]^+$ 463.2375, found 463.2391; HPLC (Method B) t_R = 14.6 min, 99.0%.

(2-Amino-6-fluorophenyl)(2-((3a*S*,4*S*,6*S*,7a*R*)-3a,5,5-trimethylhexahydro-4,6-methanobenzo[*d*][1,3,2]dioxaborol-2-yl)pyrrolidin-1-yl) methanone (3.12a) The product was synthesized following General Coupling Procedure C. The crude residue was purified by flash chromatography on a silica gel column (60:40 hexanes-EtOAc) to give a white solid (83%). R_f =

0.49 (50:50 hexanes-EtOAc); mp = 124-127°C; IR (in $CDCl_3$) cm^{-1} 3464, 3357, 2917, 1623, 1588, 1443, 1389, 1376; ^1H NMR (500 MHz, Chloroform-*d*) δ 7.05 (tdd, *J* = 8.1, 6.4, 1.4 Hz, 1H), 6.42 (d, *J* = 8.1 Hz, 1H), 6.38 (dddd, *J* = 9.1, 8.1, 2.4, 0.8 Hz, 1H), 4.41 (s, 2H), 4.34 (ddd, *J* = 20.5, 8.8, 2.1 Hz, 1H), 3.42 (dddd, *J* = 10.9, 8.0, 4.9, 3.1 Hz, 1H), 3.39 – 3.34 (m, 2H), 2.33 (dddd, *J* = 13.5, 8.9, 4.4, 2.4 Hz, 1H), 2.25 – 2.16 (m, 1H), 2.16 – 2.07 (m, 3H), 2.07 – 1.91 (m, 3H), 1.92 – 1.82 (m, 2H), 1.46 (d, *J* = 25.0 Hz, 2H), 1.43 – 1.36 (m, 2H), 1.28 (s, 3H), 0.84 (s, 3H); ^{13}C NMR (126 MHz, Chloroform-*d*) δ 164.52, 164.24, 159.74 (d, *J* = 245.0 Hz), 159.77 (d, *J* = 245.3 Hz), 146.68 (d, *J* = 6.9 Hz), 146.51 (d, *J* = 6.9 Hz), 131.16 (d, *J* = 10.7 Hz), 131.07 (d, *J* = 10.7 Hz), 111.37 (d, *J* = 2.7 Hz), 111.31 (d, *J* = 2.7 Hz), 109.87 (d, *J* = 22.1 Hz), 109.50 (d, *J* = 21.7 Hz), 104.29 (d, *J* = 11.1 Hz), 104.12 (d, *J* = 11.0 Hz), 85.99, 85.94, 78.09, 77.91, 51.55 (2C), 47.43 (d, *J* = 3.7 Hz), 47.34 (d, *J* = 3.8 Hz), 44.70, 44.68, 39.77, 39.70, 38.36, 38.34, 35.82, 35.77, 28.90, 28.79, 27.27, 27.25, 27.24, 27.22, 27.20, 27.14, 26.46, 26.36, 24.21 (2C); ^{19}F NMR (471 MHz, Chloroform-*d*) δ -115.11 (t, *J* = 7.8 Hz), -115.35 (t, *J* = 7.8 Hz); ^{11}B NMR (161 MHz, $CDCl_3$) δ 30.43; HRMS (ESI+) *m/z* calcd for $[C_{21}H_{28}O_3N_2BF + H]^+$ 387.2250, found 387.2247; HPLC (Method B) t_R = 16.7 min, 99.2%.

(2-Aminophenyl)(2-((3a*S*,4*S*,6*S*,7a*R*)-3a,5,5-trimethylhexahydro-4,6-methanobenzo[*d*][1,3,2]dioxaborol-2-yl)pyrrolidin-1-yl)methanone (3.12b) The product was synthesized following General Coupling Procedure C. The crude residue was purified by flash chromatography on a silica gel column (60:40 hexanes-EtOAc) to give the product as a yellow foam (89%); R_f = 0.38 (50:50 hexanes-EtOAc); IR (in $CDCl_3$) cm^{-1} 3468, 3333, 3067, 2916, 1617, 1573, 1534, 1387, 1370, 1122, 747; ^1H NMR (500 MHz, Chloroform-*d*) δ 7.24 (ddd, *J* = 7.9, 3.6, 1.6 Hz, 1H), 7.18 (dddd, *J* = 8.7, 7.4, 4.1, 1.6 Hz, 1H), 6.71 – 6.65 (m, 2H), 4.77 (s, 2H), 4.32 (ddd, *J* = 22.4, 8.8, 2.1 Hz, 1H), 3.60 – 3.43 (m, 2H), 3.28 – 3.16 (m, 1H), 2.36 (ddq, *J* = 13.3, 9.0, 2.0 Hz, 1H), 2.25 – 2.14 (m, 1H), 2.12 – 1.95 (m, 4H), 1.94 – 1.78 (m, 3H), 1.53 – 1.41 (m, 4H), 1.30 (s, 3H), 0.88 (s, 3H); ^{13}C NMR (126 MHz, $CDCl_3$) δ 24.26, 24.28, 26.44, 26.46, 26.53, 26.67, 27.37, 27.41, 28.07, 28.19, 29.07, 29.22, 36.29, 36.42, 38.31, 38.33, 39.96, 40.02, 47.55, 47.81, 48.81 (2C), 51.97, 52.05, 77.16, 77.25, 77.51, 84.72, 84.89, 115.95, 116.53, 116.61, 116.84, 116.91, 116.93, 128.66, 128.96, 131.72, 132.00, 146.60, 146.93, 170.18, 170.62; ^{11}B NMR (161 MHz, $CDCl_3$) δ 25.62; HRMS (ESI+) *m/z* calcd for $[C_{21}H_{29}O_3N_2B + H]^+$ 369.2344, found 369.2343; HPLC (Method B) t_R = 15.8 min, 49.2%; t_R = 16.0 min, 49.9%.

(2-Fluorophenyl)(2-((3a*S*,4*S*,6*S*,7a*R*)-3a,5,5-trimethylhexahydro-4,6-methanobenzo[*d*][1,3,2]dioxaborol-2-yl)pyrrolidin-1-yl)methanone (3.12c) The product was synthesized following General Coupling Procedure C. The crude residue was purified by flash chromatography on a silica gel column (eluent 70:30 hexanes-EtOAc) to give a clear oil as a mixture of diastereomers (89%); R_f = 0.26 (70:30 hexanes-EtOAc); IR (in $CDCl_3$) cm^{-1} 3067, 2921, 1613, 1584, 1385, 1374, 1227, 1195, 753; ^1H NMR (500 MHz, Acetone-d_6) δ 7.53 – 7.46 (m, 1H), 7.43 – 7.36 (m, 1H), 7.27 (tt, *J* = 7.5, 1.3 Hz, 1H), 7.21 (ddt, *J* = 9.8, 8.3, 1.4 Hz, 1H), 4.34 (ddd, *J* = 14.8, 8.8, 2.3 Hz, 1H), 3.37 (ddt, *J* = 11.2, 8.0, 4.1 Hz, 1H), 3.33 – 3.22 (m, 1H), 3.24 – 3.10 (m, 1H), 2.36 (ddq, *J* = 13.9, 8.9, 2.4 Hz, 1H), 2.21 – 2.11 (m, 1H), 2.12 – 2.06 (m, 1H), 2.03 – 1.96 (m, 2H), 1.95 – 1.90 (m, 1H), 1.90 – 1.85 (m, 1H), 1.85 – 1.64 (m, 2H), 1.64 – 1.41 (m, 1H), 1.41 – 1.20 (m, 6H), 1.01 – 0.78 (m, 3H); ^{13}C NMR (126 MHz, Acetone-d_6) δ 164.92, 164.79, 159.32 (2C, d, *J* = 246.8 Hz), 132.29 (d, *J* = 8.3 Hz), 132.19 (d, *J* = 8.0 Hz), 130.07 (d, *J* = 4.1 Hz), 129.95 (d, *J* = 4.0 Hz), 126.23 (d, *J* = 17.9 Hz), 126.03 (d, *J* = 17.8 Hz), 125.41, 125.38, 116.71, 116.54, 86.10, 86.07, 78.42, 78.27, 52.43, 52.39, 48.37 (d, *J* = 3.3 Hz), 48.26 (d, *J* = 3.6 Hz), 45.38 (2C), 40.49, 40.46, 38.92, 38.91, 36.42, 36.39, 30.24, 30.09, 29.15, 29.02, 28.00, 27.78, 27.73, 27.50, 26.85, 26.83, 24.30 (2C); ^{19}F NMR (471 MHz, Acetone-d_6) δ -116.21 (dt, *J* = 9.5, 6.2 Hz), -116.45 (dt, *J* = 10.1, 6.1 Hz); ^{11}B NMR (161 MHz, $CDCl_3$) δ 30.26; HRMS (ESI+) *m/z* calcd for $[C_{21}H_{27}O_3NBF + Na]^+$ 394.1960, found 394.1966; HPLC (Method B) t_R = 16.9 min, 99.7%.

(2,6-Difluorophenyl)(2-((3a*S*,4*S*,6*S*,7a*R*)-3a,5,5-trimethylhexahydro-4,6-methanobenzo[*d*][1,3,2]dioxaborol-2-yl)pyrrolidin-1-yl)methanone (3.12d). The product was synthesized following General Coupling Procedure C. The crude residue was purified by flash chromatography on a silica gel column (eluent 70:30 hexanes-EtOAc) to give a clear oil as a mixture of diastereomers (94%); R_f = 0.50 (70:30 hexanes-EtOAc); IR (in $CDCl_3$) cm^{-1} 3063, 2921, 1625, 1590, 1385, 1376, 1235, 1007, 791; ^1H NMR (500 MHz, Acetone-d_6) δ 7.60 – 7.41 (m, 1H), 7.14 – 7.05 (m, 2H), 4.35 (ddd, *J* = 14.0, 8.9, 2.2 Hz, 1H), 3.99 – 3.28 (m, 2H), 3.27 – 3.18 (m, 1H), 2.41 – 2.30 (m, 1H), 2.30 – 2.08 (m, 2H), 2.04 – 2.00 (m, 1H), 2.00 – 1.95 (m, 1H), 1.95 – 1.89 (m, 1H), 1.89 – 1.61 (m, 3H), 1.59 – 1.40 (m, 1H), 1.40 – 1.23 (m, 6H), 1.03 – 0.79 (m, 3H); ^{13}C NMR (126 MHz, Acetone-d_6) δ 159.79 (d, *J* = 248.5 Hz), 159.73 (d, *J* = 248.5 Hz), 159.59, 159.51, 132.20 (t, *J* = 9.8 Hz), 116.08 (t, *J* = 23.8 Hz), 112.73 (2C, d, *J* = 3.6 Hz), 112.56 (2C, d, *J* = 3.6 Hz), 86.39, 86.33, 78.57, 78.43, 52.31, 52.26, 48.05, 47.95, 44.95, 44.58, 40.39

(2C), 38.92, 38.90, 36.25, 36.19, 29.06, 28.94, 28.27, 27.97, 27.52 (2C), 27.47 (2C), 26.85, 26.80, 24.28 (2C); ^{19}F NMR (471 MHz, Acetone-d_6) δ -110.34 – -110.47 (m), -111.01 – -111.12 (m), -114.85 – -115.03 (m), -115.13 – -115.24 (m); ^{11}B NMR (161 MHz, Acetone) δ 31.62; ; HRMS (ESI+) *m/z* calcd for $[C_{21}H_{26}O_3NBF_2 + Na]^+$ 412.1866, found 412.1873; HPLC (Method B) t_R = 16.5 min, 19.5%; t_R = 17.1 min, 79.0%.

Phenyl(2-((3a*S*,4*S*,6*S*,7a*R*)-3a,5,5-trimethylhexahydro-4,6-methanobenzo[*d*][1,3,2]dioxaborol-2-yl)pyrrolidin-1-yl)methanone (3.12e). The product was synthesized following General Coupling Procedure C. The crude residue was purified by flash chromatography on a silica gel column (eluent 50:50 hexanes-EtOAc) to give a clear oil as a mixture of diastereomers (77%); R_f = 0.33 (50:50 hexanes-EtOAc); IR (in $CDCl_3$) cm^{-1} 3063, 2921, 1603, 1592, 1385, 1372, 1122, 1080, 698; ^{1}H NMR (500 MHz, Acetone-d_6) δ 7.70 – 7.34 (m, 5H), 4.35 – 4.20 (m, 1H), 3.74 – 3.58 (m, 1H), 3.54 – 3.44 (m, 1H), 3.18 – 3.01 (m, 1H), 2.43 – 2.28 (m, 1H), 2.28 – 2.07 (m, 1.4H), 2.03 – 1.94 (m, 2.6H), 1.94 – 1.80 (m, 2H), 1.79 – 1.66 (m, 1H), 1.64 – 1.50 (m, 1H), 1.49 – 1.31 (m, 3H), 1.30 – 1.24 (m, 3H), 1.23 – 1.05 (m, 1H), 0.95 – 0.74 (m, 3H); ^{13}C NMR (126 MHz, Acetone-d_6) δ 23.48, 23.51, 25.98, 26.08, 26.14, 26.36, 26.72, 26.75, 27.82, 27.88, 28.44, 28.58, 36.02, 36.03, 37.95, 39.78, 39.83, 47.10, 48.44, 48.49, 51.95, 51.96, 76.83, 77.02, 84.09, 84.18, 127.92 (2C), 128.11 (2C), 128.23 (2C), 128.25 (2C), 130.59, 130.77, 133.87, 134.35, 169.04, 169.28; ^{11}B NMR (161 MHz, Acetone-d_6) δ 26.68; HRMS (ESI+) *m/z* calcd for $[C_{21}H_{28}O_3NB + Na]^+$ 376.2054, found 376.2067; HPLC (Method B) t_R = 16.4 min, 35.9%; t_R = 16.5 min, 63.8%.

(2-Fluoro-6-methoxyphenyl)(2-((3a*S*,4*S*,6*S*,7a*R*)-3a,5,5-trimethylhexahydro-4,6-methanobenzo[*d*][1,3,2]dioxaborol-2-yl)pyrrolidin-1-yl)methanone (3.12f). The product was synthesized following General Coupling Procedure C. The crude residue was purified by flash chromatography on a silica gel column (eluent 50:50 hexanes-EtOAc) to give a clear oil as a mixture of diastereomers (75%). R_f = 0.34 (50:50 hexanes-EtOAc); IR (neat) cm^{-1} 3004, 2913, 1740, 1615, 1471, 1389, 1376, 1080, 908; ^{1}H NMR (500 MHz, Acetone-d_6) δ 7.37 (tdd, *J* = 8.4, 6.7, 2.2 Hz, 1H), 6.89 (d, *J* = 8.4 Hz, 1H), 6.81 – 6.66 (m, 1H), 4.38 – 4.08 (m, 1H), 3.98 – 3.81 (m, 3H), 3.76 – 3.20 (m, 2H), 3.15 (q, *J* = 8.8 Hz, 1H), 2.41 – 2.30 (m, 1H), 2.30 – 2.11 (m, 1H), 2.11 – 2.06 (m, 1H), 2.04 – 1.97 (m, 2H), 1.95 – 1.65 (m, 4H), 1.64 – 1.42 (m, 1H), 1.40 – 1.33 (m, 2H), 1.32 – 1.16 (m, 4H), 1.04 – 0.78 (m, 3H); ^{13}C NMR (126 MHz, Acetone-d_6) δ 162.17, 162.02, 160.00 (2C, d, *J* = 245.0 Hz), 158.36, 158.05, 131.51 (d, *J* = 10.1 Hz), 131.47(d, *J* = 10.2

Hz), 116.37, 116.22, 108.73 (d, *J* = 22.2 Hz), 108.66 (d, *J* = 21.7 Hz), 108.04 (2C), 86.13, 86.03, 78.45, 78.29, 56.60 (2C), 52.39, 52.36, 47.61, 47.49, 44.48 (2C), 40.46, 40.44, 38.90 (d, *J* = 4.2 Hz), 38.87 (d, *J* = 3.1 Hz), 36.30, 36.22, 29.14, 28.96, 28.30, 27.99, 27.61, 27.52, 27.51 (2C), 26.87, 26.81, 24.30 (2C); ^{19}F NMR (471 MHz, Acetone-d_6) δ -112.70 (dd, *J* = 8.3, 6.6 Hz), -113.41 (dd, *J* = 8.6, 6.7 Hz); ^{11}B NMR (161 MHz, $CDCl_3$) δ 22.45; HRMS (ESI+) *m/z* calcd for $[C_{22}H_{29}O_4NFB + Na]^+$ 424.2066, found 424.2079; HPLC (Method B) t_R = 16.0 min, 15.6%; t_R = 16.9 min, 82.0%.

(2-Methoxyphenyl)(2-((3a*S*,4*S*,6*S*,7a*R*)-3a,5,5-trimethylhexahydro-4,6-methanobenzo[*d*][1,3,2]dioxaborol-2-yl)pyrrolidin-1-yl)methanone (3.12g). The product was synthesized following General Coupling Procedure C. The crude residue was purified by flash chromatography on a silica gel column (eluent 60:40 hexanes-EtOAc) to give a clear oil as a mixture of diastereomers (75%). R_f = 0.50 (60:40 hexanes-EtOAc); IR (neat) cm^{-1} 3067, 2917, 1601, 1566, 1385, 1373, 1253, 1021, 753; ^{1}H NMR (500 MHz, Acetone-d_6) δ 7.50 – 7.32 (m, 1H), 7.31 – 7.17 (m, 1H), 7.16 – 7.05 (m, 1H), 7.02 – 6.85 (m, 1H), 4.39 – 4.03 (m, 1H), 4.00 – 3.79 (m, 3H), 3.72 – 3.13 (m, 2H), 3.13 – 3.05 (m, 1H), 2.46 – 2.29 (m, 1H), 2.28 – 2.07 (m, 1H), 2.04 – 1.93 (m, 3H), 1.92 – 1.87 (m, 1H), 1.86 – 1.77 (m, 2H), 1.76 – 1.55 (m, 1H), 1.55 – 1.33 (m, 3H), 1.32 – 1.23 (m, 3H), 1.23 – 1.16 (m, 1H), 0.98 – 0.78 (m, 3H); ^{13}C NMR (126 MHz, Acetone-d_6) δ 24.34, 24.36, 26.83, 26.91, 27.54, 27.56, 27.59, 27.78, 27.90, 27.91, 29.16, 29.33, 36.64, 36.66, 38.87 (2C), 40.56, 40.62, 45.97, 46.37, 47.62, 47.75, 52.64 (2C), 56.10, 56.13, 77.94, 78.14, 85.39, 85.51, 112.50, 112.51, 121.36 (2C), 126.29, 126.79, 129.33, 129.48, 131.62, 131.81, 156.80, 156.86, 167.69, 167.94; ^{11}B NMR (161 MHz, Acetone-d_6) δ 29.19; HRMS (ESI+) *m/z* calcd for $[C_{22}H_{30}O_4NB + Na]^+$ 406.2160, found 406.2160; HPLC (Method B) t_R = 16.6 min, 59.8%; t_R = 16.7 min, 39.4%.

(2-(Methylthio)phenyl)(2-((3a*S*,4*S*,6*S*,7a*R*)-3a,5,5-trimethylhexahydro-4,6-methanobenzo[*d*][1,3,2]dioxaborol-2-yl)pyrrolidin-1-yl)methanone (3.12h). The product was synthesized following General Coupling Procedure C. The crude residue was purified by flash chromatography on a silica gel column (eluent 60:40 hexanes-EtOAc) to give a clear oil as a mixture of diastereomers (97%). R_f = 0.46 (60:40 hexanes-EtOAc); IR (in $CHCl_3$) cm^{-1} 3055, 2921, 1611, 1590, 1385, 1376, 1203, 1031; ^{1}H NMR (500 MHz, Acetone-d_6) δ 7.45 – 7.27 (m, 2H), 7.29 – 7.13 (m, 2H), 4.39 – 4.03 (m, 1H), 3.99 – 3.09 (m, 3H), 2.60 – 2.41 (m, 3H), 2.40 – 2.29 (m, 1H), 2.28 – 2.11 (m, 1H), 2.10 – 2.03 (m, 1H), 2.02 – 1.91 (m, 2H), 1.91 – 1.87 (m, 1H), 1.87 –

1.80 (m, 2H), 1.80 – 1.58 (m, 1H), 1.58 – 1.35 (m, 3H), 1.35 – 0.99 (m, 4H), 0.99 – 0.79 (m, 3H); ^{13}C NMR (126 MHz, Acetone-d_6) δ 16.07, 16.14, 24.31 (2C), 26.80, 26.91, 27.51, 27.52, 27.86, 28.00, 28.02, 28.09, 29.01, 29.24, 29.84, 36.40 (2C), 38.88, 38.90, 40.45, 40.49, 44.96 (2C), 48.31, 48.38, 52.41, 52.45, 78.19, 78.38, 85.96, 86.03, 126.05, 126.09, 127.58, 127.64, 127.72, 127.89, 130.16, 130.21, 136.27, 136.32, 138.15, 138.27, 167.98, 168.17; ^{11}B NMR (161 MHz, Acetone-d_6) δ 30.96; HRMS (ESI+) *m/z* calcd for $[C_{22}H_{30}O_3NBS + H]^+$ 400.2112, found 400.2108; HPLC (Method B) t_R = 17.4 min, 99.2%

General Procedure for boronic ester deprotection. The boronic ester was dissolved in DCM (0.1 M), and the solution was cooled to –78°C. BCl_3 (1 M in DCM, 5 eq) was added dropwise, and the reaction stirred at –78°C for 1 hour (or at room temperature overnight for **3.12i**). The solvent and excess BCl_3 were removed *in vacuo* and co-evaporated several times with anhydrous DCM. The resultant brown residue was dissolved in H_2O and DCM, and the product was extracted with H_2O. The combined aqueous layers were washed with Et_2O and EtOAc and concentrated *in vacuo* to give the products as solids. In the case of **3.7e** and **3.7j**, deacetylated product can be re-acetylated by dissolving the solid in H_2O (0.1 M final solution), adding Ac_2O (10 eq), and sonicating the solution (with a balloon to trap AcOH vapors and prevent pressure build-up) for 30 minutes. The solution can then be concentrated *in vacuo* to give the final acetylated product.

(1-(4-Acetamidobenzoyl)pyrrolidin-2-yl)boronic acid (3.7e) The product was isolated as a white solid (91%). R_f = does not elute on silica-backed TLC plates; mp = *compound does not melt, decomposes* > 250°C; IR (neat) cm^{-1} 3202, 3009, 2865, 1681, 1598, 1443, 1194, 797; ^{1}H NMR (500 MHz, DMSO-d_6) δ 10.52 (s, 1H), 7.85 (d, *J* = 8.7 Hz, 2H), 7.80 (d, *J* = 8.7 Hz, 2H), 4.02 – 3.94 (m, 1H), 3.48 (dt, *J* = 11.6, 8.1 Hz, 1H), 2.86 (dd, *J* = 11.9, 6.4 Hz, 1H), 2.20 – 2.10 (m, 2H), 2.09 (s, 3H), 1.76 (dt, *J* = 13.0, 6.7 Hz, 1H), 1.48 (qd, *J* = 11.8, 7.8 Hz, 1H); ^{13}C NMR (126 MHz, DMSO-d_6) δ 169.53, 169.34, 144.43, 131.23 (2C), 119.26, 118.51 (2C), 58.68, 47.77, 28.92, 24.52, 24.27; ^{11}B NMR (161 MHz, DMSO-d_6) δ 20.03; HRMS (ESI+) *m/z* calcd for $[C_{13}H_{17}BN_2O_4 + Na]^+$ 299.1174, found 299.1177; HPLC (Method B) t_R = 9.7 min, 95.6%.

(1-(4-Acetamido-2-fluorobenzoyl)pyrrolidin-2-yl)boronic acid (3.7j) The product was isolated as a white solid (71%). R_f = does not elute on silica-backed TLC plates; mp = *compound does not melt, decomposes* > 250°C; IR (neat) cm^{-1} 3198, 2976, 1695, 1623, 1604, 1419, 1247, 880; ^{1}H NMR (500 MHz, DMSO-d_6) δ 10.59 (s, 1H), 7.79 (dd, *J* = 13.7, 2.0 Hz, 1H), 7.70 (t, *J* = 8.4 Hz, 1H), 7.44 (dd, *J* = 8.7, 2.0 Hz, 1H), 3.68 (dt, *J* = 12.9, 7.0 Hz, 1H), 3.35 (dt, *J* = 11.8, 7.8

Hz, 1H), 2.87 (dd, *J* = 11.5, 6.9 Hz, 1H), 2.18 – 1.98 (m, 5H), 1.80 (dq, *J* = 11.9, 5.6 Hz, 1H), 1.55 (tt, *J* = 12.0, 9.6 Hz, 1H); ^{13}C NMR (126 MHz, DMSO-d_6) δ 169.67, 167.19, 160.43 (d, *J* = 253.2 Hz), 146.06 (d, *J* = 12.2 Hz), 132.14, 114.92, 107.95 (d, *J* = 12.2 Hz), 105.93 (d, *J* = 26.9 Hz), 57.67, 47.11 (d, *J* = 5.6 Hz), 27.85, 24.75, 24.31; ^{19}F NMR (471 MHz, DMSO-d_6) δ -106.79 (dd, *J* = 13.9, 8.2 Hz); ^{11}B NMR (161 MHz, DMSO) δ 19.99; HRMS (ESI+) *m/z* calcd for $[C_{13}H_{16}BFN_2O_4 + Na]^+$ 317.1079, found 317.1086; HPLC (Method B) t_R = 10.3 min, 95.6%.

(1-(2-Amino-6-fluorobenzoyl)pyrrolidin-2-yl)boronic acid (3.12i) The product was isolated as a beige solid, which was triturated in Et_2O and filtered under vacuum to give the product as a beige solid (57%). R_f: does not elute on silica-backed TLC plates; mp = *compound does not melt, decomposes* > 250°C; IR (neat) cm^{-1} 3198, 2964, 1635, 1615, 1443, 1400, 1191, 789, 709; (NMR peaks are reported for both rotamers, ratio ~7:3) ^{1}H NMR (500 MHz, DMSO-d_6) δ 8.16 (s, 2H), 7.45 (td, *J* = 8.2, 5.7 Hz, 0.7H), 7.29 (td, *J* = 8.2, 6.5 Hz, 0.3H), 7.16 (t, *J* = 9.2 Hz, 0.7H), 7.08 (d, *J* = 7.8 Hz, 0.7H), 6.63 (d, *J* = 8.4 Hz, 0.3H), 6.45 (dd, *J* = 10.8, 8.1 Hz, 0.3H), 3.55 (dt, *J* = 13.0, 6.9 Hz, 0.3H), 3.51 – 3.38 (m, 1.4H), 3.21 (dt, *J* = 12.2, 7.9 Hz, 0.3H), 2.88 (dd, *J* = 11.4, 6.9 Hz, 0.3H), 2.43 (dd, *J* = 9.3, 3.3 Hz, 0.7H), 2.07 – 1.96 (m, 1H), 1.84 – 1.77 (m, 1H), 1.77 – 1.69 (m, 1H), 1.64 – 1.52 (m, 1H); ^{13}C NMR (126 MHz, DMSO-d_6) δ 166.93 (0.3C), 160.74 (d, *J* = 249.0 Hz), 159.60 (d, *J* = 251.40 Hz), 158.71 (0.7C), 150.25 (d, *J* = 4.7 Hz, 0.3C), 136.00 (d, *J* = 5.0 Hz, 0.7C), 134.95 (d, *J* = 11.0 Hz, 0.3C), 131.30 (d, *J* = 9.6 Hz, 0.7C), 120.01 (d, *J* = 15.8 Hz, 0.7C), 119.27 (0.7C), 114.16 (d, *J* = 21.8 Hz, 0.7C), 112.12 (0.3C), 101.85 (d, *J* = 21.8 Hz, 0.3C), 97.39 (d, *J* = 16.6 Hz, 0.3C), 46.45 (d, *J* = 5.0 Hz), 51.33 (0.7C), 56.11 (0.3C), 46.45 (d, *J* = 5.0 Hz, 0.3C), 46.14 (0.7C), 27.61 (0.3C), 26.54 (0.7C), 24.71 (0.3C), 24.21 (0.7C); ^{19}F NMR (471 MHz, DMSO-d_6) δ -111.45 (dd, *J* = 11.0, 6.8 Hz, 0.3F), -113.24 (dd, *J* = 10.1, 5.8 Hz, 0.7F). ^{11}B NMR (161 MHz, DMSO) δ 19.97; HRMS (ESI+) *m/z* calcd for $[C_{11}H_{14}BFN_2O_3 + Na]^+$ 275.0974, found 275.0968; HPLC (Method B) t_R = 11.2 min, 95.7%.

3.7 References

(1) American Cancer Society: Cancer Facts and Figures. https://www.cancer.org/research/cancer-facts-statistics/all-cancer-facts-figures/cancer-facts-figures-2018.html (accessed Sept. 10 2018).

(2) Christiansen, V. J.; Jackson, K. W.; Lee, K. N.; Downs, T. D.; McKee, P. A., Targeting Inhibition of Fibroblast Activation Protein-α and Prolyl Oligopeptidase Activities on Cells Common to Metastatic Tumor Microenvironments. *Neoplasia* **2013,** *15* (4), 348-358.

(3) Joyce, J. A.; Fearson, D. T., T cell exclusion, immune privilege, and the tumor microenvironment. *Science* **2015,** *348* (6230), 74-80.

(4) Spill, F.; Reynolds, D. S.; Kamm, R. D.; Zaman, M. H., Impact of the physical microenvironment on tumor progression and metastasis. *Curr Opin Biotechnol* **2016,** *40*, 41-8.

(5) Kelly, T.; Huang, Y.; Simms, A. E.; Mazur, A., Fibroblast Activation Protein-α. A Key Modulator of the Microenvironment in Multiple Pathologies. 2012; Vol. 297, pp 83-116.

(6) Santos, A. M.; Jung, J.; Aziz, N.; Kissil, J. L.; Puré, E., Targeting fibroblast activation protein inhibits tumor stromagenesis and growth in mice. *J Clin Invest* **2009,** *119* (12), 3613-3625.

(7) Franco, O. E.; Hayward, S. W., Targeting the Tumor Stroma as a Novel Therapeutic Approach for Prostate Cancer. *Adv Pharmacol* **2012,** *65*, 267-313.

(8) Liu, R.; Li, H.; Liu, L.; Yu, J.; Ren, X., Fibroblast activation protein: A potential therapeutic target in cancer. *Cancer Biol Ther* **2012,** *13* (3), 123-129.

(9) Koontongkaew, S., The Tumor Microenvironment Contribution to Development, Growth, Invasion and Metastasis of Head and Neck Squamous Cell Carcinomas. *J Cancer* **2013,** *4* (1), 66-83.

(10) Barar, J., Targeting Tumor Microenvironment: The Key Role of Immune System. *BioImpacts* **2012,** *2* (1), 1-3.

(11) Sung, S. Y.; Hsieh, C. L.; Wu, D.; Chung, L. W. K.; Johnstone, P. A. S., Tumor Microenvironment Promotes Cancer Progression, Metastasis, and Therapeutic Resistance. *Curr Prob Cancer* **2007,** *31* (2), 36-100.

(12) Zi, F.; He, J.; He, D.; Li, Y.; Yang, L.; Cai, Z., Fibroblast activation protein alpha in tumor microenvironment: recent progression and implications (review). *Mol Med Rep* **2015,** *11* (5), 3203-11.

(13) Myohanen, T. T.; Tenorio-Laranga, J.; Jokinen, B.; Vazquez-Sanchez, R.; Moreno-Baylach, M. J.; Garcia-Horsman, J. A.; Mannisto, P. T., Prolyl oligopeptidase induces angiogenesis both in vitro and in vivo in a novel regulatory manner. *Br J Pharmacol* **2011,** *163* (8), 1666-78.

(14) Männistö, P. T.; García-Horsman, J. A., Mechanism of Action of Prolyl Oligopeptidase (PREP) in Degenerative Brain Diseases: Has Peptidase Activity Only a Modulatory Role on the Interactions of PREP with Proteins? *Front Aging Neurosci* **2017,** *9*, 27.

(15) Hannula, M. J.; Myöhänen, T. T.; Tenorio-Laranga, J.; Männistö, P. T.; Garcia-Horsman, J. A., Prolyl oligopeptidase colocalizes with α-synuclein, β-amyloid, tau protein and astroglia in the post-mortem brain samples with Parkinson's and Alzheimer's diseases. *Neuroscience* **2013,** *242*, 140-150.

(16) Svarcbahs, R.; Julku, U. H.; Norrbacka, S.; Myöhänen, T. T., Removal of prolyl oligopeptidase reduces alpha-synuclein toxicity in cells and in vivo. *Sci Rep* **2018,** *8* (1), 1552.

(17) Lawandi, J., Gerber-Lemaire, S., Juillerat-Jeanneret, L., Moitessier, N., Inhibitors of Prolyl Oligopeptidases for the Therapy of Human Diseases: Defining Diseases and Inhibitors. *J Med Chem* **2010,** *53*, 3423–3438.

(18) Jackson, K. W.; Christiansen, V. J.; Yadav, V. R.; Silasi-Mansat, R.; Lupu, F.; Awasthi, V.; Zhang, R. R.; McKee, P. A., Suppression of Tumor Growth in Mice by Rationally Designed Pseudopeptide Inhibitors of Fibroblast Activation Protein and Prolyl Oligopeptidase. *Neoplasia* **2015,** *17*, 43-54.

(19) Teichgraber, V.; Monasterio, C.; Chaitanya, K.; Boger, R.; Gordon, K.; Dieterle, T.; Jager, D.; Bauer, S., Specific inhibition of fibroblast activation protein (FAP)-alpha prevents tumor progression in vitro. *Adv Med Sci* **2015,** *60* (2), 264-72.

(20) Tanaka, S.; Suzuki, K.; Sakaguchi, M., The prolyl oligopeptidase inhibitor SUAM-14746 attenuates the proliferation of human breast cancer cell lines in vitro. *Breast Cancer* **2017**, 1-9.

(21) Evans, D. M., Horton, J., Trim, J. E. Fap inhibitors. WO 2007085895 A2, 2007.

(22) Poplawski, S. E.; Lai, J. H.; Li, Y.; Jin, Z.; Liu, Y.; Wu, W.; Wu, Y.; Zhou, Y.; Sudmeier, J. L.; Sanford, D. G.; Bachovchin, W. W., Identification of selective and potent inhibitors of fibroblast activation protein and prolyl oligopeptidase. *J Med Chem* **2013,** *56* (9), 3467-3477.

(23) Jansen, K.; Heirbaut, L.; Verkerk, R.; Cheng, J. D.; Joossens, J.; Cos, P.; Maes, L.; Lambeir, A. M.; De Meester, I.; Augustyns, K.; Van der Veken, P., Extended structure-activity relationship and pharmacokinetic investigation of (4-quinolinoyl)glycyl-2-cyanopyrrolidine inhibitors of fibroblast activation protein (FAP). *J Med Chem* **2014,** *57* (7), 3053-74.

(24) Tsuda, M.; Muraoka, Y.; Nagai, M.; Aoyagi, T.; Takeuchi, T., Poststatin, a New Inhibitor of Prolyl Endopeptidase; VIII. Endopeptidase Inhibitory Activity of Non-peptidyl Poststatin Analogues. *J Antibiot* **1996,** *49* (10), 1022-1030.

(25) Morain, P. L., P.; De Nanteuil, G.; Jochemsen, R.; Robin,; J. L.; Guez, D. B., P. A., S 17092: A Prolyl Endopeptidase Inhibitor as a Potential Therapeutic Drug for Memory Impairment. Preclinical and Clinical Studies. *CNS Drug Rev* **2002,** *8*, 31-52.

(26) Drug Profile: S-17092. http://adisinsight.springer.com/drugs/800011104 (accessed 09 April 2016).

(27) Lawandi, J.; Toumieux, S.; Seyer, V.; Campbell, P.; Thielges, S.; Juillerat-Jeanneret, L.; Moitessier, N., Constrained Peptidomimetics Reveal Detailed Geometric Requirements of Covalent Prolyl Oligopeptidase Inhibitors. *J Med Chem* **2009,** *52*, 6672-6684

(28) De Cesco, S., Deslandes, S., Therrien, E., Levan, D., Cueto, M., Schmidt, R., ; Cantin, L.-D., Mittermaier, A., Juillerat-Jeanneret, L., Moitessier, N., Virtual Screening and Computational Optimization for the Discovery of Covalent Prolyl Oligopeptidase Inhibitors with Activity in Human Cells. *J Med Chem* **2012,** *55*, 6306−6315.

(29) Mariaule, G.; De Cesco, S.; Airaghi, F.; Kurian, J.; Schiavini, P.; Rocheleau, S.; Huskic, I.; Auclair, K.; Mittermaier, A.; Moitessier, N., 3-Oxo-hexahydro-1H-isoindole-4-carboxylic Acid as a Drug Chiral Bicyclic Scaffold: Structure-Based Design and Preparation of Conformationally Constrained Covalent and Noncovalent Prolyl Oligopeptidase Inhibitors. *J Med Chem* **2016,** *59* (9), 4221-34.

(30) Schiavini, P.; Pottel, J.; Moitessier, N.; Auclair, K., Metabolic Instability of Cyanothiazolidine-Based Prolyl Oligopeptidase Inhibitors: a Structural Assignment Challenge and Potential Medicinal Chemistry Implications. *ChemMedChem* **2015,** *10*, 1174-1183.

(31) Therrien, E.; Englebienne, P.; Arrowsmith, A. G.; Mendoza-Sanchez, R.; Corbeil, C. R.; Weill, N.; Campagna-Slater, V.; Moitessier, N., Integrating medicinal chemistry, organic/combinatorial chemistry, and computational chemistry for the discovery of selective

estrogen receptor modulators with Forecaster, a novel platform for drug discovery. *J Chem Inf Model* **2012,** *52* (1), 210-24.

(32) Corbeil, C. R.; Englebienne, P.; Moitessier, N., Docking Ligands into Flexible and Solvated Macromolecules. 1. Development and Validation of FITTED 1.0. *J Chem Inf Model* **2007,** *47*, 435-449.

(33) Moitessier, N.; Pottel, J.; Therrien, E.; Englebienne, P.; Liu, Z.; Tomberg, A.; Corbeil, C. R., Medicinal Chemistry Projects Requiring Imaginative Structure-Based Drug Design Methods. *Acc Chem Res* **2016,** *49* (9), 1646-57.

(34) De Cesco, S.; Kurian, J.; Dufresne, C.; Mittermaier, A. K.; Moitessier, N., Covalent inhibitors design and discovery. *Eur J Med Chem* **2017,** *138*, 96-114.

(35) Di Trani, J. M.; De Cesco, S.; O'Leary, R.; Plescia, J.; do Nascimento, C. J.; Moitessier, N.; Mittermaier, A. K., Rapid measurement of inhibitor binding kinetics by isothermal titration calorimetry. *Nat Commun* **2018,** *9* (1), 893.

(36) Di Trani, J. M.; Moitessier, N.; Mittermaier, A. K., Measuring Rapid Time-Scale Reaction Kinetics Using Isothermal Titration Calorimetry. *Anal Chem* **2017,** *89* (13), 7022-7030.

(37) Di Trani, J. M.; Moitessier, N.; Mittermaier, A. K., Complete Kinetic Characterization of Enzyme Inhibition in a Single Isothermal Titration Calorimetric Experiment. *Anal Chem* **2018,** *90* (14), 8430-8435.

(38) Ban, F.; Dalal, K.; Li, H.; LeBlanc, E.; Rennie, P. S.; Cherkasov, A., Best Practices of Computer-Aided Drug Discovery: Lessons Learned from the Development of a Preclinical Candidate for Prostate Cancer with a New Mechanism of Action. *J Chem Inf Model* **2017,** *57* (5), 1018-1028.

(39) Nakajima, T.; Ono, Y.; Kato, A.; Maeda, J.-i.; Ohe, T., Y-29794 — a non-peptide prolyl endopeptidase inhibitor that can penetrate into the brain. *Neurosci Lett* **1992,** *141* (2), 156-160.

(40) Kato, A.; Fukunari, A.; Sakai, Y.; Nakajima, T., Prevention of amyloid-like deposition by a selective prolyl endopeptidase inhibitor, Y-29794, in senescence-accelerated mouse. *J Pharmacol Exp Ther* **1997,** *283* (1), 328-335

(41) Kaushik, S.; Sowdhamini, R., Structural Analysis of Prolyl Oligopeptidases Using Molecular Docking and Dynamics: Insights into Conformational Changes and Ligand Binding. *PLoS ONE* **2011,** *6* (11), e26251.

(42) Plescia, J.; De Cesco, S.; Burai Patrascu, M.; Kurian, J.; Di Trani, J. M.; Dufresne, C.; Wahba, A.; Janmamode, N.; Mittermaier, A. K.; Moitessier, N., Integrated Synthetic, Biophysical and Computational Investigations of Covalent Inhibitors of Prolyl Oligopeptidase and Fibroblast Activation Protein α. *J Med Chem* **2019,** *62* (17), 7874-7884.

(43) Veber, D. F.; Johnson, S. R.; Cheng, H.-Y.; Smith, B. R.; Ward, K. W.; Kopple, K. D., Molecular Properties That Influence the Oral Bioavailability of Drug Candidates. *J Med Chem* **2002,** *45*, 2615-2623.

(44) Veera Reddy, A., Ravindranath, B., Acetylation Under Ultrasonic Conditions: Convenient Preparation of N-Acetylamino Acids. *Synth Commun* **1992,** *22* (2), 257-264.

(45) Kelly, T. A.; Fuchs, V. U.; Perry, C. W.; Snow, R. J., The efficient synthesis and simple resolution of a prolineboronate ester suitable for enzyme-inhibition studies. *Tetrahedron* **1993,** *49* (5), 1009-1016.

(46) Fukushima, H.; Hiratate, A.; Takahashi, M.; Saito, M.; Munetomo, E.; Kitano, K.; Saito, H.; Takaoka, Y.; Yamamoto, K., Synthesis and structure–activity relationships of potent 3- or 4-substituted-2-cyanopyrrolidine dipeptidyl peptidase IV inhibitors. *Bioorg Med Chem* **2004,** *12* (23), 6053-6061.

(47) Lebarbier, C.; Carreaux, F.; Carboni, B.; Boucher, J. L., Synthesis of boronic acid analogs of L-arginine as alternate substrates or inhibitors of nitric oxide synthase. *Bioorg Med Chem Lett* **1998,** *8* (18), 2573-2576.

(48) Coutts, S. J.; Kelly, T. A.; Snow, R. J.; Kennedy, C. A.; Barton, R. W.; Adams, J.; Krolikowski, D. A.; Freeman, D. M.; Campbell, S. J.; Ksiazek, J. F.; Bachovchin, W. W., Structure−Activity Relationships of Boronic Acid Inhibitors of Dipeptidyl Peptidase IV. 1. Variation of the P2 Position of Xaa-boroPro Dipeptides. *J Med Chem* **1996,** *39* (10), 2087-2094.

(This page is intentionally left blank.)

Chapter 4:

Computer-aided design, synthesis, and biological evaluation of [4.3.0] bicyclic prolyl oligopeptidase and fibroblast activation protein α dual inhibitors

This chapter is a draft of a manuscript prepared for *J Med Chem*:
Plescia, J.; Hédou, D.; Poussé, M. E.; Mittermaier, A.; Moitessier, N. Computer-aided design, synthesis, and biological evaluation of [4.3.0] bicyclic prolyl oligopeptidase and fibroblast activation protein α dual inhibitors. Prepared for *J Med Chem*.

Previous chapters have established that boronic acids are excellent electrophiles for reversible covalent drugs. Chapter 2 confirmed that they are, in fact, the optimal group for targeting both POP and FAP. Chapter 3 allowed us to further explore boronic esters for targeting POP, with various side chains or functional groups. These chapters lead us to our current study, in which we designed dual reversible covalent boronic ester/acid peptidomimetic inhibitors of POP and FAP.

Contribution(s) of authors: I designed, synthesized, and characterized all molecules presented in this chapter and conducted 90% of the *in vitro* assays, the rest of which were conducted by Naëla Janmamode. Caroline Dufresne purified the POP enzyme. Alexander S. Wahba conducted the mass spectroscopy studies. I conducted the virtual screening and analysis with aide from Professor Nicolas Moitessier.

4.1 Abstract

We have previously described several different chemical series of bicyclic prolyl oligopeptidase (POP) inhibitors as probes for neurodegenerative diseases that demonstrated nanomolar activity *in vitro* and submicromolar activity *in cellulo*. The more recent implication of POP in cancer, together with homologous fibroblast activation protein α (FAP), implicated in tumor growth, led us to consider developing POP/FAP dual inhibitors as a promising strategy for the development of cancer therapeutics. We report herein docking-guided design of a new bicyclic scaffold and synthesis of both covalent and non-covalent bicyclic inhibitors. Biological evaluation of first-of-their-kind [4.3.0] bicyclic compounds confirmed that reactive groups, or covalent warheads, are required for inhibitor activity. This work ultimately led to a dual inhibitor equipotent to the only anti-POP/FAP drug that ever-reached clinical trials.

4.2 Introduction

Prolyl oligopeptidase (POP, also referred to as PREP) and fibroblast activation protein-α (FAP, also referred to as seprase), are homologous serine proteases whose function consists of cleaving short peptides at the C-terminal end of proline residues. POP was discovered in the mid-70's, and its high concentration in the central nervous system (CNS) immediately drew attention;[1-3] early studies associated POP protease activity to neuropeptides and peptide hormones. Inhibition of this protease activity was first investigated with the reversible covalent inhibitor **4.1** over thirty years ago (Figure 4.1). However, after significant targeted research and unsuccessful clinical trials, this progress reached a plateau (Figure 4.1). In more recent years, a second boost in the development of POP inhibitors has occurred, and their potential in Alzheimer's disease (AD) and Parkinson's disease (PD) has been under further investigation.[1-4] More specifically, about 10 years ago, Lambeir and co-workers first linked POP to α-synuclein (aSyn) aggregation, a hallmark of PD,[5] and Myohanen and co-workers revealed the colocalization of POP with aSyn, amyloid beta (Aβ), and the tau protein in brain samples from patients with PD or AD.[6] The link between POP and aSyn aggregation was further supported by extensive studies by Myohanen and co-workers who first showed that aggregation is induced by POP-aSyn protein-protein interaction and is unrelated to the protease activity of POP.[7-8] The same group also demonstrated the effect of KYP-2047, a POP inhibitor (Figure 4.2), on aSyn aggregate clearance[9-10] and the restoration of motor behaviour

in mouse models, while Lee and co-workers identified POP inhibitors and confirmed their effect on aSyn expression.[11]

In addition to these recent advances in neurodegenerative research linking POP to AD and PD, this enzyme's proteolytic activity was also recently found to contribute to the release of acetyl-SDKP, a potent tetrapeptide that stimulates of angiogenesis.[12] It has since been reported that POP inhibition blocks the growth of human gastric cancer cells[13] and the proliferation of breast cancer cells.[14] We have also demonstrated that our own inhibitors (series based on **4.2** and **4.3**, Figure 4.1) can block POP protease activity in various cancer cell lines.[15-16] The endopeptidase activity of POP is shared with FAP, the latter of which is suggested to be a key modulator of the tumor microenvironment (TME)[17-19] and is thus a promising target for novel anticancer therapeutics.[20] Discovered over 10 years after POP, FAP is overexpressed in most human epithelial-derived cancers[21] and has also been suggested to promote tumor growth.[17, 22] In fact, its inhibition significantly affects stromal growth *in vivo*.[18] Most importantly, FAP is not detectable in normal tissues,[23] making it an extremely valuable target for therapeutic intervention against refractory tumors, and inhibitor development has in fact already started (Figure 4.2).[24-26]

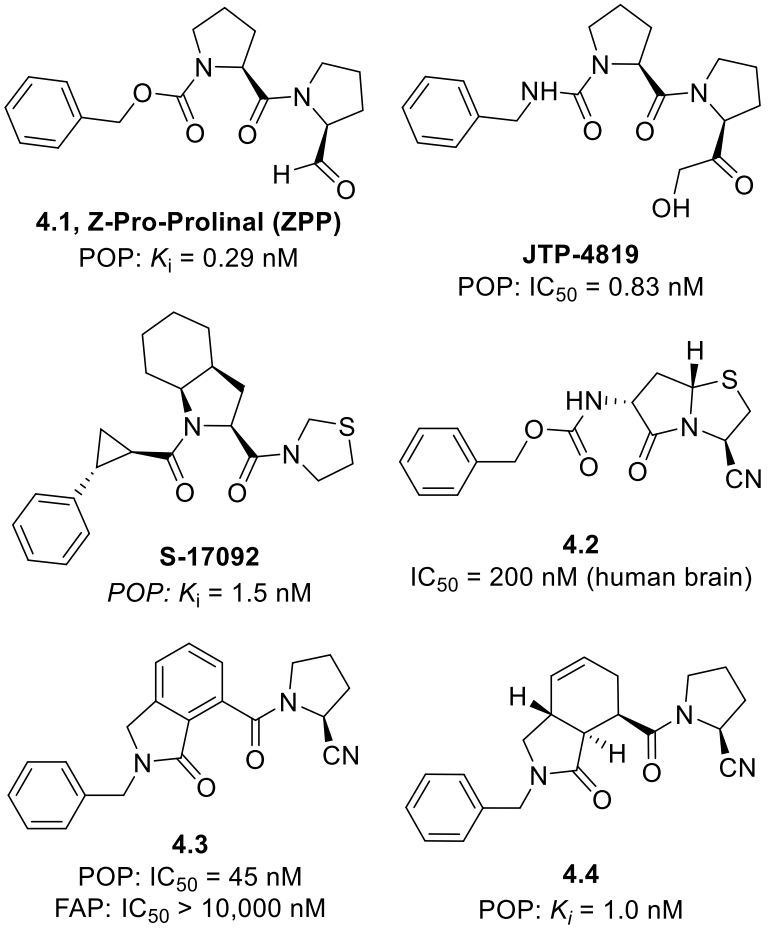

Figure 4.1. Selected POP and FAP inhibitors

In recent medicinal chemistry endeavors, selective inhibition of one enzyme over the other has been pursued. As illustrated in Figure 4.2 selectivity is very sensitive to minor structural changes. For example, while compound **4.5** is highly FAP selective, the analogue **4.6** is highly POP selective. This D-Ala-induced selectivity for FAP has been further observed recently.[27] Nevertheless, Christiansen *et al*. suggested that targeting both FAP and POP blocks stromal invasion and angiogenesis, respectively, and may alter cancer growth.[28] They designed a pseudopeptide dual inhibitor which was found to block tumor growth in mice. These findings suggest that dual inhibition is a promising strategy, though this large, non-drug-like molecule was unsuitable for further consideration.[29] Consequently, although an overview of the literature suggests that selectivity may be easier to achieve than dual inhibition, the latter may be an ideal strategy for designing and developing anti-cancer therapeutics.

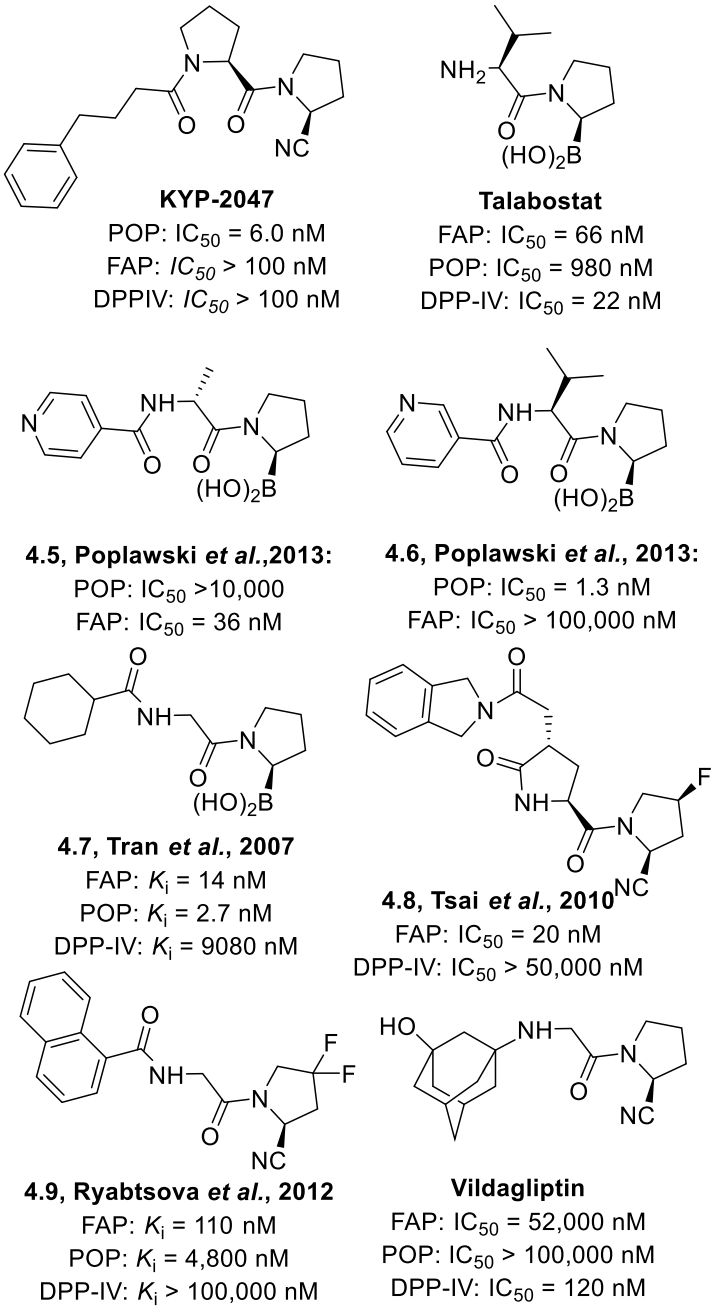

Figure 4.2. Selected known POP and FAP inhibitors and their selectivity profiles [24, 26, 30-31]

In 2009, the Moitessier group reported a series of [3.3.0] bicyclic POP inhibitors based on compound **4.2** which were found to be cell-permeant and potent in the sub-micromolar range. This series of nitrile-containing compounds were designed to act as covalent inhibitors targeting the catalytic serine in the POP active site.[15] Interestingly, a few years later, KYP-2047 was co-crystallized with POP, demonstrating the covalent nature of the binding of nitrile derivatives in

the active site of POP.[32] However, the series of inhibitors based on compound **4.2** was halted after metabolism studies revealed it to be metabolized into complex mixtures via oxidation of the sulfur.[33] A few years later, compound **4.3** was discovered via virtual screening and docking-guided optimization. This inhibitor exhibited a POP inhibitory activity five times more potent than that of the first hit **4.2** and was active in low-micromolar concentrations on human glioblastoma and endothelial cancer cells.[16] In addition, it was found that the introduction of the [4.3.0] bicyclic molecular scaffold improved the metabolic stability of the inhibitors.[16]

Three years ago, we also reported the structure-based design and synthesis of a novel class of POP inhibitors based on a hexahydroisoindole scaffold, such as **4.4** (Figure 4.1). A docking study guided the selection of structures (both in terms of stereo- and regiochemistry) for synthesis. Following the synthesis of the best virtual candidates, *in vitro* assays revealed that one member of this chemical series, compound **4.4**, was more active than any of our previous inhibitors, exhibiting a K_i of 1.0 nM. Additional assays also showed that the scaffold of this potent inhibitor, in contrast to the series based on compound **4.2**, is highly metabolically stable.[34] However, upon *in vitro* testing of **4.3** and **4.4** against recombinant FAP, they were completely inactive. Analysis of docking poses revealed a lack of stabilizing interactions with the two glutamic acid residues in the active site of FAP (Glu203 and Glu204).

With this information in hand, we became interested in the design of dual POP/FAP inhibitors. We report herein our successful efforts in the development of dual inhibitors based on an improved bicyclic core.

4.3 Results and discussion

4.3.1 Computer-aided design.

With our first three series of POP inhibitors illustrated by compounds **4.2**, **4.3** and **4.4**, we have demonstrated the accuracy of our docking program FITTED[35-37] in predicting binding modes of POP covalent inhibitors. When **4.2** and stereoisomers of **4.2** (adhering to the [3.3.0] bicyclic system) were evaluated, we found that the stereochemistry corresponding to that of D-amino acids was optimal (hydrogen atom highlighted in blue in Figure 4.3, compound **4.2**). The resultant stereochemistry upon cyclization (hydrogen atom highlighted in green in Figure 4.3) at the ring junction fortunately imposed a shape that fit best in the binding site. In this previous report,[15] computational studies also indicated that this [3.3.0] bicyclic system was less optimal for binding

to POP, and that a [4.3.0]-ring system with a specific stereochemistry should exhibit better affinity (Figure 4.3, compound **4.2a**).[18] Unfortunately, our synthetic efforts were vain, as the epimer at the ring junction (hydrogen atom highlighted in green in Figure 4.3, compound **4.2a**) was the only isomer observed experimentally but was not predicted to bind optimally in the active site of POP.

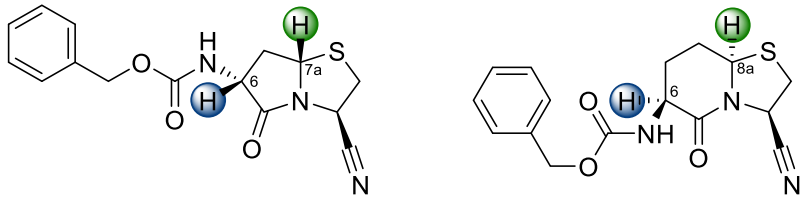

Figure 4.3. POP inhibitors designed by our group in the past, including required stereochemistry for optimal inhibitor stabilization in the active site of POP (highlighted with blue and green hydrogens).

Further computational predictions indicated that the affinity for POP could be improved by increasing the size of the western ring and inverting two stereocenters, both the carbon at the cyclic fusion (C_{7a} in **4.2**, C_{8a} in **4.2a**) and the carbon alpha to the cyclic amide (C_6). To do so, we decided to prepare a first series of analogues built around a [4.3.0]-ring system similar to that of **4.2a** but which could be accessible synthetically. After several rounds of virtual modifications and docking predictions, inhibitor structure **4.10a** was discovered. As can be seen in Figure 4.4, the predicted binding mode of nitrile **4.10a** is highly favored, featuring the same key interactions as potent aldehyde **4.1**.

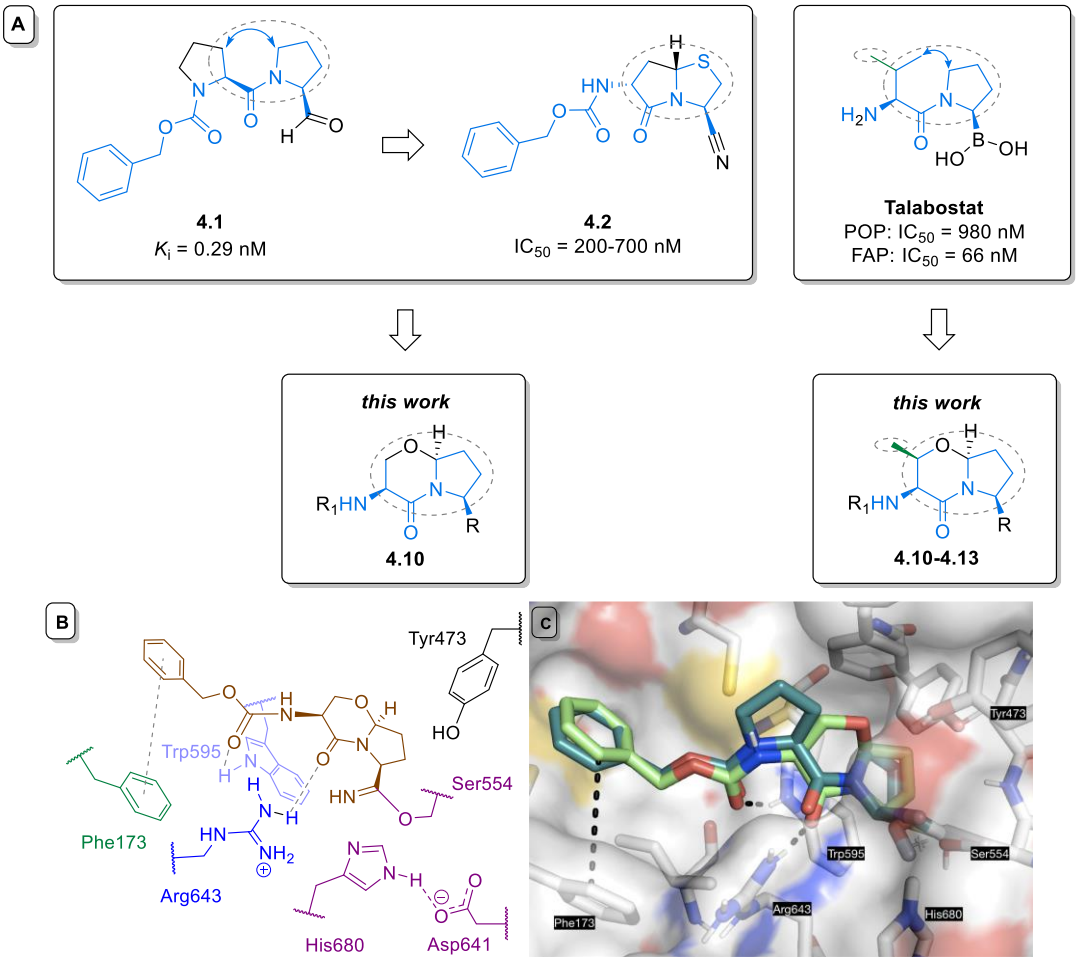

Figure 4.4. *In silico* design of a new series of bicycles. (A) Previously designed POP inhibitors and newly designed series of potential dual inhibitors. (B) Schematic representation of the predicted binding pose of **4.10** (brown) in the POP active site, catalytic triad in purple, key residues in blue/green; (C) predicted binding mode of **4.10a** (green), overlaid with the predicted binding mode of **4.1** (teal) (docked to POP using FITTED, pdb code: 2xdw)

This prediction encouraged us to pursue the synthesis of compound **4.10a** and other analogues. Our previous inhibitor **4.2a** and this newly-designed scaffold resemble previously-reported potent inhibitor **4.1** (Figure 4.4). The bicyclic scaffolds **4.2** and **4.10** were introduced by virtually rigidifying **4.1** and introducing heterocyclic alkanes to both optimize the docking pose and ensure synthetic feasibility. The valine-based side chain of Talabostat (Figure 4.2), a POP-FAP inhibitor that reached Phase III clinical trials,[38] inspired the introduction of methyl groups into **4.10a** and incorporation of the boronic acid warhead, leading to **4.12c** and **4.13b**. The complete list of new analogues selected for synthesis is provided in Table 4.1.

Table 4.1. Newly designed bicyclic analogues.

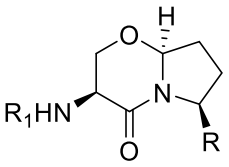

4.10

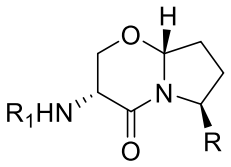

4.11

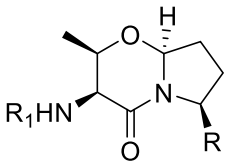

4.12

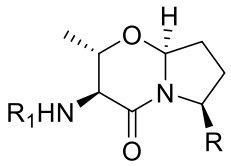

4.13

Entry	Compound #	R	R_1
1	**4.10a**	CN	Cbz
2	**4.10b**	H	Cbz
3	**4.10c**	Bpnd	Cbz
4	**4.10d**	Bpnd	Ac
5	**4.10e**	Bpnd	Boc
6	**4.10f**	$B(OH)_2$	H
7	**4.11a**	Bpnd	Boc
8	**4.11b**	$B(OH)_2$	H
9	**4.12a**	Bpnd	Cbz
10	**4.12b**	Bpnd	Boc
11	**4.12c**	$B(OH)_2$	H
12	**4.13a**	Bpnd	Boc
13	**4.13b**	$B(OH)_2$	H

A literature review of POP inhibitors revealed that many feature nitriles, activated nitriles (*i.e.*, with proximal fluorine atoms), or boronic acids, the latter two of which are more electrophilic and lead to more potent FAP inhibition. Our current version of our docking program FITTED does not consider either the reactivity of the catalytic residue nor the reactive warhead. Nevertheless, a computational study from our group on the reactivity of the catalytic serine residues in both POP and FAP suggests that the catalytic serine in POP is more nucleophilic than that in FAP and that, as a result, nitrile derivatives are unlikely to act as potent covalent inhibitors of FAP, while boronic acids are promising alternatives.[39-40] As a result, in our quest to develop dual POP/FAP inhibitors, the boronic ester or acid derivatives were also considered.

Boronic acids have been widely used in medicinal chemistry, notably as warheads of reversible covalent inhibitors of proteases,[41,42] including two approved drugs (Bortezomib and Ixazomib for the treatment of relapsed multiple myeloma and mantle cell lymphoma).[43] In addition, boronic acids are remarkably stable despite their high reactivity and consistently display very low toxicology profiles.[44-45] Consequently, we designed our bicyclic boropeptides to be structurally close to Talabostat (Figure 4.4). However, Talabostat displayed a loss in efficacy *in vivo*, believed to be a result of a reversible intramolecular cyclization into an inactive cyclic adduct.[46] The constrained scaffold of our designed boronic acids **4.10f**, **4.11b**, **4.12c**, and **4.13b** would circumvent this cyclization.

Furthermore, in both POP and FAP, the boronic acid motif may act as a transition state analogue, forming both hydrogen bonds (with His680 and Tyr473 and with His734 and Tyr571, respectively) and covalent bonds with the catalytic triad (Ser554 and Ser624, respectively) in a tetrahedral configuration, as opposed to the trigonal planar configuration conferred by nitrile-containing inhibitors (Figure 4.4). Nonetheless, the design of FAP/POP dual inhibitors remains challenging due to the difference in polarity between the active sites. While three hydrophobic or hydrogen bond donor residues contribute the necessary interactions for high inhibition of POP (aromatic interactions with Phe173 and hydrogen bonding with Trp595 and Arg643), high inhibition of FAP relies on interaction with hydrogen bond acceptors Glu203 and Glu204 in the hydrophilic pocket (Figure 4.5)

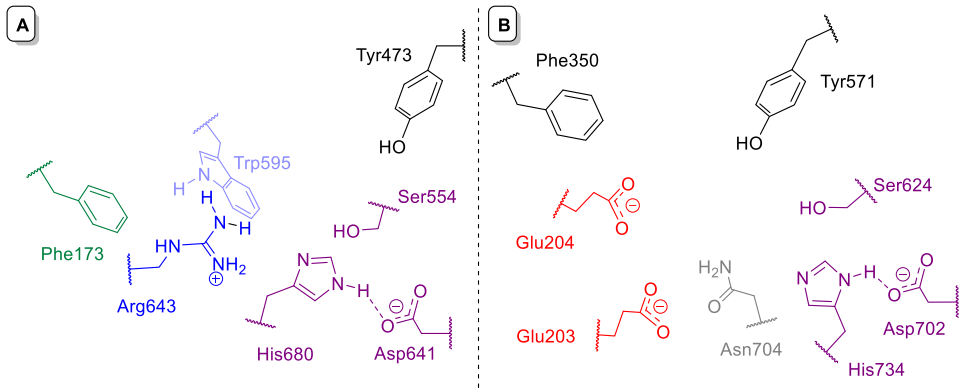

Figure 4.5. Schematic representation of the active sites of POP and FAP. Catalytic triads shown in purple. (A) POP: positively-charged pocket shown in blue, aromatic interaction residue shown in green; (B) FAP: negatively-charged pocket shown in red

Upon docking to POP, the *N*-Cbz boronic ester derivative **4.10c** was observed to fit very well into the active site of POP (Figure 4.6A), but docking to FAP gave unfavorable proposed binding modes, as the carboxybenzyl group is too large to fit into the active site (not shown). After virtual optimization of the amide side chain, the acetyl group turned out to be an excellent compromise for the design of potent dual inhibitors, as key interactions were conserved. The *N*-acetyl group may act as a hydrogen bond donor in FAP (with Glu203 or 204) and as a hydrogen bond acceptor in POP (with Trp595). The docking-predicted binding mode of the *N*-acetyl analog in both POP and FAP is shown in Figure 4.6. Furthermore, in order to evaluate the impact of the covalent warhead, the non-covalent analog **4.10b** was also prepared.

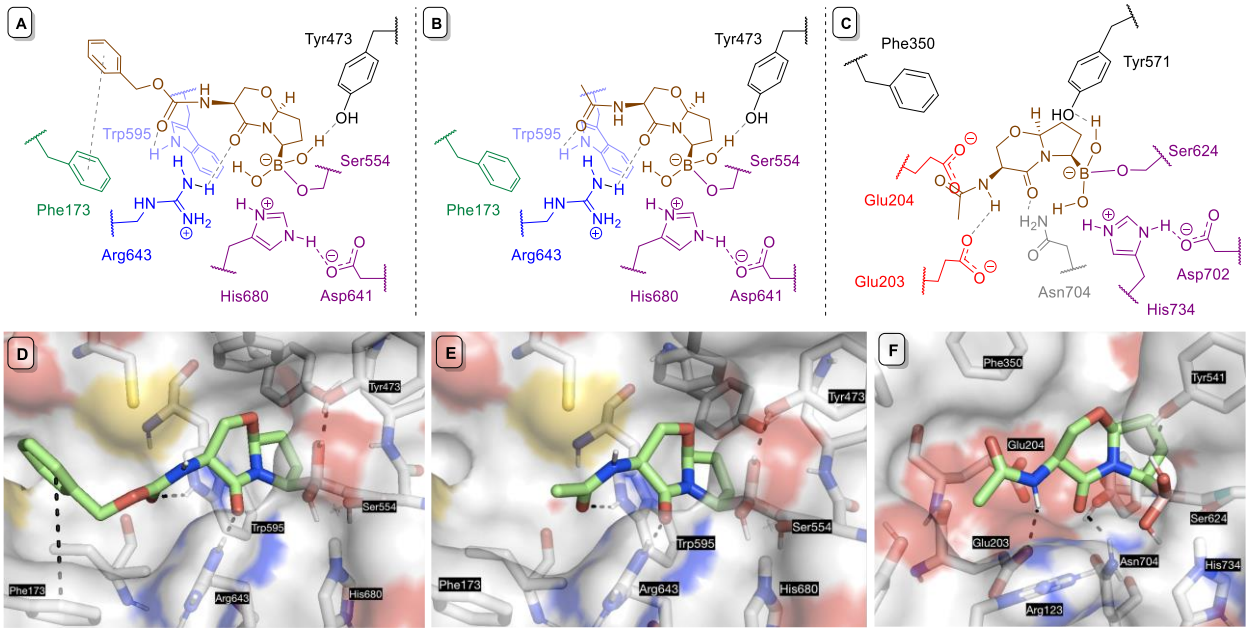

Figure 4.6. Predicted poses of compounds **4.10c** and **4.10d** in the active sites of POP and FAP.(A) schematic representation of the predicted binding mode of **4.10c** (brown) in POP; (B) schematic representation of the predicted binding mode of **4.10d** (brown) in POP; (C) Schematic representation of the predicted binding mode of **4.10d** (brown) in FAP; (D) predicted binding mode of **4.10c** (green) (pdb code: 2xdw); (E) predicted binding mode of **4.10d** (green) in POP; (F) predicted binding mode of **4.10d** (green) in FAP. All compounds were docked using FITTED. For schematic representations: catalytic triads are shown in purple, key residues are shown in blue/green (POP) and red (FAP). n.b. the hydrolyzed boronic esters (boronic acids) were docked

4.3.2 Synthesis

4.3.2.1 Non-covalent series.

The synthesis of this new [4.3.0] series started with the simplest of the analogues, the non-covalent inhibitor. Compound **4.10b** was synthesized in 3 overall steps starting with coupling *N*-Cbz-L-Ser to readily available 5-amino-1-pentene, followed by a telescoped acid-catalyzed oxidative cyclization (Scheme 4.1). Through the course of condition optimization, it was determined that performing the ozonolysis in presence of triphenylphosphine significantly increased the isolated yields and diastereoselectivity. In addition, a convenient procedure using resin-supported triphenylphosphine was developed in order to facilitate the purifications.

Scheme 4.1 Synthesis of the non-covalent series[a]

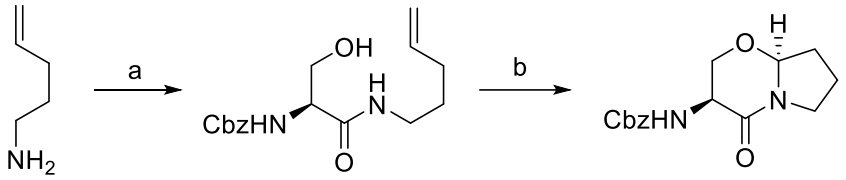

[a]a) N-Cbz-L-Ser, EDC•HCl, HOBt•H_2O, Et_3N, DCM, 0°C→rt, 18 h, 78%; b) 1) O_3, Sudan III, PPh_3, DCM, –78 °C→rt, 20 h; 2) TFA, DCM, rt, 2 h, 40% over 2 steps.

4.3.2.2 Carbonitrile series.

The synthesis of **4.10a** was unfortunately much more complex than that of the non-covalent analogue **4.10b**. Many attempts to obtain stereopure α-amino nitrile were unsuccessful; syntheses were long and yielded racemic mixtures. The synthesis was therefore redesigned, adapting chemistry from the Ellman group to obtain enantiopure sulfinylimine **4.15**,[47] followed by a modified Strecker reaction adapted from Mabic *et al.*[48] to obtain sulfinamide **4.16**, which was deprotected in HCl to obtain stereopure α-amino carbonitrile **4.17** (Scheme 4.2). This amine was subsequently coupled to *N*-Cbz-L-Ser with good yield to give dipeptide **4.18**. Subsequent acid-catalyzed oxidative cyclization gave desired diastereopure inhibitor **4.10a**.

Scheme 4.2. Synthesis of the carbonitrile series[a]

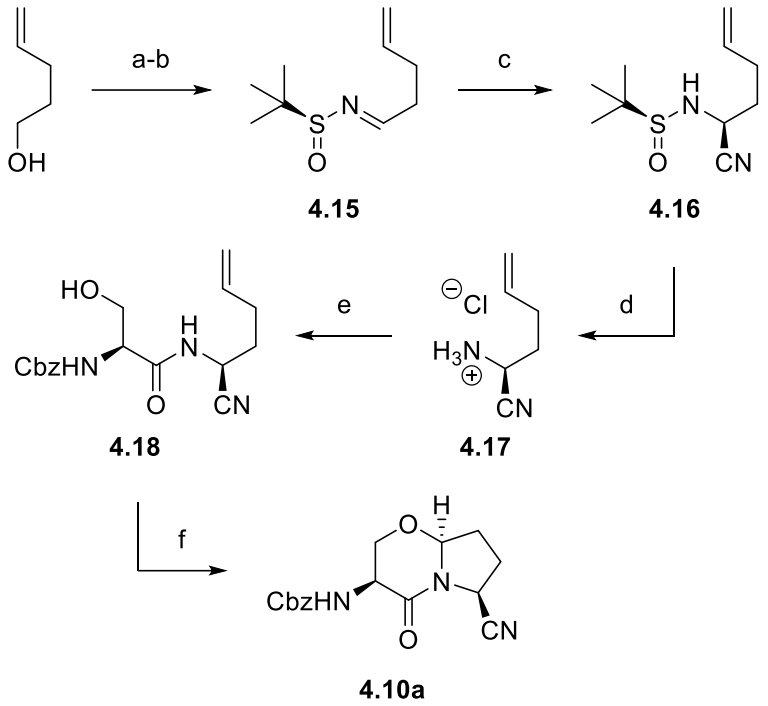

[a]a) $(COCl)_2$, DMSO, Et_3N, –78°C→rt, 2 h; b) *(S)*-(-)-tert-butyl-sulfinylamide, $CuSO_4$, DCM, rt, 18 h, 62% over two steps; c) TMSCN, $Gd(OTf)_3$, 0°C→rt, 48 h, 60%, d.r. 89:11; d) HCl, Et_2O, 0°C, 1 h, quant.; e) *N*-Cbz-L-Ser, EDC•HCl, HOBt•H_2O, Et_3N, DCM, 0°C→rt, 18 h, 80%; f) O_3, Sudan III, PPh_3, DCM, –78 °C→rt, 20 h; 2) TFA, DCM, rt, 2 h, 33% over 2 steps

4.3.2.3 Boronic ester series.

This series was prepared following a similar diastereoselective synthetic strategy, starting with the synthesis of sulfinylimine intermediate **4.15a**[47] (Scheme 4.3). The imine reacted under modified Ellman copper-catalyzed hydroboration conditions to afford the desired α-sulfinamidoboronic ester **4.19** with a good isolated yield and high diastereoselectivity.[49] A subsequent transesterification of the pinacol protecting group with the chiral (+)-pinanediol, followed by the deprotection of the sulfinamide group gave the highly diastereopure α-aminoboronic ester hydrochloride salt **4.20**. Peptide coupling of **4.20** provided the boropeptides, which were subjected to oxidative cleavage and dehydrative cyclization to obtain the corresponding bicycles as the sole diastereomers, confirmed by 1D nOe experiments (Figure 4.7).

To obtain the acetyl-protected bicyclic boronic ester, the *N*-Cbz-protected bicycle derivative **4.10c** was subjected to hydrogenation conditions, giving the free amine intermediate, which was subsequently reacted with AcCl to give the *N*-acetyl derivative **4.10d** (Scheme 4.3). Unfortunately, attempts to purify the free amine boronic ester intermediate for biological testing were unsuccessful, as purification conditions affected the boronic ester group. This led us to another route, coupling amine **4.20** to *N*-Boc-protected amino acids, followed by acid-catalyzed oxidative cyclization and subsequent simultaneous removal of the Boc and (+)-pinanediol protecting groups, obtaining the free amine boronic acid bicycles with no necessary purification. Our group has previously demonstrated that boronic esters are quickly hydrolyzed to their respective boronic acids in the basic buffer used in the *in vitro* assays.[39-40] The difference in covalent warhead within this series should therefore have negligible effect on the biological activity of these compounds. The complete synthesis of the boronic esters and acids is detailed in Scheme 4.3.

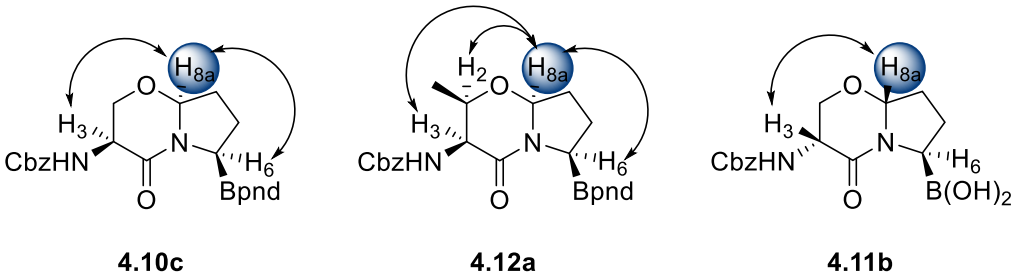

4.10c **4.12a** **4.11b**

Figure 4.7. Selected NOE signals of the boron-containing bicycles.

Scheme 4.3. Synthesis of boronic ester series[a]

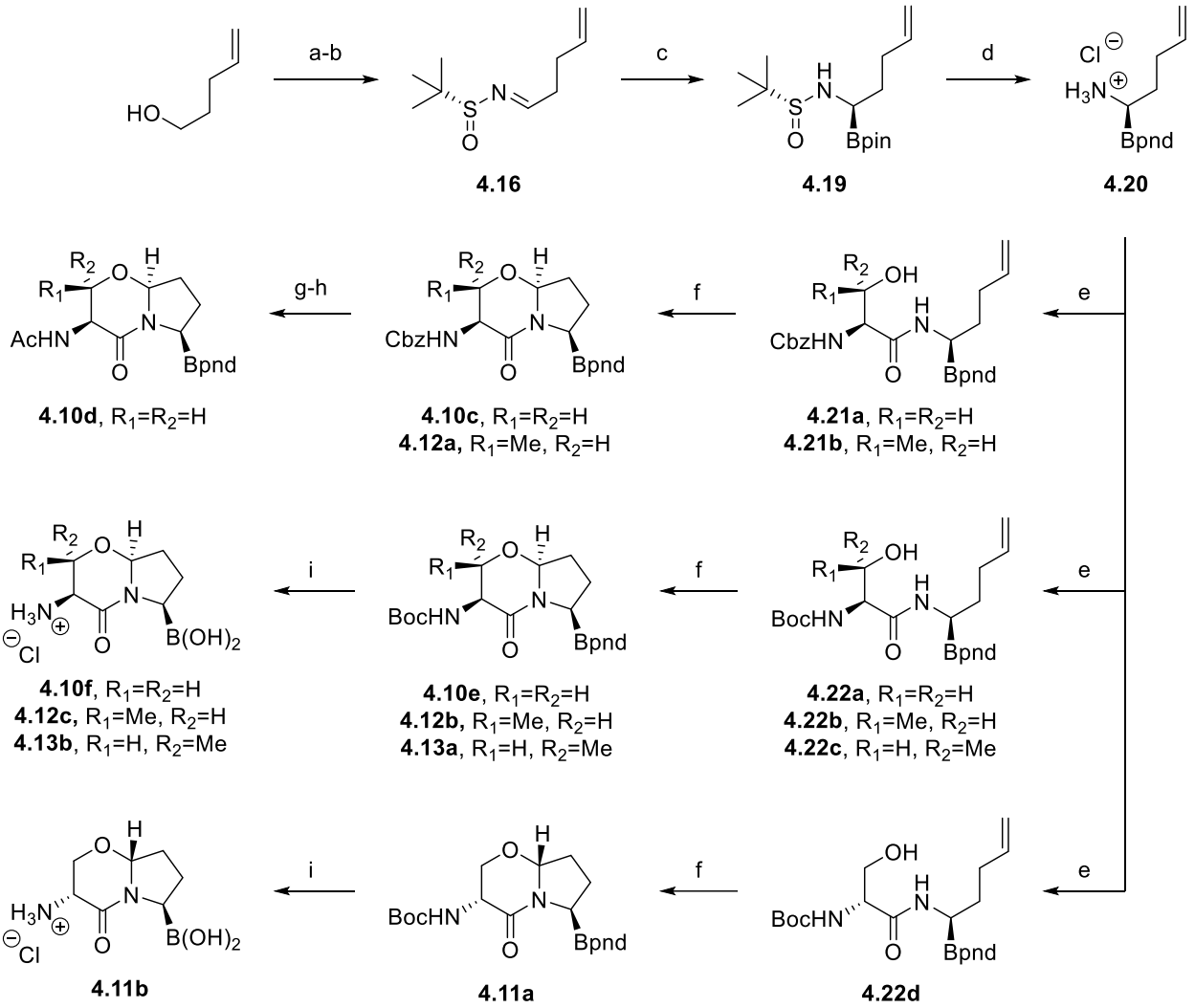

[a]a) $(COCl)_2$, DMSO, Et_3N, –78°C→rt, 2 h; b) (*R*)-(+)-*tert*-butyl-sulfinylamide, $CuSO_4$, DCM, rt, 18 h, 75% over two steps; c) B_2pin_2, $CuSO_4$•$5H_2O$, PCy_3•HBF_4, $BnNH_2$, Toluene-H_2O 5:1, rt, 18 h, 71%, d.r. > 98:2; d) 1) (+)-pinanediol, Et_2O, rt, 24 h; 2) HCl, Et_2O, 0°C, 2 h, 44% over 2 steps; e) PyBOP, L-AA (see Experimental Section), DIPEA, 0°C→rt, 18 h, 63% (**4.21a**), 48% (**4.21b**), 77% (**4.22a**), 69% (**4.22b**), 61% (**4.22c**) , 57% (**4.22d**); f) 1) O_3, DCM, PPh_3, −78 °C→rt, 20 h; 2) TFA, DCM, rt, 2 h, 58% (**4.10c**), 59% (**4.12a**), 52% (**4.10e**), 56% (**4.12b**), 60% (**4.13a**), 53% (**4.11a**); g) H_2, Pd/C, AcOH, EtOAc, rt, 15 h; h) AcCl, Et_3N, DMAP, 0°C→rt, 2 h, 63% over 2 steps; i) BCl_3, DCM, –78°C, 1 h, 34% (**4.10f**), 41% (**4.12c**), 52% (**4.13b**), 39% (**4.11b**). *pnd refers to (+)-pinanediol, pin refers to pinacol.

4.3.2.4 Linear dipeptide series

As mentioned earlier, we expect that through the loss of flexibility of the dipeptide scaffold afforded by the constrained bicyclic core, this [4.3.0] alkane series would solve the problem of the cyclization of Talabostat *in vivo*. However, the bicycles are expected to be slightly less active than their linear counterparts, as they cannot adjust their shape to the binding site. Alternatively, reduced entropy penalty may improve their binding affinity over the more flexible Talabostat. To determine the effect of rigidification of the scaffold on biological activity, several linear dipeptide probes were also synthesized, starting from protected L- or D-Ala and L-Val, the latter of which gives inhibitors resembling Talabostat. The complete list of synthesized probes can be found in Table 4.2.

Table 4.2. Selected linear dipeptide analogues of the bicyclic series.

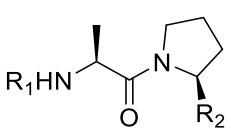

4.23

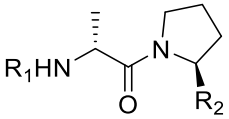

4.24

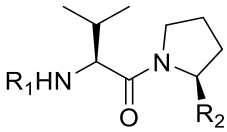

4.25

Entry	Compound	R_1	R_2
1	**4.23a**	Cbz	H
2	**4.23b**	Cbz	CN
3	**4.23c**	Cbz	Bpnd
4	**4.23d**	Boc	Bpnd
5	**4.24a**	Boc	Bpnd
6	**4.25a**	Cbz	Bpnd
7	**4.25b**	Boc	Bpnd

The synthesis of these linear analogues was rather simple. Non-covalent analogue **4.23a** was synthesized in one step, coupling Cbz-L-Ala to pyrrolidine. The carbonitrile series was previously synthesized by our group,[15] coupling readily available prolinonitrile to Cbz-L-Ala. Several boronic esters were also synthesized to probe for stereochemistry and preference of protecting group (Cbz or Boc). The synthesis of these linear peptide compounds is shown in Scheme 4.4.

Scheme 4.4. Synthesis of the linear dipeptide probes.[a]

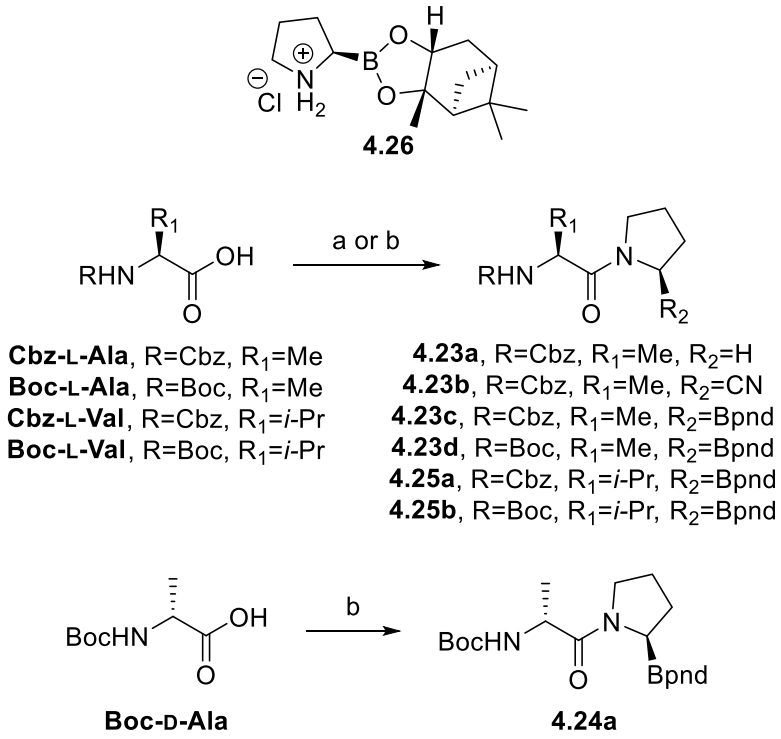

[a]a) Piv-Cl, Et_3N, pyrrolidine or prolinonitrile PTSA salt (see Experimental Section), DCM, 0°C→rt, 18 h, 49% (**4.23a**), 59% (**4.23b**); b) PyBOP, DIPEA, **4.26**, DCM, 0°C→rt, 18 h, 85% (**4.23c**), 64% (**4.23d**), 40% (**4.24a**), 60% (**4.25a**), 65% (**4.25b**). *pnd refers to (+)-pinanediol

4.3.3 Biological evaluations

The non-covalent, carbonitrile, and boronic ester/acid bicyclic series were tested *in vitro* for inhibition of POP activity. The results of these assays can be found in Table 4.3.

Table 4.3. *In vitro* activity of bicyclic and linear inhibitors against POP.

Entry	Compound	POP K_i (μM)
1	**4.10a**	0.0016 ± 0.0001
2	**4.10b**	4.4 ± 1.2
3	**4.10c**	0.0024 ± 0.0002
4	**4.10d**	1.1 ± 0.1
5	**4.10e**	0.0068 ± 0.0002
6	**4.10f**	2.2 ± 0.5
7	**4.11a**	0.34 ± 0.03
8	**4.11b**	6.2 ± 1.4
9	**4.12a**	0.0021 ± 0.0001
10	**4.12b**	0.0049 ± 0.0003
11	**4.12c**	0.84 ± 0.03
12	**4.13a**	0.12 ± 0.01
13	**4.13b**	7.2 ± 1.2
14	**4.23a**	53 ± 1
15	**4.23b**	0.00092 ± 0.00004
16	**4.23c**	0.00095 ± 0.00004
17	**4.23d**	0.0013 ± 0.00004
18	**4.24a**	1.0 ± 0.2
19	**4.25a**	0.0015 ± 0.0002
20	**4.25b**	0.0016 ± 0.00005
21	**4.1**[a]	0.00029 ± 0.00004

[a]Compound **4.1** was used as a positive control in the assay

The bicyclic boronic ester pro-drugs showed very potent *in vitro* activity against POP, with *N*-Cbz bicycles **4.10c** and **4.12a** exhibiting low single-digit nanomolar potency. This high inhibitor activity was predicted by the promising docking pose (Figure 4.6A/D) in which all three key ligand-protein interactions are fulfilled. Unexpectedly, the *N*-Boc derivative **4.10e** displayed similar potency. Although the benzyl group is missing for aromatic interactions with Phe173, the large, greasy Boc protecting group might be compensating for this loss. The acetyl derivative **4.10d** exhibited low micromolar activity, likely attributed to the lack of a large *N*-bound group to stabilize the inhibitor in the active site. The free amine boronic acid derivative **4.10f** exhibited submicromolar potency in POP. This activity can likely be attributed to the assay conditions; the pH 8.0 basic buffer likely renders the amine unionized and allows it to act as a hydrogen bond acceptor to interact with Arg643. While, in general, nitrile and boronic acids are somewhat equipotent, boronic acids are likely to exhibit longer residence times in the active sites,[39, 50] making them more suitable drug candidates. As observed previously by our group,[40] it is likely that the nitrile is not properly oriented to react covalently with the catalytic serine in POP, and therefore binds non-covalently. Dose-response curves of the most potent POP bicyclic inhibitors can be found in Figure 4.8A.

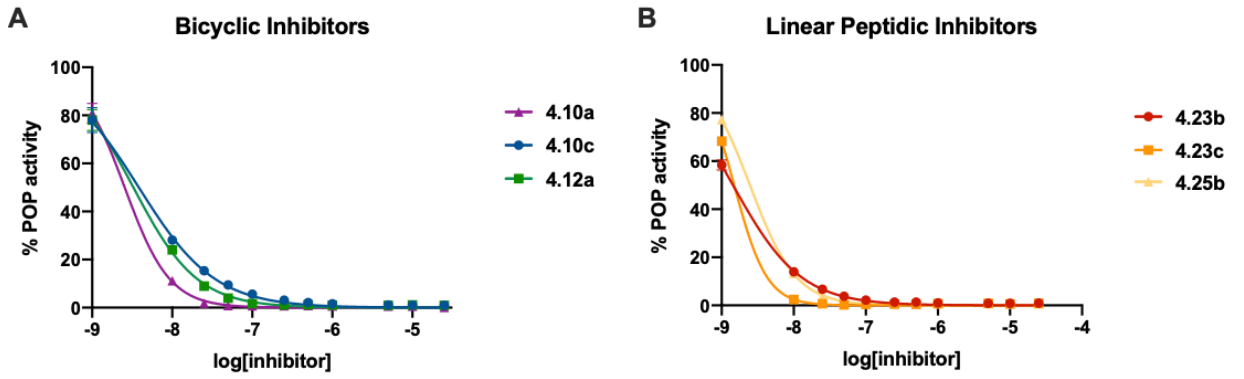

Figure 4.8. Dose response curves of the most potent POP inhibitors (A) the three most potent bicyclic inhibitors; (B) the three most potent linear peptidic inhibitors

The linear peptides displayed very high potencies against POP, demonstrating single-digit nanomolar potency or sub-nanomolar activity, the latter of which are on the same order of magnitude as aldehyde control inhibitor **4.1** and are our most potent POP inhibitors to date. The boron-containing dipeptides' trends in activity match those of their bicyclic counterparts, with D-amino acids exhibiting much lower potency than their L-amino acid analogues. Fortunately, their bicyclic analogues did not lose significant potency; L-amino acid cyclic analogues were generally in the single-digit nanomolar range. As predicted by our docking program, the designated [4.3.0] stereochemistry was optimal to inhibit the enzymes. Furthermore, the bicyclic compounds are likely to be more metabolically stable[16, 34] and more specific to our enzymatic targets *in vivo*.[51] Dose-response curves comparing of our top linear peptidic inhibitors can be found in Figure 4.8B.

The compounds predicted to be the most promising against FAP by docking, the *N*-acetyl bicyclic derivative and three of the free amines, were next tested against FAP. One of the Cbz-containing bicycles was also tested on FAP and displayed no inhibitory activity, confirming the need for smaller side chains in FAP inhibitors we proposed previously.[1] The results of the FAP assay are displayed in Table 4.4 and Figure 4.9. *In vitro* results indicate that free amine boronic acid **4.10f** exhibits nanomolar activity in FAP and low micromolar activity in POP, making it a promising dual inhibitor for future development. However, *N*-acetyl boronic ester derivative **4.12c** exhibits submicromolar activity in both enzymes and comparable potency to failed clinical trial candidate Talabostat against POP (Figure 4.1), making it a very promising drug candidate for future studies.

Table 4.4. *In vitro* activity of bicyclic dual inhibitors

Entry	Compound	POP K_i (μM)	FAP K_i (μM)
1	**4.10d**	1.1 ± 0.1	1.3 ± 0.5
2	**4.10f**	2.2 ± 0.5	0.20 ± 0.05
3	**4.11b**	6.2 ± 1.4	14 ± 2
4	**4.12c**	0.84 ± 0.03	0.72 ± 0.09
5	**4.10a**	0.0016 ± 0.0001	> 50 μM
6	**Talabostat**[a]	0.98 ± 0.06	0.066 ± 0.011

[a]Values are reported as IC_{50} concentrations by Jansen *et al.*[52]

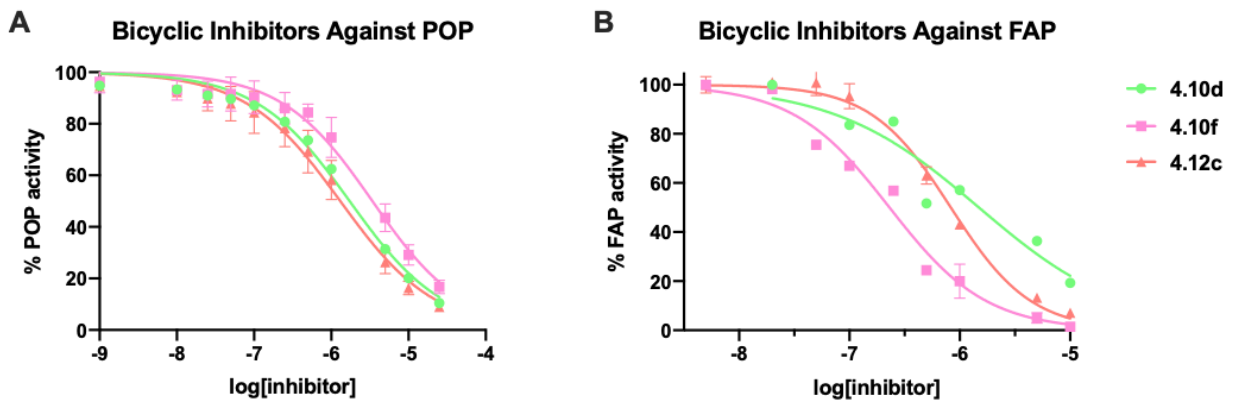

Figure 4.9. Dose response curves of our most potent dual inhibitors.(A) POP (B) FAP

4.4 Conclusion

Our group's research has previously led to potent bicycle-based POP inhibitors, revealing that the introduction of bicyclic scaffolds can enhance the metabolic stability of these inhibitors.[16, 34] In the shift toward POP-FAP dual inhibitors, we then aimed to improve these bicyclic scaffolds while simultaneously constraining the known inhibitor Cbz-Pro-Prolinal **4.1** and failed drug candidate Talabostat. Our results indicate that we were not only able to obtain potent compounds using our computationally-guided optimizations of known inhibitors, but that we were able to use this method along with synthetic developments to produce an inhibitor with comparable potency to a drug that reached Phase III clinical trials. Currently, we are carrying out cell-based assays to assess the activity of our leads *in cellulo*, as well as performing further experiments to optimize the activity and pharmacokinetic properties of our leads **4.10f** and **4.12c**.

4.5 Experimental Section

4.5.1 *In Vitro* Assays

POP *in vitro* assays were performed as previously published by our group.[16, 34, 39] The POP batch used in these assays exhibited a K_m of 141.2 μM and k_{cat} of 21.2 s^{-1}. The FAP assay was performed using the FAP Assay Kit from BPSBioscience.[53] The FAP batch used in these assays exhibited a K_m of 33 μM.

4.5.2 Chemistry

4.5.2.1 General Information

All commercially available reagents were used without further purification. All reactions, unless otherwise indicated, were carried out in flame-dried flasks under argon atmosphere with anhydrous solvents. FTIR spectra were recorded using a Perkin-Elmer Spectrum One FT-IR. ^{1}H, ^{13}C, and ^{11}B NMR spectra were recorded on a Bruker 400 or 500 MHz spectrometer. Chemical shifts are reported in ppm using the residual of deuterated solvents as an internal standard. Thin layer chromatography visualization was performed by UV or by development using $KMnO_4$, Curcumin, ninhydrin, or *p*-anisaldehyde. Chromatography was performed on silica gel 60 (230−240 mesh). High resolution mass spectrometry was performed by ESI on a Bruker Maxis Impact API QqTOF or by ESI or APCI on a ThermoFisher Exactive Plus Orbitrap-API at McGill University. All compounds were stored at –20°C.

4.5.2.2 Purity determination by High Performance Liquid Chromatography (HPLC)

Prior to biological testing, reverse-phase HPLC was used to verify the purity of compounds on an Agilent 1100 series instrument, equipped with VWD-detector, using a C18 reverse column (Agilent, Eclipse -C18 150 mm Å~ 4.6 mm, 5 μm) or Zorbax (ZORBAX Bonus-RP, 80Å, 4.6 x 150 mm, 5 μm) with UV detection at 220 or 215 nm. All tested compounds were at least 95% pure. The solvents used were H_2O (A) and MeCN (B) in a gradient. Retention times and purities are provided for each compound.

Method A: H_2O (A) and MeCN (B); t = 0 mins, 95% A / 5% B; t = 3 to 20 mins, gradually to 5% A / 95% B; t = 20 to 25 mins, 5% A / 95% B; t = 25 to 28 mins, gradually to 95% A / 5% B; t = 28 to 30 mins, 95% A / 5% B.

Method B: H_2O (A) and MeCN (B); t = 0 mins, 80% A / 20% B; t = 5 to 15 mins, gradually to 20% A / 80% B; t = 15 to 20 mins, 20% A / 80% B; t = 20 to 28 mins, gradually to 80% A / 20% B; t = 28 to 30 mins, 80% A / 20% B.

4.5.2.3 Synthesis

(*S*)-2-methyl-*N*-(pent-4-en-1-yl)propane-2-sulfinamide (4.15) and (*R*)-2-methyl-*N*-(pent-4-en-1-ylidene)propane-2-sulfinamide (4.15a) *(general procedure for both; the two sulfinimines are spectrally identical)* Oxalyl chloride (1.2 eq) was dissolved in DCM (1.5 M) under Ar, and the solution was cooled to –78°C. DMSO (2.5 eq) in DCM (7 M) was added *slowly*. The solution stirred for 5 minutes. 4-penten-1-ol (1 eq) in DCM (3 M) was added *slowly*, and the reaction stirred for 15 minutes. Triethylamine (3 eq) was added slowly, and the reaction stirred for 2 hours at room temperature. Water was added, and the product was extracted with DCM. The combined organic layers were washed with 1 M HCl, saturated $NaHCO_3$, and brine, dried over Na_2SO_4, filtered and concentrated *in vacuo* at 650 mbar, 40°C. (Some solvent remains; product is volatile.) The resultant 4-pentenal (assume 100% yield) was dissolved in anhydrous DCM (0.5 M), and (*R*)-(+)-2-methyl-2-propanesulfinamide (1 eq) *[or the (S)-(-) enantiomer for the synthesis of the (S)-sulfinimine]* and anhydrous $CuSO_4$ (3 eq) were added. The reaction stirred at room temperature overnight. The mixture was then filtered through a pad of Celite®, and the filter cake was rinsed with DCM. The filtrate was concentrated *in vacuo* to give a brown liquid, which was purified by flash chromatography on a silica gel column (85:15 hexanes-EtOAc) to give a yellow liquid (**4.15** 62%, **4.15a** 75%). R_f = 0.45 (85:15 hexanes-EtOAc); ^{1}H NMR (500 MHz, Chloroform-*d*) δ 8.07 (t, *J* = 4.4 Hz, 1H), 5.83 (ddt, *J* = 16.8, 10.2, 6.5 Hz, 1H), 5.07 (dq, *J* = 17.2, 1.7 Hz, 1H), 5.02 (dq, *J* = 10.2, 1.5 Hz, 1H), 2.62 (td, *J* = 7.3, 4.4 Hz, 2H), 2.42 – 2.36 (m, 2H), 1.18 (s, 9H). ^{13}C NMR (126 MHz, Chloroform-*d*) δ 168.94, 136.80, 115.97, 56.69, 35.41, 29.49, 22.49. Spectral and physical data were in accordance with the literature.[54-55]

(*S*)-*N*-((*S*)-1-cyanopent-4-en-1-yl)-2-methylpropane-2-sulfinamide (4.16) Imine **4.15** (462 mg, 1 eq) was dissolved in DCM (24 mL), and $Gd(OTf)_3$ (298 mg, 0.2 eq) and TMSCN (489 mg, 0.62 mL, 2 eq) were added. The reaction stirred for 48h at room temperature and was quenched with saturated $NaHCO_3$. The product was extracted with DCM, and the combined organic layers were washed with brine, dried over Na_2SO_4, and concentrated *in vacuo* to give the crude product as a brown oil, which was purified by flash chromatography on a silica gel column (eluent 70:30 hexanes-EtOAc) to give the product as a yellow oil (318 mg, 60%). R_f = 0.50 (70:30 EtOAc-hexanes); IR (film) cm^{-1} 3187, 3083, 2960, 2238, 1641, 1391, 1366, 1062, 911; ^{1}H NMR (500 MHz, Chloroform-*d*) δ 5.84 – 5.69 (m, 1H), 5.16 – 5.06 (m, 2H), 4.23 – 4.09 (m, 1H), 3.93 – 3.63 (m, 1H), 2.37 – 2.21 (m, 2H), 2.15 – 1.89 (m, 2H), 1.24 (s, 9H); ^{13}C NMR (126 MHz, Chloroform-

d) δ 22.61 (3C), 29.47, 34.01, 45.69, 57.21, 117.28, 119.19, 135.69; HRMS (ESI+) *m/z* calcd for $[C_{10}H_{18}ON_2S + Na]^+$ 237.1032, found 237.1035.

(*S*)-1-cyanopent-4-en-1-aminium chloride (4.17) Sulfinamide **4.16** (298 mg, 1 eq) was dissolved in Et_2O (12 mL), and the solution was cooled to 0°C. HCl (2 M in Et_2O, 2.1 mL, 3 eq) was added dropwise, and the resultant mixture stirred for 1h at 0°C. The solvent was removed in vacuo to give the product as a while solid, which was taken to the next step without purification (136 mg, quant.) R_f = does not elute on silica-backed TLC plates; mp = 94-97°C; IR (film) cm^{-1} 3071, 2956, 1643, 1483, 1185, 926; ^1H NMR (400 MHz, Methanol-d_4) δ 5.86 (dddd, *J* = 17.2, 10.2, 7.1, 6.1 Hz, 1H), 5.18 (dq, *J* = 17.1, 1.6 Hz, 1H), 5.11 (dq, *J* = 10.2, 1.3 Hz, 1H), 4.56 – 4.35 (m, 1H), 2.45 – 2.22 (m, 2H), 2.11 – 2.00 (m, 2H); ^{13}C NMR (101 MHz, Methanol-d_4) δ 30.23, 31.26, 42.23, 116.62, 117.59, 136.33; HRMS (ESI+) *m/z* calcd for $[C_6H_{11}N_2]^+$ 111.0917, found 111.0922.

(*R*)-2-methyl-*N*-((*R*)-1-(4,4,5,5-tetramethyl-1,3,2-dioxaborolan-2-yl)pent-4-en-1-yl)propane-2-sulfinamide (4.19) Tricyclohexylphosphonium tetrafluoroborate (63 mg, 0.1 eq) was dissolved in toluene (2.1 mL), and the solution was stirred rapidly. Copper (II) sulfate pentahydrate (43 mg, 0.1 eq) and water (0.9 mL) were added, turning the reaction light blue. Benzylamine (37 mg, 0.2 eq) was added, turning the mixture dark blue. The mixture stirred at room temperature for 10 minutes, and was then cooled to 0°C. The sulfinylimine **4.15a** (320 mg, 1 eq) in toluene (2.1 mL) was added, followed by B_2pin_2 (651 mg, 1.5 eq), and the reaction mixture turned turquoise. The reaction was kept at 0°C for 15 minutes, then was warmed to room temperature and stirred overnight, after which the reaction turned dark brown. The mixture was diluted with ethyl acetate and quenched with saturated $NaHCO_3$. The biphasic mixture stirred for 30 minutes. The product was then extracted from the aqueous layer with ethyl acetate, and the organic layer was washed with saturated NH_4Cl, saturated $NaHCO_3$ (copiously) and brine, dried over Na_2SO_4, and concentrated *in vacuo* to give the crude product as a brown oil, which was clarified with charcoal to give a clear oil (385 mg, 71%). R_f = streaks on regular silica; IR (film) cm^{-1} 3206, 3079, 2976, 1639, 1380, 1370, 1332, 1142, 1058, 910; ^1H NMR (500 MHz, Chloroform-*d*) δ 5.73 (ddt, *J* = 16.9, 10.2, 6.7 Hz, 1H), 4.96 (dq, *J* = 17.1, 1.7 Hz, 1H), 4.88 (dq, *J* = 10.1, 1.4 Hz, 1H), 3.16 (d, *J* = 7.0 Hz, 1H), 2.97 (q, *J* = 7.0 Hz, 1H), 2.07 (m, 2H), 1.77 – 1.64 (m, 2H), 1.18 (s, 6H), 1.17 (s, 6H), 1.11 (s, 9H); ^{13}C NMR (126 MHz, Chloroform-*d*) δ 22.52 (3C), 24.52 (2C), 24.92 (2C), 31.01, 32.66, 42.75, 55.97, 84.00 (2C), 115.07, 138.01; ^{11}B NMR (161

MHz, Chloroform-*d*) δ 32.41; HRMS (ESI+) *m/z* calcd for $[C_{15}H_{30}O_3NSB + Na]^+$ 338.1932, found 338.1931.

(*R*)-1-((3a*S*,4*S*,6*S*,7a*R*)-3a,5,5-trimethylhexahydro-4,6-methanobenzo[*d*][1,3,2] dioxaborol-2-yl)pent-4-en-1-aminium chloride (4.20) The aminoboronic ester **4.19** (11.51 g, 1 eq) was dissolved in Et_2O (120 mL), and (+)-pinanediol (6.22 g, 1 eq) was added. The solution stirred at room temperature for 24 hours. The solvent was removed in vacuo, the residue was re-dissolved in Et_2O (75 mL), and the solution was cooled to 0°C. HCl (2 M in Et_2O, 24 mL, 1.3 eq) was added dropwise, and the argon balloon was removed. After 2 h of stirring at room temperature, the solvent was removed *in vacuo* to give a white solid, which was triturated at 0°C in 2:1 *n*-hexane/Et_2O and filtered, rinsing with cold 2:1 *n*-hexane/Et_2O, to give the boroamine salt **4.20** as a fluffy white solid (4.85 g, 44% over 2 steps). R_f = does not elute on silica-backed TLC plates; mp = 168–171ºC; IR (film) cm^{-1} 3130, 2921, 1605, 1405, 1389, 1076, 1029; ^1H NMR (500 MHz, Chloroform-*d*) δ 8.31 (s, br, 3H), 5.78 (ddt, *J* = 16.6, 11.1, 6.0 Hz, 1H), 5.13 (d, *J* = 16.9 Hz, 1H), 4.99 (d, *J* = 10.0 Hz, 1H), 4.38 (d, *J* = 8.2 Hz, 1H), 2.97 (s, br, 1H), 2.43 – 2.14 (m, 4H), 2.16 – 1.95 (m, 3H), 1.98 – 1.88 (m, 2H), 1.41 (s, 3H), 1.27 (s, 3H), 1.17 (d, *J* = 10.9 Hz, 1H), 0.81 (s, 3H); ^{13}C NMR (126 MHz, $CDCl_3$) δ 24.08, 26.71, 27.13, 28.61, 29.04, 30.71, 35.17, 37.12, 38.25, 39.57, 51.21, 77.16, 78.88, 87.74, 116.27, 137.12; ^{11}B NMR (161 MHz, $CDCl_3$) δ 32.35; HRMS (APCI+) *m/z* calcd for $[C_{15}H_{26}O_2NB + H]^+$ 264.2129, found 264.2129.

General peptide coupling procedure A. The protected amino acid (1 eq) was suspended in DCM (0.1 M), and HOBt•H_2O (1.2 eq) was added, followed by EDC•HCl (1.2 eq). The reaction stirred at 0°C for one hour. The amine salt (1 eq) was then added, followed by Et_3N (3 eq). The reaction stirred at 0°C for one hour, then at room temperature overnight. Water was added, and the product was extracted with DCM. The combined organic layers were washed with saturated NH_4Cl, saturated $NaHCO_3$, and brine, dried over Na_2SO_4, filtered, and concentrated *in vacuo* to give the crude product. The crude material was purified by flash chromatography on a silica gel column to give the corresponding dipeptide.

General peptide coupling procedure B. The protected amino acid (1 eq) was suspended in DCM (0.1 M), and Et_3N (5 eq) was added, followed by Piv-Cl (1.1 eq). The reaction stirred at 0°C for one hour. The amine salt (1 eq) was then added. The reaction stirred at 0°C for one hour, then at room temperature overnight. Water was added, and the product was extracted with DCM. The combined organic layers were washed with saturated NH_4Cl, saturated $NaHCO_3$, and brine, dried

over Na_2SO_4, filtered, and concentrated *in vacuo* to give the crude product. The crude material was purified by flash chromatography on a silica gel column to give the corresponding dipeptide.

General peptide coupling procedure C. The protected amino acid (1 eq) was suspended in DCM (0.1 M), and PyBOP (1.2 eq) was added, followed by the amine (1 eq), then DIPEA (3 eq). The reaction stirred at 0°C for one hour, then at room temperature overnight. Water was added, and the product was extracted with DCM. The combined organic layers were washed with saturated NH_4Cl, saturated $NaHCO_3$, and brine, dried over Na_2SO_4, filtered, and concentrated *in vacuo* to give the crude product. The crude material was purified by flash chromatography on a silica gel column to give the corresponding dipeptide.

General peptide coupling procedure D. The protected amino acid (1 eq) was dissolved in DMF (0.3 M), and the solution was cooled to 0°C. HATU (1.2 eq) was added, followed by the amine (1 eq), then Et_3N (10 eq). The reaction stirred at room temperature overnight. Water was added, and the product was extracted with DCM. The combined organic layers were washed with saturated NH_4Cl, saturated $NaHCO_3$, and brine, dried over Na_2SO_4, filtered, and concentrated *in vacuo* to give the crude product. The crude material was purified by flash chromatography on a silica gel column to give the corresponding dipeptide.

Benzyl (S)-(3-hydroxy-1-oxo-1-(pent-4-en-1-ylamino)propan-2-yl)carbamate (4.14) Dipeptide **4.14** was prepared following general peptide coupling procedure A, using Z-L-Ser as the amino acid and 5-amino-1-pentene as the amine. The crude product was purified by flash chromatography on a silica gel column (eluent 70:30 EtOAc-hexanes) to give the product as a white solid (78%). R_f = 0.43 (80:20 EtOAc-hexanes); mp = 143-145°C; IR (film) cm^{-1} 3316, 3068, 2937, 1709, 1651, 1532, 1239, 1060, 913; ^1H NMR (500 MHz, Chloroform-*d*) δ 7.39 – 7.30 (m, 5H), 6.64 (s, 1H), 5.87 (d, *J* = 7.6 Hz, 1H), 5.77 (ddt, *J* = 16.9, 10.2, 6.6 Hz, 1H), 5.13 (s, 2H), 5.02 (dq, *J* = 17.2, 1.7 Hz, 1H), 4.98 (dq, *J* = 10.2, 1.4 Hz, 1H), 4.17 (ddd, *J* = 7.8, 4.9, 3.2 Hz, 1H), 4.15 – 4.05 (m, 1H), 3.71 – 3.60 (m, 1H), 3.25 (q, *J* = 6.7 Hz, 2H), 3.20 (s, 1H), 2.06 (q, *J* = 7.2 Hz, 2H), 1.59 (p, *J* = 7.3 Hz, 2H); ^{13}C NMR (126 MHz, Chloroform-*d*) δ 28.58, 31.09, 39.15, 55.29, 62.91, 67.51, 115.55, 128.23 (2C), 128.50, 128.74 (2C), 136.06, 137.64, 156.93, 171.00; HRMS (ESI+) *m/z* calcd for $[C_{16}H_{22}O_4N_2 + Na]^+$ 329.1472, found 329.1464.

benzyl ((*S*)-1-(((*S*)-1-cyanopent-4-en-1-yl)amino)-3-hydroxy-1-oxopropan-2-yl)carbamate (4.18) The product was synthesized following general coupling procedure D, using **4.17** as the amine. The crude product was purified by silica gel (eluent 60:40 EtOAc-hexanes) to

give the product as a white foam (80%). R_f = 0.27 (60:40 EtOAc-hexanes); mp = 87-91°C; IR (film) cm^{-1} 3409, 3321, 3278, 3020, 2940, 1707, 1671, 1516, 1217, 1058; ^{1}H NMR (500 MHz, Acetone-d_6) δ 8.20 – 7.95 (m, 1H), 7.47 – 7.18 (m, 5H), 6.48 (d, J = 8.7 Hz, 1H), 5.82 (ddt, J = 17.0, 10.1, 6.7 Hz, 1H), 5.15 – 5.04 (m, 3H), 5.01 (dq, J = 10.2, 1.3 Hz, 1H), 4.33 – 4.18 (m, 2H), 3.87 (dt, J = 10.3, 5.0 Hz, 1H), 3.81 (dt, J = 10.7, 5.2 Hz, 1H), 2.23 (q, J = 7.4 Hz, 2H), 2.01 – 1.91 (m, 2H); ^{13}C NMR (126 MHz, Acetone-d_6) δ 30.09, 32.56, 40.53, 57.85, 62.99, 67.01, 116.59, 119.55, 128.70 (2C), 128.71, 129.24 (2C), 137.34, 137.98, 157.01, 171.22; HRMS (ESI+) *m/z* calcd for $[C_{17}H_{21}O_4N_3 + Na]^+$ 354.1424, found 354.1417.

benzyl ((*S*)-3-hydroxy-1-oxo-1-(((*R*)-1-((3a*S*,4*S*,6*S*,7a*R*)-3a,5,5-trimethylhexahydro-4,6-methanobenzo[*d*][1,3,2]dioxaborol-2-yl)pent-4-en-1-yl)amino)propan-2-yl)carbamate

(4.21a) The product was synthesized following general coupling procedure C, using **4.20** as the amine. The crude product was purified by silica gel (eluent 60:40 EtOAc-hexanes) to give the product as a white foam (63%). R_f = 0.23 (50:50 EtOAc-hexanes); IR (film) cm^{-1} 3310, 3071, 2929, 1722, 1701, 1522, 1385, 1372, 1247, 1078, 1052, 906; ^{1}H NMR (500 MHz, Acetone-d_6) δ 8.04 (s, 1H), 7.46 – 7.21 (m, 5H), 6.63 – 6.43 (m, 1H), 5.82 (ddt, J = 17.0, 10.3, 6.7 Hz, 1H), 5.10 (s, 2H), 4.99 (dq, J = 17.1, 1.8 Hz, 1H), 4.91 (ddt, J = 10.2, 2.2, 1.2 Hz, 1H), 4.44 – 4.35 (m, 1H), 4.31 (dt, J = 7.9, 5.1 Hz, 1H), 4.24 (dd, J = 8.8, 2.2 Hz, 1H), 3.85 (dt, J = 10.8, 5.3 Hz, 1H), 3.77 (dt, J = 11.3, 5.8 Hz, 1H), 2.84 (ddd, J = 7.8, 6.3, 4.3 Hz, 1H), 2.31 (ddt, J = 13.9, 8.7, 2.5 Hz, 1H), 2.22 – 2.09 (m, 3H), 1.94 (t, J = 5.6 Hz, 1H), 1.84 (tt, J = 5.9, 3.0 Hz, 1H), 1.78 (ddd, J = 14.2, 3.2, 2.1 Hz, 1H), 1.73 – 1.64 (m, 1H), 1.64 – 1.57 (m, 1H), 1.48 – 1.40 (m, 1H), 1.34 (s, 3H), 1.27 (s, 3H), 0.86 (s, 3H); ^{13}C NMR (126 MHz, Acetone-d_6) δ 24.35, 26.98, 27.56, 29.25, 31.32, 32.08, 36.74, 38.77, 39.73, 40.62, 52.70, 56.55, 63.10, 66.99, 77.75, 85.09, 114.89, 128.62 (2C), 128.65, 129.19 (2C), 137.96, 139.69, 156.93, 173.39; ^{11}B NMR (161 MHz, Acetone-d_6) δ 26.64; HRMS (APCI+) *m/z* calcd for $[C_{26}H_{37}O_6N_2B + Na]^+$ 507.2637, found 507.2652.

benzyl ((2*S*,3*R*)-3-hydroxy-1-oxo-1-(((*R*)-1-((3a*S*,4*S*,6*S*,7a*R*)-3a,5,5-trimethylhexahydro-4,6-methanobenzo[*d*][1,3,2]dioxaborol-2-yl)pent-4-en-1-yl)amino)butan-2-yl)carbamate

(4.21b) The product was synthesized following general coupling procedure C, using **4.20** as the amine. The crude product was purified by silica gel (eluent 60:40 EtOAc-hexanes) to give the product as a white solid (48%). R_f = 0.38 (50:50 EtOAc-hexanes); mp = 44–47°C; IR (film) cm^{-1} 3322, 3068, 2922, 1722, 1699, 1606, 1515, 1383, 1373, 1247, 1120, 1070, 908; ^{1}H NMR (500 MHz, Acetone-d_6) δ 7.91 (s, 1H), 7.43 – 7.28 (m, 5H), 6.25 (d, J = 8.2 Hz, 1H), 5.82 (ddt, J = 17.0,

10.2, 6.7 Hz, 1H), 5.11 (s, 2H), 4.99 (dq, *J* = 17.2, 1.7 Hz, 1H), 4.91 (ddt, *J* = 10.1, 2.3, 1.2 Hz, 1H), 4.30 (d, *J* = 4.3 Hz, 1H), 4.25 (dd, *J* = 8.8, 2.2 Hz, 1H), 4.22 – 4.13 (m, 2H), 2.87 – 2.81 (m, 1H), 2.31 (ddt, *J* = 14.0, 8.8, 2.5 Hz, 1H), 2.21 – 2.07 (m, 3H), 1.95 (dd, *J* = 11.1, 5.6 Hz, 1H), 1.84 (tq, *J* = 6.0, 3.1 Hz, 1H), 1.81 – 1.74 (m, 1H), 1.74 – 1.65 (m, 1H), 1.65 – 1.44 (m, 1H), 1.45 – 1.37 (m, 1H), 1.34 (s, 3H), 1.27 (s, 3H), 1.22 – 1.15 (m, 3H), 0.86 (s, 3H); ^{13}C NMR (126 MHz, Acetone-d_6) δ 19.59, 24.36, 26.99, 27.56, 29.25, 31.32, 32.14, 36.72, 38.80, 39.44, 40.62, 52.69, 59.82, 67.00, 67.96, 77.85, 85.23, 114.93, 128.57 (2C), 128.66, 129.21 (2C), 138.04, 139.64, 157.12, 173.17; ^{11}B NMR (161 MHz, Acetone-d_6) δ 27.32; HRMS (ESI+) *m/z* calcd for $[C_{27}H_{39}O_6N_2B + Na]^+$ 521.2793, found 521.2804.

***tert*-butyl ((*S*)-3-hydroxy-1-oxo-1-(((*R*)-1-((3a*S*,4*S*,6*S*,7a*R*)-3a,5,5-trimethylhexahydro-4,6-methanobenzo[*d*][1,3,2]dioxaborol-2-yl)pent-4-en-1-yl)amino)propan-2-yl)carbamate (4.22a)** The product was synthesized following general coupling procedure C, using Boc-L-Ser as the amino acid and **4.20** as the amine. The crude product was purified by silica gel (eluent 70:30 EtOAc-hexanes) to give the product as a white solid (77%). R_f = 0.23 (60:40 hexanes-EtOAc); mp = 49-52°C; IR (film) cm^{-1} 3425, 3345, 3079, 3020, 2980, 1709, 1653, 1607, 1504, 1389, 1368, 1215, 1167, 1054; ^{1}H NMR (400 MHz, Acetone-d_6) δ 7.87 (s, 1H), 6.04 (d, *J* = 8.4 Hz, 1H), 5.83 (ddt, *J* = 17.0, 10.2, 6.7 Hz, 1H), 5.00 (dq, *J* = 17.1, 1.7 Hz, 1H), 4.91 (ddt, *J* = 10.2, 2.4, 1.2 Hz, 1H), 4.25 (dd, *J* = 8.7, 2.2 Hz, 1H), 4.23 – 4.15 (m, 2H), 3.82 (dt, *J* = 11.0, 5.5 Hz, 1H), 3.77 – 3.68 (m, 1H), 2.88 – 2.78 (m, 1H), 2.31 (ddt, *J* = 13.9, 8.8, 2.5 Hz, 1H), 2.21 – 2.07 (m, 3H), 2.00 – 1.91 (m, 1H), 1.85 (tt, *J* = 5.7, 3.0 Hz, 1H), 1.78 (ddd, *J* = 14.2, 3.3, 2.2 Hz, 1H), 1.75 – 1.65 (m, 1H), 1.65 – 1.56 (m, 1H), 1.42 (s, 9H), 1.34 (s, 3H), 1.27 (s, 3H), 0.86 (s, 3H); ^{13}C NMR (101 MHz, Acetone-d_6) δ 23.48, 26.13, 26.70, 27.64 (3C), 28.41, 30.55, 31.22, 35.89, 37.92, 38.45, 39.76, 51.85, 55.31, 62.30, 76.95, 78.75, 84.29, 113.99, 138.87, 155.39, 172.64; ^{11}B NMR (128 MHz, Acetone-d_6) δ 26.33; HRMS (ESI+) *m/z* calcd for $[C_{23}H_{39}O_6N_2B + Na]^+$ 473.2793, found 473.2794.

***tert*-butyl ((2*S*,3*R*)-3-hydroxy-1-oxo-1-(((*R*)-1-((3a*S*,4*S*,6*S*,7a*R*)-3a,5,5-trimethylhexahydro-4,6-methanobenzo[*d*][1,3,2]dioxaborol-2-yl)pent-4-en-1-yl)amino)butan-2-yl)carbamate (4.22b)** The product was synthesized following general coupling procedure C, using Boc-L-Thr as the amino acid and **4.20** as the amine. The crude product was purified by silica gel (eluent 60:40 EtOAc-hexanes) to give the product as a white solid (69%). R_f = 0.50 (60:40 EtOAc-hexanes); mp = 54-57°C; IR (film) cm^{-1} 3492, 3349, 3198, 3079, 2976,

1720, 1695, 1607, 1500, 1391, 1368, 1238, 1167, 1078, 1052, 884; ^{1}H NMR (500 MHz, Acetone-d_6) δ 7.99 (s, 1H), 5.94 – 5.72 (m, 2H), 5.00 (dq, J = 17.1, 1.7 Hz, 1H), 4.91 (ddd, J = 10.1, 2.3, 1.2 Hz, 1H), 4.38 (d, J = 4.7 Hz, 1H), 4.24 (dd, J = 8.8, 2.2 Hz, 1H), 4.18 (dq, J = 11.1, 6.2, 5.0 Hz, 1H), 4.15 – 3.93 (m, 1H), 2.82 (td, J = 6.9, 4.1 Hz, 1H), 2.31 (ddt, J = 14.0, 8.7, 2.5 Hz, 1H), 2.25 – 2.07 (m, 3H), 2.00 – 1.91 (m, 1H), 1.91 – 1.83 (m, 1H), 1.79 (ddd, J = 14.1, 3.2, 2.3 Hz, 1H), 1.75 – 1.67 (m, 1H), 1.66 – 1.48 (m, 2H), 1.43 (s, 9H), 1.35 (s, 3H), 1.27 (s, 3H), 1.16 (d, J = 6.2 Hz, 3H), 0.86 (s, 3H); ^{13}C NMR (126 MHz, Acetone-d_6) δ 19.71, 24.38, 27.04, 27.59, 28.51 (3C), 31.44, 32.18, 35.24, 36.85, 38.79, 39.85, 40.66, 52.79, 59.24, 67.95, 77.72, 79.66, 85.00, 114.87, 139.72, 156.48, 173.95; ^{11}B NMR (161 MHz, Acetone-d_6) δ 26.18; HRMS (ESI+) *m/z* calcd for $[C_{24}H_{41}O_6N_2B + H]^+$ 465.3130, found 465.3140.

***tert*-butyl ((2*S*,3*S*)-3-hydroxy-1-oxo-1-(((*R*)-1-((3a*S*,4*S*,6*S*,7a*R*)-3a,5,5-trimethylhexahydro-4,6-methanobenzo[*d*][1,3,2]dioxaborol-2-yl)pent-4-en-1-yl)amino)butan-2-yl)carbamate (4.22c)** The product was synthesized following general coupling procedure C, using Boc-L-*allo*-Thr as the amino acid and **4.20** as the amine. The crude product was purified by silica gel (eluent 60:40 EtOAc-hexanes) to give the product as a white solid (61%). R_f = 0.38 (70:30 hexanes-EtOAc); mp = 49-52°C; IR (film) cm^{-1} 3424, 3310, 3075, 2976, 1720, 1697, 1641, 1607, 1500, 1451, 1389, 1368, 1218, 1167, 1080, 1020, 908; ^{1}H NMR (500 MHz, Acetone-d_6) δ 7.87 (s, 1H), 6.05 (d, J = 8.4 Hz, 1H), 5.82 (ddt, J = 17.0, 10.2, 6.7 Hz, 1H), 5.00 (dq, J = 17.1, 1.8 Hz, 1H), 4.91 (ddd, J = 10.2, 2.2, 1.2 Hz, 1H), 4.27 – 4.22 (m, 2H), 4.08 (t, J = 7.1 Hz, 1H), 4.00 (h, J = 6.3 Hz, 1H), 2.86 – 2.79 (m, 1H), 2.31 (ddt, J = 14.0, 8.7, 2.4 Hz, 1H), 2.22 – 2.08 (m, 3H), 1.94 (t, J = 5.6 Hz, 1H), 1.85 (tt, J = 5.7, 2.9 Hz, 1H), 1.78 (ddd, J = 14.3, 3.3, 2.2 Hz, 1H), 1.74 – 1.65 (m, 1H), 1.65 – 1.57 (m, 1H), 1.42 (s, 9H), 1.34 (s, 3H), 1.27 (s, 3H), 1.19 (d, J = 6.3 Hz, 3H), 0.86 (s, 3H); ^{13}C NMR (126 MHz, Acetone-d_6) δ 19.85, 24.36, 26.98, 27.57, 28.52 (3C), 29.29, 31.30, 32.11, 36.74, 38.80, 39.21, 40.63, 52.70, 59.42, 68.79, 77.89, 79.60, 85.24, 114.90, 139.70, 156.47, 173.34; ^{11}B NMR (161 MHz, Acetone-d_6) δ 27.43; HRMS (ESI+) *m/z* calcd for $[C_{24}H_{41}O_6N_2B + H]^+$ 465.3130, found 465.3142.

***tert*-butyl ((2*R*)-3-hydroxy-1-oxo-1-(((1*R*)-1-((3a*S*,4*S*,6*S*)-3a,5,5-trimethylhexahydro-4,6-methanobenzo[*d*][1,3,2]dioxaborol-2-yl)pent-4-en-1-yl)amino)propan-2-yl)carbamate (4.22d)** The product was synthesized following general coupling procedure C, using Boc-D-Ser as the amino acid and **4.20** as the amine. The crude product was purified by silica gel (eluent 60:40 EtOAc-hexanes) to give the product as a white solid (57%). R_f = 0.31 (70:30 hexanes-EtOAc); mp

= 47–51°C; IR (film) cm^{-1} 3412, 3302, 3075, 2929, 1701, 1657, 1607, 1452, 1391, 1368, 1219, 1167, 1054, 910; ^{1}H NMR (500 MHz, Acetone-d_6) δ 8.01 – 7.20 (m, 1H), 6.05 (d, J = 7.2 Hz, 1H), 5.82 (ddt, J = 16.9, 10.2, 6.7 Hz, 1H), 5.00 (dq, J = 17.1, 1.7 Hz, 1H), 4.91 (ddt, J = 10.2, 2.3, 1.2 Hz, 1H), 4.25 (dd, J = 8.7, 2.2 Hz, 1H), 4.22 – 4.19 (m, 1H), 4.14 (s, 1H), 3.82 (dd, J = 11.3, 4.8 Hz, 1H), 3.73 (dd, J = 10.8, 5.6 Hz, 1H), 2.86 (ddt, J = 8.5, 6.3, 3.1 Hz, 1H), 2.31 (ddt, J = 13.9, 8.8, 2.5 Hz, 1H), 2.21 – 2.08 (m, 3H), 1.95 (t, J = 5.6 Hz, 1H), 1.85 (tt, J = 5.8, 2.9 Hz, 1H), 1.81 – 1.74 (m, 1H), 1.69 (ddt, J = 13.1, 9.2, 6.5 Hz, 1H), 1.66 – 1.57 (m, 1H), 1.42 (s, 10H), 1.34 (s, 3H), 1.27 (s, 3H), 0.86 (s, 3H); ^{13}C NMR (126 MHz, Acetone-d_6) δ 24.35, 26.98, 27.56, 28.52 (3C), 29.27, 31.38, 32.05, 36.71, 38.81, 39.34, 40.61, 52.68, 56.00, 63.23, 77.87, 79.63, 85.28, 114.89, 139.73, 156.29, 173.32; ^{11}B NMR (161 MHz, Acetone-d_6) δ 27.28; HRMS (ESI+) *m/z* calcd for $[C_{23}H_{39}O_6N_2B + H]^+$ 451.2974, found 451.2985.

benzyl (*S*)-(1-oxo-1-(pyrrolidin-1-yl)propan-2-yl)carbamate (4.23a) The product was synthesized following general coupling procedure B, using Z-L-Ala as the amino acid and pyrrolidine as the amine, to give a white solid (49%). R_f = 0.49 (50:50 Hexanes-EtOAc); ^{1}H NMR (500 MHz, Acetone-d_6) δ 7.44 – 7.27 (m, 5H), 6.34 (d, J = 7.9 Hz, 1H), 5.08 (s, 2H), 4.43 (p, J = 7.1 Hz, 1H), 3.65 (dt, J = 9.9, 6.7 Hz, 1H), 3.51 (dt, J = 9.9, 6.9 Hz, 1H), 3.42 (dt, J = 11.8, 7.1 Hz, 1H), 3.33 (dt, J = 11.7, 6.8 Hz, 1H), 1.98 (p, J = 6.8 Hz, 2H), 1.85 (p, J = 6.9 Hz, 2H), 1.28 (d, J = 6.9 Hz, 3H); ^{13}C NMR (126 MHz, Acetone-d_6) δ 18.29, 24.71, 26.76, 46.51, 46.71, 49.16, 66.57, 128.61 (3C), 129.19 (2C), 138.31, 156.33, 171.19. Spectral and physical data were in accordance with the literature.[56] HPLC (Method A) t_R = 13.0 min, 96.5%.

benzyl ((*S*)-1-((*S*)-2-cyanopyrrolidin-1-yl)-1-oxopropan-2-yl)carbamate (4.23b) The product was synthesized following general coupling procedure B, using Z-L-Ala as the amino acid and prolinonitrile PTSA salt as the amine, to give the product as a clear oil (59%). R_f = 0.50 (50:50 Hexanes-EtOAc); ^{1}H NMR (500 MHz, Chloroform-*d*) δ 7.39 – 7.28 (m, 5H), 5.56 (d, J = 8.2 Hz, 1H), 5.15 – 5.02 (m, 2H), 4.82 – 4.72 (m, 1H), 4.48 (dt, J = 13.8, 7.2 Hz, 1H), 3.74 – 3.59 (m, 2H), 2.36 – 2.08 (m, 4H), 1.39 (d, J = 6.9 Hz, 3H). Spectral and physical data were previously published by our group.[15] HPLC (Method A) t_R = 13.2 min, 96.3%.

benzyl ((*S*)-1-oxo-1-((*R*)-2-((3a*S*,4*S*,6*S*,7a*R*)-3a,5,5-trimethylhexahydro-4,6-methanobenzo[*d*][1,3,2]dioxaborol-2-yl)pyrrolidin-1-yl)propan-2-yl)carbamate (4.23c) The product was synthesized following general coupling procedure C, using Z-L-Ala as the amino acid and **4.26** as the amine, to give a white foam (85%). R_f = 0.42 (50:50 Hexanes-EtOAc); IR (film)

cm^{-1} 3302, 3036, 2921, 1719, 1625, 1498, 1453, 1387, 1374, 1240, 1054, 1029, 741; ^{1}H NMR (500 MHz, Acetone-d_6) δ 8.08 – 7.10 (m, 10H), 6.62 – 6.30 (m, 1H), 6.29 – 5.90 (m, 1H), 5.15 – 4.97 (m, 4H), 4.51 – 4.35 (m, 2H), 4.26 (ddd, J = 8.9, 7.2, 2.3 Hz, 2H), 4.00 – 3.68 (m, 1H), 3.66 – 3.28 (m, 3H), 3.04 (dd, J = 10.1, 6.8 Hz, 1H), 2.96 (dd, J = 9.8, 7.0 Hz, 1H), 2.43 – 2.24 (m, 2H), 2.11 (ddtt, J = 10.8, 6.3, 4.6, 2.1 Hz, 4H), 2.03 – 1.91 (m, 6H), 1.90 – 1.75 (m, 4H), 1.74 – 1.65 (m, 2H), 1.64 – 1.45 (m, 2H), 1.44 – 1.36 (m, 2H), 1.35 (s, 3H), 1.27 (d, J = 5.0 Hz, 10H), 1.26 – 1.20 (m, 3H), 0.85 (d, J = 5.3 Hz, 6H); ^{13}C NMR (126 MHz, Acetone-d_6) δ 17.99, 18.37, 24.27 (2C), 26.72, 26.79, 27.39, 27.46, 27.48, 27.80, 28.11, 28.18, 28.99, 29.06, 36.26, 36.34, 38.83, 38.87, 40.43 (2C), 45.41 (2C), 46.73, 46.79, 48.50, 48.68, 52.23, 52.38, 66.56, 66.58, 78.26, 78.26, 85.83, 85.98, 128.56 (2C), 128.58 (2C), 128.60 (2C), 129.17 (4C), 138.28 (2C), 156.20, 156.32, 171.04, 171.17; ^{11}B NMR (161 MHz, Acetone-d_6) δ 31.39; HRMS (ESI+) *m/z* calcd for [$C_{25}H_{35}O_5N_2B$ + H]$^+$ 455.2712, found 455.2711; HPLC (Method A) t_R = 14.1 min, 95.6%.

***tert*-butyl ((*S*)-1-oxo-1-((*R*)-2-((3a*S*,4*S*,6*S*,7a*R*)-3a,5,5-trimethylhexahydro-4,6-methanobenzo[*d*][1,3,2]dioxaborol-2-yl)pyrrolidin-1-yl)propan-2-yl)carbamate (4.23d)** The product was synthesized following general coupling procedure C, using Boc-L-Ala as the amino acid and **4.26** as the amine, to give a white foam (64%). R_f = 0.41 (60:40 Hexanes-EtOAc); IR (film) cm^{-1} 3321, 2924, 1710, 1627, 1451, 1389, 1366, 1242, 1167, 1054, 1029; ^{1}H NMR (500 MHz, Acetone-d_6) δ 5.87 (d, J = 7.8 Hz, 1H), 5.78 (d, J = 8.2 Hz, 1H), 4.34 (p, J = 7.0 Hz, 2H), 4.27 (ddd, J = 11.3, 8.9, 2.3 Hz, 2H), 3.73 – 3.67 (m, 1H), 3.65 – 3.52 (m, 2H), 3.49 – 3.39 (m, 1H), 3.03 (dd, J = 10.1, 6.7 Hz, 1H), 2.94 (dd, J = 9.8, 7.0 Hz, 1H), 2.42 – 2.25 (m, 2H), 2.17 – 2.07 (m, 4H), 2.03 – 1.91 (m, 6H), 1.89 – 1.82 (m, 2H), 1.82 – 1.76 (m, 1H), 1.76 – 1.57 (m, 3H), 1.52 – 1.44 (m, 2H), 1.42 – 1.38 (m, 18H), 1.35 (s, 3H), 1.30 (s, 3H), 1.27 (s, 6H), 1.25 (d, J = 4.4 Hz, 3H), 1.22 (d, J = 4.2 Hz, 3H), 0.85 (s, 6H); ^{13}C NMR (126 MHz, Acetone-d_6) δ 18.12, 18.35, 24.26 (2C), 26.71, 26.78, 27.38, 27.46, 27.48, 27.77, 28.11, 28.19, 28.56 (3C), 28.59 (3C), 28.98, 29.12, 36.25, 36.38, 38.83, 38.86, 40.42, 40.45, 45.35 (2C), 46.67, 46.76, 47.96, 48.12, 52.23, 52.41, 78.21, 78.23, 79.00, 79.01, 85.80, 85.97, 155.70, 155.72, 171.33, 171.56; ^{11}B NMR (161 MHz, Acetone-d_6) δ 31.17; HRMS (ESI+) *m/z* calcd for [$C_{22}H_{37}O_5N_2B$ + H]$^+$ 421.2868, found 421.2864; HPLC (Method A) t_R = 1.5 min, 35.1%; t_R = 16.7 min, 62.2%.

***tert*-butyl ((*R*)-1-oxo-1-((*R*)-2-((3a*S*,4*S*,6*S*,7a*R*)-3a,5,5-trimethylhexahydro-4,6-methanobenzo[*d*][1,3,2]dioxaborol-2-yl)pyrrolidin-1-yl)propan-2-yl)carbamate (4.24a)** The product was synthesized following general coupling procedure C, using Boc-D-Ala as the amino

acid and **4.26** as the amine, to give a mixture of diastereomers as a white foam (40%). R_f = 0.39 (60:40 Hexanes-EtOAc); IR (film) cm^{-1} 3317, 2928, 1713, 1629, 1451, 1389, 1366, 1243, 1165, 1031; ^{1}H NMR (500 MHz, Acetone-d_6) δ 5.86 (d, J = 7.8 Hz, 1H), 5.77 (d, J = 7.8 Hz, 1H), 4.35 (td, J = 7.3, 3.1 Hz, 2H), 4.29 (dd, J = 8.9, 2.3 Hz, 1H), 4.24 (dd, J = 8.8, 2.2 Hz, 1H), 3.76 – 3.67 (m, 1H), 3.65 – 3.51 (m, 2H), 3.44 (td, J = 9.4, 6.7 Hz, 1H), 3.03 (dd, J = 10.3, 6.8 Hz, 1H), 2.97 – 2.89 (m, 1H), 2.39 – 2.26 (m, 2H), 2.20 – 2.07 (m, 4H), 2.03 – 1.90 (m, 6H), 1.85 (tq, J = 5.8, 2.9 Hz, 2H), 1.82 – 1.64 (m, 4H), 1.43 – 1.41 (m, 10H), 1.41 – 1.39 (m, 10H), 1.36 (s, 3H), 1.30 (s, 3H), 1.28 (s, 3H), 1.27 (s, 3H), 1.26 – 1.23 (m, 3H), 1.22 (s, 3H), 0.85 (s, 3H), 0.85 (s, 3H).; ^{13}C NMR (126 MHz, Acetone-d_6) δ 18.25, 18.60, 24.26, 24.28, 26.80 (2C), 27.46, 27.49, 27.55, 27.70, 28.18 (2C), 28.58 (3C), 28.59 (3C), 28.94, 29.06, 36.35 (2C), 38.85 (2C), 40.40, 40.44, 45.38 (2C), 46.65, 46.83, 47.99, 48.16, 52.33, 52.37, 78.05, 78.33, 78.96, 79.06, 85.84, 86.00, 155.54, 155.68, 171.18, 171.43; ^{11}B NMR (161 MHz, Acetone-d_6) δ 31.25; HRMS (ESI+) *m/z* calcd for $[C_{22}H_{37}O_5N_2B + H]^+$ 421.2868, found 421.2869; HPLC (Method A) t_R = 16.5 min, 98.3%

benzyl ((2*S*)-3-methyl-1-oxo-1-(2-((3a*S*,4*S*,6*S*,7a*R*)-3a,5,5-trimethylhexahydro-4,6-methanobenzo[*d*][1,3,2]dioxaborol-2-yl)pyrrolidin-1-yl)butan-2-yl)carbamate (4.25a) The product was synthesized following general coupling procedure C, using Z-L-Val as the amino acid and **4.26** as the amine, to give a white foam (60%). R_f = 0.31 (65:45 Hexanes-EtOAc); IR (film) cm^{-1} 3250, 3067, 2968, 1715, 1619, 1502, 1451, 1389, 1376, 1368, 1217, 1078, 1028; ^{1}H NMR (500 MHz, Acetone-d_6) δ 7.91 – 6.90 (m, 10H), 6.26 (d, J = 9.0 Hz, 1H), 6.15 (d, J = 9.2 Hz, 1H), 5.18 – 4.96 (m, 4H), 4.44 – 4.12 (m, 4H), 4.01 – 3.78 (m, 1H), 3.73 – 3.40 (m, 3H), 3.32 – 2.93 (m, 2H), 2.41 – 2.20 (m, 2H), 2.15 – 2.07 (m, 3H), 2.03 – 1.90 (m, 6H), 1.90 – 1.66 (m, 6H), 1.63 – 1.45 (m, 2H), 1.35 – 1.33 (m, 3H), 1.27 (s, 12H), 1.00 – 0.92 (m, 12H), 0.86 – 0.82 (m, 6H); ^{13}C NMR (126 MHz, Acetone-d_6) δ 18.30 (2C), 19.42, 19.66, 24.28 (2C), 26.82 (2C), 27.30, 27.47, 27.50, 27.92, 28.17 (2C), 29.05, 29.09, 31.58, 31.60, 36.24, 36.42, 38.82, 38.86, 40.41, 40.47, 45.28 (2C), 47.03, 47.20, 52.22, 52.42, 58.12, 58.30, 66.63, 66.69, 78.20, 78.26, 85.67, 86.08, 128.42 (2C), 128.56 (4C), 129.17 (4C), 138.29, 138.35, 157.07, 157.10, 170.48, 170.79; ^{11}B NMR (161 MHz, Acetone-d_6) δ 30.84; HRMS (ESI+) *m/z* calcd for $[C_{27}H_{39}O_5N_2B + H]^+$ 483.3025, found 483.3027; HPLC (Method A) t_R = 17.7 min, 45.2%; t_R = 18.4 min, 53.6%;

***tert*-butyl ((*S*)-3-methyl-1-oxo-1-((*R*)-2-((3a*S*,4*S*,6*S*,7a*R*)-3a,5,5-trimethylhexahydro-4,6-methanobenzo[*d*][1,3,2]dioxaborol-2-yl)pyrrolidin-1-yl)butan-2-yl)carbamate (4.25b)** The product was synthesized following general coupling procedure C, using Boc-L-Val as the amino

acid and **4.26** as the amine, to give a white foam (65%). R_f = 0.36 (70:30 Hexanes-EtOAc; IR (film) cm^{-1} 3321, 2968, 1715, 1619, 1449, 1389, 1366, 1169, 1076, 1032; ^{1}H NMR (500 MHz, Acetone-d_6) δ 5.72 (d, J = 8.8 Hz, 1H), 5.64 (d, J = 9.2 Hz, 1H), 4.32 – 4.22 (m, 2H), 4.20 – 3.91 (m, 2H), 3.77 (ddd, J = 10.6, 8.5, 2.8 Hz, 1H), 3.67 (dt, J = 10.0, 7.6 Hz, 1H), 3.59 (ddd, J = 10.2, 8.1, 4.2 Hz, 1H), 3.48 (td, J = 9.7, 6.8 Hz, 1H), 3.01 (dd, J = 10.7, 6.8 Hz, 1H), 2.96 (dd, J = 9.5, 7.1 Hz, 1H), 2.38 – 2.26 (m, 2H), 2.18 – 2.07 (m, 4H), 2.03 – 1.90 (m, 8H), 1.88 – 1.82 (m, 2H), 1.82 – 1.58 (m, 4H), 1.48 (dd, J = 15.0, 10.7 Hz, 2H), 1.40 (s, 18H), 1.34 (s, 3H), 1.30 (s, 3H), 1.27 (s, 3H), 1.27 (s, 3H), 0.97 – 0.92 (m, 6H), 0.92 – 0.88 (m, 6H), 0.85 (s, 6H). ^{13}C NMR (126 MHz, Acetone-d_6) δ 17.14, 17.32, 18.66, 18.84, 23.41 (2C), 25.93, 25.95, 26.42 (2C), 26.60, 26.63, 27.02 (2C), 27.31 (2C), 27.68 (3C), 27.72 (3C), 28.18, 28.29, 30.71, 30.80, 35.38, 35.62, 37.96, 37.99, 39.54, 39.62, 44.36 (2C), 46.08, 46.24, 51.36, 51.62, 56.54, 56.61, 77.28, 77.38, 84.77, 85.19, 155.56, 155.62, 169.76, 170.19; ^{11}B NMR (161 MHz, Acetone-d_6) δ 30.70; HRMS (ESI+) *m/z* calcd for $[C_{22}H_{41}O_5N_2B + H]^+$ 449.3181, found 449.3180; HPLC (Method A) t_R = 18.3 min, 95.4%

General acid-catalyzed oxidative cyclization procedure A. The dipeptide (1 eq) was diluted in anhydrous DCM (0.02 M), and 2-3 drops of Sudan III solution (1 mg/mL in DCM) were added (enough to reach a pink color). The solution was cooled to –78°C, and N_2 gas was bubbled into the solution for 5 minutes, followed by ozone (~80% ozone output). When the solution turned dark blue, ozone addition was stopped, and N_2 was bubbled until the solution was colorless. Polymer-bound triphenylphospine (1.5 eq, ~3 mmol/g loading, CAS 39319-11-4) was added, and the mixture stirred for 5 minutes at –78°C, then at room temperature overnight under argon atmosphere, after which the mixture became slightly opaque. TFA (1.5 eq) was added at room temperature, and the mixture was stirred for 2 h. The mixture was filtered through Celite®. The solid was rinsed with DCM, and the filtrate was concentrated *in vacuo*. The residue was redissolved in EtOAc and washed with saturated NH_4Cl and brine. The organic layer was dried over Na_2SO_4, filtered, and concentrated *in vacuo* to give the crude product, which was purified by flash chromatography on a silica gel column to give the pure product.

General acid-catalyzed oxidative cyclization procedure B. The dipeptide (1 eq) was diluted in anhydrous DCM (0.02 M) and cooled to –78°C. N_2 gas was bubbled into the solution for 5 minutes, followed by ozone (~80% output). When the solution turned a deep blue, ozone addition was immediately stopped, and N_2 was bubbled until the solution was colorless. Polymer-bound triphenylphospine (1.5 eq, ~3 mmol/g loading, CAS 39319-11-4) was added, and the mixture

stirred for 5 minutes at –78°C, then at room temperature overnight, after which the mixture became slightly opaque. TFA (1.5 eq) was added at room temperature, and the mixture was stirred for 2h. The mixture was filtered through Celite®. The solid was rinsed with DCM, and the filtrate was concentrated *in vacuo*. The residue was redissolved in EtOAc and washed with saturated NH_4Cl and brine. The organic layer was dried over Na_2SO_4, filtered, and concentrated *in vacuo* to give the crude product, which was purified by flash chromatography on a silica gel column to give the pure product.

benzyl ((3*S*,6*S*,8a*S*)-6-cyano-4-oxohexahydro-2*H*-pyrrolo[2,1-*b*][1,3]oxazin-3-yl)carbamate (4.10a) The product was synthesized according to general acid-catalyzed oxidative cyclization procedure B from peptide **4.18** and purified by flash chromatography on a silica gel column (eluent 80-20 EtOAc-hexanes) to give the product as a white solid (33%). R_f = 0.56 (100% EtOAc); mp = 167-170°C; IR (film) cm^{-1} 3361, 3031, 2952, 1719, 1685, 1532, 1433, 1257, 1064, 1064, 1018, 698; ^{1}H NMR (500 MHz, Acetone-d_6) δ 7.59 – 7.23 (m, 5H), 6.71 (d, J = 8.4 Hz, 1H), 5.41 (t, J = 6.5 Hz, 1H), 5.12 (s, 2H), 4.69 (dd, J = 5.3, 3.5 Hz, 1H), 4.62 (q, J = 8.6 Hz, 1H), 4.38 (t, J = 9.6 Hz, 1H), 3.78 (t, J = 8.5 Hz, 1H), 2.52 (ddt, J = 13.2, 5.6, 3.3 Hz, 1H), 2.33 (dq, J = 9.9, 3.0 Hz, 2H), 2.08 – 1.97 (m, 1H); ^{13}C NMR (126 MHz, Acetone-d_6) δ 28.41, 32.01, 45.59, 50.42, 67.02, 68.85, 88.52, 118.79, 128.64 (2C), 128.69, 129.22 (2C), 138.03, 157.29, 167.37; HRMS (ESI+) *m/z* calcd for $[C_{16}H_{17}O_4N_3 + Na]^+$ 338.1111, found 338.1102.

benzyl ((3*S*,8a*S*)-4-oxohexahydro-2*H*-pyrrolo[2,1-*b*][1,3]oxazin-3-yl)carbamate (4.10b) The product was synthesized according to general acid-catalyzed oxidative cyclization procedure A from peptide **4.14** and purified by flash chromatography on a silica gel column (eluent 80-20 EtOAc-hexanes) to give the product as a white solid (40%). R_f = 0.39 (100% EtOAc); mp = 118-122°C; IR (film) cm^{-1} 3305, 3063, 2980, 1717, 1669, 1530, 1443, 1217, 1064, 1018, 695; ^{1}H NMR (500 MHz, Acetone-d_6) δ 7.48 – 7.25 (m, 5H), 6.50 (s, 1H), 5.20 (t, J = 5.3 Hz, 1H), 5.10 (s, 2H), 4.44 (q, J = 7.4 Hz, 1H), 4.28 (dd, J = 10.2, 8.1 Hz, 1H), 3.76 – 3.66 (m, 2H), 3.26 (ddd, J = 11.9, 7.3, 5.1 Hz, 1H), 2.23 (td, J = 10.4, 10.0, 4.9 Hz, 1H), 1.96 – 1.87 (m, 1H), 1.87 – 1.76 (m, 2H); ^{13}C NMR (126 MHz, Acetone-d_6) δ 21.89, 33.03, 45.26, 50.22, 66.92, 68.81, 88.01, 128.65 (3C), 129.19 (2C), 138.06, 157.14, 166.64; HRMS (ESI+) *m/z* calcd for $[C_{15}H_{18}O_4N_2 + Na]^+$ 313.1159, found 313.1163; HPLC (Method A) t_R = 10.6 min, 96.0%.

benzyl ((3*S*,6*R*,8a*S*)-4-oxo-6-((3a*S*,4*S*,6*S*,7a*R*)-3a,5,5-trimethylhexahydro-4,6-methanobenzo[*d*][1,3,2]dioxaborol-2-yl)hexahydro-2*H*-pyrrolo[2,1-*b*][1,3]oxazin-3-

yl)carbamate (4.10c) The product was synthesized according to general acid-catalyzed oxidative cyclization procedure B from peptide **4.21a** and purified by flash chromatography on a silica gel column (eluent 50:50 hexanes-EtOAc) to give the product as a white foam (58%). R_f = 0.47 (50:50 hexanes-EtOAc); IR (film) cm^{-1} 3325, 3067, 2921, 1720, 1673, 1586, 1451, 1391, 1376, 1219, 1029; ^1H NMR (500 MHz, Acetone-d_6) δ 7.44 – 7.26 (m, 5H), 6.25 (d, J = 6.9 Hz, 1H), 5.20 (dd, J = 6.1, 4.0 Hz, 1H), 5.11 (s, 2H), 4.41 (q, J = 6.6 Hz, 1H), 4.29 (dd, J = 8.8, 2.1 Hz, 1H), 4.24 (dd, J = 10.4, 7.4 Hz, 1H), 3.72 (dd, J = 10.5, 6.2 Hz, 1H), 3.05 (t, J = 7.3 Hz, 1H), 2.33 (ddt, J = 14.1, 8.9, 2.5 Hz, 1H), 2.26 – 2.18 (m, 1H), 2.14 (ddt, J = 10.2, 7.7, 3.9 Hz, 1H), 2.01 – 1.93 (m, 3H), 1.91 – 1.83 (m, 2H), 1.78 (ddd, J = 14.4, 3.3, 2.2 Hz, 1H), 1.39 (s, 3H), 1.34 – 1.29 (m, 1H), 1.28 – 1.19 (m, 3H), 0.85 (s, 3H); ^{13}C NMR (126 MHz, Acetone-d_6) δ 24.25, 24.96, 26.82, 27.43, 28.75, 33.71, 36.17, 38.86, 40.38, 43.46, 50.00, 52.21, 66.97, 68.80, 78.36, 86.48, 88.29, 128.66 (3C), 129.20 (2C), 138.04, 157.03, 166.39; ^{11}B NMR (161 MHz, Acetone-d_6) δ 31.58; HRMS (ESI+) *m/z* calcd for $[C_{25}H_{33}O_6N_2B + Na]^+$ 491.2324, found 491.2331; HPLC (Method A) t_R = 16.4 min, 96.0%.

***tert*-butyl ((3S,6R,8aS)-4-oxo-6-((3aS,4S,6S,7aR)-3a,5,5-trimethylhexahydro-4,6-methanobenzo[d][1,3,2]dioxaborol-2-yl)hexahydro-2H-pyrrolo[2,1-b][1,3]oxazin-3-yl)carbamate (4.10e)** The product was synthesized according to general acid-catalyzed oxidative cyclization procedure B from peptide **4.22a** and purified by flash chromatography on a silica gel column (eluent 60:40 hexanes-EtOAc) to give the product as a white solid (52%). R_f = 0.39 (60:40 hexanes-EtOAc); mp = 144–147°C; IR (film) cm^{-1} 3337, 2924, 1715, 1673, 1449, 1391, 1368, 1165, 1078, 1030; ^1H NMR (500 MHz, Acetone-d_6) δ 5.75 (d, J = 6.6 Hz, 1H), 5.18 (t, J = 5.1 Hz, 1H), 4.34 – 4.26 (m, 2H), 4.20 (dd, J = 10.3, 7.2 Hz, 1H), 3.67 (dd, J = 10.3, 6.2 Hz, 1H), 3.06 (t, J = 7.2 Hz, 1H), 2.35 (ddt, J = 14.1, 8.8, 2.5 Hz, 1H), 2.26 – 2.18 (m, 1H), 2.18 – 2.13 (m, 1H), 2.02 – 1.92 (m, 3H), 1.92 – 1.85 (m, 2H), 1.79 (ddd, J = 14.4, 3.3, 2.2 Hz, 1H), 1.43 (s, 9H), 1.40 (s, 3H), 1.34 – 1.31 (m, 1H), 1.29 (s, 3H), 0.87 (s, 3H); ^{13}C NMR (126 MHz, Acetone-d_6) δ 24.25, 24.95, 26.82, 27.45, 28.49 (3C), 28.76, 33.73, 36.18, 38.88, 40.39, 43.62, 49.63, 52.21, 69.00, 78.39, 79.61, 86.48, 88.20, 156.28, 166.63; ^{11}B NMR (161 MHz, Acetone-d_6) δ 31.59; HRMS (ESI+) *m/z* calcd for $[C_{22}H_{35}O_6N_2B + H]^+$ 435.2661, found 435.2667; HPLC (Method A) t_R = 16.6 min, 98.8%.

***tert*-butyl ((3*R*,6*R*,8a*R*)-4-oxo-6-((3a*S*,4*S*,6*S*,7a*R*)-3a,5,5-trimethylhexahydro-4,6-methanobenzo[*d*][1,3,2]dioxaborol-2-yl)hexahydro-2*H*-pyrrolo[2,1-*b*][1,3]oxazin-3-**

yl)carbamate (4.11a) The product was synthesized according to general acid-catalyzed oxidative cyclization procedure B from peptide **4.22d** and purified by flash chromatography on a silica gel column (eluent 70:30 hexanes-EtOAc) to give the product as a white foam (53%). R_f = 0.31 (70:30 hexanes-EtOAc); IR (film) cm^{-1} 3349, 2925, 1709, 1671, 1449, 1389, 1378, 1370, 1215, 1163, 1076; ^1H NMR (500 MHz, Acetone-d_6) δ 6.02 (d, J = 6.5 Hz, 1H), 5.22 (t, J = 6.1 Hz, 1H), 4.33 (dt, J = 8.8, 1.6 Hz, 2H), 4.26 (dd, J = 11.5, 7.2 Hz, 1H), 3.67 (dd, J = 10.3, 6.1 Hz, 1H), 3.36 (dd, J = 10.3, 6.9 Hz, 1H), 2.41 – 2.27 (m, 2H), 2.21 – 2.11 (m, 1H), 2.09 (td, J = 6.1, 5.4, 2.8 Hz, 1H), 1.98 (t, J = 5.7 Hz, 1H), 1.95 – 1.81 (m, 2H), 1.83 – 1.76 (m, 2H), 1.78 – 1.69 (m, 1H), 1.42 (s, 9H), 1.36 (s, 3H), 1.28 (s, 3H), 0.86 (s, 3H); ^{13}C NMR (126 MHz, Acetone-d_6) δ 166.41, 156.43, 88.87, 86.78, 79.50, 78.62, 69.94, 52.08, 49.77, 43.44, 40.26, 38.86, 36.09, 34.28, 28.93, 28.50 (3C), 27.38, 26.83, 25.11, 24.19; ^{11}B NMR (161 MHz, Acetone-d_6) δ 31.87; HRMS (ESI+) *m/z* calcd for $[C_{22}H_{35}O_6N_2B + Na]^+$ 457.2480, found 457.2468; HPLC (Method A) t_R = 16.7 min, 98.2%.

benzyl ((2*R*,3*S*,6*R*,8a*S*)-2-methyl-4-oxo-6-((3a*S*,4*S*,6*S*,7a*R*)-3a,5,5-trimethylhexahydro-4,6-methanobenzo[*d*][1,3,2]dioxaborol-2-yl)hexahydro-2*H*-pyrrolo[2,1-*b*][1,3]oxazin-3-yl)carbamate (4.12a) The product was synthesized according to general acid-catalyzed oxidative cyclization procedure B from peptide **4.21b** and purified by flash chromatography on a silica gel column (eluent 50:50 hexanes-EtOAc) to give the product as a clear oil (59%). R_f = 0.58 (50:50 hexanes-EtOAc); IR (film) cm^{-1} 3409, 1720, 1675, 1504, 1454, 1391, 1376, 1217, 1056, 1028; ^1H NMR (500 MHz, Acetone-d_6) δ 7.46 – 7.30 (m, 5H), 6.06 (d, J = 8.0 Hz, 1H), 5.23 (t, J = 5.1 Hz, 1H), 5.12 (s, 2H), 4.43 (dd, J = 7.9, 5.5 Hz, 1H), 4.34 (p, J = 6.2 Hz, 1H), 4.29 (dd, J = 8.9, 2.2 Hz, 1H), 3.08 (dd, J = 8.2, 6.0 Hz, 1H), 2.32 (ddt, J = 14.1, 8.9, 2.5 Hz, 1H), 2.25 – 2.15 (m, 1H), 2.11 (dtd, J = 10.9, 6.4, 2.3 Hz, 1H), 2.02 – 1.83 (m, 5H), 1.78 (ddd, J = 14.4, 3.3, 2.2 Hz, 1H), 1.37 (s, 3H), 1.36 – 1.31 (m, 1H), 1.24 (s, 3H), 1.12 (d, J = 6.3 Hz, 3H), 0.85 (s, 3H); ^{13}C NMR (126 MHz, Acetone-d_6) δ 17.05, 24.26, 24.57, 26.80, 27.43, 28.80, 33.52, 36.15, 38.87, 40.39, 43.07, 52.18, 53.55, 67.00, 73.39, 78.46, 86.50, 87.46, 128.59 (2C), 128.67, 129.22 (2C), 138.12, 157.11, 166.11; ^{11}B NMR (161 MHz, Acetone-d_6) δ 31.95; HRMS (ESI+) *m/z* calcd for $[C_{26}H_{35}O_6N_2B + Na]^+$ 505.2480, found 505.2489; HPLC (Method A) t_R = 16.8 min, 95.3%.

***tert*-butyl ((2*R*,3*S*,6*R*,8a*S*)-2-methyl-4-oxo-6-((3a*S*,4*S*,6*S*,7a*R*)-3a,5,5-trimethylhexahydro-4,6-methanobenzo[*d*][1,3,2]dioxaborol-2-yl)hexahydro-2*H*-pyrrolo[2,1-*b*][1,3]oxazin-3-yl)carbamate (4.12b)** The product was synthesized according to

general acid-catalyzed oxidative cyclization procedure B from peptide **4.22b** and purified by flash chromatography on a silica gel column (eluent 60:40 hexanes-EtOAc) to give the product as a white solid (56%). R_f = 0.34 (60:40 hexanes-EtOAc); mp = 131-134°C; IR (film) cm^{-1} 3333, 1717, 1675, 1453, 1391, 1368, 1165, 1058, 1030; ^1H NMR (400 MHz, Acetone-d_6) δ 5.57 (d, J = 7.0 Hz, 1H), 5.23 (dd, J = 5.5, 4.4 Hz, 1H), 4.39 – 4.26 (m, 3H), 3.09 (dd, J = 8.3, 5.7 Hz, 1H), 2.35 (ddt, J = 14.0, 8.8, 2.5 Hz, 1H), 2.26 – 2.11 (m, 2H), 2.03 – 1.96 (m, 2H), 1.95 – 1.89 (m, 2H), 1.89 – 1.84 (m, 1H), 1.80 (ddd, J = 14.3, 3.3, 2.2 Hz, 1H), 1.44 (s, 9H), 1.39 (s, 3H), 1.37 – 1.32 (m, 1H), 1.29 (s, 3H), 1.09 (d, J = 6.1 Hz, 3H), 0.87 (s, 3H); ^{13}C NMR (101 MHz, Acetone-d_6) δ 165.37, 155.28, 86.26, 85.53, 78.50, 77.54, 72.36, 52.06, 51.18, 42.17, 39.41, 37.92, 35.15, 32.59, 27.83, 27.51 (3C), 26.48, 25.80, 23.66, 23.26, 16.02; ^{11}B NMR (161 MHz, Acetone-d_6) δ 31.80; HRMS (ESI+) *m/z* calcd for $[C_{23}H_{37}O_6N_2B + H]^+$ 449.2817, found 449.2814; HPLC (Method A) t_R = 18.1 min, 98.0%.

***tert*-butyl ((2*S*,3*S*,6*R*,8a*S*)-2-methyl-4-oxo-6-((3a*S*,4*S*,6*S*,7a*R*)-3a,5,5-trimethylhexahydro-4,6-methanobenzo[*d*][1,3,2]dioxaborol-2-yl)hexahydro-2*H*-pyrrolo[2,1-*b*][1,3]oxazin-3-yl)carbamate (4.13a)** The product was synthesized according to general acid-catalyzed oxidative cyclization procedure B from peptide **4.22c** and purified by flash chromatography on a silica gel column (eluent 60:40 hexanes-EtOAc) to give the product as a white foam (60%). R_f = 0.43 (70:30 hexanes-EtOAc); IR (film) cm^{-1} 3329, 2929, 1717, 1671, 1449, 1389, 1376, 1368, 1165, 1054, 1031; ^1H NMR (500 MHz, Acetone-d_6) δ 5.89 (d, J = 8.6 Hz, 1H), 5.40 (dd, J = 6.3, 2.3 Hz, 1H), 4.29 (dd, J = 8.8, 2.1 Hz, 1H), 4.19 (t, J = 9.0 Hz, 1H), 3.74 – 3.56 (m, 1H), 2.99 (t, J = 8.1 Hz, 1H), 2.34 (ddt, J = 14.2, 8.8, 2.5 Hz, 1H), 2.25 – 2.12 (m, 2H), 2.01 – 1.96 (m, 2H), 1.96 – 1.90 (m, 2H), 1.90 – 1.85 (m, 1H), 1.78 (ddd, J = 14.5, 3.4, 2.1 Hz, 1H), 1.43 (s, 9H), 1.41 (s, 3H), 1.32 (d, J = 6.2 Hz, 3H), 1.28 (d, J = 3.0 Hz, 4H), 0.87 (s, 3H); ^{13}C NMR (126 MHz, Acetone-d_6) δ 167.88, 156.81, 86.47, 84.11, 79.51, 78.29, 73.80, 55.75, 52.25, 44.12, 40.40, 38.84, 36.15, 34.36, 28.67, 28.49 (3C), 27.44, 26.86, 26.35, 24.25, 19.50; ^{11}B NMR (161 MHz, Acetone-d_6) δ 31.74; HRMS (ESI+) *m/z* calcd for $[C_{23}H_{37}O_6N_2B + H]^+$ 449.2817, found 449.2811; HPLC (Method A) t_R = 17.8 min, 96.8%.

***N*-((3S,6R,8aS)-4-oxo-6-((3aS,4S,6S,7aR)-3a,5,5-trimethylhexahydro-4,6-methanobenzo[d][1,3,2]dioxaborol-2-yl)hexahydro-2H-pyrrolo[2,1-b][1,3]oxazin-3-yl)acetamide (4.10d)** Bicycle **4.10c** (175 mg) was dissolved in EtOAc (15 mL), and AcOH was added (~5 drops). The solution was purged with Ar (bubbled into the solution) for 15 minutes. The

Pd/C catalyst was then added, and the mixture was purged with Ar (bubbled into the solution) for 5 minutes. The Ar balloon was replaced with an H_2 balloon, and the mixture stirred overnight. The solid was then filtered through Celite® and rinsed with EtOAc. The filtrate was concentrated *in vacuo* to give a yellow oil, which was dissolved in DCM (10 mL), and the solution was cooled to 0°C. Et_3N (113 mg, 0.16 mL, 3 eq) was added, followed by acetyl chloride (35 mg, 0.031 mL, 1.2 eq) and DMAP (5 mg, 0.1 eq). The solution was warmed to room temperature and stirred for 2 h. Water was added, and the product was extracted with DCM. The combined organic layers were washed with brine, dried over Na_2SO_4, and concentrated *in vacuo*. The crude product was purified by flash chromatography on a silica gel column (eluent 100% EtOAc) to give the product as a white solid (89 mg, 63% over 2 steps). R_f = 0.17 (eluent 100% EtOAc); ^{1}H NMR (500 MHz, Acetone-d_6) δ 7.16 (s, 1H), 5.18 (dd, J = 6.0, 4.0 Hz, 1H), 4.60 (dtd, J = 7.3, 6.4, 0.9 Hz, 1H), 4.29 (dd, J = 8.8, 2.2 Hz, 1H), 4.22 (dd, J = 10.4, 7.5 Hz, 1H), 3.57 (dd, J = 10.4, 6.4 Hz, 1H), 3.04 (t, J = 7.2 Hz, 1H), 2.35 (ddt, J = 14.2, 8.8, 2.5 Hz, 1H), 2.27 – 2.19 (m, 1H), 2.16 (dtd, J = 10.7, 6.1, 2.2 Hz, 1H), 2.01 – 1.96 (m, 2H), 1.96 – 1.92 (m, 4H), 1.92 – 1.85 (m, 2H), 1.78 (ddd, J = 14.4, 3.3, 2.2 Hz, 1H), 1.40 (s, 3H), 1.35 – 1.29 (m, 1H), 1.28 (s, 3H), 0.87 (s, 3H); ^{13}C NMR (126 MHz, Acetone-d_6) δ 170.20, 166.57, 88.20, 86.43, 78.34, 68.98, 52.24, 48.43, 43.39, 40.39, 38.86, 36.21, 33.74, 28.76, 27.43, 26.84, 25.07, 24.25, 22.65; ^{11}B NMR (161 MHz, Acetone-d_6) δ 31.51, 22.62; HRMS (ESI+) *m/z* calcd for $[C_{19}H_{29}O_5N_2B + H]^+$ 377.2242, found 377.2244; HPLC (Method A) t_R = 12.9 min, 95.1%.

General procedure for the deprotection of *N*-Boc protected boronic esters. The boronic ester (1 eq) was dissolved in DCM (0.1 M), and the solution was cooled to –78°C. BCl_3 (1 M in DCM, 3.5 eq) was added dropwise, and the solution was stirred at –78°C for 1 h. MeOH (12 eq) was added *slowly* at –78°C. The solution was concentrated *in vacuo*, and the residue was dissolved in DCM. The product was extracted with water, and the combined aqueous phases were washed with Et_2O and concentrated *in vacuo* to give the product as a solid with no further purification necessary.

(3*S*,6*R*,8a*S*)-6-borono-4-oxohexahydro-2*H*-pyrrolo[2,1-*b*][1,3]oxazin-3-aminium chloride (4.10f) The product was synthesized from bicycle **4.10e** according to the general procedure for the deprotection of *N*-Boc protected boronic esters, giving a sticky white solid (34%). R_f = does not elute on silica-backed TLC plates; IR (film) cm^{-1} 3206, 3194, 2845, 1647, 1477, 1022; ^{1}H NMR (500 MHz, DMSO-d_6) δ 8.68 (s, 3H), 5.02 (dd, J = 6.9, 5.5 Hz, 1H), 4.14

(dd, *J* = 12.1, 6.2 Hz, 1H), 4.08 (dd, *J* = 12.1, 3.5 Hz, 1H), 3.91 – 3.85 (m, 1H), 2.98 (dd, *J* = 9.4, 4.1 Hz, 1H), 2.14 (dtd, *J* = 10.7, 5.6, 3.3 Hz, 1H), 1.93 – 1.80 (m, 2H), 1.79 – 1.73 (m, 1H); ^{13}C NMR (126 MHz, DMSO) δ 22.65, 31.19, 45.20, 46.71, 66.09, 88.62, 161.45; ^{11}B NMR (161 MHz, DMSO) δ 20.23; HRMS (ESI+) *m/z* calcd for $[C_7H_{13}O_4N_2B + H]^+$ 201.1041, found 201.1039; HPLC (Method B) t_R = 1.7 min, 96.2%.

(3*R*,6*R*,8a*R*)-6-borono-4-oxohexahydro-2*H*-pyrrolo[2,1-*b*][1,3]oxazin-3-aminium chloride (4.11b) The product was synthesized from bicycle **4.11a** according to the general procedure for the deprotection of *N*-Boc protected boronic esters, giving a sticky white solid (39%). R_f = does not elute on silica-backed TLC plates; IR (film) cm^{-1} 3206, 2980, 1653, 1447, 1191, 1056; ^{1}H NMR (500 MHz, DMSO-d_6) δ 8.60 (s, 3H), 5.05 (dd, *J* = 7.9, 5.4 Hz, 1H), 4.19 (dd, *J* = 12.1, 7.1 Hz, 1H), 4.05 (dd, *J* = 12.1, 3.4 Hz, 1H), 3.97 – 3.86 (m, 1H), 3.21 (dd, *J* = 10.9, 7.5 Hz, 1H), 2.21 (dtd, *J* = 11.3, 5.8, 1.6 Hz, 1H), 2.00 (dtd, *J* = 12.3, 7.1, 1.5 Hz, 1H), 1.66 (tt, *J* = 11.5, 7.3 Hz, 1H), 1.56 (qd, *J* = 11.8, 5.9 Hz, 1H); ^{13}C NMR (126 MHz, DMSO) δ 23.05, 32.39, 46.12, 46.81, 66.38, 89.33, 161.95; ^{11}B NMR (161 MHz, DMSO) δ 20.15; HRMS (ESI+) *m/z* calcd for $[C_7H_{13}O_4N_2B + H]^+$ 201.1041, found 201.1041; HPLC (Method B) t_R = 1.8 min, 96.0%.

(2*R*,3*S*,6*R*,8a*S*)-6-borono-2-methyl-4-oxohexahydro-2*H*-pyrrolo[2,1-*b*][1,3]oxazin-3-aminium chloride (4.12c) The product was synthesized from bicycle **4.12b** according to the general procedure for the deprotection of *N*-Boc protected boronic esters, giving a sticky white solid (41%). R_f = does not elute on silica-backed TLC plates; IR (film) cm^{-1} 3194, 2892, 1651, 1445, 1193, 1046; ^{1}H NMR (500 MHz, DMSO-d_6) δ 8.54 (d, *J* = 5.4 Hz, 3H), 5.12 (t, *J* = 5.9 Hz, 1H), 4.34 (p, *J* = 6.4 Hz, 1H), 3.98 (p, *J* = 5.6 Hz, 1H), 2.97 (dd, *J* = 9.1, 4.5 Hz, 1H), 2.18 – 2.03 (m, 1H), 1.93 – 1.73 (m, 3H), 1.21 (d, *J* = 6.5 Hz, 3H); ^{13}C NMR (126 MHz, DMSO) δ 16.54, 23.13, 31.42, 45.49, 50.31, 70.67, 87.24, 161.95; ^{11}B NMR (161 MHz, DMSO) δ 19.64; HRMS (ESI+) *m/z* calcd for $[C_8H_{15}O_4N_2B + H]^+$ 215.1198, found 215.1192; HPLC (Method B) t_R = 1.8 min, 95.3%.

(2*S*,3*S*,6*R*,8a*S*)-6-borono-2-methyl-4-oxohexahydro-2*H*-pyrrolo[2,1-*b*][1,3]oxazin-3-aminium chloride (4.13b) The product was synthesized from bicycle **4.13a** according to the general procedure for the deprotection of *N*-Boc protected boronic esters, giving a sticky white solid (52%). R_f = does not elute on silica-backed TLC plates; IR (film) cm^{-1} 3198, 2948, 1653, 1477, 1193, 1138; ^{1}H NMR (500 MHz, DMSO-d_6) δ 8.63 (d, *J* = 4.7 Hz, 3H), 5.40 – 5.19 (m, 1H), 4.28 – 3.79 (m, 2H), 3.21 – 2.87 (m, 1H), 2.24 – 1.98 (m, 1H), 1.98 (s, 3H), 1.39 (d, *J* = 6.3 Hz,

3H); ^{13}C NMR (126 MHz, DMSO) δ 18.85, 24.70, 31.99, 46.74, 52.40, 70.24, 83.35, 162.86; ^{11}B NMR (161 MHz, DMSO) δ 20.09; HRMS (ESI+) $[C_8H_{15}O_4N_2B + H]^+$ 215.1198, found 215.1190; HPLC (Method B) t_R = 1.8 min, 97.3%.

4.6 References

(1) Lawandi, J.; Gerber-Lemaire, S.; Juillerat-Jeanneret, L.; Moitessier, N., Inhibitors of prolyl oligopeptidases for the therapy of human diseases: Defining diseases and inhibitors. *J Med Chem* **2010,** *53* (9), 3423-3438

(2) Lambeir, A. M., Translational research on prolyl oligopeptidase inhibitors: The long road ahead. *Exp Opin Therap Pat* **2011,** *21* (7), 977-981.

(3) López, A.; Tarragó, T.; Giralt, E., Low molecular weight inhibitors of Prolyl Oligopeptidase: A review of compounds patented from 2003 to 2010. *Exp Opin Therap Pat* **2011,** *21* (7), 1023-1044.

(4) Van Der Veken, P.; Fülöp, V.; Rea, D.; Gerard, M.; Van Elzen, R.; Joossens, J.; Cheng, J. D.; Baekelandt, V.; De Meester, I.; Lambeir, A. M.; Augustyns, K., P2-substituted N-acylprolylpyrrolidine inhibitors of prolyl oligopeptidase: Biochemical evaluation, binding mode determination, and assessment in a cellular model of synucleinopathy. *J Med Chem* **2012,** *55* (22), 9856-9867.

(5) Brandt, I.; Gérard, M.; Sergeant, K.; Devreese, B.; Baekelandt, V.; Augustyns, K.; Scharpé, S.; Engelborghs, Y.; Lambeir, A.-M., Prolyl oligopeptidase stimulates the aggregation of α-synuclein. *Peptides* **2008,** *29* (9), 1472-1478.

(6) Hannula, M. J.; Myöhänen, T. T.; Tenorio-Laranga, J.; Männistö, P. T.; Garcia-Horsman, J. A., Prolyl oligopeptidase colocalizes with α-synuclein, β-amyloid, tau protein and astroglia in the post-mortem brain samples with Parkinson's and Alzheimer's diseases. *Neuroscience* **2013,** *242*, 140-150.

(7) Savolainen, M. H.; Yan, X.; Myöhänen, T. T.; Huttunen, H. J., Prolyl Oligopeptidase Enhances α-Synuclein Dimerization via Direct Protein-Protein Interaction. *J Biol Chem* **2015,** *290* (8), 5117-5126.

(8) Svarcbahs, R.; Julku, U. H.; Norrbacka, S.; Myöhänen, T. T., Removal of prolyl oligopeptidase reduces alpha-synuclein toxicity in cells and in vivo. *Sci Rep* **2018,** *8* (1), 1552.

(9) Savolainen, M. H.; Richie, C. T.; Harvey, B. K.; Männistö, P. T.; Maguire-Zeiss, K. A.; Myöhänen, T. T., The beneficial effect of a prolyl oligopeptidase inhibitor, KYP-2047, on alpha-synuclein clearance and autophagy in A30P transgenic mouse. *Neurobiol Dis* **2014,** *68*, 1-15.

(10) Myöhänen, T. T.; Norrbacka, S.; Savolainen, M. H., Prolyl oligopeptidase inhibition attenuates the toxicity of a proteasomal inhibitor, lactacystin, in the alpha-synuclein overexpressing cell culture. *Neurosci Lett* **2017,** *636*, 83-89.

(11) Kumar, R.; Bavi, R.; Jo, M. G.; Arulalapperumal, V.; Baek, A.; Rampogu, S.; Kim, M. O.; Lee, K. W., New compounds identified through in silico approaches reduce the α-synuclein expression by inhibiting prolyl oligopeptidase in vitro. *Sci Rep* **2017,** *7* (1), 10827.

(12) Liu, J. M.; Kusinski, M.; Ilic, V.; Bignon, J.; Hajem, N.; Komorowski, J.; Kuzdak, K.; Stepien, H.; Wdzieczak-Bakala, J., Overexpression of the angiogenic tetrapeptide AcSDKP in human malignant tumors. *Anticancer Res* **2008,** *28* (5 A), 2813-2817.

(13) Suzuki, K.; Sakaguchi, M.; Tanaka, S.; Yoshimoto, T.; Takaoka, M., Prolyl oligopeptidase inhibition-induced growth arrest of human gastric cancer cells. *Biochem Biophys Res Commun* **2014,** *443*, 91-96.

(14) Tanaka, S.; Suzuki, K.; Sakaguchi, M., The prolyl oligopeptidase inhibitor SUAM-14746 attenuates the proliferation of human breast cancer cell lines in vitro. *Breast Cancer* **2017**, 1-9.

(15) Lawandi, J.; Toumieux, S.; Seyer, V.; Campbell, P.; Thielges, S.; Juillerat-Jeanneret, L.; Moitessier, N., Constrained Peptidomimetics Reveal Detailed Geometric Requirements of Covalent Prolyl Oligopeptidase Inhibitors. *J Med Chem* **2009,** *52*, 6672-6684

(16) De Cesco, S.; Deslandes, S.; Therrien, E.; Levan, D.; Cueto, M.; Schmidt, R.; Cantin, L. D.; Mittermaier, A.; Juillerat-Jeanneret, L.; Moitessier, N., Virtual screening and computational optimization for the discovery of covalent prolyl oligopeptidase inhibitors with activity in human cells. *J Med Chem* **2012,** *55* (14), 6306-6315.

(17) Kelly, T.; Huang, Y.; Simms, A. E.; Mazur, A., Fibroblast Activation Protein-α. A Key Modulator of the Microenvironment in Multiple Pathologies. *Int Rev Cell Mol Biol* **2012,** *297*, 83-116.

(18) Santos, A. M.; Jung, J.; Aziz, N.; Kissil, J. L.; Puré, E., Targeting fibroblast activation protein inhibits tumor stromagenesis and growth in mice. *J Clin Invest* **2009,** *119* (12), 3613-3625.

(19) Franco, O. E.; Hayward, S. W., Targeting the Tumor Stroma as a Novel Therapeutic Approach for Prostate Cancer. *Adv Pharmacol* **2012,** *65*, 267-313.

(20) Liu, R.; Li, H.; Liu, L.; Yu, J.; Ren, X., Fibroblast activation protein: A potential therapeutic target in cancer. *Cancer Biol Ther* **2012,** *13* (3), 123-129.

(21) Park, J. E.; Lenter, M. C.; Zimmermann, R. N.; Garin-Chesa, P.; Old, L. J.; Rettig, W. J., Fibroblast activation protein, a dual specificity serine protease expressed in reactive human tumor stromal fibroblasts. *J Biol Chem* **1999,** *274* (51), 36505-36512.

(22) Cheng, J. D.; Dunbrack Jr, R. L.; Valianou, M.; Rogatko, A.; Alpaugh, R. K.; Weiner, L. M., Promotion of tumor growth by murine fibroblast activation protein, a serine protease, in an animal model. *Cancer Res* **2002,** *62* (16), 4767-4772.

(23) Rettig, W. J.; Garin-Chesa, P.; Healey, J. H.; Su, S. L.; Ozer, H. L.; Schwab, M.; Albino, A. P.; Old, L. J., Regulation and heteromeric structure of the fibroblast activation protein in normal and transformed cells of mesenchymal and neuroectodermal origin. *Cancer Res* **1993,** *53* (14), 3327-3335.

(24) Ryabtsova, O.; Jansen, K.; Van Goethem, S.; Joossens, J.; Cheng, J. D.; Lambeir, A. M.; De Meester, I.; Augustyns, K.; Van Der Veken, P., Acylated Gly-(2-cyano)pyrrolidines as inhibitors of fibroblast activation protein (FAP) and the issue of FAP/prolyl oligopeptidase (PREP)-selectivity. *Bioorg Med Chem Lett* **2012,** *22* (10), 3412-3417.

(25) Jansen, K.; Heirbaut, L.; Cheng, J. D.; Joossens, J.; Ryabtsova, O.; Cos, P.; Maes, L.; Lambeir, A. M.; De Meester, I.; Augustyns, K.; Van Der Veken, P., Selective inhibitors of fibroblast activation protein (FAP) with a (4-quinolinoyl)-glycyl-2-cyanopyrrolidine scaffold. *ACS Med Chem Lett* **2013,** *4* (5), 491-496.

(26) Poplawski, S. E.; Lai, J. H.; Li, Y.; Jin, Z.; Liu, Y.; Wu, W.; Wu, Y.; Zhou, Y.; Sudmeier, J. L.; Sanford, D. G.; Bachovchin, W. W., Identification of selective and potent inhibitors of fibroblast activation protein and prolyl oligopeptidase. *J Med Chem* **2013,** *56* (9), 3467-3477.

(27) Bainbridge, T. W.; Dunshee, D. R.; Kljavin, N. M.; Skelton, N. J.; Sonoda, J.; Ernst, J. A., Selective Homogeneous Assay for Circulating Endopeptidase Fibroblast Activation Protein (FAP). *Sci Rep* **2017**.

(28) Christiansen, V. J.; Jackson, K. W.; Lee, K. N.; Downs, T. D.; McKee, P. A., Targeting Inhibition of Fibroblast Activation Protein-alpha and Prolyl Oligopeptidase Activities on Cells Common to Metastatic Tumor Microenvironments *Neoplasia* **2013,** *15*.

(29) Jackson, K. W.; Christiansen, V. J.; Yadav, V. R.; Silasi-Mansat, R.; Lupu, F.; Awasthi, V.; Zhang, R. R.; McKee, P. A., Suppression of Tumor Growth in Mice by Rationally Designed Pseudopeptide Inhibitors of Fibroblast Activation Protein and Prolyl Oligopeptidase. *Neoplasia* **2015,** *17*, 43-54.

(30) Tsai, T.-Y.; Yeh, T.-K.; Chen, X.; Hsu, T.; Jao, Y.-C.; Huang, C.-H.; Song, J.-S.; Huang, Y.-C.; Chien, C.-H.; Chiu, J.-H.; Yen, S.-C.; Tang, H.-K.; Chao, Y.-S.; Jiaang, W.-T., Substituted 4-Carboxymethylpyroglutamic Acid Diamides as Potent and Selective Inhibitors of Fibroblast Activation Protein. *J Med Chem* **2010,** *53* (18), 6572-6583.

(31) Tran, T.; Quan, C.; Edosada, C. Y.; Mayeda, M.; Wiesmann, C.; Sutherlin, D.; Wolf, B. B., Synthesis and structure-activity relationship of N-acyl-Gly-, N-acyl-Sar- and N-blocked-boroPro inhibitors of FAP, DPP4, and POP. *Bioorg Med Chem Lett* **2007,** *17* (5), 1438-1442.

(32) Kaszuba, K.; Róg, T.; Danne, R.; Canning, P.; Fülöp, V.; Juhász, T.; Szeltner, Z.; St. Pierre, J. F.; García-Horsman, A.; Männistö, P. T.; Karttunen, M.; Hokkanen, J.; Bunker, A., Molecular dynamics, crystallography and mutagenesis studies on the substrate gating mechanism of prolyl oligopeptidase. *Biochimie* **2012,** *94* (6), 1398-1411.

(33) Schiavini, P.; Pottel, J.; Moitessier, N.; Auclair, K., Metabolic Instability of Cyanothiazolidine-Based Prolyl Oligopeptidase Inhibitors: A Structural Assignment Challenge and Potential Medicinal Chemistry Implications. *ChemMedChem* **2015,** *10* (7), 1174-1183.

(34) Mariaule, G.; De Cesco, S.; Airaghi, F.; Kurian, J.; Schiavini, P.; Rocheleau, S.; Huskić, I.; Auclair, K.; Mittermaier, A.; Moitessier, N., 3-Oxo-hexahydro-1H-isoindole-4-carboxylic acid as a drug chiral bicyclic scaffold: structure-based design and preparation of conformationally constrained covalent and noncovalent prolyl oligopeptidase inhibitors. *J Med Chem* **2016,** *59*, 4221–4234.

(35) Corbeil, C. R.; Englebienne, P.; Moitessier, N., Docking Ligands into Flexible and Solvated Macromolecules. 1. Development and Validation of FITTED 1.0. *J Chem Inf Model* **2007,** *47*, 435-449.

(36) Moitessier, N.; Corbeil, C. R., Docking ligands into flexible and solvated macromolecules. 3. Impact of input ligand conformation, protein flexibility, and water molecules on the accuracy of docking programs. *J Chem Inf Model* **2009,** *49* (4), 997-1009.

(37) Moitessier, N.; Pottel, J.; Therrien, E.; Englebienne, P.; Liu, Z.; Tomberg, A.; Corbeil, C. R., Medicinal Chemistry Projects Requiring Imaginative Structure-Based Drug Design Methods. *Acc Chem Res* **2016,** *49* (9), 1646-57.

(38) Cunningham, C. C., Talabostat. *Exp Opin Investig Drugs* **2007,** *16* (9), 1459-65.

(39) Plescia, J.; De Cesco, S.; Patrascu, M. B.; Kurian, J.; Di Trani, J.; Dufresne, C.; Wahba, A. S.; Janmamode, N.; Mittermaier, A. K.; Moitessier, N., Integrated Synthetic, Biophysical, and Computational Investigations of Covalent Inhibitors of Prolyl Oligopeptidase and Fibroblast Activation Protein α. *J Med Chem* **2019,** *62* (17), 7874-7884.

(40) Plescia, J.; Dufresne, C.; Janmamode, N.; Wahba, A. S.; Mittermaier, A. K.; Moitessier, N., Discovery of covalent prolyl oligopeptidase boronic ester inhibitors. *Eur J Med Chem* **2020,** *185*, 111783.

(41) Smoum, R.; Rubinstein, A.; Dembitsky, V. M.; Srebnik, M., Boron Containing Compounds as Protease Inhibitors. *Chem Rev* **2012,** *112* (7), 4156-4220.

(42) Trippier, P. C.; McGuigan, C., Boronic acids in medicinal chemistry: anticancer, antibacterial and antiviral applications. *MedChemComm* **2010,** *1* (3), 183.

(43) Gentile, M.; Offidani, M.; Vigna, E.; Corvatta, L.; Recchia, A. G.; Morabito, L.; Morabito, F.; Gentili, S., Ixazomib for the treatment of multiple myeloma. *Exp Opin Investig Drugs* **2015,** *24* (9), 1287-1298.

(44) Michaelis, A.; Becker, P., Ueber Monophenylborchlorid und die Valenz des Bors. *Berichte der deutschen chemischen Gesellschaft* **1880,** *13* (1), 58-61.

(45) Michaelis, A.; Becker, P., Ueber Monophenylborchlorid und einige Derivate desselben. *Berichte der deutschen chemischen Gesellschaft* **1882,** *15* (1), 180-185.

(46) Lai, J. H.; Wu, W.; Zhou, Y.; Maw, H. H.; Liu, Y.; Milo Jr, L. J.; Poplawski, S. E.; Henry, G. D.; Sudmeier, J. L.; Sanford, D. G.; Bachovchin, W. W., Synthesis and characterization of constrained peptidomimetic dipeptidyl peptidase IV inhibitors: Amino-lactam boroalanines. *J Med Chem* **2007,** *50* (10), 2391-2398.

(47) Liu, G.; Cogan, D. A.; Owens, T. D.; Tang, T. P.; Ellman, J. A., Synthesis of Enantiomerically Pure N-tert-Butanesulfinyl Imines (tert-Butanesulfinimines) by the Direct Condensation of tert-Butanesulfinamide with Aldehydes and Ketones. *J Org Chem* **1999,** *64* (4), 1278-1284.

(48) Mabic, S.; Cordi, A. A., Synthesis of enantiomerically pure ethylenediamines from chiral sulfinimines: a new twist to the Strecker reaction. *Tetrahedron* **2001,** *57*, 8861-8866.

(49) Beenen, M. A.; An, C.; Ellman, J. A., Asymmetric Copper-Catalyzed Synthesis of α-Amino Boronate Esters from N-tert-Butanesulfinyl Aldimines. *J Am Chem Soc* **2008,** *130* (22), 6910-6911.

(50) Li, C.; Wang, J.; Barton, L. M.; Yu, S.; Tian, M.; Peters, D. S.; Kumar, M.; Yu, A. W.; Johnson, K. A.; Chatterjee, A. K.; Yan, M.; Baran, P. S., Decarboxylative borylation. *Science* **2017,** *356* (6342).

(51) Rhodes, C. A.; Pei, D., Bicyclic Peptides as Next-Generation Therapeutics. *Chemistry* **2017,** *23* (52), 12690-12703.

(52) Jansen, K.; Heirbaut, L.; Verkerk, R.; Cheng, J. D.; Joossens, J.; Cos, P.; Maes, L.; Lambeir, A. M.; De Meester, I.; Augustyns, K.; Van der Veken, P., Extended structure-activity relationship and pharmacokinetic investigation of (4-quinolinoyl)glycyl-2-cyanopyrrolidine inhibitors of fibroblast activation protein (FAP). *J Med Chem* **2014,** *57* (7), 3053-74.

(53) Abagyan, R.; Totrov, M., Biased Probability Monte Carlo Conformational Searches and Electrostatic Calculations for Peptides and Proteins. *J Mol Biol* **1994,** *235* (3), 983-1002 Monte Carlo; conformational search; global energy minimization; NMR structure determination; protein folding.

(54) Fustero, S.; Diego Jiménez; Sánchez-Roselló, M.; Pozo, C. d., Microwave-Assisted Tandem Cross Metathesis Intramolecular Aza-Michael Reaction: An Easy Entry to Cyclic B-Amino Carbonyl Derivatives. *J Am Chem Soc* **2007,** *129*, 6700-6701.

(55) Babij, N. R.; Wolfe, J. P., Asymmetric Total Synthesis of (+)-Merobatzelladine B. *Angew Chem Int Ed* **2012,** *51*, 4128-4130.

(56) Saito, Y.; Ouchi, H.; Takahata, H., Carboxamidation of carboxylic acids with 1-tert-butoxy-2-tert-butoxycarbonyl-1,2-dihydroisoquinoline (BBDI) without bases. *Tetrahedron* **2008,** *64* (49), 11129-11135.

Chapter 5:

A stereochemical study of acid-catalyzed oxidative cyclizations and asymmetric Strecker reactions in the synthesis of [4.3.0] azabicyclic peptidomimetics

This chapter is a draft of a manuscript prepared as:
Plescia, J.; Hédou, D.; Burai Patrascu, M.; Gerlovin, B.; Moitessier, N. A stereochemical study of acid-catalyzed oxidative cyclizations and asymmetric Strecker reactions in the synthesis of [4.3.0] azabicyclic peptidomimetics. *J. Org. Chem.*

While Chapters 2-4 focused on design, synthesis, and biological evaluation of POP and FAP inhibitors, they largely remain focused on inhibitor design and medicinal chemistry. Chapter 4 describes the preparation of inhibitors containing a [4.3.0] azabicylic scaffold, synthesized via a telescoped oxidative cleavage and acid-catalyzed cyclization. Herein we further explore this reaction to determine the effect of certain substituents on the stereoselectivity of the reaction.

Contribution(s) of authors: I synthesized and characterized all molecules presented in this chapter, with help in synthetic optimization from a summer intern student Benjamin Gerlovin. Dr. Damien Hédou contributed to the optimization of the syntheses. All computational work was done by Wanlei Wei.

5.1 Abstract

Over the past several years, our group has focused on the discovery of fused bicyclic inhibitors of prolyl oligopeptidase (POP) inhibitors as neurodegenerative and anti-cancer therapeutics. In our studies, we have applied several synthetic approaches to obtain these bicyclic scaffolds, including Diels-Alder reactions and peptide synthesis. Herein we report the synthesis of a [4.3.0] azabicyclic scaffold obtained from an acid-catalyzed oxidative cyclization reaction. Unexpectedly, while performing the reaction with both differing reducing reagents and starting materials varying in substitution patterns and stereochemistry, interesting patterns were observed. Thus, by changing some reaction conditions, we were able to select for certain stereochemistry. While these results are very recent, we propose tentative mechanisms to explain our results.

5.2 Introduction

Over the past fifteen years, our research group has focused on the synthesis of computationally-designed prolyl oligopeptidase (POP) inhibitors for the treatment of both neurodegenerative diseases and endothelial cancers (**5.1**-**5.3**, Figure 5.1).[1-4] In more recent medicinal chemistry projects, we have become interested in the preparation of inhibitors based around a [4.3.0] azabicyclic scaffold, as in compound **5.4** (Figure 5.2). Our approach to the design of these compounds stemmed from *in silico* optimization of **5.1**, as the sulfur rendered the inhibitor metabolically unstable,[5] and other linear peptides that are potent POP inhibitors. Using our in-house docking program FITTED,[6-7] we selected this scaffold for synthesis and elucidated the most promising structures, including various side chains and their optimal regio- and stereochemisty.

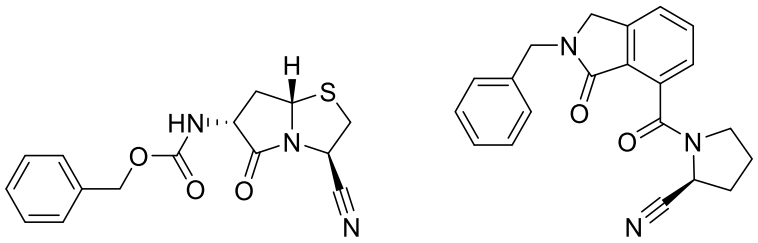

5.1
IC_{50} = 200 nM

5.2
K_i = 25 nM

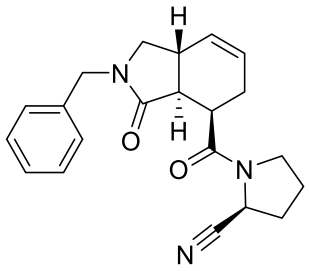

5.3
K_i = 1.0 nM

Figure 5.1. Our previous computationally designed prolyl oligopeptidase (POP) inhibitors **5.1-5.3.**

The preparation of this [4.3.0]-scaffold was first described in 1993 by Baldwin *et al.*, intending for analysis as *β*-turn-inducing mimetics.[8] Different conditions (*e.g.* Rh-catalyzed cyclohydrocarbonylation,[9] $SnCl_2$-mediated deacetalization-bicyclization sequence,[10] Ugi reaction[11]) were developed for the cyclization of this bicyclic core. The Baldwin procedure relies on the oxidative cleavage ($OsO_4/NaIO_4$[8] or O_3/PPh_3[12]) of alkene **A** (Figure 5.2) to afford a mixture of aldehyde/hemiaminal **B/C,** which undergo cyclization upon heating in presence of trifluoroacetic acid (TFA). The group studied both the stability of this bicyclic scaffold under basic and acidic conditions and, using nOe experiments, the stereocontrol of the cyclization reaction for both L- and D-serine derivatives. However, to the best of our knowledge, no study describing the effect of the substitution and stereochemistry at C_2 and C_6 on the stereocontrol of the cyclization has been reported. Herein we described the cyclization of polysubstituted [4.3.0] azabicyclic scaffold **5.4** and its stereocontrol induced by the presence and stereochemistry of substituents at C_2 and/or C_6. Furthermore, to the best of our knowledge, no studies have been reported that analyze the effect of reducing agents dimethyl sulfide (DMS) or triphenylphosphine (PPh_3) on the

stereochemistry of the ring closure. A summary of Baldwin's and our study can be found in Figure 5.2.

Based on studies involving docking-guided peptidomimetics, our group has chosen this scaffold as synthetic targets for potential POP inhibitors. Because our aim is to synthesize reversible covalent inhibitors,[13] and many active inhibitors of POP contain the nitrile reactive group to react with the enzyme's catalytic serine,[2] we have opted to synthesize both the covalent series (R_3 = CN in **5.4**) and the non-covalent series (R_3 = H in **5.4**) to compare biological activities.

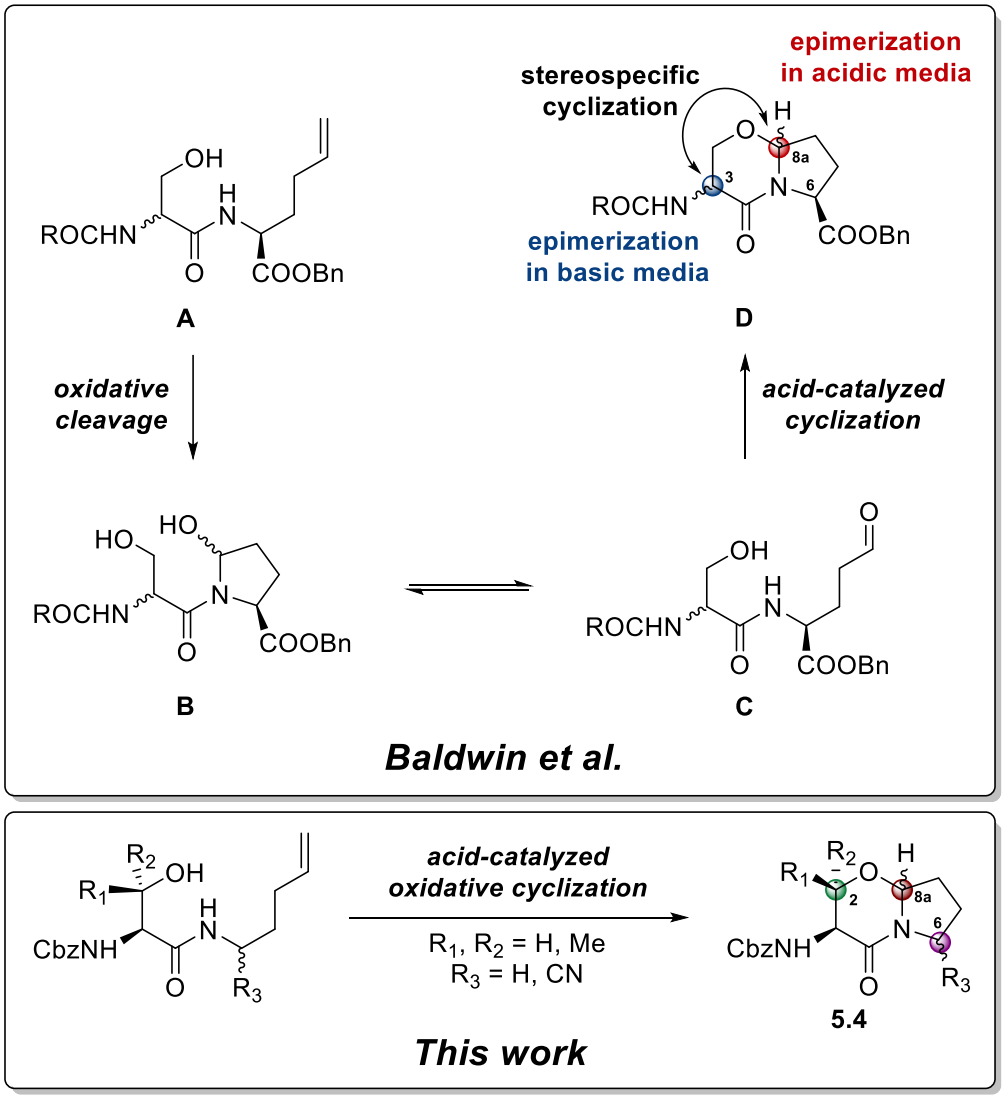

Figure 5.2. A summary of Baldwin's and our work on acid-catalyzed oxidative cleavage[8, 12]

5.3 Results and Discussion

5.3.1 Synthesis of the non-covalent series

The synthesis of this new inhibitor series began with the simpler of the two bicyclic systems, the non-covalent series lacking a reactive functional group at C_6. The first step was a coupling of readily available 4-pentene-1-amine, and *N*-Cbz-protected amino acids L-serine, L-threonine, and L-*allo*-threonine (Scheme 5.1). Following modified Baldwin procedures, we obtained our final bicycles by telescoping the oxidative cleavage via ozonolysis and acid-catalyzed cyclization reactions, totaling two overall steps. Interestingly, the diastereomeric ratios varied when the cyclization step was carried out at various temperatures and with different reducing agents (Table 5.1).

Scheme 5.1. Synthesis of the bicyclic non-covalent series lacking substituents at C_6[a]

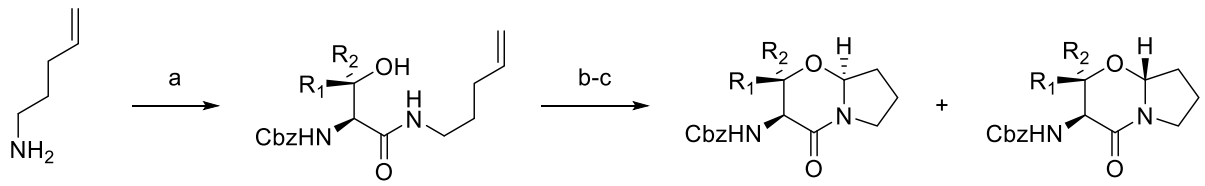

5.5, R_1 = H, R_2 = H (Z-Ser)
5.6, R_1 = Me, R_2 = H (Z-Thr)
5.7, R_1 = H, R_2 = Me (Z-*allo*-Thr)

5.8a/b, R_1 = H, R_2 = H (Z-Ser)
5.9a/b, R_1 = Me, R_2 = H (Z-Thr)
5.10a/b, R_1 = H, R_2 = Me (Z-*allo*-Thr)

[a]a) Z-L-AA, EDC•HCl, HOBt•H_2O, Et_3N, DCM, 0°C→rt, 18 h, 78% (**5.5**), 81% (**5.6**), 74% (**5.7**); b) O_3, CH_2Cl_2, −78°C; DMS or PPh_3, −78°C→rt, 18 h; c) TFA, DCM, rt or reflux, 2 h

Table 5.1. Diastereomeric ratios of the non-covalent dipeptide cyclization step at various temperatures.[a]

Entry	Starting dipeptide	Reducing agent	Cyclization temperature	Diastereomeric ratio (a:b)*	Yield of major diastereomer (%)
1	**5.5**	PPh_3	rt	92:8	40
2		PPh_3	reflux	89:11	32
3		DMS	rt	53:47	18:21
4		DMS	reflux	49:51	16:19
5		DMS[b]	rt	52:48	21:24
6		PPh_3[b]	rt	96:4	51
7		PPh_3[c]	rt	96:4	n/a[d]
8	**5.6**	PPh_3	rt	89:11	58
9		PPh_3	reflux	87:13	56
10		DMS	rt	73:27	53
11		DMS	reflux	67:33	38
12		DMS[b]	rt	74:26	45
13		PPh_3[b]	rt	93:7	52
14	**5.7**	PPh_3	rt	89:11	49
15		PPh_3	reflux	91:9	51
16		DMS	rt	25:75	37
17		DMS	reflux	24:76	46
18		DMS[b]	rt	26:73	48
19		PPh_3[b]	rt	74:26	30

[a]Conditions: (1) O_3, CH_2Cl_2, −78°C then DMS or PPh_3, −78°C→rt, 18 h; (2) TFA, DCM, rt/reflux, 2 h

[b]TFA was added without first removing DMS or PPh_3

[c]Free (upsupported) PPh_3 was used

[d]product was inseparable from $OPPh_3$ and residual PPh_3

*ratios determined from crude NMR

One-dimensional and two-dimensional NMR analysis were performed on the crude bicyclic product mixtures to determine (1) the stereochemistry of the major diastereomer, and (2) the ratio of diastereomer **a** to **b**. Irradiation of the hemiaminal-ethereal proton H_{8a} in 1D nuclear Overhauser effect experiments (Figure 5.3) revealed that for the L-serine-derived bicycle, diastereomer **5.8a** was preferred over **5.8b** upon room temperature cyclization when using PPh_3 as a reducing agent. For the compounds containing a methyl group at C_2, diastereomer **a** was preferred in a much higher ratio than that of **5.8a** when DMS is used as the reducing agent. It is clear that the methyl group somehow influences the closure of the bicyclic structure. Furthermore, there seems to be a match/mismatch case; the effects of the stereochemistry at C_2 and C_3 seem to be additive for the L-threonine-derived bicycle, giving **5.9a** as the major diastereomer in all cases. For the L-*allo*-threonine-derived bicycle, however, while the PPh_3 reactions gave mostly diastereomer **5.10a**, the DMS reactions gave the opposite diastereomer **5.10b** as the major product in a lower ratio. The opposite stereochemistry of the methyl C_2 group and C_3–NHCbz group seem to compete in the stereocontrol of this reaction (mismatched case).

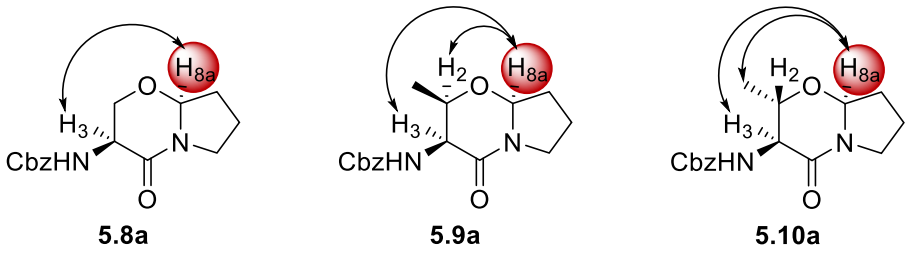

Figure 5.3. Selected 1D nOe experiments from the non-covalent inhibitor series. Red sphere indicates irradiation of H_{8a} proton.

Both DMS and PPh_3 are commonly used reducing agents in quenching the ozonolysis reaction. One result that we did not expect, however, was the significant difference in diastereomeric ratios upon using PPh_3 as the reducing agent in lieu of DMS. To assess the possibility of side reactions or influence of either reagent, both reducing reagents are removed before addition of the TFA: DMS is evaporated *in vacuo*, co-evaporating with DCM to ensure removal, and the resin-supported PPh_3 is filtered out of the mixture through Celite® to ensure full removal. Despite their full removal before addition of acid, PPh_3 gives significantly higher ratios of a:b than does DMS. To determine whether there would be a difference in diastereomeric ratios if the reducing agents were

not removed before addition of acid, two experiments were conducted introducing TFA into the reaction mixture containing either DMS or PPh_3. However, adding TFA to the reaction directly led to negligible differences in diastereometric ratios (within the error of NMR). This (1) eliminates the possibility of the steric bulk of PPh_3 contributing to the kinetically-favored diastereomer, and (2) confirms that the heat applied during rotoevaporator-mediated removal of DMS does not affect the diastereomeric ratio.

To determine whether the cyclization step was reversible, isolated **5.8a**, **5.9a**, and **5.10a** were subjected to reflux in the presence of TFA for 24 hours. The results are summarized in Table 5.2.

Table 5.2. Results of the cyclization reversibility of purified diastereomer **a**.

Entry	Starting bicycle	Diastereomeric ratio (a:b)[a]	Diastereomeric ratio (a:b)[b]
1	**5.8a**	53:47	47:51
2	**5.9a**	73:27	97:3
3	**5.10a**	25:75	26:74

[a]Original ratio of cyclization using DMS: TFA (1.5 eq), DCM, rt, 2 h,
[b]TFA (1.5 eq), DCM, reflux, 24 h

It appears that, although the initial cyclization with PPh_3 gave diastereomer **5.8a** selectively, refluxing **5.8a** in the presence of TFA lead to partial conversion (1:1) of diastereomer **5.8a** to diastereomer **5.8b**, indicating that the cyclization step is, in fact, reversible or that **5.8a** can epimerize through a different mechanism into **5.8b**. Interestingly, this ratio is the same as the one observed when the ozonolysis/cyclization was performed with DMS. The same epimerization occurs for the *allo*-threonine derivative **5.10a**. Unusual results lie with the L-threonine derivative: 24 h of refluxing in the presence of TFA gives little to no conversion to diastereomer **5.9b**. Since the only difference in structure is the methyl substituent at C_2, it is clear that this stereocenter plays a role in controlling the stereochemistry of the bicycle. For more insight into the mechanism, we proceeded with the synthesis of the nitrile-containing analogues which will introduce another potential stereodirecting group.

5.3.2 Synthesis of the nitrile series

All of these results intrigued us to study the effect of not only the substituent at C_2, but also at C_6, i.e. the potential covalent inhibitor series. However, the synthesis towards the final nitrile-containing scaffold was a bit more challenging than that of the non-covalent series. Preparations of nitrile-containing amines were lengthy, not reproducible, and gave racemic salts that would not allow for kinetic analysis. To remedy these shortcomings, the preparation of the amine started with synthesis of an enantiopure sulfinyl imine,[14] followed by the asymmetric diastereoselective addition of the cyano group using trimethylsilyl carbonitrile (TMSCN) (Scheme 5.2). The diastereoselectivity was not so straight-forward, however. During optimization of the reaction conditions, it was discovered that certain Lewis acids favored one diastereomer over the other. The steric bulk of the chiral auxiliary was expected to direct the TMSCN to the opposite side; the bulky lanthanide Lewis acids $Yb(OTf)_3$ and $Gd(OTf)_3$ were therefore expected to give the *anti* diastereomer, but instead gave the *syn* diastereomer, as did boron trifluoride. The results specific to these Lewis acids contradict a study of various Lewis acids on the Strecker reaction by Mabic *et al.*[15] and syntheses by Gu *et al.*[16] and Plant *et al*.[17] Even the reaction without a Lewis acid catalyst was expected to give diastereopure sulfinamide,[18] but no conversion was observed. When the lanthanide catalyst was replaced with ZnI_2, the desired *anti* diastereomer was finally observed.

Table 5.3 contains a summary of optimization conditions.

Scheme 5.2. Synthetic optimization of the diastereopure sulfinamide[a]

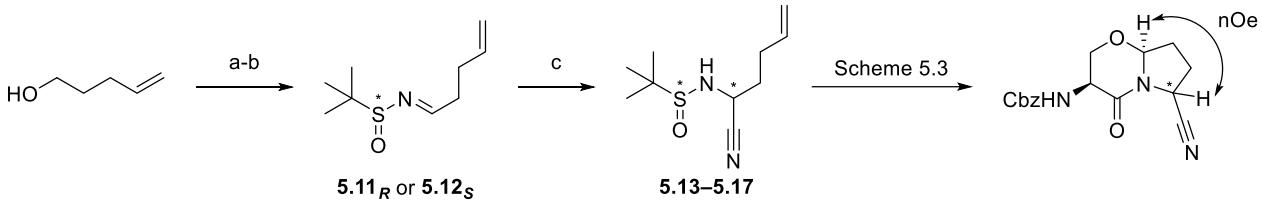

[a]a) $(COCl)_2$, DMSO, Et_3N, –78°C→rt, 2 h; b) (*R*)-(+)- or (*S*)-(-)-*tBu*-sulfinamide, $CuSO_4$, DCM, rt, 18 h, 75% (**5.11**), 62% (**5.12**); c) Lewis acid, TMSCN, DCM, 0°C→rt, 48 h

Table 5.3. Diastereoselectivity of various Lewis acids in the Strecker reaction.

Entry	Chiral auxiliary: *R* (5.11) *or* *S* (5.12)	Compound	Lewis Acid	Diastereoselectivity (syn:anti)	Yield (%)[a]
1	*R*	-	None[b]	n/a[c]	n/a[c]
2	*R*	**5.13**	$Gd(OTf)_3$	89:11	84
3	*R*	**5.14**	$Yb(OTf)_3$	90:10	73
4	*R*	**5.15**	$BF_3•OEt_2$	64:36	n/a[d]
5	*R*	**5.16**	ZnI_2	20:80	75
6	*S*	**5.17**	$Yb(OTf)_3$	89:11	82

[a]the diastereomers were inseparable; [b]hexane was used as the solvent[18]; [c]the reaction did not proceed; [d]the product was not purified

While the mechanism is still under investigation, we propose that the reaction involves three different methods of activation (Figure 5.4A-C). We hypothesize that the lanthanide-containing Lewis acids proceed through a six-membered transition state (A) to give the *syn* product, while the ZnI_2 could proceed through one of two mechanisms (B-C) to give the *anti* product.

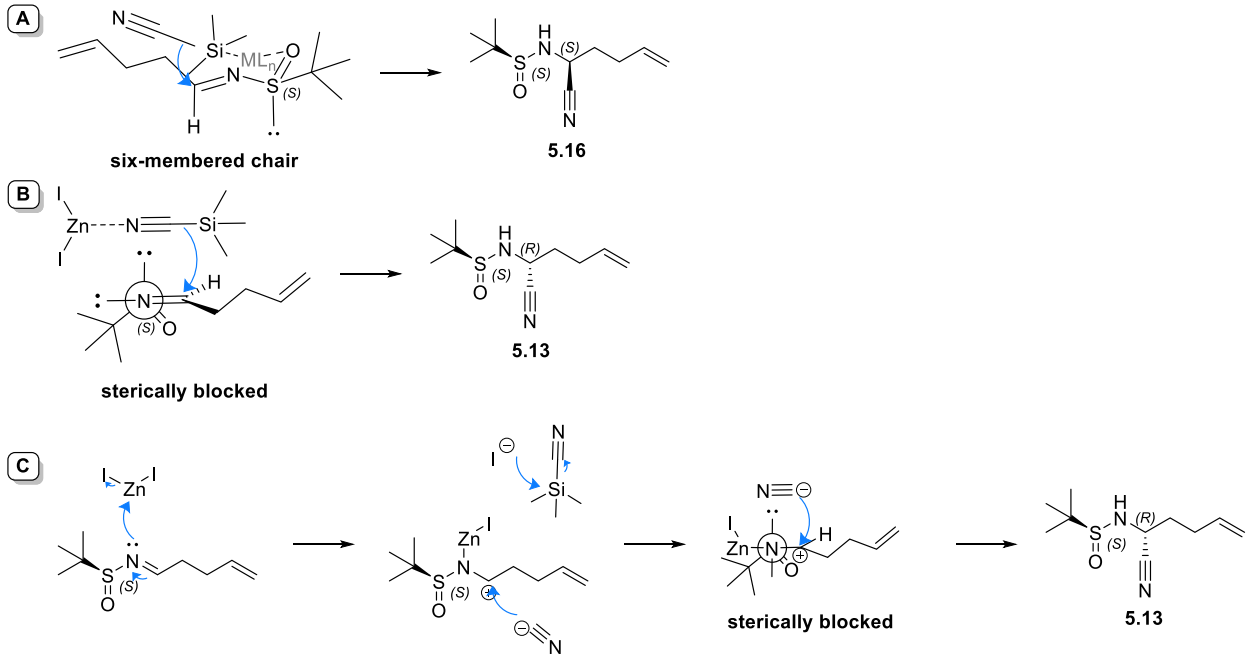

Figure 5.4. Proposed modes of sulfinimine activation by Lewis acids (A) $Gd(OTf)_3$ or (B-C) ZnI_2

The *syn* sulfinamides were carried forward to synthesize the nitrile-containing bicycles. (Scheme 5.3).

Scheme 5.3. Synthesis towards the covalent inhibitors.[a]

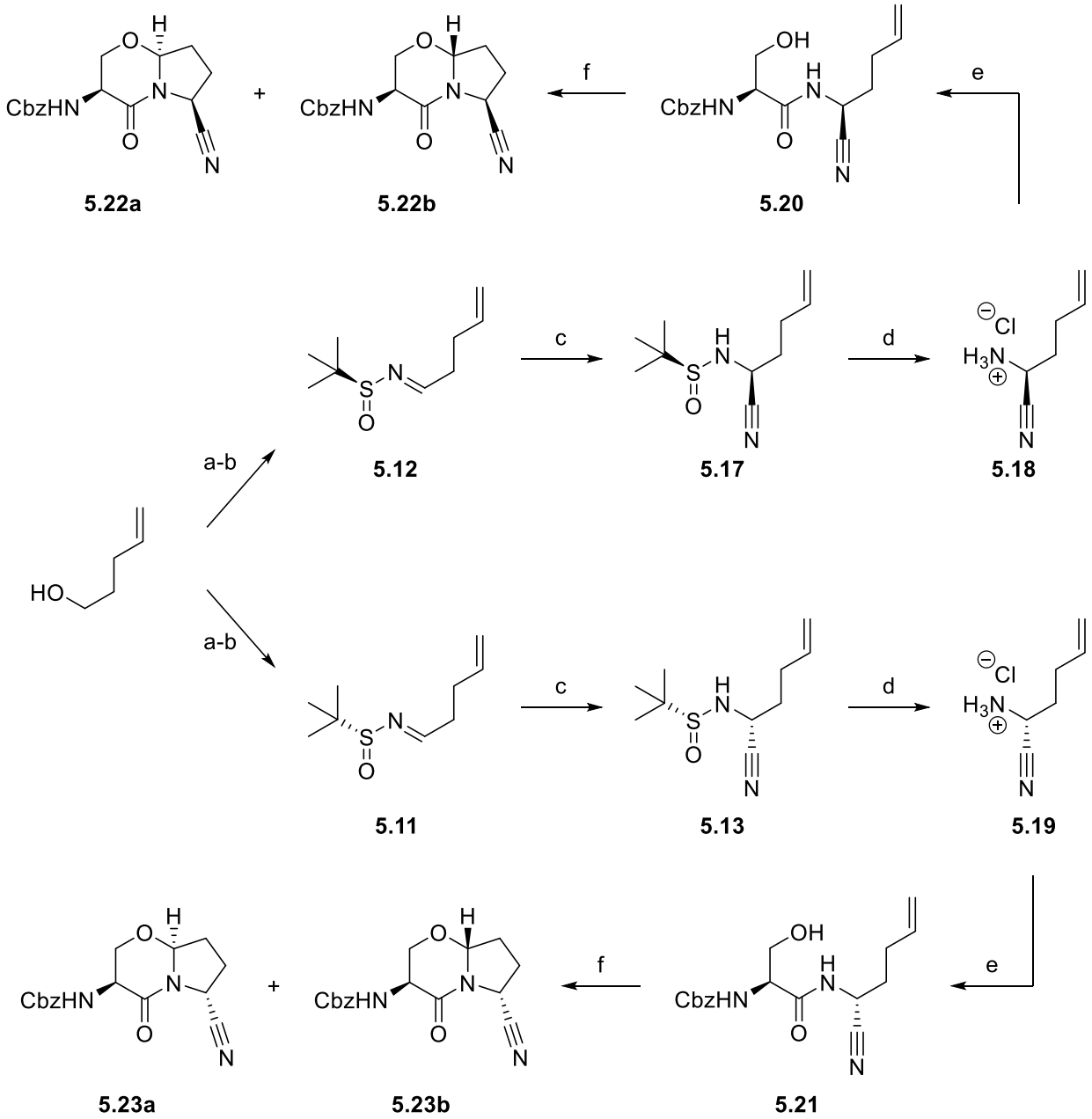

[a]a) $(COCl)_2$, DMSO, Et_3N, –78°C→rt, 2 h; b) (*R*)-(+)-*tBu*-sulfinamide (**5.11**) or (*S*)-(-)-*tBu*-sulfinamide (**5.12**), $CuSO_4$, DCM, rt, 18 h, 75% (**5.11**), 62% (**5.12**); c) $Gd(OTf)_3$, TMSCN, DCM, 0°C→rt, 48 h, 74% (**5.13**), 60% (**5.17**) ; d) HCl, Et_2O, 0°C, 1 h; e) Cbz-protected amino acid,

HATU, Et_3N, DMF, rt, 80% (**5.20**), 76% (**5.21**); f) 1) O_3, Sudan III, PPh_3 or DMS, −78°C→rt, 18 h; 2) TFA, DCM, reflux, 2 h

The sulfinylamide was deprotected with HCl, and the resultant ammonium was coupled to the corresponding *N*-Cbz-protected amino acid (Scheme 5.3). Cyclization to the bicycles was performed using the same conditions as with the non-covalent inhibitor series, with the use of indicator dye Sudan III to determine the end of the alkene's ozonolysis.[19-20] Interestingly, the second step of the cyclization did not proceed at room temperature, but only at reflux. It's likely that the electron-withdrawing nitrile is rendering the system less reactive. We verified the nitrile stereochemistry of the ammonium salt by cyclizing the corresponding dipeptides and conducting 1D nOe experiments (Figure 5.5).

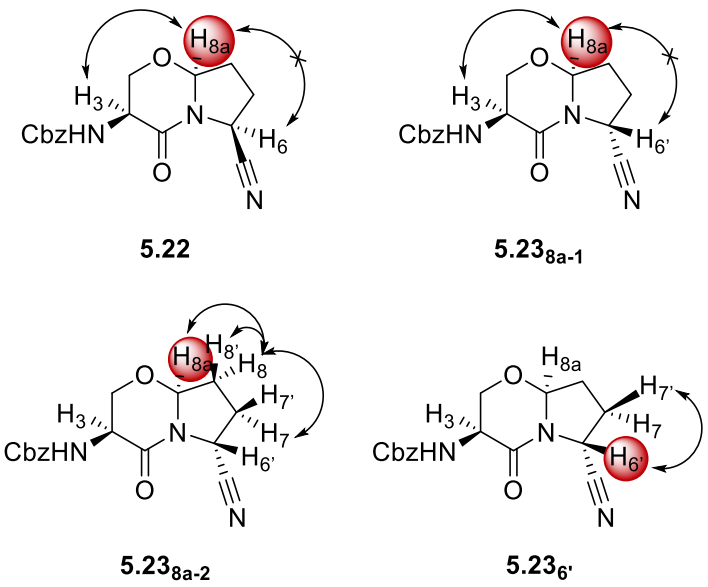

Figure 5.5. Selected NOE signals of the bicyclic nitrile series.

Table 5.4. Diastereomeric ratios of the dipeptide cyclization step.[a]

Entry	Starting dipeptide	Reducing agent	Diastereomeric ratio (a:b)*	Yield of major diastereomer (%)
1	**5.20**	PPh_3	91:9	54%
2		DMS	90:10	40%
3	**5.21**	PPh_3	86:14	53%
4		DMS	82:18	36%

[a]Conditions: (1) O_3, CH_2Cl_2, −78°C then DMS or PPh_3, −78°C→rt, 18 h; (2) TFA, DCM, reflux, 2 h

*ratios determined from crude NMR

The results in Table 5.4 indicate that the stereochemistry at C_6 unexpectedly has little to no effect on the diastereoselectivity of the cyclization. Whether or not the nitrile is *cis* to the amide, the effect on stereocontrol is weak, with stereoselectivity remaining ≥ 9:1, regardless of whether or not DMS or PPh_3 is used as the reducing agent. The nitriles, regardless of stereochemistry, give the same preferred diastereomer with high selectivity. These ratios are surprising, considering that the non-covalent serine analogue gave an approximately even 1:1 ratio. All of these results shed light on the possible mechanisms of the cyclization.

5.3.3 Mechanism Proposals

While these results are very recent and require much further analysis, we have some proposals about the possible mechanism of the reaction. Firstly, a preliminary NMR of the cyclization of the L-serine derived non-covalent inhibitor peptide **5.5** revealed that only trace amounts of aldehyde were present, i.e. a cyclization of some sort had already taken place. Furthermore, a time-monitored experiment (Figure 5.6) indicated that after addition of TFA, complete conversion to the fused bicycles was rapid; over the experiment of two hours at room temperature, the observable differences were minor changes in the baseline.

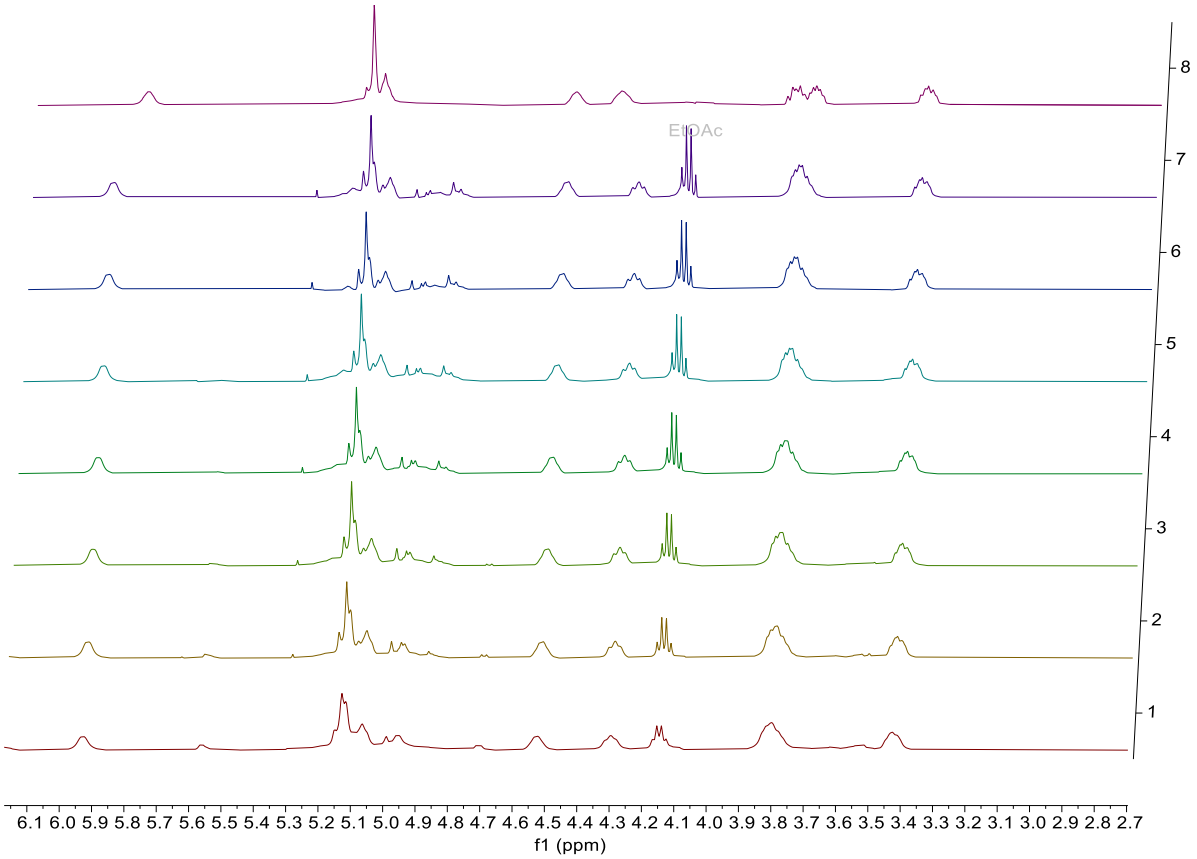

Figure 5.6. NMR time- monitored experiment of acid catalyzed cyclization of dipeptide **5.5**.NMR spectra of reaction mixture over 2 hours. (1–7) t_1 = 5 mins, $t_{2\text{-}7}$ = time measured every 20 mins; (8) NMR spectrum after TFA was removed from the mixture.

To account for (1) the differences observed with DMS or PPh_3, and (2) the stereoselectivity differences among the three different peptides, we propose that after the first step of the ozonolysis, the hydroxyl group attacks the carbonyl oxide (Figure 5.7), as has been reported with ozonolysis reactions in methanol.[21]

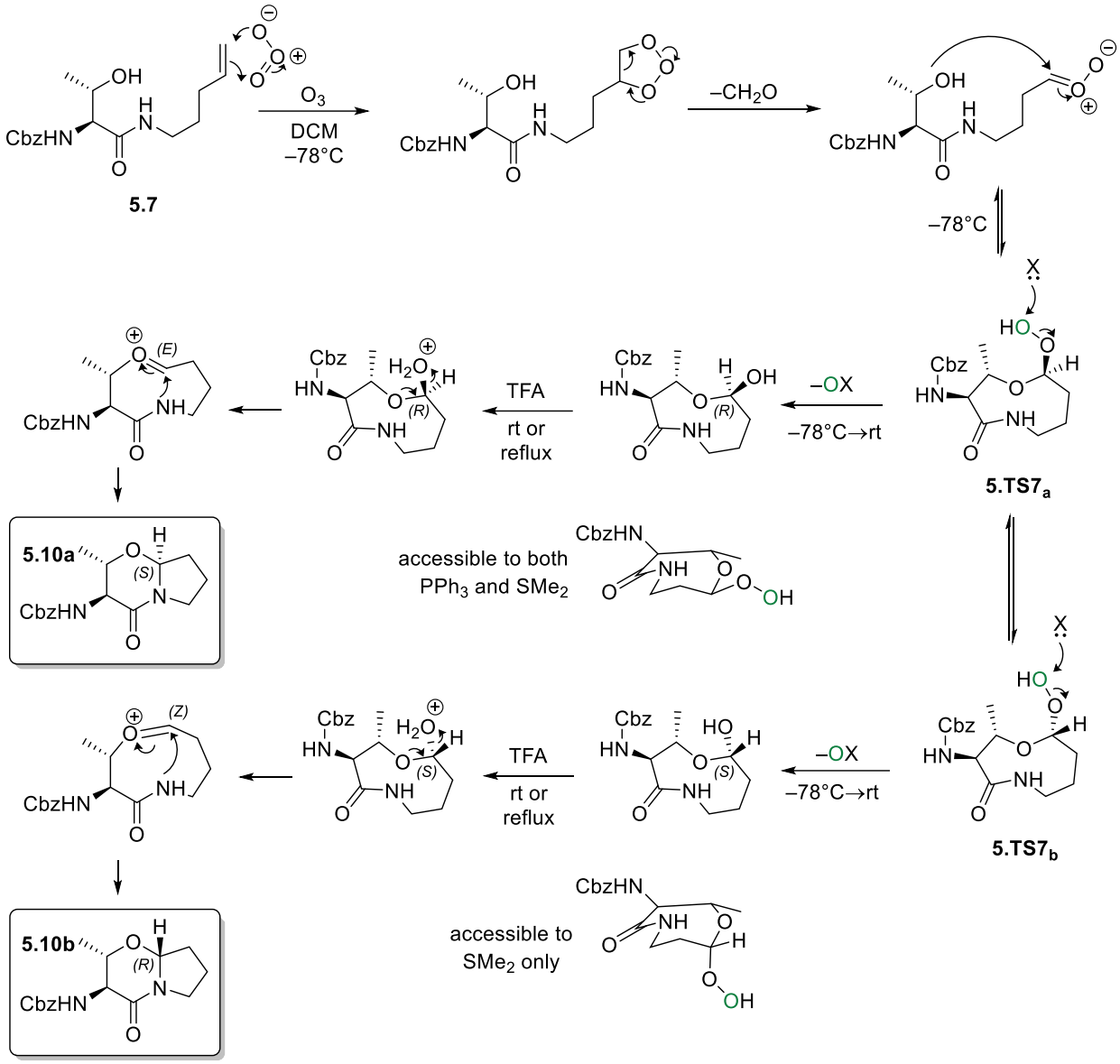

Figure 5.7. Proposed mechanism of the acid-catalyzed oxidative cyclization, illustrated with the L-*allo*-threonine derivative

This would give hydroperoxy acetal **5.TS7b**, in equilibrium with **5.TS7a**. We hypothesize that the reason reaction with PPh_3 gives such high diastereomeric ratios is that its size renders it unable to quench the hydroperoxy acetal when it is trans to the *N*-Cbz-amide, or **5.TS7b**. To examine this further, we converted the transition states to optimized 3D models using the CONVERT[22] function on the Forecaster platform. Figure 5.8 contains the optimized 3D structures of **5.TS7a** and **5.TS7b**.

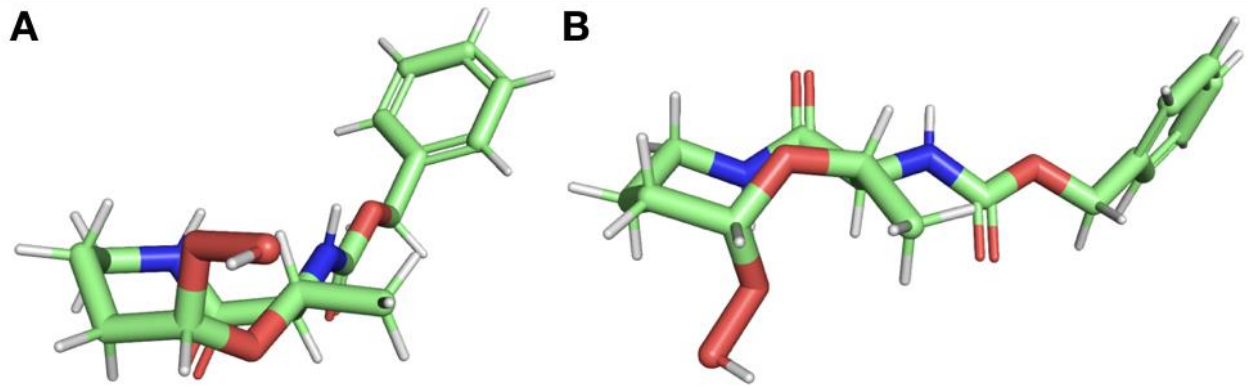

Figure 5.8. Optimized 3D structures of possible transitions states in the cyclization of the *allo*-threonine bicycle.**5.TS7a** (A) and **5.TS7b** (B) using CONVERT.[22]

From Figure 5.8, we see that the hydroperoxy group *cis* to the *N*-Cbz-amide (A) is much more accessible to PPh_3, a much more sterically hindered reducing agent, as the *trans* hydroperoxy is pseudo-axial and is less accessible. Furthermore, while we thought the PPh_3 might be blocked from the bottom face because of the methyl of the *allo*-threonine, its 3D model indicates that is an unlikely explanation. It's more likely that the methyl group is not sterically directing but instead conformationally directing; the two macrocycles differ in 3D conformation. These proposals are a preliminary hypothesis of this complex system's mechanism. However, to gain an understanding of the mechanism of this complex system, particularly the preference of **5.10b** in the presence of DMS, we require computational studies of the nine-membered ring system.

As for the mechanism of the reversed reaction, we saw that the threonine derivative did not epimerize under acidic conditions upon refluxing, while the *allo*-threonine and serine derivatives did, and they reached the ratios of the DMS room temperature reactions. To account for this, we propose that the mechanism of the reverse reaction goes through an imine intermediate (Figure 5.9).

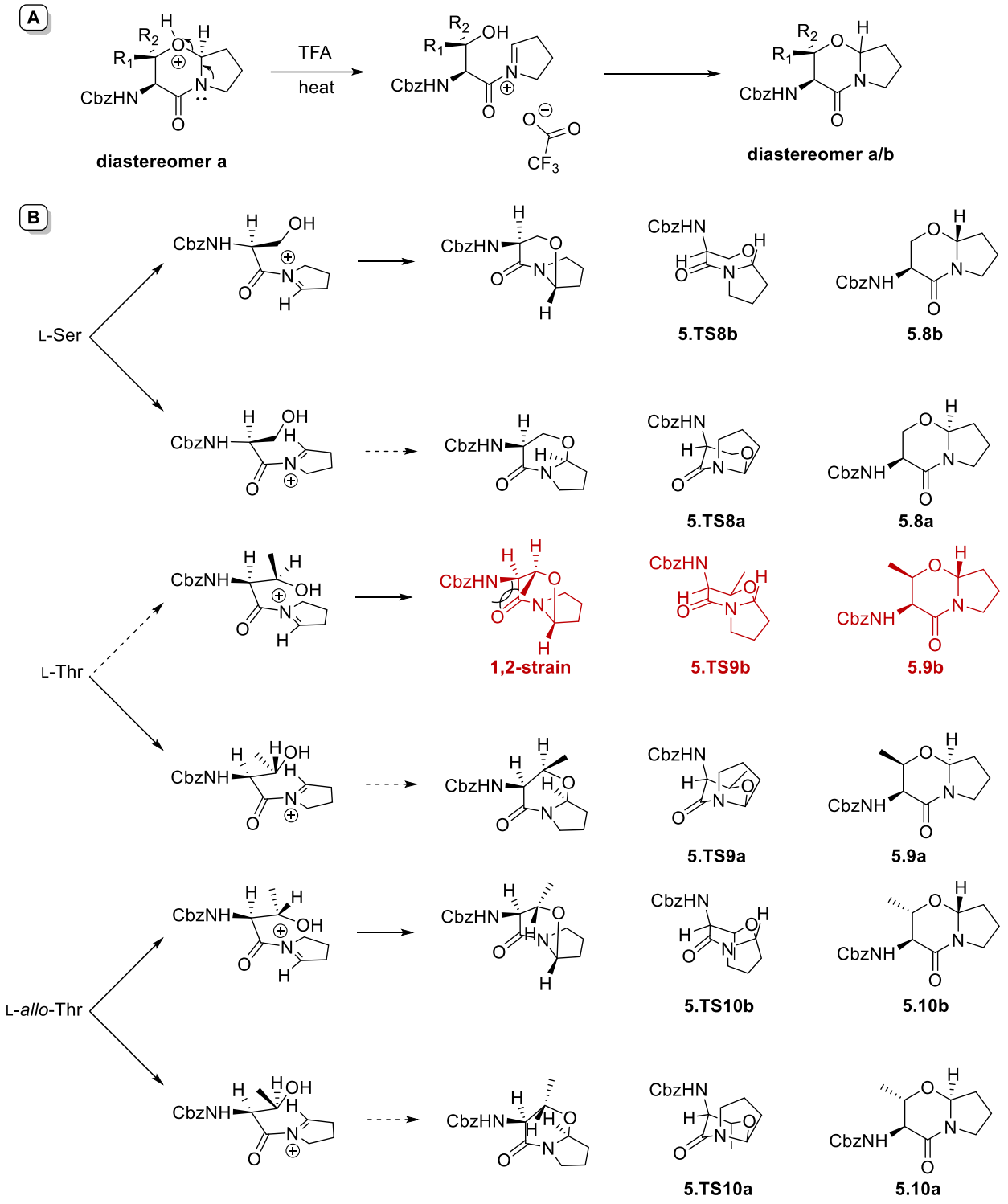

Figure 5.9. Proposed mechanism of the reverse cyclization (epimerization) reaction of the non-covalent series. (A) general scheme; (B) transition state proposals for each dipeptide

This preliminary mechanism highlights the different transition states observed for diastereomers **a** and **b**; diastereomer **a** appears to form through a chair-like transition state, while diastereomer **b** appears to form through a boat-like transition state. However, this does not explain the observed diastereomeric ratios. To understand the preference of **5.10b** over **5.10a** and the approximate 1:1 ratio of **5.8a** and **5.8b**, we require calculations of the relative energies of the products and transition states. These calculations are being performed by Wanlei Wei, a computational chemist in our group.

For the nitrile, if the reaction proceeded through a macrocyclic transition state, the nitrile should have little to no effect on the stereochemistry of the cyclization, as both nitriles give the same preferred diastereomer. Instead, because of the very high ratio favoring one diastereomer, it is possible that the reaction proceeds through the similar iminium ion, especially since the reaction does not proceed at room temperature with TFA (Figure 5.10). Considering the boat and chair transition states better explains the similar ratios; the transition states are very similar despite the opposite configuration of the nitriles. However, these proposals do not explain why with serine, previously known to give both epimers at C_{8a}, gives only **5.22a** and **5.23a**. It is therefore imperative to study this reaction using computational analysis.

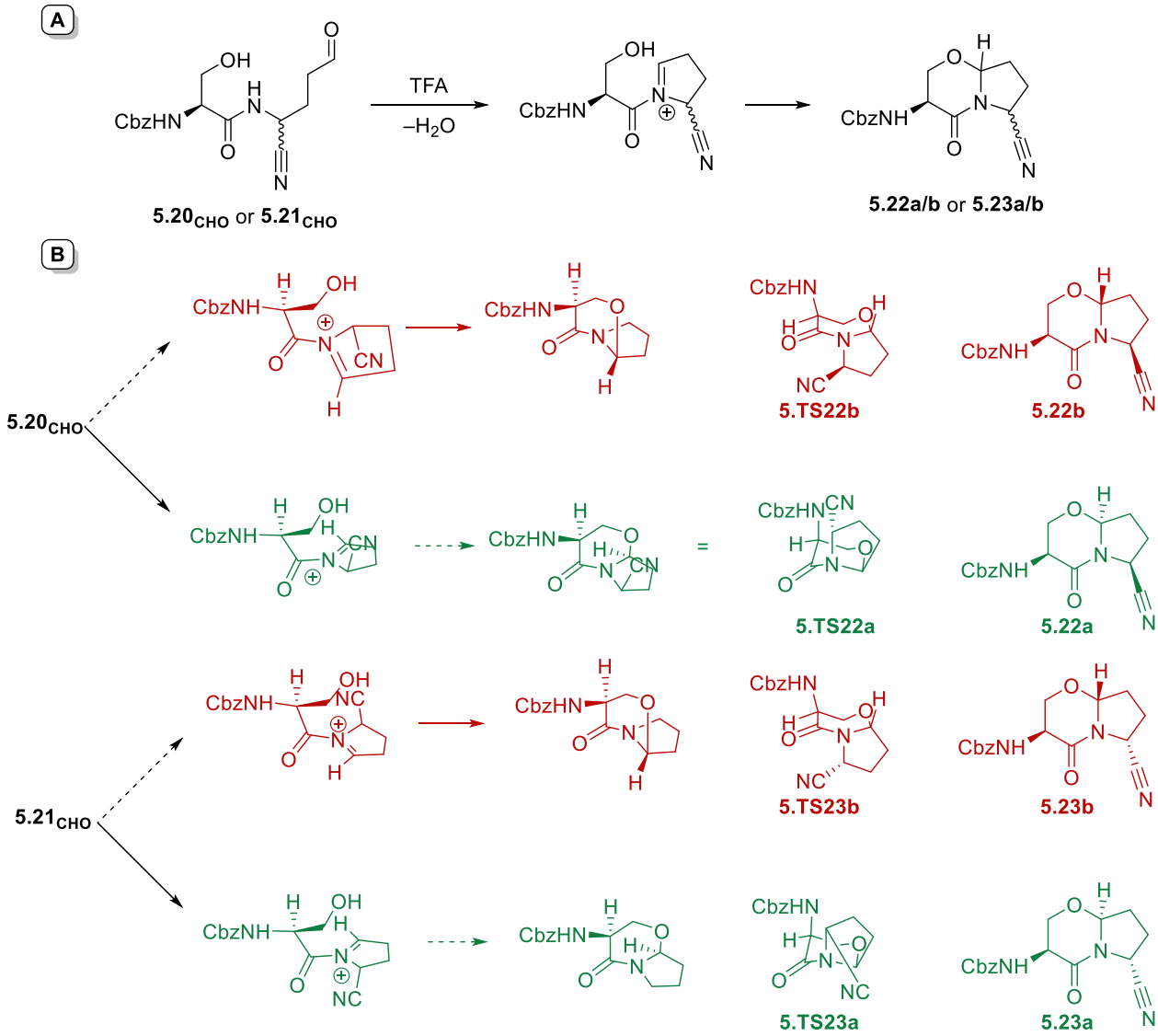

Figure 5.10. Proposed mechanism of the nitrile series cyclization through an iminium intermediate.(A) general scheme; (B) transition state proposals for each dipeptide

5.3.4 Computational analysis

The various diastereomeric ratios in the cyclization step of both series and the uncertainty of the mechanism have intrigued us to study the kinetics of the cyclizations from a computational perspective. These computational studies will explore the relative difference in energies of the products in the cyclization of the non-covalent series, as well as relative energies of the possible transition states in both series. The results will hopefully shed light on the difference in the observed diastereoselectivities.

5.4 Conclusion

Our work in discovery of bicyclic POP inhibitors has led us to several potent constrained peptidomimetic scaffolds. In this study, we expand upon an interesting reaction observed during acid-catalyzed oxidative cyclizations of our [4.3.0] azabicylic series. With this reaction, we observed diastereoselectivity facilitated both by stereochemistry of the scaffold's substituents and the reducing agents used in the ozonolysis first step. This work expands upon a previously reported study from Baldwin *et al*.,[12] providing insight into stereocontrol of the reaction. Although these results are very recent, we propose a few tentative mechanisms. To understand the complex mechanisms, computational studies are currently underway.

5.5 Experimental Section

5.5.1 Synthesis – General Information

All commercially available reagents were used without further purification. All reactions, unless otherwise indicated, were carried out in flame-dried flasks under argon atmosphere with anhydrous solvents. FTIR spectra were recorded using a Perkin-Elmer Spectrum One FT-IR. ^{1}H and ^{13}C NMR spectra were recorded on a Bruker 400 or 500 MHz spectrometer. Chemical shifts are reported in ppm using the residual of deuterated solvents as an internal standard. Thin layer chromatography visualization was performed by UV or by development using *p*-anisaldehyde, Seebach's stain, $KMnO_4$. Optical rotations were measured at the wavelength 589 nm (sodium D line) on a Jasco DIP-140 digital polarimeter. Chromatography was performed on silica gel 60 (230−240 mesh). High resolution mass spectrometry was performed by ESI on a Bruker Maxis Impact API QqTOF or by ESI or APCI on a ThermoFisher Exactive Plus Orbitrap-API at McGill University. All compounds were stored at –20°C.

5.5.2 Chemistry

General Coupling Procedure A (for the coupling of 4-pentene-1-amine to *N*-Cbz-protected amino acids). The *N*-Cbz-protected amino acid (1 eq) was suspended in DCM (0.1 M) and cooled to 0°C. HOBt•H_2O (1.2 eq) was added, followed by EDC•HCl (1.2 eq). The resultant solution stirred for 1h at 0°C. The amine (1 eq in DCM, 1 M) was then added, followed by Et_3N (5 eq). The reaction stirred at 0°C for 10 minutes, and then was warmed to room temperature and stirred overnight. Water was added, and the product was extracted with DCM. The combined organic layers were washed with saturated NH_4Cl, saturated $NaHCO_3$, and brine, dried over Na_2SO_4, filtered, and concentrated *in vacuo* to give the crude product. The crude material was purified by flash chromatography on a silica gel column to give the corresponding dipeptide.

General Coupling Procedure B (for the coupling of nitrile-containing aminium chloride salts to *N*-Cbz-protected amino acids). The *N*-Cbz-protected amino acid (1 eq) was dissolved in DMF (0.3 M), and the solution was cooled to 0°C. HATU (1.2 eq) was added, followed by the amine (1 eq), then Et_3N (10 eq). The reaction stirred at room temperature overnight. Water was added, and the product was extracted with DCM. The combined organic layers were washed with saturated NH_4Cl, saturated $NaHCO_3$, and brine, dried over Na_2SO_4, filtered, and concentrated *in vacuo* to give the crude product. The crude material was purified by flash chromatography on a silica gel column to give the corresponding dipeptide.

Benzyl (S)-(3-hydroxy-1-oxo-1-(pent-4-en-1-ylamino)propan-2-yl)carbamate (5.5) Dipeptide **5.5** was both prepared following General Coupling Procedure A, using Z-L-Ser as the amino acid. The crude product was purified by flash chromatography on a silica gel column (eluent 70:30 EtOAc-hexanes) to give the products as a white solid (78%). R_f = 0.43 (80:20 EtOAc-hexanes); mp = 143-145°C; $[\alpha]_D^{22}$ = –37.2° (*c* = 1.0, $CHCl_3$); IR (film) cm^{-1} 3316, 3068, 2937, 1709, 1651, 1532, 1239, 1060, 913 ^{1}H NMR (500 MHz, Chloroform-*d*) δ 7.39 – 7.30 (m, 5H), 6.64 (s, 1H), 5.87 (d, *J* = 7.6 Hz, 1H), 5.77 (ddt, *J* = 16.9, 10.2, 6.6 Hz, 1H), 5.13 (s, 2H), 5.02 (dq, *J* = 17.2, 1.7 Hz, 1H), 4.98 (dq, *J* = 10.2, 1.4 Hz, 1H), 4.17 (ddd, *J* = 7.8, 4.9, 3.2 Hz, 1H), 4.15 – 4.05 (m, 1H), 3.71 – 3.60 (m, 1H), 3.25 (q, *J* = 6.7 Hz, 2H), 3.20 (s, 1H), 2.06 (q, *J* = 7.2 Hz, 2H), 1.59 (p, *J* = 7.3 Hz, 2H); ^{13}C NMR (126 MHz, Chloroform-*d*) δ 28.58, 31.09, 39.15, 55.29, 62.91, 67.51, 115.55, 128.23 (2C), 128.50, 128.74 (2C), 136.06, 137.64, 156.93, 171.00; HRMS (ESI+) *m/z* calcd for $[C_{16}H_{22}O_4N_2 + Na]^+$ 329.1472, found 329.1464.

benzyl ((2*S*,3*R*)-3-hydroxy-1-oxo-1-(pent-4-en-1-ylamino)butan-2-yl)carbamate (5.6) Dipeptide **5.6** was prepared following General Coupling Procedure A, using Z-L-Thr as the amino acid. The crude product was purified by flash chromatography on a silica gel column (eluent 80:20 EtOAc-hexanes) to give the product as a white solid (81%). R_f = 0.55 (80:20 EtOAc-hexanes); mp = 101-104°C; $[\alpha]_D^{22}$ = –48.0° (*c* = 1.0, $CHCl_3$); IR (film) cm^{-1} 3357, 3298, 3067, 2976, 1693, 1643, 1542, 1227, 1066, 910; ^{1}H NMR (500 MHz, Chloroform-*d*) δ 7.38 – 7.28 (m, 5H), 6.73 (t, *J* = 6.0 Hz, 1H), 5.95 (d, *J* = 8.0 Hz, 1H), 5.76 (ddt, *J* = 16.9, 10.2, 6.7 Hz, 1H), 5.15 – 5.07 (m, 2H), 5.01 (dq, *J* = 17.1, 1.7 Hz, 1H), 4.97 (dq, *J* = 10.3, 1.5 Hz, 1H), 4.32 (dt, *J* = 8.1, 4.1 Hz, 1H), 4.10 – 4.06 (m, 1H), 3.82 (s, 1H), 3.30 – 3.14 (m, 2H), 2.13 – 2.04 (m, 2H), 1.57 (p, *J* = 7.3 Hz, 2H), 1.15 (d, *J* = 6.4 Hz, 3H); ^{13}C NMR (126 MHz, Chloroform-*d*) δ 18.33, 28.53, 31.06, 39.06, 58.69, 66.81, 67.36, 115.46, 128.06 (2C), 128.37, 128.66 (2C), 136.10, 137.60, 157.12, 170.98; HRMS (ESI+) *m/z* calcd for $[C_{17}H_{24}O_4N_2 + Na]^+$ 343.1628, found 343.1623.

benzyl ((2*S*,3*S*)-3-hydroxy-1-oxo-1-(pent-4-en-1-ylamino)butan-2-yl)carbamate (5.7) Dipeptide **5.7** was prepared following General Coupling Procedure A, using Z-L-*allo*-Thr as the amino acid. The crude product was purified by flash chromatography on a silica gel column (eluent 80:20 EtOAc-hexanes) to give the product as a white solid (74%). R_f = 0.55 (80:20 EtOAc-hexanes); mp = 128–132°C; $[\alpha]_D^{22}$ = –26.5° (*c* = 1.0, $CHCl_3$); IR (film) cm^{-1} 3290, 3071, 2968, 1691, 1647, 1534, 1288, 1241, 1038, 910; ^{1}H NMR (500 MHz, Acetone-d_6) δ 7.45 – 7.24 (m, 5H), 6.43 (s, 1H), 5.82 (ddt, *J* = 16.9, 10.2, 6.7 Hz, 1H), 5.13 – 5.05 (m, 2H), 5.01 (dq, *J* = 17.1, 1.8 Hz,

1H), 4.93 (ddt, *J* = 10.3, 2.5, 1.2 Hz, 1H), 4.32 (d, *J* = 5.0 Hz, 1H), 4.05 (dd, *J* = 8.6, 6.3 Hz, 1H), 4.01 – 3.96 (m, 1H), 3.22 (q, *J* = 6.7 Hz, 2H), 2.16 – 2.06 (m, 2H), 1.58 (p, *J* = 7.2 Hz, 2H), 1.29 (s, 1H), 1.16 (d, *J* = 6.3 Hz, 3H); ^{13}C NMR (126 MHz, Acetone-*d*$_6$) δ 20.00, 29.45, 31.67, 39.32, 60.95, 66.91, 68.80, 115.19, 128.59 (2C), 128.63, 129.18 (2C), 138.07, 139.06, 157.18, 171.48; HRMS (APCI+) *m/z* calcd for $[C_{17}H_{24}N_2O_4 + Na]^+$ 321.1809, found 321.1816.

General Procedure for the acid-catalyzed oxidative cyclization of dipeptides using PPh$_3$. The dipeptide (1 eq) was dissolved in DCM (0.025 M), 2–3 drops of a 1 mg/mL Sudan III DCM solution was added, and the solution was cooled to –78°C. N_2 was bubbled into the solution for 5 minutes, followed by O_3 until the solution was dark blue. N_2 was then bubbled into the solution until the blue color disappeared. The reducting agent resin-supported PPh_3 (~3 mmol/g loading, CAS 39319-11-4, 1.5 eq) was added. The reaction stirred for 5 minutes at –78°C, then room temperature overnight. PPh_3 was filtered over Celite®, and the filtrate was concentrated *in vacuo*, and the residue was re-dissolved in DCM (0.05 M) (Some experiments in Table 5.1 add TFA directly to the reaction mixture.). TFA (1.5 eq) was added at room temperature, and the reaction stirred either at room temperature or reflux for 2 hours. The TFA was removed *in vacuo*, and crude NMR was taken to determine the diastereomeric ratio. The crude products were purified on a silica gel column to give the pure major diastereomer.

General Procedure for the acid-catalyzed oxidative cyclization of dipeptides using DMS. The dipeptide (1 eq) was dissolved in DCM (0.025 M), 2–3 drops of a 1 mg/mL Sudan III DCM solution was added, and the solution was cooled to –78°C. N_2 was bubbled into the solution for 5 minutes, followed by O_3 until the solution was dark blue. N_2 was then bubbled into the solution until the blue color disappeared. The reducing agent DMS (10 eq) was added. The reaction stirred for 5 minutes at –78°C, then room temperature overnight. The solution was concentrated *in vacuo*, and the residue was re-dissolved in DCM (0.05 M). TFA (1.5 eq) was added at room temperature, and the reaction stirred either at room temperature or reflux for 2 hours (Some experiments in Table 5.1 add TFA directly to the reaction mixture.). The TFA was removed *in vacuo*, and crude NMR was taken to determine the diastereomeric ratio. The crude products were purified on a silica gel column to give the pure major diastereomer.

benzyl ((3*S*,8a*S*)-4-oxohexahydro-2*H*-pyrrolo[2,1-*b*][1,3]oxazin-3-yl)carbamate (5.8a) Bicycle **5.8a** was synthesized from dipeptide **5.5**, and the crude product was purified by flash chromatography on a silica gel column (eluent 80:20 EtOAc-hexanes) to give the product as a

white solid. R_f = 0.39 (100% EtOAc); mp = 118-122°C; $[\alpha]_D^{22}$ = +31.4° (*c* = 1.0, $CHCl_3$); IR (film) cm^{-1} 3306, 3063, 2980, 1717, 1669, 1530, 1217, 1064; ^1H NMR (500 MHz, Acetone-d_6) δ 7.48 – 7.25 (m, 5H), 6.50 (s, 1H), 5.20 (t, *J* = 5.3 Hz, 1H), 5.10 (s, 2H), 4.44 (q, *J* = 7.4 Hz, 1H), 4.28 (dd, *J* = 10.2, 8.1 Hz, 1H), 3.76 – 3.66 (m, 2H), 3.26 (ddd, *J* = 11.9, 7.3, 5.1 Hz, 1H), 2.23 (td, *J* = 10.4, 10.0, 4.9 Hz, 1H), 1.96 – 1.87 (m, 1H), 1.87 – 1.76 (m, 2H); ^{13}C NMR (126 MHz, Acetone-d_6) δ 21.89, 33.03, 45.26, 50.22, 66.92, 68.81, 88.01, 128.65 (3C), 129.19 (2C), 138.06, 157.14, 166.64; HRMS (ESI+) *m/z* calcd for $[C_{15}H_{18}N_2O_4 + Na]^+$ 313.1159, found 313.1163.

benzyl ((3*S*,8a*R*)-4-oxohexahydro-2*H*-pyrrolo[2,1-*b*][1,3]oxazin-3-yl)carbamate (5.8b) Bicycle **5.8b** was synthesized from dipeptide **5.5**, and the crude product was purified by flash chromatography on a silica gel column (eluent 80:20 EtOAc-hexanes) to give the product as a white solid. R_f = 0.28 (100% EtOAc); mp = 123-126°C; $[\alpha]_D^{22}$ = –104.0° (*c* = 0.01, $CHCl_3$); IR (film) cm^{-1} 3306, 3019, 2893, 1715, 1657, 1529, 1452, 1058, 1022; ^1H NMR (500 MHz, Acetone-d_6) δ 7.47 – 7.24 (m, 5H), 6.67 – 6.21 (m, 1H), 5.14 – 4.98 (m, 3H), 4.23 (dd, *J* = 10.9, 7.4 Hz, 1H), 4.10 – 4.02 (m, 1H), 3.80 (t, *J* = 10.9 Hz, 1H), 3.58 (q, *J* = 9.3 Hz, 1H), 3.32 (t, *J* = 10.5 Hz, 1H), 2.27 – 2.14 (m, 1H), 2.00 – 1.90 (m, 1H), 1.88 – 1.77 (m, 1H), 1.77 – 1.64 (m, 1H); ^{13}C NMR (101 MHz, Acetone-d_6) δ 20.14, 32.38, 43.99, 50.23, 66.88, 69.27, 90.46, 128.70 (3C), 129.23 (2C), 138.11, 157.14, 165.77; HRMS (ESI+) *m/z* calcd for $[C_{15}H_{18}N_2O_4 + Na]^+$ 313.1159, found 313.1148.

benzyl ((2*R*,3*S*,8a*S*)-2-methyl-4-oxohexahydro-2*H*-pyrrolo[2,1-*b*][1,3]oxazin-3-yl)carbamate (5.9a) Bicycle **5.9a** was synthesized from dipeptide **5.6**, and the crude product was purified by flash chromatography on a silica gel column (eluent 70:30 EtOAc-hexanes) to give the product as a white solid. R_f = 0.34 (70:30 EtOAc-hexanes); mp = 120-123°C ; $[\alpha]_D^{22}$ = +36.3° (*c* = 1.0, $CHCl_3$); IR (film) cm^{-1} 3313, 3063, 2980, 1720, 1675, 1530, 1454, 1259, 1064; ^1H NMR (500 MHz, Acetone-d_6) δ 7.47 – 7.25 (m, 5H), 6.46 (d, *J* = 7.7 Hz, 1H), 5.20 (t, *J* = 5.5 Hz, 1H), 5.10 (d, *J* = 3.3 Hz, 2H), 4.43 (dd, *J* = 7.9, 6.0 Hz, 1H), 4.35 (p, *J* = 6.2 Hz, 1H), 3.68 (dt, *J* = 11.5, 7.4 Hz, 1H), 3.25 (ddd, *J* = 12.0, 7.5, 4.9 Hz, 1H), 2.19 (dt, *J* = 11.9, 5.9 Hz, 1H), 1.96 – 1.87 (m, 1H), 1.86 – 1.74 (m, 2H), 1.08 (d, *J* = 6.3 Hz, 3H); ^{13}C NMR (126 MHz, Acetone-d_6) δ 17.21, 21.35, 32.85, 44.84, 53.84, 66.92, 73.61, 87.43, 128.59 (2C), 128.65, 129.20 (2C), 138.15, 157.23, 166.12; HRMS (APCI+) *m/z* calcd for $[C_{16}H_{20}N_2O_4 + H]^+$ 305.1496, found 305.1497.

benzyl ((2*S*,3*S*,8a*S*)-2-methyl-4-oxohexahydro-2*H*-pyrrolo[2,1-*b*][1,3]oxazin-3-yl)carbamate (5.10a) Bicycle **5.10a** was synthesized from dipeptide **5.7**, and the crude product

was purified by flash chromatography on a silica gel column (eluent 80:20 EtOAc-hexanes) to give the product as a white solid. R_f = 0.53 (70:30 EtOAc-hexanes); mp = 142-145°C; $[\alpha]_D^{22}$ = +3.8° (*c* = 1.0, $CHCl_3$); IR (film) cm^{-1} 3298, 3063, 2976, 1720, 1669, 1534, 1437, 1241, 1042, 989; ^1H NMR (500 MHz, Acetone-d_6) δ 7.47 – 7.20 (m, 5H), 6.43 (d, *J* = 9.1 Hz, 1H), 5.42 (dd, *J* = 6.1, 2.9 Hz, 1H), 5.11 (s, 2H), 4.23 (t, *J* = 9.1 Hz, 1H), 3.82 – 3.74 (m, 1H), 3.75 – 3.67 (m, 1H), 3.23 (dt, *J* = 11.0, 6.6 Hz, 1H), 2.23 (tt, *J* = 11.0, 5.0 Hz, 1H), 1.95 – 1.79 (m, 3H), 1.34 (d, *J* = 6.3 Hz, 3H). ^{13}C NMR (126 MHz, Acetone-d_6) δ 19.56, 22.79, 33.25, 45.55, 56.79, 66.93, 73.81, 83.94, 128.61 (2C), 128.65, 129.20 (2C), 138.12, 157.62, 167.83; HRMS (ESI+) *m/z* calcd for $[C_{16}H_{20}N_2O_4 + Na]^+$ 327.1315, found 327.1316.

benzyl ((2*S*,3*S*,8a*R*)-2-methyl-4-oxohexahydro-2*H*-pyrrolo[2,1-*b*][1,3]oxazin-3-yl)carbamate (5.10b) Bicycle **5.10b** was synthesized from dipeptide **7**, and the crude product was purified by flash chromatography on a silica gel column (eluent 80:20 EtOAc-hexanes) to give the product as a clear oil. R_f = 0.30 (100% EtOAc); $[\alpha]_D^{22}$ = –98.3° (*c* = 0.04, $CHCl_3$); IR (film) cm^{-1} 3298, 3063, 2976, 1713, 1649, 1528, 1454, 1240, 1044; ^1H NMR (500 MHz, Acetone-d_6) δ 7.44 – 7.23 (m, 5H), 6.78 (d, *J* = 8.6 Hz, 1H), 5.18 – 5.04 (m, 3H), 4.05 – 3.91 (m, 1H), 3.71 – 3.49 (m, 2H), 3.31 (ddd, *J* = 11.8, 8.9, 2.9 Hz, 1H), 2.23 – 2.13 (m, 1H), 1.99 – 1.90 (m, 1H), 1.88 – 1.77 (m, 1H), 1.72 (tt, *J* = 11.8, 8.2 Hz, 1H), 1.27 (d, *J* = 6.1 Hz, 3H); ^{13}C NMR (126 MHz, Acetone-d_6) δ 18.64, 19.29, 31.55, 43.21, 56.13, 65.92, 75.22, 88.35, 127.71 (2C), 127.76, 128.33 (2C), 137.31, 156.49, 165.07; HRMS (ESI+) *m/z* calcd for $[C_{16}H_{20}N_2O_4 + Na]^+$ 327.1315, found 327.1304.

General procedure for determining the reversibility of the acid-catalyzed cyclization reaction. The pure diastereomer **a** was dissolved in DCM (0.05 M), and TFA (1.5 eq) was added. The solution refluxed for 24 h. The solvent was removed *in vacuo*, and crude NMR was taken to determine the diastereomeric ratio.

(*R*)-2-methyl-*N*-(pent-4-en-1-ylidene)propane-2-sulfinamide (5.11) and (*S*)-2-methyl-*N*-(pent-4-en-1-yl)propane-2-sulfinamide (5.12) *(general procedure for both; the two sulfinimines are spectrally identical)* Oxalyl chloride (1.2 eq) was dissolved in DCM (1.5 M) under Ar, and the solution was cooled to –78°C. DMSO (2.5 eq) in DCM (7 M) was added *slowly*. The solution stirred for 5 minutes. 4-penten-1-ol (1 eq) in DCM (3 M) was added *slowly*, and the reaction stirred for 15 minutes. Triethylamine (3 eq) was added slowly, and the reaction stirred for 2 hours at room temperature. Water was added, and the product was extracted with DCM. The combined organic

layers were washed with 1M HCl, saturated $NaHCO_3$, and brine, dried over Na_2SO_4, filtered and concentrated *in vacuo* at 650 mbar, 40°C. (Some solvent remains; product is volatile.) The resultant 4-pentenal (assume 100% yield) was dissolved in anhydrous DCM (0.5 M), and (*R*)-(+)-2-methyl-2-propanesulfinamide (1 eq) *[or the (S)-(-) enantiomer for the synthesis of the (S)-sulfinimine]* and anhydrous CuSO4 (3 eq) were added. The reaction stirred at room temperature overnight. The mixture was then filtered through a pad of Celite®, and the filter cake was rinsed with DCM. The filtrate was concentrated *in vacuo* to give a brown liquid, which was purified by flash chromatography on a silica gel column (85:15 hexanes-EtOAc) to give a yellow liquid (**5.11** 75%, **5.12** 62%). R_f = 0.45 (85:15 hexanes-EtOAc); IR (film) cm^{-1} 3079, 2960, 1699, 1621, 1362, 1084, 914; ^{1}H NMR (500 MHz, Chloroform-*d*) δ 8.07 (t, *J* = 4.4 Hz, 1H), 5.83 (ddt, *J* = 16.8, 10.2, 6.5 Hz, 1H), 5.07 (dq, *J* = 17.2, 1.7 Hz, 1H), 5.02 (dq, *J* = 10.2, 1.5 Hz, 1H), 2.62 (td, *J* = 7.3, 4.4 Hz, 2H), 2.42 – 2.36 (m, 2H), 1.18 (s, 9H). ^{13}C NMR (126 MHz, Chloroform-*d*) δ 168.94, 136.80, 115.97, 56.69, 35.41, 29.49, 22.49. Spectral and physical data were in accordance with the literature.[23-24]

(*R*)-*N*-((*R*)-1-cyanopent-4-en-1-yl)-2-methylpropane-2-sulfinamide (5.13) and (*S*)-*N*-((*S*)-1-cyanopent-4-en-1-yl)-2-methylpropane-2-sulfinamide (5.17) *(general procedure for both; the two sulfinamides are spectrally identical)* The imine (1 eq) was dissolved in DCM (0.1 M), and $Gd(OTf)_3$ (0.2 eq) and TMSCN (2 eq) were added. The reaction stirred for 48 h at room temperature and was quenched with $NaHCO_3$. The product was extracted with DCM, and the combined organic layers were washed with brine, dried over Na_2SO_4, and concentrated *in vacuo* to give the crude product as a brown oil, which was purified by flash chromatography on a silica gel column (eluent 70:30 hexanes-EtOAc) to give the product as a yellow oil (**5.13** 74%, **5.17** 60%). R_f = 0.50 (70:30 EtOAc-hexanes); **(5.13)** $[\alpha]_D^{22}$ = –37.9° (*c* = 1.0, $CHCl_3$); **(5.17)** $[\alpha]_D^{22}$ = +48.1° (*c* = 1.0, $CHCl_3$); IR (film) cm^{-1} 3187, 3083, 2960, 2238, 1641, 1062, 912; ^{1}H NMR (500 MHz, Chloroform-*d*) δ 5.84 – 5.69 (m, 1H), 5.16 – 5.06 (m, 2H), 4.23 – 4.09 (m, 1H), 3.93 – 3.63 (m, 1H), 2.37 – 2.21 (m, 2H), 2.15 – 1.89 (m, 2H), 1.24 (s, 9H); ^{13}C NMR (126 MHz, Chloroform-*d*) δ 22.61 (3C), 29.47, 34.01, 45.69, 57.21, 117.28, 119.19, 135.69; HRMS (ESI+) *m/z* calcd for $[C_{10}H_{18}ON_2S + Na]^+$ 237.1032, found 237.1035.

***(R)-N-((S)*-1-cyanopent-4-en-1-yl)-2-methylpropane-2-sulfinamide (5.16)** Imine **5.11** (359 mg, 1 eq) was dissolved in DCM (20 mL), and ZnI_2 (122 mg, 0.2 eq) and TMSCN (380 mg, 0.48 mL, 2 eq) were added. The reaction stirred for 48h at room temperature and was quenched with

$NaHCO_3$. The product was extracted with DCM, and the combined organic layers were washed with brine, dried over Na_2SO_4, and concentrated *in vacuo* to give the crude product as a brown oil, which was purified by flash chromatography on a silica gel column (eluent 70:30 hexanes-EtOAc) to give the product as a yellow oil (75%). R_f = 0.50 (70:30 EtOAc-hexanes); IR (film) cm^{-1} 3198, 3083, 2980, 2254, 1643, 1475, 1391, 1366, 1066, 905; *Peaks reported for major diastereomer.* ^1H NMR (500 MHz, Chloroform-*d*) δ 5.91 – 5.63 (m, 1H), 5.17 (dt, *J* = 17.1, 1.6 Hz, 1H), 5.13 – 5.03 (m, 1H), 4.29 (q, *J* = 7.0 Hz, 1H), 3.62 – 3.36 (m, 1H), 2.44 – 2.32 (m, 1H), 2.32 – 2.25 (m, 1H), 2.10 – 1.91 (m, 2H), 1.24 (s, 9H); ^{13}C NMR (126 MHz, Chloroform-*d*) δ 22.44 (3C), 29.63, 34.09, 47.73, 57.00, 117.53, 118.70, 135.63.

(*S*)-1-cyanopent-4-en-1-aminium (18) and (*R*)-1-cyanopent-4-en-1-aminium (5.19) *(general procedure for both; the two amines are spectrally identical)* R_f = does not elute on silica-backed TLC plates; The sulfinamide (1 eq) was dissolved in Et_2O (0.1 M) under argon, and the solution was cooled to 0°C. HCl (2M in Et_2O, 3 eq) was added dropwise, and the argon balloon was removed. After 2 h of stirring at 0°C, the solvent was removed *in vacuo* to give a beige solid (trituration and filtration not possible due to solubility and sticking issues), which was carried to the next step without purification. R_f = does not elute on silica-backed TLC plates; IR (film) cm^{-1} 3071, 2956, 1643, 1483, 1185, 926; mp = 94-97°C; **(5.18)** $[\alpha]_D^{22}$ = +15.7° (*c* = 1.0, MeOH); **(5.19)** $[\alpha]_D^{22}$ = –11.3° (*c* = 1.0, MeOH); ^1H NMR (400 MHz, Methanol-d_4) δ 5.86 (dddd, *J* = 17.2, 10.2, 7.1, 6.1 Hz, 1H), 5.18 (dq, *J* = 17.1, 1.6 Hz, 1H), 5.11 (dq, *J* = 10.2, 1.3 Hz, 1H), 4.56 – 4.35 (m, 1H), 2.45 – 2.22 (m, 2H), 2.11 – 2.00 (m, 2H); ^{13}C NMR (101 MHz, Methanol-d_4) δ 30.23, 31.26, 42.23, 116.62, 117.59, 136.33; HRMS (ESI+) *m/z* calcd for $[C_6H_{11}N_2]^+$ 111.0917, found 111.0922.

benzyl ((*S*)-1-(((*S*)-1-cyanopent-4-en-1-yl)amino)-3-hydroxy-1-oxopropan-2-yl)carbamate (5.20) The product was synthesized following General Coupling Procedure B, using **5.18** as the amine. The crude product was purified by silica gel (eluent 60:40 EtOAc-hexanes) to give the product as a white solid (80%). R_f = 0.27 (60:40 EtOAc-hexanes); mp = 87-91°C; $[\alpha]_D^{22}$ = –24.1° (*c* = 1.0, MeOH); IR (film) cm^{-1} 3409, 3321, 3278, 3020, 2940, 1707, 1671, 1516, 1217, 1058; ^1H NMR (500 MHz, Acetone-d_6) δ 8.20 – 7.95 (m, 1H), 7.47 – 7.18 (m, 5H), 6.48 (d, *J* = 8.7 Hz, 1H), 5.82 (ddt, *J* = 17.0, 10.1, 6.7 Hz, 1H), 5.15 – 5.04 (m, 3H), 5.01 (dq, *J* = 10.2, 1.3 Hz, 1H), 4.33 – 4.18 (m, 2H), 3.87 (dt, *J* = 10.3, 5.0 Hz, 1H), 3.81 (dt, *J* = 10.7, 5.2 Hz, 1H), 2.23 (q, *J* = 7.4 Hz, 2H), 2.01 – 1.91 (m, 2H); ^{13}C NMR (126 MHz, Acetone-d_6) δ 30.09, 32.56, 40.53,

57.85, 62.99, 67.01, 116.59, 119.55, 128.70 (2C), 128.71, 129.24 (2C), 137.34, 137.98, 157.01, 171.22; HRMS (ESI+) *m/z* calcd for $[C_{17}H_{21}O_4N_3 + Na]^+$ 354.1424, found 354.1417.

benzyl ((*S*)-1-(((*R*)-1-cyanopent-4-en-1-yl)amino)-3-hydroxy-1-oxopropan-2-yl)carbamate (5.21) The product was synthesized following General Coupling Procedure B, using **5.19** as the amine. The crude product was purified by silica gel (eluent 60:40 EtOAc-hexanes) to give the product as a beige solid (76%). R_f = 0.58 (80:20 EtOAc-hexanes); mp = 103-106°C; $[\alpha]_D^{22}$ = +11.0° (*c* = 1.0, MeOH); IR (in $CHCl_3$) cm^{-1} 3381, 3321, 3274, 3067, 2937, 1707, 1667, 1524, 1241, 1058, 917; ^1H NMR (500 MHz, Acetone-d_6) δ 8.29 – 8.03 (m, 1H), 7.41 – 7.26 (m, 5H), 6.60 – 6.37 (m, 1H), 5.82 (ddt, *J* = 16.9, 10.0, 6.7 Hz, 1H), 5.10 (qd, *J* = 6.2, 2.8 Hz, 3H), 5.01 (dq, *J* = 10.2, 1.4 Hz, 1H), 4.87 (q, *J* = 7.9 Hz, 1H), 4.32 – 4.19 (m, 2H), 3.88 (dt, *J* = 10.9, 5.4 Hz, 1H), 3.84 – 3.73 (m, 1H), 2.23 (q, *J* = 7.6 Hz, 2H), 2.03 – 1.90 (m, 2H); ^{13}C NMR (126 MHz, Acetone-d_6) δ 32.62, 38.73, 40.46, 57.94, 63.06, 66.99, 116.63, 119.57, 128.65 (2C), 128.69, 129.22 (2C), 137.31, 138.00, 156.99, 171.18; HRMS (ESI+) *m/z* calcd for $[C_{17}H_{21}O_4N_3 + Na]^+$ 354.1424, found 354.1416.

benzyl ((3*S*,6*S*,8a*S*)-6-cyano-4-oxohexahydro-2*H*-pyrrolo[2,1-*b*][1,3]oxazin-3-yl)carbamate (5.22a) The product was cyclized from peptide **5.20** and purified by flash chromatography on a silica gel column (eluent 80-20 EtOAc-hexanes) to give the product as a white solid (33%). R_f = 0.56 (100% EtOAc); mp = 167-170°C; $[\alpha]_D^{22}$ = –60.0° (*c* = 1.0, $CHCl_3$); IR (film) cm^{-1} 3361, 3032, 2952, 1719, 1685, 1532, 1433, 1257, 1213, 1064, 1019, 914; ^1H NMR (500 MHz, Acetone-d_6) δ 7.59 – 7.23 (m, 5H), 6.71 (d, *J* = 8.4 Hz, 1H), 5.41 (t, *J* = 6.5 Hz, 1H), 5.12 (s, 2H), 4.69 (dd, *J* = 5.3, 3.5 Hz, 1H), 4.62 (q, *J* = 8.6 Hz, 1H), 4.38 (t, *J* = 9.6 Hz, 1H), 3.78 (t, *J* = 8.5 Hz, 1H), 2.52 (ddt, *J* = 13.2, 5.6, 3.3 Hz, 1H), 2.33 (dq, *J* = 9.9, 3.0 Hz, 2H), 2.08 – 1.97 (m, 1H); ^{13}C NMR (126 MHz, Acetone-d_6) δ 28.41, 32.01, 45.59, 50.42, 67.02, 68.85, 88.52, 118.79, 128.64 (2C), 128.69, 129.22 (2C), 138.03, 157.29, 167.37; HRMS (ESI+) *m/z* calcd for $[C_{16}H_{17}O_4N_3 + Na]^+$ 338.1111, found 338.1102.

benzyl ((3*S*,6*R*,8a*S*)-6-cyano-4-oxohexahydro-2*H*-pyrrolo[2,1-*b*][1,3]oxazin-3-yl)carbamate (5.23a) The product was cyclized from peptide **5.21** and purified by flash chromatography on a silica gel column (eluent 80-20 EtOAc-hexanes) to give the product as a white solid. R_f = 0.27 (80:20 EtOAc-hexanes); mp = 157-161°C; $[\alpha]_D^{22}$ = +108.9° (*c* = 1.0, $CHCl_3$); IR (film) cm^{-1} 3317, 3031, 2953, 2250, 1719, 1687, 1526, 1425, 1256, 102z1, 914; ^1H NMR (500 MHz, Chloroform-*d*) δ 7.45 – 7.28 (m, 5H), 5.89 – 5.66 (m, 1H), 5.25 (dd, *J* = 5.8, 2.9 Hz, 1H),

5.12 (s, 2H), 5.00 (dd, J = 7.8, 3.9 Hz, 1H), 4.56 (dd, J = 7.2, 6.6 Hz, 1H), 4.47 (t, J = 9.5 Hz, 1H), 3.65 (dd, J = 10.3, 7.2 Hz, 1H), 2.45 (ddt, J = 12.5, 9.2, 6.3 Hz, 1H), 2.43 – 2.32 (m, 1H), 2.26 – 2.17 (m, 1H), 2.14 – 2.06 (m, 1H); ^{13}C NMR (126 MHz, CD Chloroform-*d* Cl_3) δ 27.77, 31.65, 46.10, 49.70, 67.51, 68.54, 87.31, 117.60, 128.30 (2C), 128.47, 128.73 (2C), 136.02, 156.27, 166.99; HRMS (ESI+) *m/z* calcd for $[C_{16}H_{17}O_4N_3 + Na]^+$ 338.1111, found 338.1114.

5.6 References

(1) De Cesco, S.; Deslandes, S.; Therrien, E.; Levan, D.; Cueto, M.; Schmidt, R.; Cantin, L. D.; Mittermaier, A.; Juillerat-Jeanneret, L.; Moitessier, N., Virtual screening and computational optimization for the discovery of covalent prolyl oligopeptidase inhibitors with activity in human cells. *J Med Chem* **2012,** *55* (14), 6306-6315.

(2) Lawandi, J.; Gerber-Lemaire, S.; Juillerat-Jeanneret, L.; Moitessier, N., Inhibitors of prolyl oligopeptidases for the therapy of human diseases: Defining diseases and inhibitors. *J Med Chem* **2010,** *53* (9), 3423-3438

(3) Lawandi, J.; Toumieux, S.; Seyer, V.; Campbell, P.; Thielges, S.; Juillerat-Jeanneret, L.; Moitessier, N., Constrained Peptidomimetics Reveal Detailed Geometric Requirements of Covalent Prolyl Oligopeptidase Inhibitors. *J Med Chem* **2009,** *52*, 6672-6684

(4) Mariaule, G.; De Cesco, S.; Airaghi, F.; Kurian, J.; Schiavini, P.; Rocheleau, S.; Huskić, I.; Auclair, K.; Mittermaier, A.; Moitessier, N., 3-Oxo-hexahydro-1H-isoindole-4-carboxylic acid as a drug chiral bicyclic scaffold: structure-based design and preparation of conformationally constrained covalent and noncovalent prolyl oligopeptidase inhibitors. *J Med Chem* **2016,** *59*, 4221–4234.

(5) Schiavini, P.; Pottel, J.; Moitessier, N.; Auclair, K., Metabolic Instability of Cyanothiazolidine-Based Prolyl Oligopeptidase Inhibitors: A Structural Assignment Challenge and Potential Medicinal Chemistry Implications. *ChemMedChem* **2015,** *10* (7), 1174-1183.

(6) Corbeil, C. R.; Englebienne, P.; Moitessier, N., Docking Ligands into Flexible and Solvated Macromolecules. 1. Development and Validation of FITTED 1.0. *J Chem Inf Model* **2007,** *47*, 435-449.

(7) Moitessier, N.; Corbeil, C. R., Docking ligands into flexible and solvated macromolecules. 3. Impact of input ligand conformation, protein flexibility, and water molecules on the accuracy of docking programs. *J Chem Inf Model* **2009,** *49* (4), 997-1009.

(8) Baldwin, J. E.; Hulme, C.; Schofield, C. J.; Edwards, A. J., Synthesis of potential [small beta]-turn bicyclic dipeptide mimetics. *J Chem Soc, Chem Commun* **1993,** (11), 935-936.

(9) Chiou, W.-H.; Mizutani, N.; Ojima, I., Highly Efficient Synthesis of Azabicyclo[x.y.0]alkane Amino Acids and Congeners by Means of Rh-Catalyzed Cyclohydrocarbonylation. *J Org Chem* **2007,** *72* (6), 1871-1882.

(10) Cayley, A. N.; Gallagher, K. A.; Ménard-Moyon, C.; Schmidt, J. P.; Diorazio, L. J.; Taylor, R. J. K., Preparation of Novel Polycyclic Heterocycles Using a Tin(II) Chloride Dihydrate-Mediated Deacetalisation-Bicyclisation Sequence. *Synthesis* **2008,** *2008* (23), 3846-3856.

(11) Vamos, M.; Welsh, K.; Finlay, D.; Lee, P. S.; Mace, P. D.; Snipas, S. J.; Gonzalez, M. L.; Ganji, S. R.; Ardecky, R. J.; Riedl, S. J.; Salvesen, G. S.; Vuori, K.; Reed, J. C.; Cosford, N. D. P., Expedient Synthesis of Highly Potent Antagonists of Inhibitor of Apoptosis Proteins (IAPs) with Unique Selectivity for ML-IAP. *ACS Chem Biol* **2013,** *8* (4), 725-732.

(12) Claridge, T. D. W.; Hulme, C.; Kelly, R. J.; Lee, V.; Nash, I. A.; Schofield, C. J., Synthesis and analysis of Leu-enkephalin analogues containing reverse turn peptidomimetics. *Bioorg Med Chem Lett* **1996,** *6* (4), 485-490.

(13) De Cesco, S.; Kurian, J.; Dufresne, C.; Mittermaier, A. K.; Moitessier, N., Covalent inhibitors design and discovery. *Eur J Med Chem* **2017,** *138*, 96-114.

(14) Liu, G.; Cogan, D. A.; Owens, T. D.; Tang, T. P.; Ellman, J. A., Synthesis of Enantiomerically Pure N-tert-Butanesulfinyl Imines (tert-Butanesulfinimines) by the Direct Condensation of tert-Butanesulfinamide with Aldehydes and Ketones. *J Org Chem* **1999,** *64* (4), 1278-1284.

(15) Mabic, S.; Cordi, A. A., Synthesis of enantiomerically pure ethylenediamines from chiral sulfinimines: a new twist to the Strecker reaction. *Tetrahedron* **2001,** *57*, 8861-8866.

(16) Gu, Z.; Zakarian, A., Concise total synthesis of sintokamides A, B, and E by a unified, protecting-group-free strategy. *Angew Chem Int Ed Engl* **2010,** *49* (50), 9702-5.

(17) Plant, A.; Thompson, P.; Williams, D. M., Stereoselective Synthesis of Novel Uracil Polyoxin C Conjugates as Substrate Analogues of Chitin Synthase. *J Org Chem* **2008,** *73*, 3714–3724.

(18) Wang, H.; Zhao, X.; Li, Y.; Lu, L., Solvent-Controlled Asymmetric Strecker Reaction: Stereoselective Synthesis of α-Trifluoromethylated α-Amino Acids. *Org Lett* **2006,** *8* (7), 1379-1381.

(19) Veysoglu, T.; Mitscher, L. A.; Swayze, J. K., A Convenient Method for the Control of Selective Ozonizations of Olefins. *Synthesis* **1980,** *10*, 807-810.

(20) Hamzik, P. J.; Goutierre, A. S.; Sakai, T.; Danheiser, R. L., Aza Diels-Alder Reactions of Nitriles, N,N-Dimethylhydrazones, and Oximino Ethers. Application in Formal [2 + 2 + 2] Cycloadditions for the Synthesis of Pyridines. *J Org Chem* **2017,** *82* (24), 12975-12991.

(21) Bailey, P. S., Ozonolysis of Cyclohexene in Methanol. *J Org Chem* **1957,** *22* (1548-1551).

(22) Therrien, E.; Englebienne, P.; Arrowsmith, A. G.; Mendoza-Sanchez, R.; Corbeil, C. R.; Weill, N.; Campagna-Slater, V.; Moitessier, N., Integrating medicinal chemistry, organic/combinatorial chemistry, and computational chemistry for the discovery of selective estrogen receptor modulators with Forecaster, a novel platform for drug discovery. *J Chem Inf Model* **2012,** *52* (1), 210-24.

(23) Fustero, S.; Diego Jiménez; Sánchez-Roselló, M.; Pozo, C. d., Microwave-Assisted Tandem Cross Metathesis Intramolecular Aza-Michael Reaction: An Easy Entry to Cyclic B-Amino Carbonyl Derivatives. *J Am Chem Soc* **2007,** *129*, 6700-6701.

(24) Babij, N. R.; Wolfe, J. P., Asymmetric total synthesis of (+)-merobatzelladine B. *Angew Chem Int Ed Engl* **2012,** *51* (17), 4128-30.

Chapter 6:

Virtual Screening, Computational Optimization, and Synthesis of a [4.3.0] Bicyclic Borinic Ester Targeting Prolyl Oligopeptidase and Fibroblast Activation Protein α

This Chapter is a draft of a manuscript prepared for *J Med Chem*.

We have now seen that boronic esters and acids are the optimal group for targeting POP and FAP. Chapters 3 and 4 describe the design of POP or POP/FAP inhibitors through docking-guided optimization of known actives. In this study, we conduct the first known FAP virtual screening to date, and we design non-peptidic dual FAP-POP potential inhibitors by modifying virtual hits. This chapter describes the design and synthetic plan of these potential inhibitors.

Contribution(s) of authors: I designed, synthesized, and characterized all molecules presented in this chapter, with help in synthetic optimization from a summer intern student Yufei Wang, who also wrote the majority of this chapter's introduction. The virtual screening and analysis were conducted by myself and Dr. Stéphane De Cesco.

6.1 Abstract

Our group has focused on two serine proteases implicated in cancer and the tumour microenvironment, prolyl oligopeptidase (POP) and fibroblast activation protein alpha (FAP). In the past, we have designed POP-selective constrained peptidomimetics of a [4.3.0] bicyclic system that inhibit POP in the nanomolar range *in vitro* and *in cellulo*. We have since progressed to dual POP-FAP inhibitors of the same [4.3.0] skeleton. Our computationally-guided modifications of Talabostat, a failed drug candidate that reached Phase III clinical trials, led us to sub-micromolar potent dual inhibitors. With these compounds, we have new information regarding the structures of bicyclic compounds that can inhibit both enzymes simultaneously. We have since moved on to more advanced inhibitor design. Herein we describe the first virtual screening of FAP reported to date and subsequent optimization of hits to a [4.3.0] scaffold that could potentially inhibit POP and FAP. The synthesis of these compounds is currently in progress.

6.2 Introduction

According to the World Health Organization, cancer is currently the second largest global cause of death.[1] Research into anti-cancer therapeutics has increasingly demonstrated the importance of understanding the tumor microenvironment (TME) in cancer pathology.[2] Within the TME, cancer-associated fibroblasts are thought to play a major role,[3] and their expression of the serine protease fibroblast activation protein α (FAP) has been of particular interest, due to its contribution to tumour growth and metastasis through its peptidase and collagenase activity.[4] Present in the TME is another homologous enzyme of the same S9 family, prolyl oligopeptidase (POP). This protease is known to contribute to cleavage of thymosin-β4 and consequent release of acetyl-SDKP, a tetrapeptide which is a potent angiogenesis stimulator and is implicated in cell proliferation.[5-6]

Under healthy physiological conditions, FAP is not expressed by adult tissues, though it is expressed transiently during healing processes. In contrast, this enzyme is abundantly expressed by tumor stromal fibroblasts.[7] Furthermore, in pancreatic and rectal cancer samples, FAP expression levels are positively correlated with a more serious prognosis.[4] POP, on the other hand, is expressed in normal cells throughout the body. Its high concentration in the brain led to its initial discovery as a target for neurodegenerative diseases (e.g. Parkinson's, Alzheimer's).[8] More recently, however, it has been discovered to be overexpressed in certain epithelial cancers and

associated with tumour expansion.[9] Both *in vitro* and *in vivo* studies have shown that POP and/or FAP inhibition lead to attenuation of tumour progression,[6, 9-10] and Christiansen *et al.* have demonstrated with *in vivo* models the possibility that dual inhibition could be synergystic.[5]

Currently, there exist no POP nor FAP inhibiting drugs on the market nor in clinical trials, although one drug candidate marketed as Talabostat (Figure 6.1), a boronic acid dipeptide multi-target drug, did reach Phase III clinical trials but was ultimately halted[11-12] due to inefficacy.[13] This attrition was likely due to its rapid inactivation via intramolecular cyclization at physiological pH.[14-15] However, its failure was also suggested to be due to toxicity at dosage levels needed for therapeutic effect.[15] Thus, in recent years, our group has been interested in the discovery of potent dual inhibitors that move away from the common peptidic scaffold resembling Talabostat exploited by many groups (**6.1-6.3**, Figure 6.1).[16-18] Using combinations of virtual screening and docking-guided design, we have discovered several series of potent peptidomimetic inhibitors against POP in the low-nanomolar range *in vitro* (**6.4-6.5**, Figure 6.1)[19-21] and micromolar against cancer cell lines[19, 22] and against POP-FAP in the micromolar range *in vitro*.[23] Further, our collaborative efforts have demonstrated that boronic acid is the ideal functional group for POP-FAP dual covalent inhibition, as it demonstrates longer residence times and higher reactivity with the less-reactive catalytic serine of FAP.[24] Herein we describe a bicyclic borinic acid scaffold optimized from results of the first ever reported virtual screening on FAP. However, this discovery of an innovative class of potential reversible covalent POP-FAP dual inhibitors represents a clear synthetic challenge.

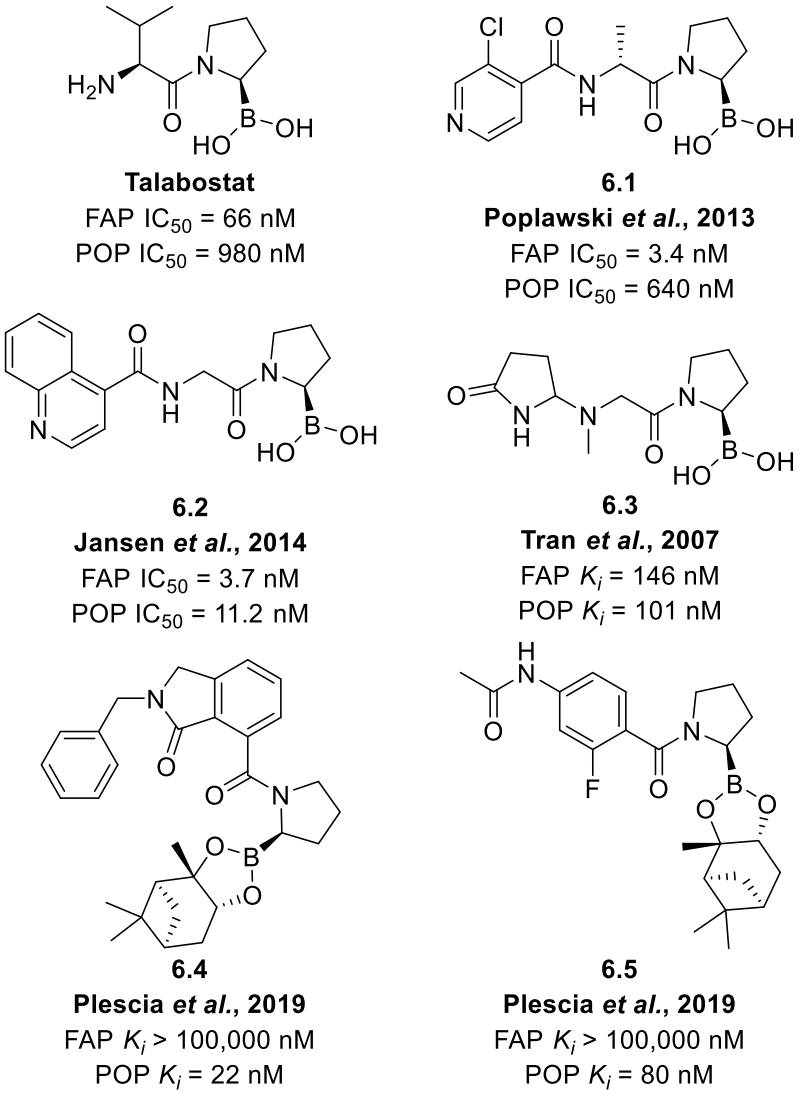

Figure 6.1. Boronic acids and esters as dual inhibitors of FAP and POP

6.3 Virtual Screening Design

6.3.1 Crystal Structure Preparation

In our past docking studies to POP and FAP, we established the key residues for the stabilization of inhibitors in the enzymes' respective active sites,[21] allowing us to move forward with a virtual screening. Unfortunately, the only crystal structure for FAP available on the Protein Data Bank is of the apo form,[25] or not bound to a substrate nor inhibitor. This lack of ligand prohibits the docking program from recognizing the active site and therefore where to dock the ligand. To prepare the FAP crystal structure (pdb code: 1z68[25]) for docking, we thought to align it to a homologous enzyme, dipeptidyl peptidase IV (DPP-IV), that has been co-crystallized with a

ligand. The aligned FAP structure was prepared by first aligning two DPP-IV crystal structures (pdb codes: 2rgu,[26] 3bjm[27]), using the MATCH-UP function on the Forecaster platform to obtain an average structure, followed by aligning FAP to the average DPP-IV structure. The FAP/DPP-IV superposition is shown in Figure 6.2. The ligands were simultaneously aligned with FAP and were extracted from the DPP-IV active site to be used as the "FAP ligand" in the final docking protocol. The workflow for aligning FAP to DPP-IV is included in Figure 6.4.

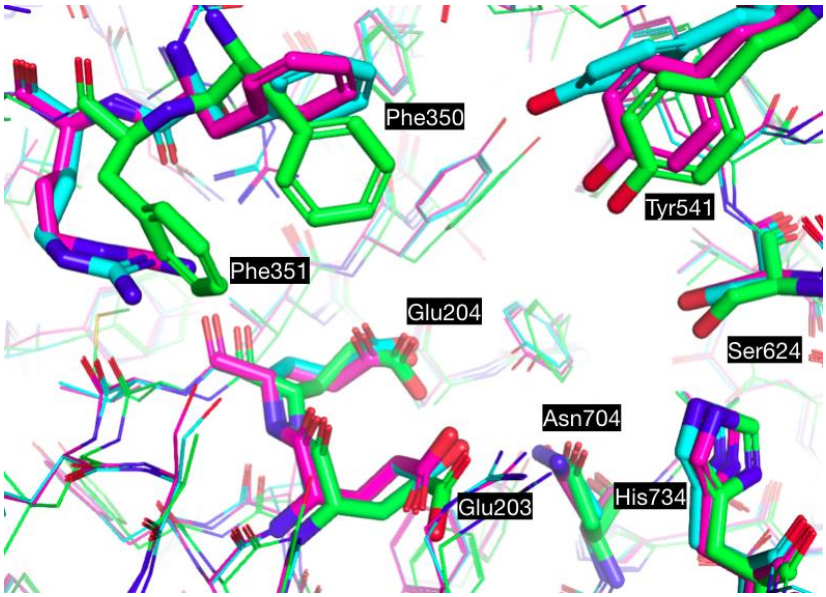

Figure 6.2. FAP crystal structure aligned to DPP-IV. (FAP in green, pdb 1z68[25]; DPP-IV pdb 2rgu[26] in cyan and pdb 3bjm[27] in magenta). Key residues are thickened and labeled following FAP numbering.

From Figure 6.2, it is apparent that the key glutamic acid residues for substrate binding are conserved, along with several key residues in the active site. One major difference resides in the Phe350/351 pair in FAP. In DPP-IV, it appears that one of these Phe is replaced with a positively charged Arg residue. This difference in polarity, among others in the residues surrounding the active site (e.g. Ala207 in FAP is Ser209 in DPP-IV), can be later exploited to assure specificity for FAP over DPP-IV, a target for antidiabetic treatment.[28]

6.3.2 Virtual Screening Preparation

Once the FAP crystal structure for docking was ready, the virtual screening was prepared. Figure 6.3 shows the overall methodology of our virtual screening.

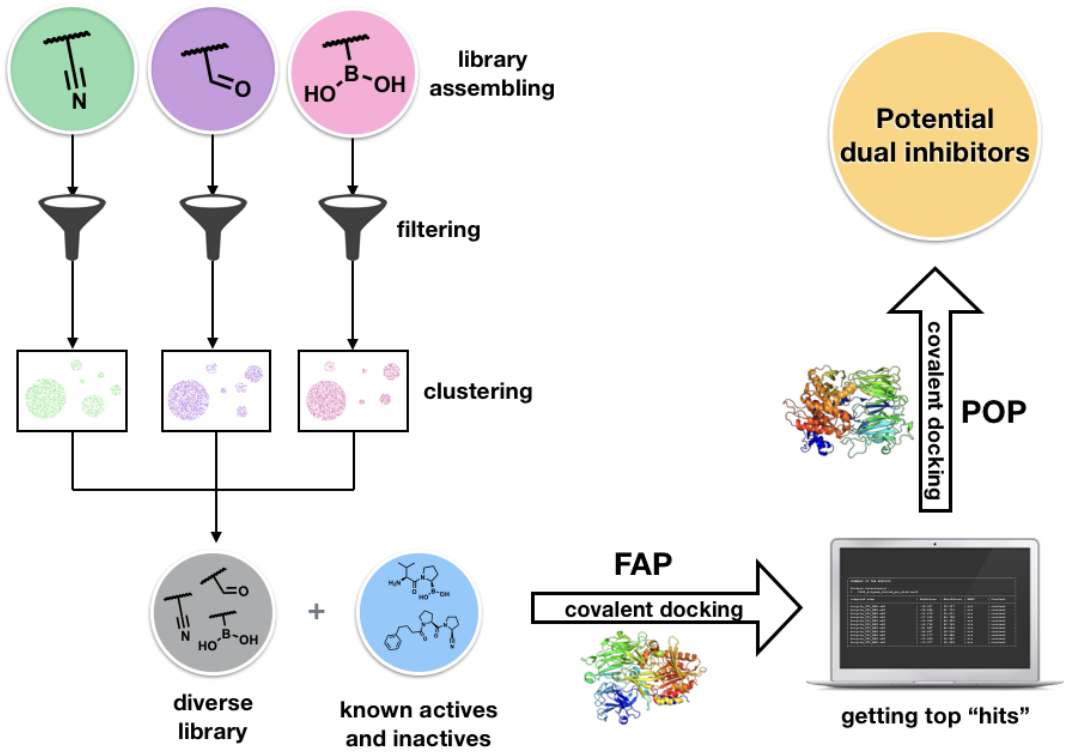

Figure 6.3. Virtual screening methodology for new FAP-POP dual inhibitors

Because our search would ultimately lead to potential covalent inhibitors, our first step was to assemble a library of structures containing covalently reactive groups. The focus was on nitriles, aldehydes, and boronic acids, all well-established groups for covalent inhibition.[29] Thus, a library of compounds containing each functional group was collected from the ZINC15[30] and ChEMBL[31] databases. We further concentrated this library to eventually lead to a drug-like potential FAP-POP dual inhibitor. The library was processed using Forecaster's[32] SMART function to add descriptors, or quantifiable parameters (e.g. logP, number of rotatable bonds, number of hydrogen donors/acceptors, etc.), that would be used in the subsequent filtering process. Filtering was performed using the REDUCE function to remove undesirable compounds, such as those containing more than one covalent group and/or do not adhere to Lipinski's Rule of Five[33] or Veber's rules.[34] The remaining molecules were clustered using the SELECT function into a set of representative

molecules. It was also necessary to assemble a library of known active and inactive compounds for both FAP and POP in order to have a reference against which to compare the library of unknowns. The final compound libraries and proteins were then virtually prepared for docking (using PREPARE and PROCESS) and docked using FITTED.[35-37] Finally, because the pharmacophore of POP covalent inhibitors allows for a larger diversity of inhibitor structure,[8] whereas the majority of FAP covalent inhibitors have been modified dipeptides,[16-17] we started our screening by docking the compound library to the more restrictive active site of FAP. Figure 6.4 shows the Forecaster workflow used for the protein alignment, library preparation, and virtual screening.

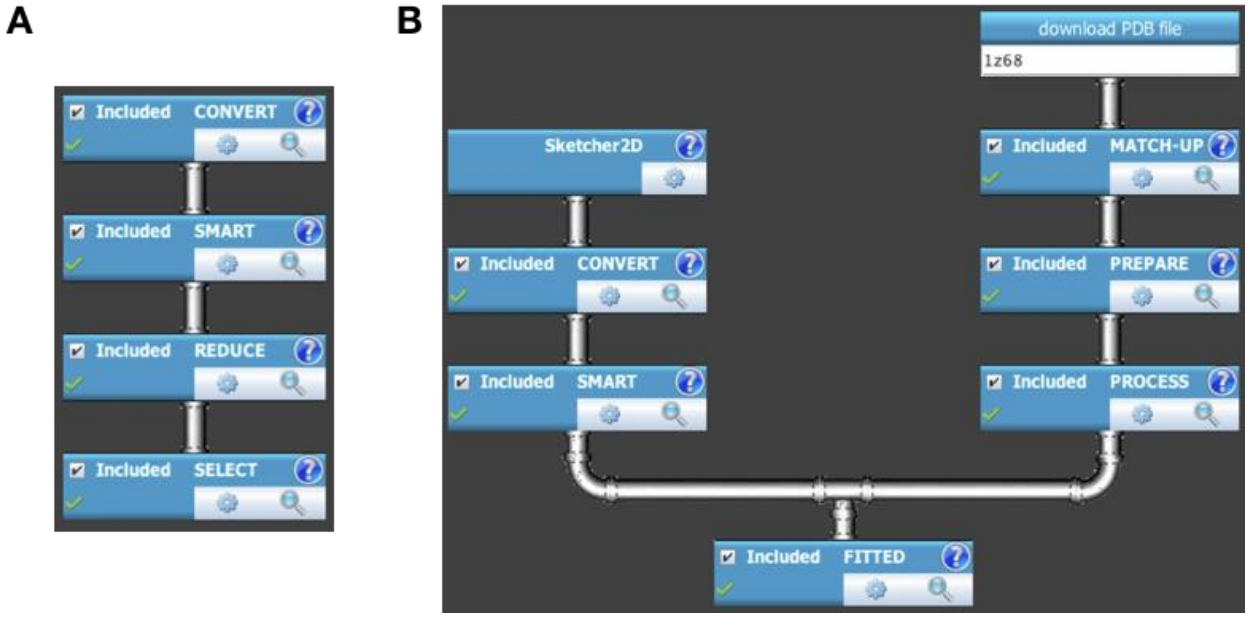

Figure 6.4. The Forecaster workflows for virtual screening. (A) Workflow for cleaning up each ligand library; (B) Workflow for aligning FAP to DPPIV structures and for docking the ligand libraries to FAP

Upon docking each compound, FITTED uses an implemented scoring function to calculate two values: RankScore and MatchScore. In brief, RankScore sums the total favorable interactions between the ligand and the protein and estimates the solvation/desolvation energy and the entropy change of the ligand upon binding, while MatchScore sums the total matching interactions (e.g., hydrogen bond donor in the protein with hydrogen bond acceptor in the ligand) between the ligand and each residue in the active site. Furthermore, the FITTED output includes several energy terms (e.g. van der Waals, hydrogen bonding).[35-37] Different weights were applied to each term to obtain

an optimized score so as to indirectly allocate the highest scores to known actives, thereby allowing the most promising unknown compounds to be easily identified using definite, quantitative descriptors.

6.3.3 Virtual Screening Results

Upon analysis of the ranked results, one third of the top 100 compounds (out of 5237) in FAP were known actives, either from the known library of actives/inactives or in the library of unknown compounds. This result not only indicated that many unknowns within the top 100 would potentially be active against FAP, but it also confirms that our docking software can be used to successfully identify active compounds in a screening library. Docking the top 100 to POP gave us a better sense of which molecules could potentially be dual inhibitors. Among the virtual hits were many amines and anilines/anilides. This result is not surprising, as the glutamic acids 203 and 204 in the active site (Figure 6.5A) act as hydrogen bond acceptors for the natural peptidic substrate and potent peptidic inhibitors. The aromatic amines/anilides were also promising in POP, participating in aromatic interactions with Phe173 in POP (Figure 6.5B). The anilines also participated in aromatic interactions with the phenylalanine pair in FAP (Figure 6.5A), as did other hits containing aromatic rings. Some anilide compounds containing fluorine also ranked highly, potentially participating in halogen bonds or weak hydrogen bonds with the active site residues in both enzymes.

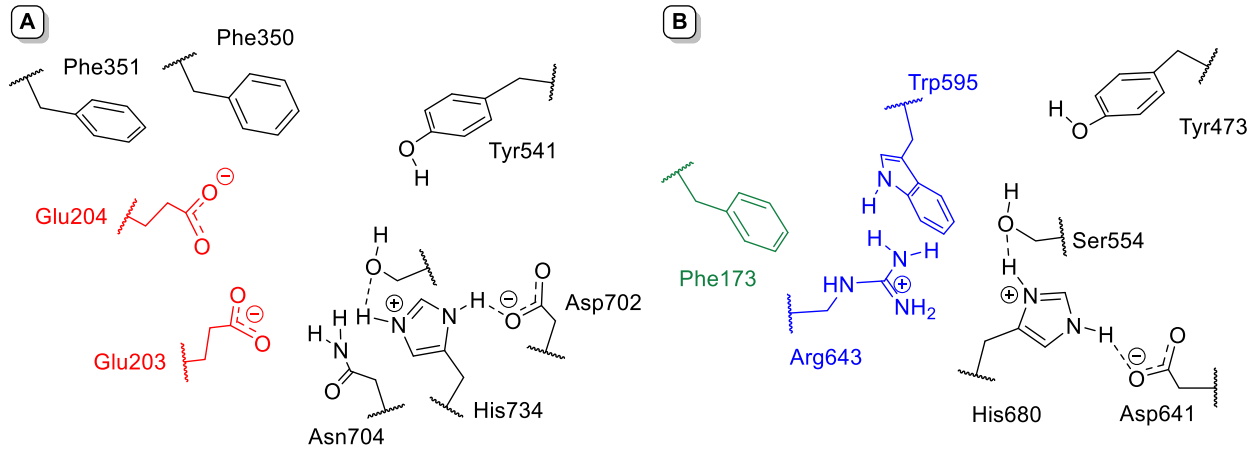

Figure 6.5. Schematic diagram of the POP and FAP active sites. (A) FAP, key hydrogen bond acceptors highlighted in red; (B) POP, key hydrogen bond donors highlighted in blue and aromatic interaction residue in green

Several benzoxaboroles were also among the top hits in the screening. The benzoxaborole presents an interesting functional group, as the boronic acid reactive group is locked into a [4.3.0] bicyclic structure (Figure 6.6, **6.7**-**6.9**). This fused bicycle was present in many of the unknown compounds and several in the top 100 compounds. The benzoxaborole is a common scaffold used in anti-fungal[38] and dermatological[39] drug discovery, and is present in two FDA-approved drugs, Crisaborole[40] and Tavaborole[41] (Figure 6.6).[42] Interestingly, the 1,4-dicarbonyl moiety (found in dipeptides **6.1**, **6.2**, and **6.4**) of potent POP and FAP inhibitors was present almost exclusively in hits that are known active compounds. Instead, the virtual hits contained 1,4-heteroatom connections (e.g. aminoalcohol, diol), such as in compounds **6.6** and **6.7** (Figure 6.6). The alcohol or phenol group could act as a hydrogen bond acceptor for Arg643 and Trp595 in the POP active site (Figure 6.5, B) or as a hydrogen bond donor for Glu203/204 in the FAP active site (Figure 6.5, A). A few selected hits are shown in Figure 6.6.

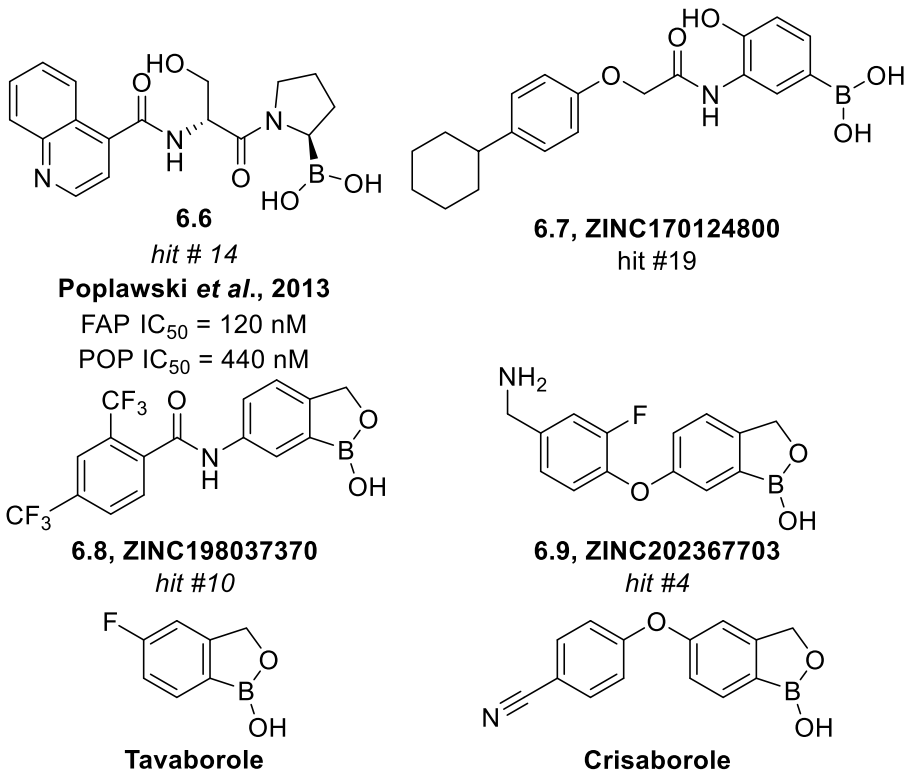

Figure 6.6. Selected virtual hits from the screening, including one active FAP-POP dual inhibitor from the library of unknowns. [18]

With these hits in hand, it was next necessary to conduct *in silico* modifications to optimize the docking poses, while maintaining synthetic feasibility. We chose the known active **6.6** and benzoxaborole **6.8** as starting points. We first virtually reduced the flat aromatic system to its aliphatic analogue to introduce two stereocenters for specificity. Next, maintaining the 1,4-amidoalcohol relationship of **6.6** and the fluorinated aromatic side chain of **6.8**, several rounds of docking-guided optimizations involving modifying side chains and stereochemistry, led to compound **6.10** (Figure 6.7). We next removed the *cis*-aminoalcohol and moved the alcohol to the aromatic ring to allow for some flexibility in the hydrogen bond donors and acceptors, giving compound **6.11** (Figure 6.7).

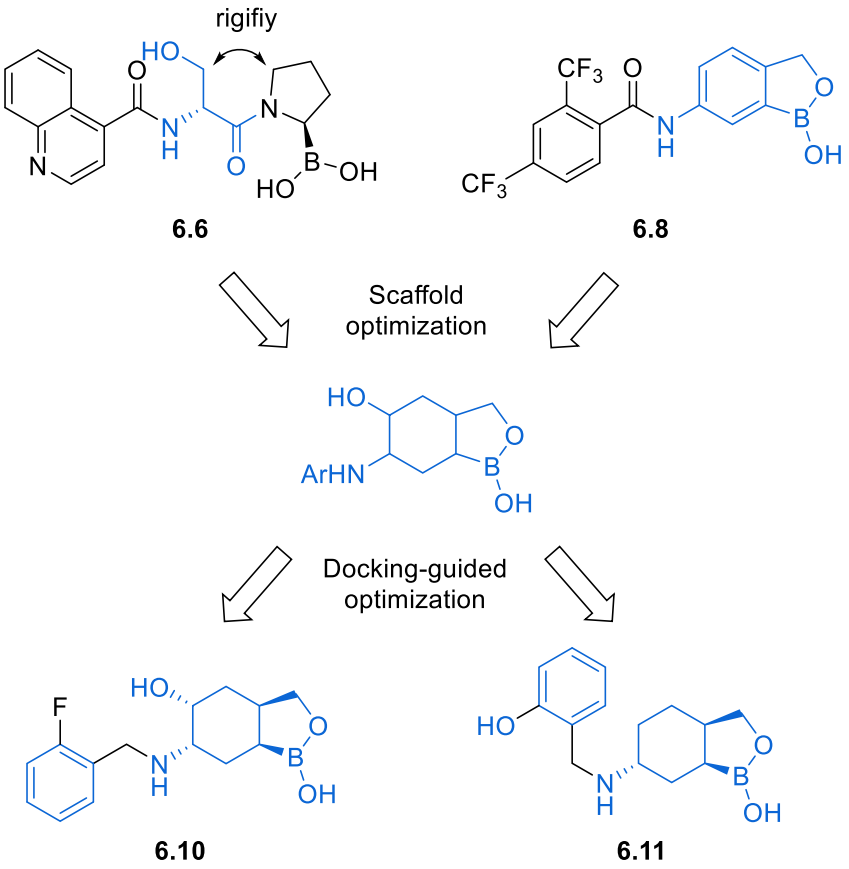

Figure 6.7. Synthetic targets obtained by docking-guided optimization of selected virtual hits. Retained scaffolds and functional groups highlighted in blue.

Figure 6.8 gives the docking pose of compound **6.10** in both POP and FAP. From the docking poses, it is clear that the selected functional groups serve their intended purpose. In POP, the benzylic group participates in edge-to face interactions with Phe173, with the fluorine facing the Arg643 residue, potentially interacting in weak hydrogen bonding. Although the hydroxyl group does not interact with the Trp595, it is in position to hydrogen bond with Cys255, previously unconsidered. The amine, though positively charged in the docking pose, is likely to be only partially ionized *in vitro*; not only is our *in vitro* assay done in slightly basic conditions, but the binding pocket of POP is hydrophobic, potentially leading to decreased ionization. Furthermore, some kinetic studies have found that the optimal pH for POP activity (*in vitro*) has been measured to be approximately pH 8,[43-44] though optimal pH of the active site *in vivo* is not known. This opens an opportunity of the amine in **6.10** to potentially act as a hydrogen bond acceptor to the Arg643. In FAP, the pose is very promising. Both the alcohol and the amine interact with Glu203/204 as hydrogen bond donors. Furthermore, the benzylic group is positioned in a way so as to interact in aromatic interactions simultaneously with Phe350 and Tyr541. This compound was thus selected as a synthetic target.

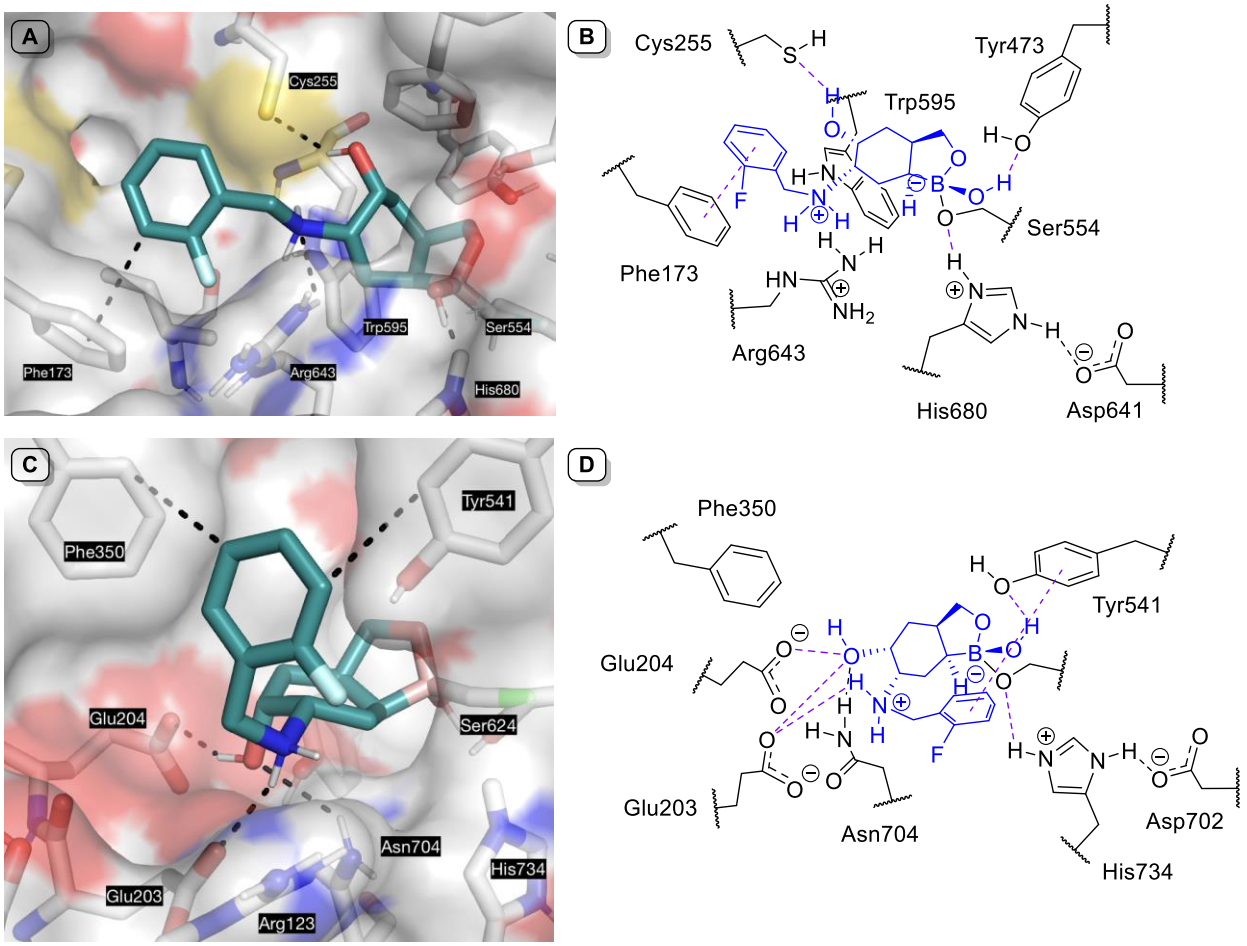

Figure 6.8. Predicted docking poses of compound **6.10** in POP and FAP. (A, B) POP; (C, D) FAP. The compound is highlighted in blue, and key observed interactions are highlighted in violet.

Figure 6.9 gives the docking pose of compound **6.11** in both POP and FAP. From the docking poses, compound **6.11** also looks promising. In POP, the slightly-further phenolic hydroxyl restores desired hydrogen bonding interactions with Trp595 while maintaining aromatic interactions with Phe173. Furthermore, the potential amine-Arg643 interaction is maintained. In FAP, both the phenolic hydroxyl and amine interact with Glu203/204 as hydrogen bond donors. (The 3D docking pose shows the oxygen hydrogen bonding to the oxygen, but the phenolic hydrogen is randomly placed *in silico*. The analysis of interactions considered this.) The benzylic group of compound **6.11** also appears to be participating in aromatic interactions with Phe350. Compound **6.11** was therefore also selected as a synthetic target.

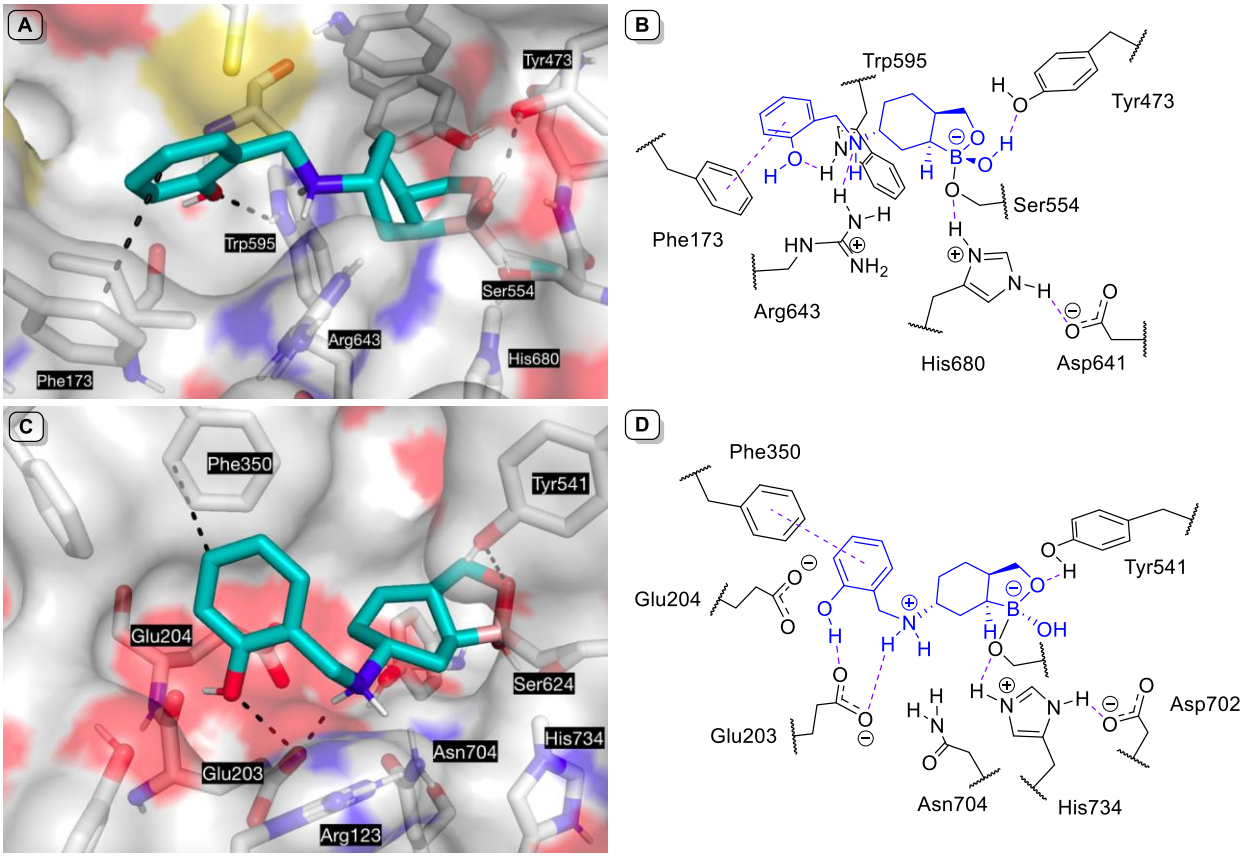

Figure 6.9. Predicted docking poses of compound **6.11** in POP and FAP. (A, B) POP; (C, D) FAP. The compound is highlighted in blue, and key observed interactions are highlighted in violet.

6.4 Chemistry

The separate syntheses were first optimized using the same *meso*-anhydride **6.12** to synthesize the desired final products as racemic mixtures. Upon optimization, the *meso*-anhydride will require enantiomeric resolution so as to provide the corresponding enantiopure starting materials for the synthesis of enantiopure inhibitors **6.10** and **6.11** for testing.

6.4.1 First hit synthesis

The synthesis began with alcoholysis of commercially available *meso*-anhydride **6.12**, using *t*-butyl alcohol to give the *t*-butyl hemiester, followed by a simple benzylation procedure to give mixed ester **6.13** (Scheme 6.1).

Scheme 6.1. Synthesis of **6.10**[a]

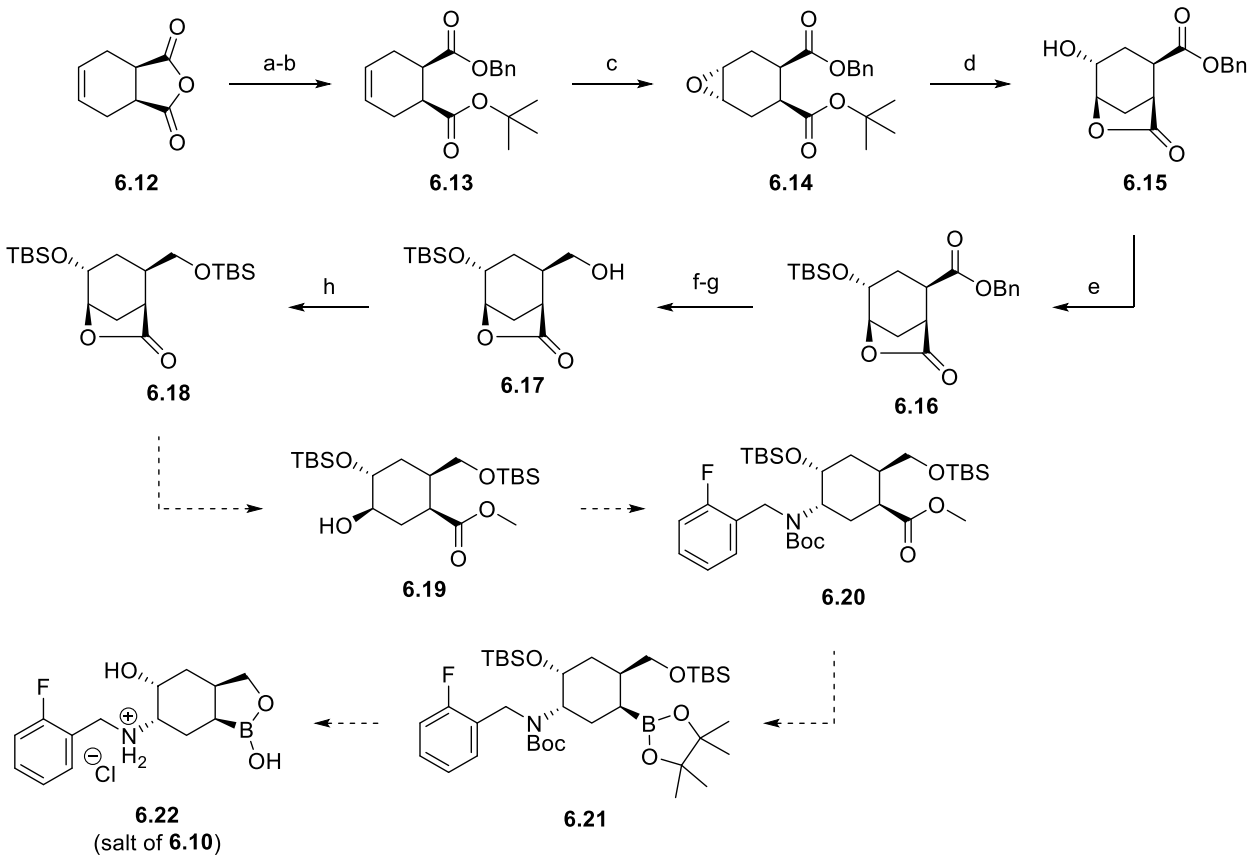

[a](a) DMAP, *t*-BuOH, reflux, 4 d; (b) K_2CO_3, BnBr, acetone, rt, 20 h, 84% over 2 steps; (c) mCPBA, DCM, 0°C→rt, 16 h, 73%, 3.5:1 d.r.; (d) TFA, 0°C→rt, 2 h, 72%; (e) TBSCl, Im, DMAP, DMF, 0°C→rt, 20 h, 78%; (f) H_2, Pd/C, EtOAc, rt, 20 h; (g) (1) Et_3N, EtOCOCl, THF, –78°C, 1 h; (2) $NaBH_4$, H_2O, 0°C, 3 h, 57% over 3 steps; (h) TBSCl, Im, DMF, 0°C→rt, 20 h, 89%

The benzylated di-ester was then subjected to epoxidation conditions with *m*-CPBA to give the *trans* epoxide **6.14** with high diastereoselectivity. Different combinations of di-esters (e.g. methyl/benzyl, *tert*-butyl/methyl) were tested during stereochemical optimization, but most gave lower diastereomeric ratios and more difficult chromatographic separations; the *tert*-butyl/benzyl di-ester combination was found to be the optimal system. Cyclization of this system to the desired lactone was not so straight-forward. De-benzylation via hydrogenolysis only gave 5% cyclization products, even upon addition of base. However, use of BF_3•OEt_2 on the debenzylated product did result in cyclization and also removed the *tert*-butyl group. Unfortunately, reproducibility was low,

and the high polarity of the product led to isolation and purification issues. Finally, TFA was used on the epoxide **6.14** to give the cyclized alcohol **6.15** in good yield, simultaneously deprotecting the *tert*-butyl ester and cyclizing the system to the lactone. Subsequent protection of the hindered secondary alcohol gave low yield, but improved significantly upon addition of DMAP as a catalyst. To convert the remaining benzyl ester to the primary alcohol **6.17**, we telescoped the de-benzylation of **6.16** and reduction of the resultant carboxylic acid via a mixed anhydride, then protected the alcohol using TBSCl to give **6.18**. Unfortunately, several attempts to open the lactone through methanolysis or with lithium methoxide failed. We will next test saponification conditions and selective methylation of the resultant carboxylic acid to give **6.19** in telescoped steps. Although the synthesis is still in progress, we have successfully established our desired stereocenters so far. We next envision displacing the alcohol with a Mitsunobu reaction to obtain the amine, followed by several functionalization steps to obtain **6.20**, a decarboxylative borylation developed by the Baran lab[45] to convert the methyl ester to the pinacol boronic ester **6.21**, and finally deprotection steps to obtain **6.22**, the hydrochloride salt of **6.10**.

6.4.2 Second hit synthesis

The synthesis began with the same alcoholysis of commercially available *meso*-anhydride **6.12**, followed instead by iodolactonization in a one-pot procedure to give **6.23** in good yield (Scheme 6.2).

Scheme 6.2. Synthesis of inhibitor **6.11**[a]

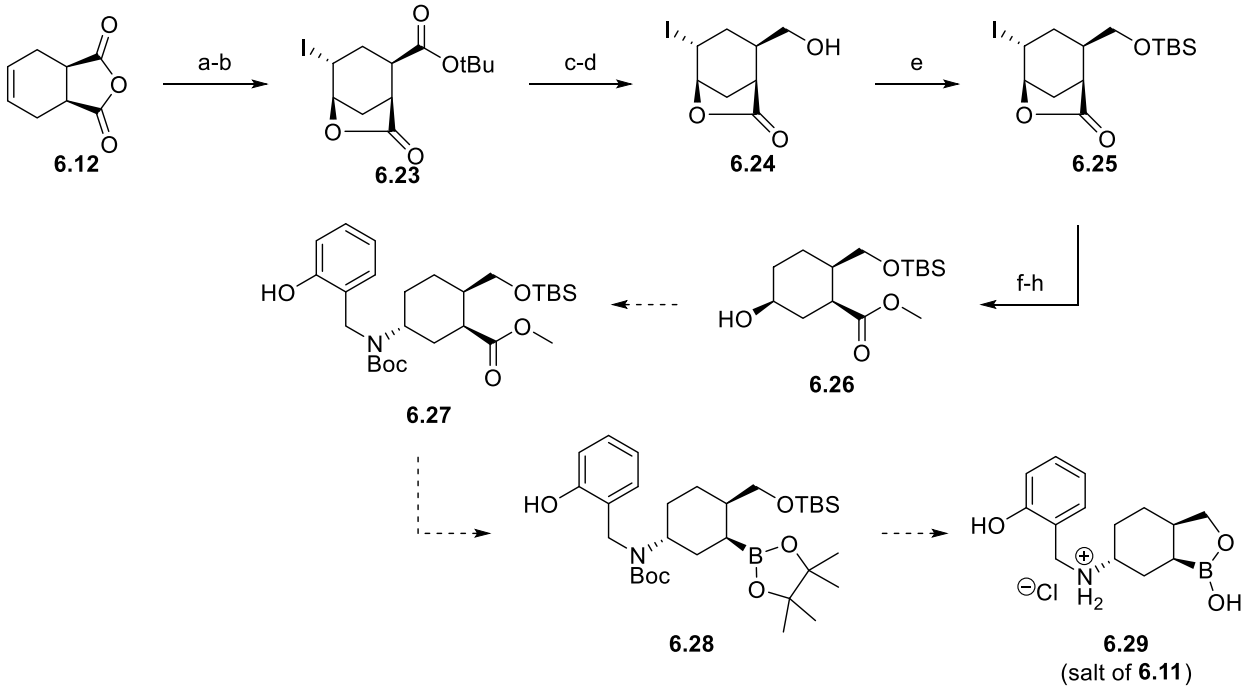

[a](a) DMAP, *t*-BuOH, reflux, 4 d; (b) $NaHCO_3$, I_2, KI, DCM-H_2O; 0°C→rt, 18 h, 73% over 2 steps; (c) TFA, DCM, 0°C→rt, 20 h; (d) (1) Et_3N, EtOCOCl, THF, –78°C, 1 h; (2) $NaBH_4$, H_2O, 0°C, 3 h, 89% over 2 steps; (e) TBSCl, Im, DMF, 0°C→rt, 20 h, 74%; (f) LiOAc•$2H_2O$, H_2, Pd/C, MeOH, rt, 16 h; (g) LiOH, THF-H_2O, 0°C→rt, 20 h; (h) K_2CO_3, MeI, rt, 18 h, 53% over 3 steps

Following procedures adapted from the literature,[46] the deprotection of the *tert*-butyl ester proceeded smoothly, giving the carboxylic acid, which was selectively reduced and protected to give **6.25**, as in **6.17** in Scheme 6.1. Deiodination was conducted using H_2 and Pd/C, adapting procedures from Wang *et al.*[47] The lactone was then opened using LiOH to saponify the lactone, followed by selective methylation, giving alcohol **6.26**. Converting the remaining secondary alcohol to an amine with inverted stereochemistry has been quite a challenge so far. Reactions

with nosyl chloride or triflic anhydride to create leaving group were unsuccessful, but upon successful mesylation of **6.26**, SN_2 attempts with amines or sodium azide failed, even under reflux conditions; starting material was recovered nearly quantitatively. Currently, we are in a similar phase of the synthesis as in that of **6.10**. The next few steps should be very similar, and we can hopefully obtain our two racemic synthetic targets. When both syntheses are optimized, we can proceed to the synthesis of the enantiopure analogues.

6.4.3 Enantiomeric Resolution

Once the synthetic strategy is established and fully optimized, it will be necessary to synthesize the enantiopure desired inhibitor should the racemic mixture show inhibition. We envision that the enantiomeric synthetic target **6.11** could be obtained through enzymatic resolution of the di-ester **6.*rac*-30** using pig liver esterase (Scheme 6.3) as originally reported by Kobayashi *et al.*[48] The di-ester **6.*rac*-30** can be synthesized via a procedure adapted from Sabitha *et al.*,[49] giving the desired product in quantitative yield with no necessary flash chromatography.

Scheme 6.3. Preparation of enantiopure starting material of compound **6.11**[a]

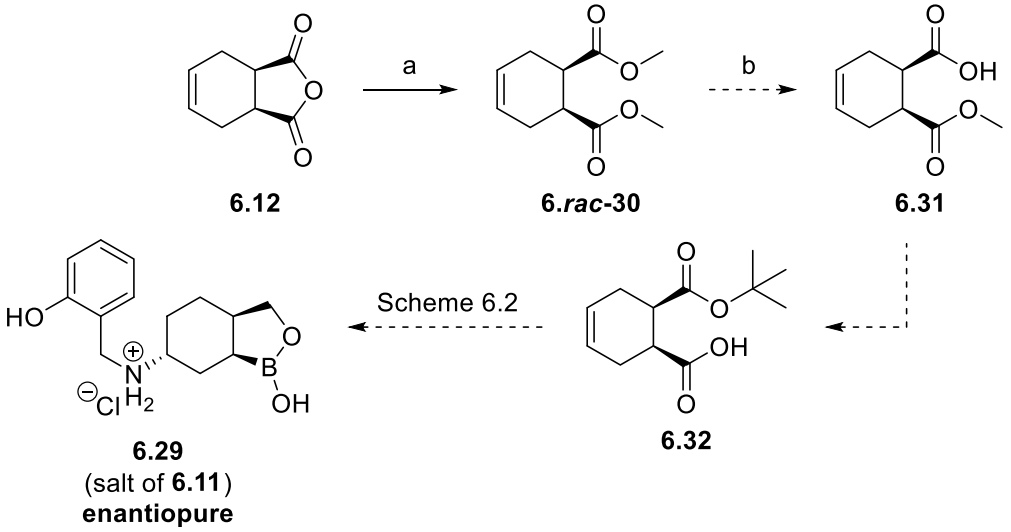

[a](a) MeOH, BF_3•OEt_2, 0°C→rt, 18 h, quant.; (b) pig liver esterase, KH_2PO_4, NaOH, H_2O-acetone, rt, 5 d[48]

Although desymmetrization of **6.*rac*-30** has been achieved synthetically through the use of the cinchona alkaloids quinidine or quinine,[50-51] enzymatic resolution allows for a more scalable preparation of this particular starting material.[48] To obtain the desired enantiomer of compound **6.10** (as well as **6.11**), the desymmetrization of the *meso*-anhydride **6.12** can be achieved via adaptation of a enantioselective methanolysis by Manzano *et al.*,[52] using enantiopure L- or D-valine-derived thiourea catalyst **6.33** or **6.ent-33** in the to give the hemi-ester **6.31** with high enantioselectivity (Scheme 6.4). The synthesis of catalysts **6.33** and **6.ent-33** can be performed as described by Andrés *et al.*[53]

Scheme 6.4. Preparation of enantiopure starting material of compounds **6.10** and **6.11**[a]

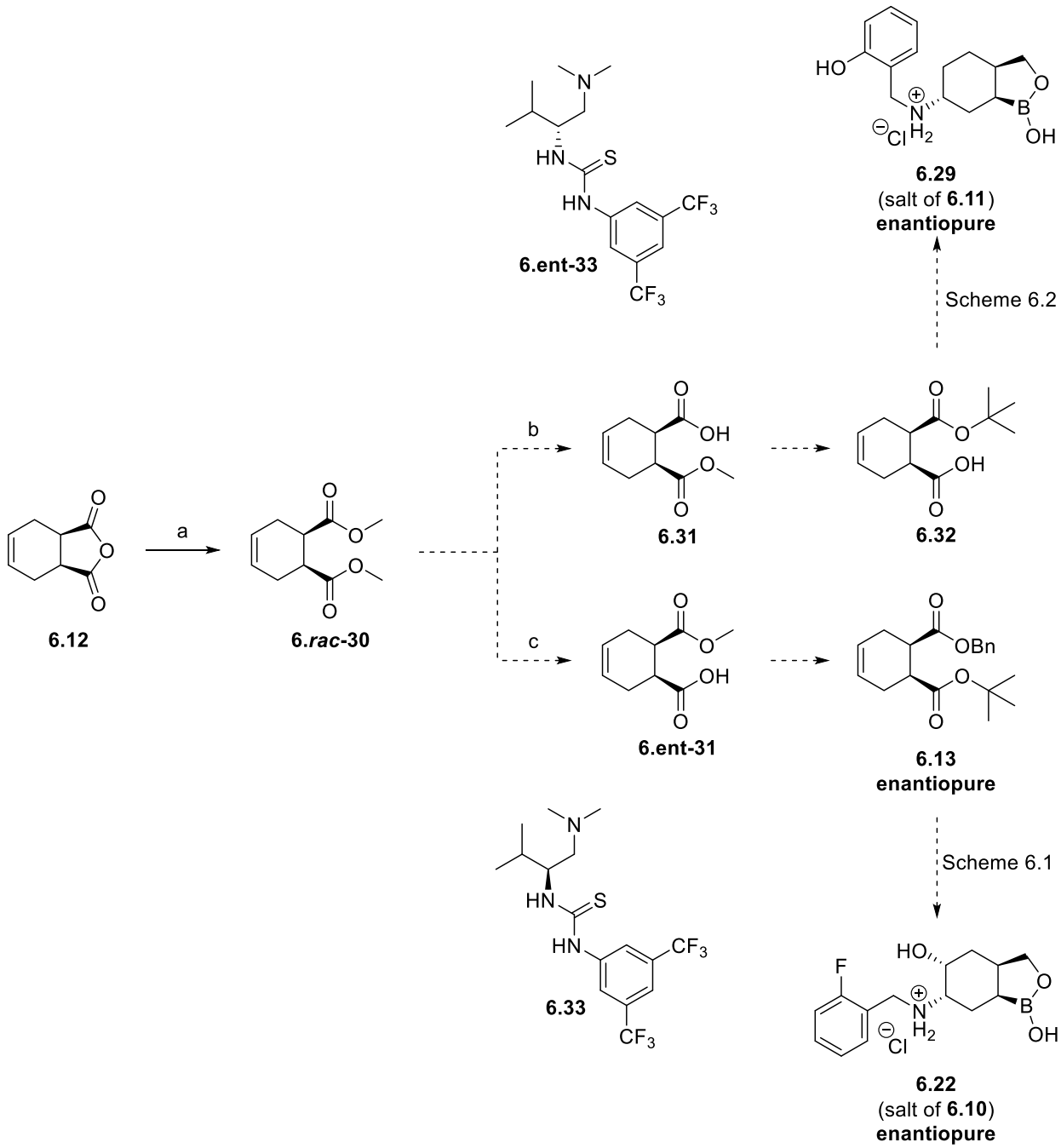

[a](a) MeOH, BF_3•OEt_2, 0°C→rt, 18 h, quant.;(b) MeOH, catalyst **6.ent-33**, tBuOMe, rt, 12 h;[52] (c) MeOH, catalyst **6.33**, tBuOMe, rt, 12 h[52]

With these enantiopure compounds in hand, it will finally be possible to test their ability to inhibit POP and FAP *in vitro*. Because we used the crystal structures of DPP4 to prepare that of FAP, it will also be necessary to test the compounds on DPP4 to ensure selectivity for POP/FAP.

6.5 Conclusion

Our group has successfully utilized docking software in the past to conduct computer-aided drug design, whether through *in silico* modification of known actives[21] or substrates,[22-23] or through virtual screening.[19] We have recently expanded our studies from POP-selective inhibition to POP-FAP. After a comprehensive virtual screening, we obtained two promising synthetic targets of a borinic acid scaffold. Our synthetic efforts have thus far led us to an advanced intermediate, and we hope to reach the desired targets soon.

6.6 Experimental Section

6.6.1 Protein alignment.

The FAP (pdb 1z68[25]) and DPP-IV (pdb 2rgu,[26] 3bjm[27]) protein structures were obtained from the Protein Data Bank[54] (https://www.rcsb.org). The proteins were aligned using the Match function on the Forecaster platform.

6.6.2 Virtual Screening.

The original libraries were obtained from both the ZINC15[30] and ChEMBL[31] databases. Corresponding libraries (nitriles, aldehydes, and boronic acids) were combined, and duplicate compounds were removed. In the boronic acid library, boronic esters were virtually deprotected, or converted to the respective boronic acids; duplicate boronic acids were then removed. Each 2D library was converted to 3D using Forecaster's Convert function. Each compound in the 3D library was assigned descriptors using the Smart function. Each library (nitrile, aldehyde, boronic acid) was filtered using the Reduce function to set minimum and maximum values on quantitative descriptors and to remove unwanted functional groups. While the final aldehyde and boronic acid libraries contained less than 2500 compounds each, the nitrile library was set to 2500 clusters using the Select function. The individually filtered libraries were then combined and prepared for docking using the Smart function. The libraries were then docked to FAP using Fitted. The results sorted by optimized score, obtained by assigning weights to the various energy terms and scores to maximize the area under the receiver operating characteristic curve. The top compounds were docked to POP using Fitted and their docking poses analyzed to determine which compounds would be selected for virtual optimization of potential dual inhibitors.

6.6.3 Synthesis.

6.6.3.1 General Information

All commercial reagents were used without purification. All reactions, unless under aqueous conditions, were carried out in flame-dried flasks under argon atmosphere with anhydrous solvents. FTIR spectra were recorded using a Perkin-Elmer Spectrum One FT-IR. ^{1}H and ^{13}C NMR spectra were recorded on Bruker 400 or 500 MHz or Varian 500 MHz spectrometers. Chemical shifts are reported in ppm using the residual of deuterated solvents as the internal standard. Thin Layer Chromatography visualization was performed under UV light or by development using

$KMnO_4$ or *p*-anisaldehyde stains. Chromatography was performed on silica gel 60 (230–40 mesh). High resolution mass spectrometry was performed by ESI on a Bruker Maxis Impact API QqTOF or by ESI or APCI on a ThermoFisher Exactive Plus Orbitrap-API at McGill University. All compounds were stored at –20°C.

6.6.3.2 Chemistry

1-benzyl 2-(*tert*-butyl) (1*R*,2*S*)-cyclohex-4-ene-1,2-dicarboxylate (6.13) The anhydride **6.12** (7.50 g, 49.3 mmol, 1 eq) was suspended in *t*-BuOH (40 mL), and DMAP (602 mg, 4.93 mmol, 0.1 eq) was added. The mixture was refluxed for 4 days. Water was added, and the product was extracted with Et_2O. The combined organic layers were washed with brine, dried over Na_2SO_4, filtered, and concentrated *in vacuo* to give the intermediate hemiester as a beige oil (84% conversion). (The conversion was determined by NMR to calculate the stoichiometric amounts in the next step.) The crude hemi ester (1 g, 1 eq) was dissolved in acetone (44 mL). K_2CO_3 (1.83 g, 3 eq) was added, followed by BnBr (0.45g, 0.8 eq). The reaction stirred overnight at room temperature. Water was added, and the product was extracted with Et_2O. The combined organic layers were washed with saturated $NaHCO_3$ and brine, dried over Na_2SO_4, filtered, and concentrated *in vacuo*. The crude product was purified by flash chromatography on a silica gel column to give the product as a clear oil (eluent 90:10 hexanes-EtOAc) to give the product as a clear oil (0.99 g, 84% over 2 steps). R_f = 0.50 (90:10 hexanes-EtOAc); IR (film) cm^{-1} 3036, 2980, 1724, 1367, 1393, 1153, 908; ^1H NMR (500 MHz, Chloroform-*d*) δ 7.41 – 7.28 (m, 5H), 5.68 (d, *J* = 1.7 Hz, 2H), 5.18 – 5.11 (m, 2H), 3.06 (td, *J* = 5.8, 3.5 Hz, 1H), 2.99 (ddd, *J* = 7.9, 5.8, 3.4 Hz, 1H), 2.59 – 2.54 (m, 1H), 2.54 – 2.50 (m, 1H), 2.39 – 2.33 (m, 1H), 2.32 – 2.24 (m, 1H), 1.39 (s, 9H); ^{13}C NMR (126 MHz, Chloroform-*d*) δ 25.65, 26.38, 28.04 (3C), 40.17, 40.69, 66.41, 80.90, 125.15, 125.54, 128.25 (2C), 128.39, 128.63 (2C), 136.19, 172.31, 173.40; HRMS (ESI+) *m/z* calcd for $[C_{19}H_{24}O_4 + Na]^+$ 339.1567, found 339.1560.

3-benzyl 4-(*tert*-butyl) (1*R*,3*R*,4*S*,6*S*)-7-oxabicyclo[4.1.0]heptane-3,4-dicarboxylate (6.14) The alkene **6.13** (2.83 g, 1 eq) was dissolved in DCM (30 mL), and the solution was cooled to 0°C. mCPBA (1.85 g, 1.2 eq) was added, and the reaction stirred overnight at room temperature. Saturated $NaHCO_3$ was added, and the mixture stirred for 20 minutes. The product was extracted with DCM, and the combined organic layers were washed twice with saturated $Na_2S_2O_5$, twice with saturated $NaHCO_3$, and twice with brine, dried over Na_2SO_4, filtered, and concentrated *in vacuo*. The crude product (d.r. 3.5:1, *trans*:*cis*) was purified by flash chromatography on a silica

gel column (eluent 80:20 hexanes-EtOAc) to give the desired diastereomer as a clear oil (2.20 g, 73%). R_f = 0.55 (80:20 hexanes-EtOAc); IR (film) cm^{-1} 2980, 1726, 1386, 1391, 1171, 1153, 909; ^1H NMR (500 MHz, Chloroform-*d*) δ 7.40 – 7.29 (m, 5H), 5.15 (d, *J* = 12.4 Hz, 1H), 5.10 (d, *J* = 12.2 Hz, 1H), 3.26 – 3.20 (m, 2H), 2.93 – 2.85 (m, 2H), 2.34 – 2.22 (m, 2H), 2.18 (ddd, *J* = 15.6, 8.2, 2.6 Hz, 1H), 2.07 (dd, *J* = 15.6, 5.8 Hz, 1H), 1.39 (s, 9H); ^{13}C NMR (126 MHz, Chloroform-*d*) δ 24.64, 25.27, 28.04 (3C), 37.90, 38.86, 51.56, 52.08, 66.68, 81.40, 128.35 (2C), 128.41, 128.68 (2C), 135.89, 172.07, 173.08; HRMS (ESI+) *m/z* calcd for $[C_{19}H_{24}O_5 + Na]^+$ 355.1516, found 355.1509.

benzyl (1*S*,2*R*,4*R*,5*R*)-4-hydroxy-7-oxo-6-oxabicyclo[3.2.1]octane-2-carboxylate (6.15) The epoxide **6.14** (312 mg, 1 eq) was dissolved in DCM (9 mL), and the solution was cooled to 0°C. TFA (535 mg, 0.36 mL, 5 eq) was added, and the solution stirred at 0°C for 2 hours (with a glass septum). The solution was concentrated *in vacuo*, and the crude product was purified by flash chromatography on a silica gel column (eluent 60:40 EtOAc-hexanes) to give the cyclized lactone as a clear oil (187 mg, 72%). R_f = 0.38 (60:40 EtOAc-hexanes); IR (film) cm^{-1} 3484, 2984, 1774, 1731, 1165, 1138, 1054, 908; ^1H NMR (500 MHz, Chloroform-*d*) δ 7.43 – 7.30 (m, 5H), 5.16 (s, 2H), 4.65 (t, *J* = 5.2 Hz, 1H), 4.26 (dt, *J* = 7.0, 2.7 Hz, 1H), 3.07 (dd, *J* = 5.1, 2.8 Hz, 1H), 2.98 (ddd, *J* = 11.8, 6.6, 2.0 Hz, 1H), 2.51 – 2.36 (m, 1H), 2.34 – 2.23 (m, 1H), 2.16 – 2.06 (m, 2H); ^{13}C NMR (126 MHz, Chloroform-*d*) δ 30.08, 31.24, 39.22, 40.47, 64.70, 67.17, 78.31, 128.39 (2C), 128.50, 128.73 (2C), 135.61, 171.54, 176.00; HRMS (ESI+) *m/z* calcd for $[C_{15}H_{16}O_5 + Na]^+$ 299.0890, found 299.0890.

benzyl (1*S*,2*R*,4*R*,5*R*)-4-((*tert*-butyldimethylsilyl)oxy)-7-oxo-6-oxabicyclo[3.2.1]octane-2-carboxylate (6.16) The lactone **6.15** (936 mg, 1 eq) was dissolved in DMF (11 mL), and the solution was cooled to 0°C. DMAP (42 mg, 0.1 eq) was added, followed by imidazole (461 mg, 2 eq) and TBSCl (613 mg, 1.2 eq). The reaction stirred overnight at room temperature without argon atmosphere. Water was added, and the product was extracted with Et_2O. The combined organic layers were washed with brine, dried over Na_2SO_4, filtered, and concentrated *in vacuo*. The crude product was purified by flash chromatography on a silica gel column (eluent 80:20 hexanes-EtOAc) to give the product as a clear oil (1.035 g, 78%). R_f = 0.33 (80:20 hexanes-EtOAc); IR (film) cm^{-1} 3019, 2952, 1786, 1732, 1162, 1064; ^1H NMR (500 MHz, Chloroform-*d*) δ 7.48 – 7.29 (m, 5H), 5.17 (s, 2H), 4.50 (t, *J* = 5.3 Hz, 1H), 4.26 – 4.04 (m, 1H), 3.05 (dt, *J* = 5.5, 1.7 Hz, 1H), 2.93 (ddd, *J* = 12.6, 5.6, 2.0 Hz, 1H), 2.42 (dd, *J* = 12.0, 6.2 Hz, 1H), 2.25 (dt, *J* = 11.6, 5.7 Hz,

1H), 2.17 – 2.08 (m, 1H), 2.05 – 1.97 (m, 1H), 0.89 (s, 9H), 0.08 (s, 3H), 0.06 (s, 3H); ^{13}C NMR (126 MHz, Chloroform-*d*) δ -4.85, -4.73, 18.04, 25.81 (3C), 30.37, 31.39, 39.30, 40.49, 65.47, 67.15, 78.61, 128.45 (2C), 128.49, 128.74 (2C), 135.70, 171.64, 175.84; ^{13}C NMR (126 MHz, Chloroform-*d*) δ -4.85, -4.73, 18.04, 25.81 (3C), 30.37, 31.39, 39.30, 40.49, 65.47, 67.15, 78.61, 128.45 (2C), 128.49, 128.74 (2C), 135.70, 171.64, 175.84; HRMS (ESI+) *m/z* calcd for $[C_{21}H_{30}O_5Si + Na]^+$ 413.1755, found 413.1751.

(1*S*,2*R*,4*R*,5*R*)-4-((*tert*-butyldimethylsilyl)oxy)-2-(hydroxymethyl)-6-oxabicyclo[3.2.1]octan-7-one (6.17) The benzyl ester **6.16** (347 mg, 1 eq) was dissolved in EtOAc (25 mL). Argon was bubbled into the solution for 5 minutes, and Pd/C (10 wt%) was added. Argon was bubbled into the solution for 5 more minutes. The argon balloon was replaced with an H_2 balloon, and H_2 was then bubbled into the solution overnight. The catalyst was filtered through Celite®, and the filter cake was rinsed with EtOAc. The filtrate was concentrated in vacuo, and the crude carboxylic acid was dissolved in THF (4 mL), and the solution was cooled to –78°C. Et_3N (117 mg, 0.16 mL, 1.3 eq) was added, followed by EtOCOCl (116 mg, 0.10 mL, 1.2 eq). The resultant mixture was stirred for 1 hour at –78°C and was then warmed to 0°C. H_2O (1.6 mL) was added, followed by $NaBH_4$ (67 mg, 2 eq) *slowly*. The reaction stirred at 0°C for 2 h, and then quenched with saturated sodium bicarbonate. The product was extracted with EtOAc, and the combined organic layers were washed with saturated $NaHCO_3$ and brine, dried over Na_2SO_4, filtered, and concentrated *in vacuo*. The crude product was purified by flash chromatography on a silica gel column (eluent 60:40 hexanes-EtOAc) to give the product as a clear oil (146 mg, 57% over 3 steps). R_f = 0.41 (60:40 hexanes-EtOAc); IR (film) cm^{-1} 3440, 2956, 1776, 1389, 1364, 1102, 1064, 876; ^{1}H NMR (500 MHz, Chloroform-*d*) δ 4.52 (t, *J* = 5.2 Hz, 1H), 4.12 (ddd, *J* = 5.5, 3.2, 1.0 Hz, 1H), 3.60 – 3.45 (m, 2H), 2.72 (dt, *J* = 5.7, 1.7 Hz, 1H), 2.39 (d, *J* = 11.8 Hz, 1H), 2.26 (dt, *J* = 11.8, 5.8 Hz, 1H), 2.23 – 2.17 (m, 1H), 2.00 – 1.93 (m, 1H), 1.73 (dd, *J* = 14.9, 5.3 Hz, 1H), 1.54 (ddd, *J* = 14.9, 12.7, 4.2 Hz, 1H), 0.89 (s, 9H), 0.08 (s, 3H), 0.06 (s, 3H); ^{13}C NMR (126 MHz, Chloroform-*d*) δ -4.83, -4.73, 18.05 (3C), 25.81, 30.95, 31.51, 36.87, 40.14, 64.57, 65.80, 79.70, 178.15; HRMS (ESI+) *m/z* calcd for $[C_{14}H_{26}O_4Si + Na]^+$ 309.1493, found 309.1496.

(1*S*,2*R*,4*R*,5*R*)-4-((*tert*-butyldimethylsilyl)oxy)-2-(((*tert*-butyldimethylsilyl)oxy)methyl)-6-oxabicyclo[3.2.1]octan-7-one (6.18) The alcohol **6.17** (132 mg, 1 eq) was dissolved in DMF (4 mL), and the solution was cooled to 0°C. Imidazole (63 mg, 2 eq) was added, followed by TBSCl (83 mg, 1.2 eq). The reaction stirred overnight at room temperature without argon atmosphere.

Water was added, and the product was extracted with Et_2O. The combined organic layers were washed with brine, dried over Na_2SO_4, filtered, and concentrated *in vacuo*. The crude product was purified by flash chromatography on a silica gel column (eluent 90:10 hexanes-EtOAc) to give the product as a clear oil (165 mg, 89%). R_f = 0.61 (90:10 hexanes-EtOAc); IR (film) cm^{-1} 2952, 1792, 1782, 1257, 1096, 1064, 836; ^1H NMR (500 MHz, Chloroform-*d*) δ 4.49 (t, *J* = 5.2 Hz, 1H), 4.10 (t, *J* = 4.2 Hz, 1H), 3.51 (dd, *J* = 10.1, 8.5 Hz, 1H), 3.39 (dd, *J* = 10.1, 5.9 Hz, 1H), 2.67 (d, *J* = 5.6 Hz, 1H), 2.37 (d, *J* = 11.8 Hz, 1H), 2.23 (dt, *J* = 11.8, 5.8 Hz, 1H), 2.20 – 2.13 (m, 1H), 1.75 (dd, *J* = 14.9, 5.2 Hz, 1H), 1.40 (ddd, *J* = 14.9, 12.8, 4.2 Hz, 1H), 0.90 (s, 18H), 0.08 (s, 6H), 0.06 (s, 3H), 0.06 (s, 3H); ^{13}C NMR (126 MHz, Chloroform-*d*) δ -5.29, -5.25, -4.81, -4.72, 18.07, 18.43, 25.83 (3C), 26.04 (3C), 31.28, 31.61, 37.36, 39.57, 64.62, 65.96, 79.47, 177.38; HRMS (ESI+) *m/z* calcd for $[C_{20}H_{40}O_4Si_2 + Na]^+$ 423.2357, found 423.2355.

***tert*-butyl (1S,2R,4R,5R)-4-iodo-7-oxo-6-oxabicyclo[3.2.1]octane-2-carboxylate (6.23)** The anhydride **6.12** (7.50 g, 49.3 mmol, 1 eq) was suspended in *t*-BuOH (40 mL), and DMAP (602 mg, 4.93 mmol, 0.1 eq) was added. The mixture was refluxed for 4 days. Water was added, and the product was extracted with Et_2O. The combined organic layers were washed with brine, dried over Na_2SO_4, filtered, and concentrated *in vacuo* to give the intermediate hemiester as a beige oil (84% conversion). (The conversion was determined by NMR to calculate the stoichiometric amounts in the next step.) The crude product (8.26 g, 36.5 mmol, 1 eq) was dissolved in DCM (40 mL) and H_2O (120 mL), and the resultant mixture was cooled to 0°C. $NaHCO_3$ (6.13 g, 71.3 mmol, 2 eq) was added slowly, followed by I_2 (10.2 g, 40.2 mmol, 1.1 eq), and KI (12.1 g, 72.9 mmol, 2 eq). The mixture was stirred overnight at room temperature. The reaction was then cooled to 0°C, and saturated $Na_2S_2O_3$ was added slowly until the mixture became colorless. The product was then extracted with DCM, and the combined organic layers were washed with saturated $Na_2S_2O_3$ and brine, dried over Na_2SO_4, filtered, and concentrated *in vacuo*. The crude product was then purified by flash chromatography on a silica gel column (eluent 85:15 hexanes-EtOAc) to give the pure iodolactone **6.23** as a white solid (11.2 g, 73% over 2 steps). R_f = 0.43 (85:15 hexanes-EtOAc); mp = 86-89°C; IR (film) cm^{-1} 2976, 1784, 1724, 1367, 1393, 1144, 1114, 951; ^1H NMR (500 MHz, Chloroform-*d*) δ 4.78 (dd, *J* = 5.8, 4.0 Hz, 1H), 4.52 (dd, *J* = 5.7, 4.0 Hz, 1H), 3.15 – 3.02 (m, 1H), 2.85 – 2.74 (m, 2H), 2.54 (ddd, *J* = 16.7, 12.6, 5.7 Hz, 1H), 2.45 (dtd, *J* = 12.7, 5.8, 1.5 Hz, 1H), 2.33 (dd, *J* = 16.6, 5.3 Hz, 1H), 1.45 (s, 9H); ^{13}C NMR (126 MHz,

Chloroform-*d*) δ 22.30, 28.05 (3C), 31.98, 34.41, 40.22, 40.98, 79.41, 82.18, 169.79, 175.12; HRMS (ESI+) *m/z* calcd for $[C_{12}H_{17}O_4I + Na]^+$ 375.0064, found 375.0065.

(1*S*,2*R*,4*R*,5*R*)-2-(hydroxymethyl)-4-iodo-6-oxabicyclo[3.2.1]octan-7-one (6.24) The iodolactone **6.23** (11.2 g, 31.8 mmol) was dissolved in DCM (100 mL), and the solution was cooled to 0°C. Trifluoroacetic acid (18.1 g, 12.1 mL, 5 eq) was added slowly (without a septum). The reaction stirred at room temperature overnight (with a glass stopper). The solution was then concentrated *in vacuo* to give a beige oil, which was precipitated in hexanes to give the carboxylic acid product as a white solid. The crude carboxylic acid (*only some taken to next step*: 810 mg, 2.74 mmol, 1 eq) was dissolved in THF (25 mL), and the solution was cooled to –78°C. Et_3N (332 mg, 3.28 mmol, 0.46 mL, 1.2 eq) was added, followed by EtOCOCl (327 mg, 3.01 mmol, 0.29 mL, 1.1 eq). The resultant mixture was stirred for 1 hour at –78°C and was then warmed to 0°C. H_2O (10 mL) was added, followed by $NaBH_4$ (207 mg, 5.48 mmol, 2 eq) *slowly*. The reaction stirred at 0°C for 2h, and then quenched with 1M HCl. The product was extracted with Et_2O, and the combined organic layers were washed with brine, dried over Na_2SO_4, filtered, and concentrated *in vacuo*. The crude product was purified by flash chromatography on a silica gel column (eluent 60:40 EtOAc-hexanes) to give the alcohol **6.24** as a white solid (770 mg, 89% over 2 steps). R_f = 0.42 (60:40 EtOAc-hexanes); ^{1}H NMR (500 MHz, Chloroform-*d*) δ 4.86 (dd, *J* = 5.8, 4.0 Hz, 1H), 4.55 (ddt, *J* = 5.6, 3.3, 1.6 Hz, 1H), 3.68 – 3.55 (m, 2H), 2.87 – 2.73 (m, 2H), 2.53 – 2.45 (m, 1H), 2.32 – 2.24 (m, 1H), 2.23 – 2.10 (m, 2H). Physical and spectral properties were in agreement with the literature.[46]

(1*S*,2*R*,4*R*,5*R*)-2-(((*tert*-butyldimethylsilyl)oxy)methyl)-4-iodo-6-oxabicyclo[3.2.1]octan-7-one (6.25) The alcohol **6.24** (753 mg, 1 eq) was dissolved in DMF (13 mL), and the solution was cooled to 0°C. Imidazole (363 mg, 2 eq) was added, followed by TBSCl (483 mg, 1.2 eq). The reaction stirred overnight at room temperature without argon atmosphere. The reaction was then quenched with water, and the product was extracted with Et_2O. The combined layers were washed with water and brine, dried over Na_2SO_4, filtered, and concentrated *in vacuo*. The crude product was purified by flash chromatography on a silica gel column (eluent 90:10 hexanes-EtOAc) to give the product as a clear oil (787 mg, 74%). R_f = 0.41 (91:10 hexanes-EtOAc); ^{1}H NMR (500 MHz, Chloroform-*d*) δ 4.81 (dd, *J* = 5.8, 4.1 Hz, 1H), 4.52 – 4.49 (m, 1H), 3.55 (dd, *J* = 10.1, 8.3 Hz, 1H), 3.47 – 3.39 (m, 1H), 2.82 – 2.71 (m, 2H), 2.52 – 2.40 (m, 1H), 2.32 – 2.19

(m, 1H), 2.16 (dd, J = 16.1, 5.0 Hz, 1H), 1.96 (ddd, J = 16.1, 12.5, 5.7 Hz, 1H), 0.90 (s, 9H), 0.08 (s, 3H), 0.06 (s, 3H).). Physical and spectral properties were in agreement with the literature.[46]

methyl (1*S*,2*R*,5*S*)-2-(((*tert*-butyldimethylsilyl)oxy)methyl)-5-hydroxycyclohexane-1-carboxylate (6.26) The iodolactone **6.25** (738 mg, 1 eq) was dissolved in MeOH (18 mL), and LiOAc•2H_2O (418 mg, 2.2 eq) was added. Argon was bubbled into the solution for 5 minutes, and Pd/C (10 wt%) was added. Argon was bubbled into the solution for 5 minutes. The argon balloon was replaced with an H_2 balloon, and H_2 was then bubbled into the solution overnight. The catalyst was filtered through Celite®, and the filter cake was rinsed with EtOAc. Saturated $Na_2S_2O_3$ was added, and the product was extracted with EtOAc. The combined organic layers were washed with saturated $Na_2S_2O_3$ and brine, dried over Na_2SO_4, and concentrated *in vacuo*. The crude residue was redissolved in THF-H_2O (5:1, 9 mL), and LiOH (133 mg, 3 eq) was added. The reaction stirred overnight at room temperature. The solvent was removed *in vacuo*, and the residue was dissolved in H_2O and EtOAc, cooled to 0°C, and 10% citric acid was added until pH 4 was reached. The product was extracted with EtOAc, and the combined organic layers were washed with brine, dried over Na_2SO_4, filtered, and evaporated to give the product as a white solid, which was dissolved in acetone (19 mL). K_2CO_3 (771 mg, 3 eq) was added, followed by MeI (316 mg, 0.14 mL, 1.2 eq). The reaction stirred overnight at room temperature. Water was added, and the product was extracted with Et_2O. The combined organic layers were washed with saturated $NaHCO_3$ and brine, dried over Na_2SO_4, filtered, and concentrated *in vacuo*. The crude product was purified by flash chromatography on a silica gel column (eluent 70:30 hexanes-EtOAc) to give the product as a clear oil (298 mg, 53% over 3 steps). R_f = 0.24 (70:30 hexanes-EtOAc); IR (film) cm^{-1} 3397, 2952, 1736, 1255, 1094, 836; ^{1}H NMR (500 MHz, Chloroform-*d*) δ 3.78 (q, J = 5.5 Hz, 1H), 3.67 (s, 3H), 3.65 – 3.45 (m, 2H), 2.73 (dt, J = 7.6, 4.9 Hz, 1H), 2.05 – 1.98 (m, 1H), 1.94 – 1.86 (m, 2H), 1.86 – 1.79 (m, 1H), 1.67 – 1.62 (m, 2H), 1.48 – 1.38 (m, 1H), 1.33 – 1.25 (m, 1H), 0.88 (s, 9H), 0.03 (s, 3H), 0.02 (s, 3H); ^{13}C NMR (126 MHz, Chloroform-*d*) δ -5.34, -5.31, 22.03, 26.04 (3C), 31.52, 31.73, 33.04, 39.51, 41.21, 51.81, 63.26, 68.02, 176.17; HRMS (ESI+) *m/z* calcd for $[C_{15}H_{30}O_4Si + Na]^+$ 325.1806, found 325.1804.

dimethyl (1*R*,2*S*)-cyclohex-4-ene-1,2-dicarboxylate (6.*rac*-30) The anhydride **6.12** (200 mg, 1 eq) was suspended in MeOH (0.78 mL, 20 eq), and the mixture was cooled to 0°C. BF_3•OEt_2 (140 mg, 0.12 mL, 0.75 eq) was added dropwise, and the mixture was warmed to room temperature and stirred overnight. Water was added, and the product was extracted with Et_2O. The combined

organic layers were washed with brine, dried over Na_2SO_4, filtered, and concentrated *in vacuo* to give the pure di-ester as a clear oil (459 mg, quant.). R_f = 0.58 (60:40 EtOAc-hexanes); ^{1}H NMR (500 MHz, Chloroform-*d*) δ 5.95 – 5.29 (m, 2H), 3.69 (s, 6H), 3.04 (t, *J* = 5.4 Hz, 2H), 2.60 – 2.50 (m, 2H), 2.42 – 2.25 (m, 2H). Physical and spectral properties were in agreement with the literature.[55]

6.7 References

(1) Cancer: Key facts. https://www.who.int/news-room/fact-sheets/detail/cancer (accessed 4 Dec 2019).

(2) Roma-Rodrigues, C.; Mendes, R.; Baptista, P. V.; Fernandes, A. R., Targeting Tumor Microenvironment for Cancer Therapy. *Int J Mol Sci* **2019,** *20* (4).

(3) Li, M.; Li, M.; Yin, T.; Shi, H.; Wen, Y.; Zhang, B.; Chen, M.; Xu, G.; Ren, K.; Wei, Y., Targeting of cancerassociated fibroblasts enhances the efficacy of cancer chemotherapy by regulating the tumor microenvironment. *Mol Med Rep* **2016,** *13* (3), 2476-84.

(4) Zi, F.; He, J.; He, D.; Li, Y.; Yang, L.; Cai, Z., Fibroblast activation protein alpha in tumor microenvironment: recent progression and implications (review). *Mol Med Rep* **2015,** *11* (5), 3203-11.

(5) Christiansen, V. J.; Jackson, K. W.; Lee, K. N.; Downs, T. D.; McKee, P. A., Targeting inhibition of fibroblast activation protein-alpha and prolyl oligopeptidase activities on cells common to metastatic tumor microenvironments. *Neoplasia* **2013,** *15* (4), 348-58.

(6) Cao, H.; Zhao, X.; Lu, S.; Wang, Z., Prolyl oligopeptidase inhibitor suppresses the upregulation of ACSDKP in patients with acute myeloid leukemia. *Exp Ther Med* **2018,** *15* (6), 5431-5435.

(7) Henry, L. R.; Lee, H. O.; Lee, J. S.; Klein-Szanto, A.; Watts, P.; Ross, E. A.; Chen, W. T.; Cheng, J. D., Clinical implications of fibroblast activation protein in patients with colon cancer. *Clin Cancer Res* **2007,** *13* (6), 1736-41.

(8) Lawandi, J.; Gerber-Lemaire, S.; Juillerat-Jeanneret, L.; Moitessier, N., Inhibitors of prolyl oligopeptidases for the therapy of human diseases: defining diseases and inhibitors. *J Med Chem* **2010,** *53* (9), 3423-38.

(9) Jackson, K. W.; Christiansen, V. J.; Yadav, V. R.; Silasi-Mansat, R.; Lupu, F.; Awasthi, V.; Zhang, R. R.; McKee, P. A., Suppression of tumor growth in mice by rationally designed pseudopeptide inhibitors of fibroblast activation protein and prolyl oligopeptidase. *Neoplasia* **2015,** *17* (1), 43-54.

(10) Tanaka, S.; Suzuki, K.; Sakaguchi, M., The prolyl oligopeptidase inhibitor SUAM-14746 attenuates the proliferation of human breast cancer cell lines in vitro. *Breast Cancer* **2017,** *24* (5), 658-666.

(11) Study of Talabostat and Pemetrexed vs. Pemetrexed in Stage IIIB/IV Non-Small Cell Lung Cancer (NSCLC) After Failure of Platinum-Based Chemotherapy. https://ClinicalTrials.gov/show/NCT00290017.

(12) Study of Talabostat + Docetaxel Versus Docetaxel in Stage IIIB/IV Non-Small Cell Lung Cancer (NSCLC) After Failure of Platinum-Based Chemotherapy. https://ClinicalTrials.gov/show/NCT00243204.

(13) Haas, M. J., Truly boronic. *Sci Bus Exch* **2008,** *1*, 1-3.

(14) Kelly, T. A.; Adams, J.; Bachovchin, W. W.; Barton, L. M.; Campbel, S. J.; Coutts, S. J.; Kennedy, C. A.; Snow, R. J., Immunosuppressive Boronic Acid Dipeptides Correlation between Conformation and Activity. *J Am Chem Soc* **1993,** *115*, 12637-12638.

(15) Poplawski, S. E.; Lai, J. H.; Sanford, D. G.; Sudmeier, J. L.; Wu, W.; Bachovchin, W. W., Pro-soft Val-boroPro: a strategy for enhancing in vivo performance of boronic acid inhibitors of serine proteases. *J Med Chem* **2011,** *54* (7), 2022-8.

(16) Jansen, K.; Heirbaut, L.; Verkerk, R.; Cheng, J. D.; Joossens, J.; Cos, P.; Maes, L.; Lambeir, A. M.; De Meester, I.; Augustyns, K.; Van der Veken, P., Extended structure-activity relationship and pharmacokinetic investigation of (4-quinolinoyl)glycyl-2-cyanopyrrolidine inhibitors of fibroblast activation protein (FAP). *J Med Chem* **2014,** *57* (7), 3053-74.

(17) Poplawski, S. E.; Lai, J. H.; Li, Y.; Jin, Z.; Liu, Y.; Wu, W.; Wu, Y.; Zhou, Y.; Sudmeier, J. L.; Sanford, D. G.; Bachovchin, W. W., Identification of selective and potent inhibitors of fibroblast activation protein and prolyl oligopeptidase. *J Med Chem* **2013,** *56* (9), 3467-77.

(18) Tran, T.; Quan, C.; Edosada, C. Y.; Mayeda, M.; Wiesmann, C.; Sutherlin, D.; Wolf, B. B., Synthesis and structure-activity relationship of N-acyl-Gly-, N-acyl-Sar- and N-blocked-boroPro inhibitors of FAP, DPP4, and POP. *Bioorg Med Chem Lett* **2007,** *17* (5), 1438-42.

(19) De Cesco, S.; Deslandes, S.; Therrien, E.; Levan, D.; Cueto, M.; Schmidt, R.; Cantin, L. D.; Mittermaier, A.; Juillerat-Jeanneret, L.; Moitessier, N., Virtual screening and computational optimization for the discovery of covalent prolyl oligopeptidase inhibitors with activity in human cells. *J Med Chem* **2012,** *55* (14), 6306-15.

(20) Mariaule, G.; De Cesco, S.; Airaghi, F.; Kurian, J.; Schiavini, P.; Rocheleau, S.; Huskic, I.; Auclair, K.; Mittermaier, A.; Moitessier, N., 3-Oxo-hexahydro-1H-isoindole-4-

carboxylic Acid as a Drug Chiral Bicyclic Scaffold: Structure-Based Design and Preparation of Conformationally Constrained Covalent and Noncovalent Prolyl Oligopeptidase Inhibitors. *J Med Chem* **2016,** *59* (9), 4221-34.

(21) Plescia, J.; Dufresne, C.; Janmamode, N.; Wahba, A. S.; Mittermaier, A. K.; Moitessier, N., Discovery of covalent prolyl oligopeptidase boronic ester inhibitors. *Eur J Med Chem* **2019**, 111783.

(22) Lawandi, J.; Toumieux, S.; Seyer, V.; Campbell, P.; Thielges, S.; Juillerat-Jeanneret, L.; Moitessier, N., Constrained peptidomimetics reveal detailed geometric requirements of covalent prolyl oligopeptidase inhibitors. *J Med Chem* **2009,** *52* (21), 6672-84.

(23) Plescia, J.; Hédou, D.; Poussé, M. E.; Labarre, A.; Dufresne, C.; Mittermaier, A.; Moitessier, N., Computer-aided design, synthesis, and biological evaluation of [4.3.0] bicyclic prolyl oligopeptidase and fibroblast activation protein alpha dual inhibitors. McGill University: 2019.

(24) Plescia, J.; De Cesco, S.; Patrascu, M. B.; Kurian, J.; Di Trani, J.; Dufresne, C.; Wahba, A. S.; Janmamode, N.; Mittermaier, A. K.; Moitessier, N., Integrated Synthetic, Biophysical, and Computational Investigations of Covalent Inhibitors of Prolyl Oligopeptidase and Fibroblast Activation Protein alpha. *J Med Chem* **2019,** *62* (17), 7874-7884.

(25) Aertgeerts, K., Levin, I., Shi, L., Snell, G.P., Jennings, A., Prasad, G.S., Zhang, Y., Kraus, M.L., Salakian, S., Sridhar, V., Wijnands, R., Tennant, M.G., Structural and kinetic analysis of the substrate specificity of human fibroblast activation protein alpha. *J Biol Chem* **2005,** *280*, 19441-19444.

(26) Eckhardt, M., Langkopf, E., Mark, M., Tadayyon, M., Thomas, L., Nar, H., Pfrengle, W., Guth, B., Lotz, R., Sieger, P., Fuchs, H., Himmelsbach, F., 8-(3-(R)-Aminopiperidin-1-yl)-7-but-2-ynyl-3-methyl-1-(4-methyl-quinazolin-2-ylmethyl)-3,7-dihydropurine-2,6-dione (BI 1356), a Highly Potent, Selective, Long-Acting, and Orally Bioavailable DPP-4 Inhibitor for the Treatment of Type 2 Diabetes. *J Med Chem* **2007,** *50*, 6450-6453.

(27) Metzler, W. J., Yanchunas, J., Weigelt, C., Kish, K., Klei, H.E., Xie, D., Zhang, Y., Corbett, M., Tamura, J.K., He, B., Hamann, L.G., Kirby, M.S., Marcinkeviciene, J., Involvement of DPP-IV catalytic residues in enzyme-saxagliptin complex formation. *Protein Sci* **2008,** *17*, 240-250.

(28) Ji, X.; Xia, C.; Wang, J.; Su, M.; Zhang, L.; Dong, T.; Li, Z.; Wan, X.; Li, J.; Li, J.; Zhao, L.; Gao, Z.; Jiang, H.; Liu, H., Design, synthesis and biological evaluation of 4-fluoropyrrolidine-2-carbonitrile and octahydrocyclopenta[b]pyrrole-2-carbonitrile derivatives as dipeptidyl peptidase IV inhibitors. *Eur J Med Chem* **2014,** *86*, 242-56.

(29) De Cesco, S.; Kurian, J.; Dufresne, C.; Mittermaier, A. K.; Moitessier, N., Covalent inhibitors design and discovery. *Eur J Med Chem* **2017,** *138*, 96-114.

(30) Sterling, T.; Irwin, J. J., ZINC 15--Ligand Discovery for Everyone. *J Chem Inf Model* **2015,** *55* (11), 2324-37.

(31) European Molecular Biology Laboratory – ChEMBL database. https://www.ebi.ac.uk/chembl/ (accessed 2019).

(32) Therrien, E.; Englebienne, P.; Arrowsmith, A. G.; Mendoza-Sanchez, R.; Corbeil, C. R.; Weill, N.; Campagna-Slater, V.; Moitessier, N., Integrating medicinal chemistry, organic/combinatorial chemistry, and computational chemistry for the discovery of selective estrogen receptor modulators with Forecaster, a novel platform for drug discovery. *J Chem Inf Model* **2012,** *52* (1), 210-24.

(33) Lipinski, C. A.; Lombardo, F.; Dominy, B. W.; Feeney, P. J., Experimental and computational approaches to estimate solubility and permeability in drug discovery and development settings. *Adv Drug Deliv Rev* **1997,** *23* (1-3), 3-25.

(34) Veber, D. F.; Johnson, S. R.; Cheng, H.-Y.; Smith, B. R.; Ward, K. W.; Kopple, K. D., Molecular Properties That Influence the Oral Bioavailability of Drug Candidates. *J Med Chem* **2002,** *45*, 2615-2623.

(35) Corbeil, C. R.; Englebienne, P.; Moitessier, N., Docking Ligands into Flexible and Solvated Macromolecules. 1. Development and Validation of FITTED 1.0. *J Chem Inf Model* **2007,** *47*, 435-449.

(36) Moitessier, N.; Corbeil, C. R., Docking ligands into flexible and solvated macromolecules. 3. Impact of input ligand conformation, protein flexibility, and water molecules on the accuracy of docking programs. *J Chem Inf Model* **2009,** *49* (4), 997-1009.

(37) Moitessier, N.; Pottel, J.; Therrien, E.; Englebienne, P.; Liu, Z.; Tomberg, A.; Corbeil, C. R., Medicinal Chemistry Projects Requiring Imaginative Structure-Based Drug Design Methods. *Acc Chem Res* **2016,** *49* (9), 1646-57.

(38) Baker, S. J.; Zhang, Y.-K.; Tsutomu, A.; Lau, A.; Zhou, H.; Hernandez, V.; Mao, W.; Alley, M. R. K.; Sanders, V.; Plattner, J. J., Discovery of a New Boron-Containing Antifungal Agent, 5-Fluoro-1,3-dihydro-1-hydroxy-2,1benzoxaborole (AN2690), for the Potential Treatment of Onychomycosis. *J Med Chem* **2006,** *49* (15), 4447-4450.

(39) Akama, T.; Baker, S. J.; Zhang, Y. K.; Hernandez, V.; Zhou, H.; Sanders, V.; Freund, Y.; Kimura, R.; Maples, K. R.; Plattner, J. J., Discovery and structure-activity study of a novel benzoxaborole anti-inflammatory agent (AN2728) for the potential topical treatment of psoriasis and atopic dermatitis. *Bioorg Med Chem Lett* **2009,** *19* (8), 2129-32.

(40) Danehy, S., Pfizer Receives FDA Approval for EUCRISA™ (crisaborole) a Novel Non-Steroidal Topical Ointment for Mild to Moderate Atopic Dermatitis (Eczema). 2017.

(41) Markham, A., Tavaborole: first global approval. *Drugs* **2014,** *74* (13), 1555-8.

(42) Plescia, J.; Moitessier, N. Design and Discovery of Boronic Acid Drugs. *Eur J Med Chem* **2020**, 112270.

(43) Van Elzen, R.; Schoenmakers, E.; Brandt, I.; Van Der Veken, P.; Lambeir, A. M., Ligand-induced conformational changes in prolyl oligopeptidase: a kinetic approach. *Protein Eng Des Sel* **2017,** *30* (3), 217-224.

(44) Goossens, F.; De Meester, I.; Vanhoof, G.; Hendriks, G.; Vriend, G.; Scharpé, S., The purification, characterization and analysis of primary and secondary-structure of prolyl oligopeptidase from human lymphocytes: Evidence that the enzyme belongs to the a/b hydrolase fold family. *Eur J Biochem* **1995,** *233*, 432-441.

(45) Li, C.; Wang, J.; Barton, L. M.; Yu, S.; Tian, M.; Peters, D. S.; Kumar, M.; Yu, A. W.; Johnson, K. A.; Chatterjee, A. K.; Yan, M.; Baran, P. S., Decarboxylative borylation. *Science* **2017,** *356* (6342), 1-8.

(46) Kobayashi, S.; Eguchi, Y.; Shimada, M.; Ohno, M., Enantioselective synthesis of cyclohexenone derivatives by a chemicoenzymatic approach: stereo- and regioselective route to potential intermediates of compactin (ML 236B) and mevinolin. *Chem Pharm Bull* **1990,** *38* (6), 1479-84.

(47) Wang, H.; Yan, L.; Wu, Y.; Lu, Y.; Chen, F., Asymmetric Synthesis of Vitamin D3 Analogues: Organocatalytic Desymmetrization Approach toward the A-Ring Precursor of Calcifediol. *Org Lett* **2015,** *17* (21), 5452-5.

(48) Kobayashi, S.; Kamiyama, K.; Ohno, M., Chiral Synthon Obtained with Pig Liver Esterase: Introduction of Chiral Centers into Cyclohexene Skeleton. *Chem Pharm Bull* **1990,** *38* (2), 350-354.

(49) Sabitha, G.; Srividya, R.; Yadav, J. S., Ring Opening of Cyclic Anhydrides: Synthesis of Achiral Half-Esters Using Lewis Acids. *Tetrahedron* **1999,** *55*, 4015-4018.

(50) Bolm, C.; Schiffers, I.; Dinter, C. L.; Gerlach, A., Practical and Highly Enantioselective Ring Opening of Cyclic Meso-Anhydrides Mediated by Cinchona Alkaloids. *J Org Chem* **2000,** *65*, 6984-6991.

(51) Henderson, A. R.; Stec, J.; Owen, D. R.; Whitby, R. J., The first total synthesis of (+)-mucosin. *Chem Commun (Camb)* **2012,** *48* (28), 3409-11.

(52) Manzano, R.; Andres, J. M.; Muruzabal, M. D.; Pedrosa, R., Synthesis of both enantiomers of hemiesters by enantioselective methanolysis of meso cyclic anhydrides catalyzed by alpha-amino acid-derived chiral thioureas. *J Org Chem* **2010,** *75* (15), 5417-20.

(53) Andres, J. M.; Manzano, R.; Pedrosa, R., Novel bifunctional chiral urea and thiourea derivatives as organocatalysts: enantioselective nitro-Michael reaction of malonates and diketones. *Chemistry* **2008,** *14* (17), 5116-9.

(54) Berman, H. M.; Westbrook, J.; Feng, Z.; Gilliland, G.; Bhat, T. N.; Weissig, H.; Shindyalov, I. N.; Bourne, P. E., The Protein Data Bank. *Nucleic Acids Res* **2000,** *28*, 235-242.

(55) Fuchs, M.; Furstner, A., trans-Hydrogenation: application to a concise and scalable synthesis of brefeldin A. *Angew Chem Int Ed Engl* **2015,** *54* (13), 3978-82.

Chapter 7:

Conclusions and Perspectives

7.1 Conclusions

As discussed in Chapter 1, boronic acids are present ubiquitously in nature and are generally safe reversibly covalent warheads. Their studies and uses in scientific endeavours have increased in the past few decades, including their use in drug discovery programs. Many research groups have taken advantage of their unique properties, and thus far, five boronic acid drugs have been approved, with several others in clinical trials. In our own research group, we have studied several electrophilic groups in the development of reversible covalent serine protease inhibitors and found that boronic acids are most beneficial, offering high potencies and relatively long residence times compared to other reversibly covalent warheads (Chapter 2). We hope to further develop our boronic acids into pre-clinical candidates with our expert biological and pharmacological collaborators.

As we have shown in Chapters 3, 4, and 6, our approach of computational drug design, whether it be through computationally-guided medicinal chemistry optimizations, constrained peptidomimetics, or virtual screening, has the potential to lead to very potent POP and FAP inhibitors. We are able to start from a known active compound and virtually optimize the structure, dock our designs into the protein targets, and choose the most promising analogues for synthesis. Furthermore, we can screen virtual libraries of thousands of compounds and use our scoring function to determine the most promising inhibitors. These methods have proven very successful for us in the past, and they have led us to nanomolar-potent selective POP inhibitors and dual POP/FAP inhibitors. Following the findings in this dissertation, our research group is currently applying these methods to other enzymatic targets. As shown in Chapters 5 and 6, we also have the synthetic expertise to develop complex asymmetric syntheses of compounds with multiple stereocenters.

The following summaries outline in more detail the conclusions that can be drawn from this dissertation.

In Chapter 2, we presented a collaborative effort of synthetic chemists, biophysicists, and computational chemists to study the druggability of POP and FAP in terms of which covalent

groups are best accommodated in each enzyme. We synthesized a series of compounds differing only in the electrophilic warhead that targets the catalytic serine of POP. Our *in vitro* assays revealed that, in POP, the nitrile and boronic acid exhibited very similar activities, with the aldehyde being more potent by an order of magnitude. However, further biophysical kinetics assays used to determine the inhibitors residence time in the active site demonstrated that, while the nitrile and boronic acid did have similar inhibition constants, the boronic acid led to residence time which was approximately 70 minutes, while that of the nitrile and the non-covalent analogue were less than one minute, indicating that the nitrile might not even form a covalent bond with the catalytic serine, i.e. the inhibitor may be binding non-covalently or through a quickly-reversible covalent bond. Furthermore, the more potent aldehyde remained in the active site for only 20 minutes, less than a third of the time as the boronic acid (likely due to the boronic acid's extra hydrogen bonds of its hydroxyl groups, as discussed in Chapter 2). These results were mirrored in the computational studies of the activation energy of bond formation between the enzyme and electrophiles. Because longer residence time is generally associated with high *in vivo* efficacy of a drug,[1] and aldehydes do not make ideal drug candidates due to their high intrinsic reactivities,[2] we have decided to move forth with boronic acids as future POP/FAP inhibitors. Although their synthesis is generally not as straightforward or malleable as that of a nitrile or an aldehyde, they seem to be the ideal electrophilic warhead for our enzymatic targets.

In Chapter 3, we presented a series of highly potent POP inhibitors that was virtually derived from Y-29794, an existing failed drug. The synthesis of this new series was optimized to be just 1-2 steps, 3 including a final "unnecessary" deprotection step. Taking advantage of this efficient synthesis, we prepared many analogues to probe the active site of POP and explore a wider inhibitor scope than what is currently presented in the literature. We found that the original required pharmacophore for potent compounds is in fact not entirely essential; replacing one greasy functional group (e.g. benzyl, alkyl chain) with either a fluorine atom or a methoxy group gave equal if not higher potency. This study gave us a better understanding of the requirements for potent POP inhibitors and further widened the potential scope of our future endeavours in POP inhibition. Our work also provides biophysicists and biologists with inhibitors that are readily available in just 1-2 steps for studies pertaining to POP's activity in neurodegenerative diseases or cancer.

In Chapter 4, we presented a series of dual inhibitors based on a [4.3.0] heterobicyclic scaffold which was virtually optimized from Talabostat, a drug that failed in Phase III clinical trials. This attrition was due to inefficacy likely caused by intramolecular cyclization of the dipeptidic structure, rendering it inactive. Our solution to this problem was the virtual rigidification of the dipeptide to the corresponding bicyclic scaffold, followed by docking-guided optimizations to improve the predicted docking modes and chemical modifications to ensure synthetic feasibility.

The synthesis of the bicyclic structures was not straightforward, as they contain several stereocenters. Initial synthesis attempts led to mixtures of stereoisomers and difficult chromatographic separations. Synthetic optimization using chiral auxiliaries finally led to series of diastereopure [4.3.0] heterocyclic nitriles and boronic esters and acids. Analogues with different substituents and stereochemistry were synthesized to probe the active site and determine the optimal stereochemistry and substitution. Dipeptide acyclic analogues were also synthesized to determine the effect of rigidity on inhibitor activity. It was found that the most active inhibitors were boronic ester analogues of L-serine and L-threonine. Furthermore, the rigid bicyclic analogues exhibited inhibitory potency on the same order of magnitude as the acyclic inhibitors. The bicyclic inhibitors have higher potential for developability, as they are more rigid, specific to their targets (reduced off-target binding), and generally more metabolically stable. From these peptidomimetic designs, we obtained our first-ever POP/FAP dual inhibitors, exhibiting submicromolar activity *in vitro*. We learned which substituents and stereochemistry offer the highest inhibitor potency, which will be applied to pharmacokinetic optimization of these compounds and to future POP/FAP inhibitor designs.

In Chapter 5, we further explored the oxidative cyclization reaction encountered in Chapter 4. During the course of optimization of the reaction conditions, we noticed that altering stereochemistry at certain stereocenters, as well as changing the reducing agent, gave us interesting results. Although the results are very recent and are still under analysis, we propose that our oxidative cyclization proceeds through a macrocyclic intermediate. Furthermore, the major diastereomer of the product depends on both the established stereocenters and on the reducing agent utilized, resulting in a match/mismatch case.

In our synthesis of the bicyclic nitrile analogue, we also obtained interesting results from a modified Strecker reaction. Using the Ellman auxiliary and various Lewis acids, we were able to selectively synthesize either the (*S*)- or (*R*)- nitrile synthetic intermediate with high

diastereoselectivity. We also noticed that the stereochemistry of the nitrile does not particularly influence the reaction mechanism. These results led us to believe that the reaction was more complex and may occur through more than one mechanism. Currently, we are performing computational calculations to study the reaction and hopefully explain the results.

In Chapter 6, we presented a series of promising potential POP/FAP dual inhibitors based on the first FAP virtual screening reported to date. After many rounds of synthetic optimization, we arrived at two promising borinic ester synthetic targets that contain functional groups designed to be compatible with the binding sites of both POP and FAP. Once more, the synthesis of these compounds has proven to be very challenging, as the compounds contain multiple stereocenters and functional groups that are not always compatible from step to step. So far, we have achieved a highly stereoselective syntheses, but we still have several challenging steps ahead. We hope that upon completion of the syntheses, along with those of a few analogues, we will have obtained dual POP/FAP inhibitors with a bicyclic borinic ester scaffold.

Overall, we have successfully applied our drug discovery approach several times to obtain POP and POP/FAP inhibitors. From our synthetic endeavours, we learned unfortunately that synthesis involving boronic esters and acids is very tricky, as these functional groups are very polar, not as easily obtained as nitriles or aldehydes, and quite sensitive to reaction conditions. Nevertheless, we have found ways to incorporate the boronic esters so that their introduction is either followed by mild reaction conditions or is at the end of the inhibitor synthesis. Our optimized syntheses led to pure, nanomolar-potent boronic esters and acids. We hope to be able to apply these synthetic methods to future drug discovery endeavours.

7.2 Perspectives

The studies laid out in this dissertation provide potential for future studies both in our own research group and in the field as a whole.

7.2.1 Near future

Within the next few years, our group has the potential to improve our current data to optimize activity of our hit compounds.

7.2.1.1 Analogues for activity

In Chapter 4, we achieved nanomolar potency for our hits, and we are currently awaiting cell assays. Based on these results, we may require compound optimization to increase activity, such as to improve cell penetration. Upon completion of the synthesis and testing of the synthetic targets in Chapter 6, we may also need to improve *in vitro* activity. The Forecaster software we used to discover these compounds also has two other functions, REACTS2D and FINDERS,[3] which would allow us to virtually synthesize a library of analogues – through combinatorial chemistry – and subsequently screen them to POP and FAP. Figure 7.1 illustrates our plan for compound optimization.

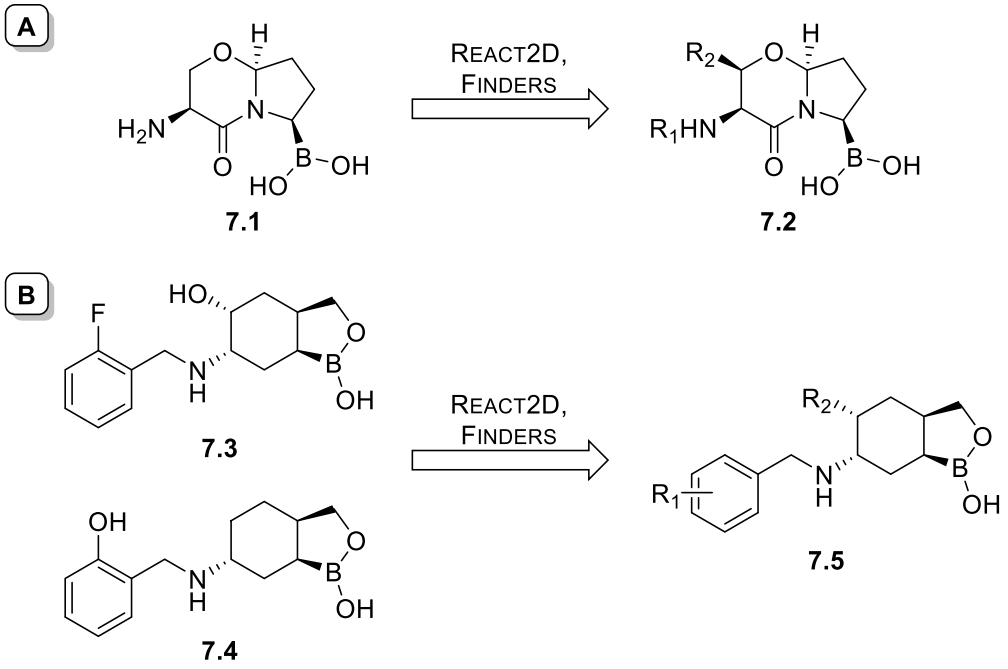

Figure 7.1. Computational optimization of inhibitors from (A) Chapter 4 (B) Chapter 6

7.2.1.2 Applying our compounds to different targets

Based on the findings laid out in this dissertation, our research group has begun to carry our similar studies on different enzymatic targets implicated in various diseases.

As mentioned in Chapters 4 and 6, the dipeptidyl peptidase (DPP) family, including DPP4/8/9, possesses highly polar active sites that highly resemble that of FAP. These enzymes are also cancer-associated, though through different biochemical pathways. It is possible that our POP/FAP dual inhibitors (Chapter 4) are also active in the DPP enzymes, as they contain primary amines and boronic acids, rendering them very polar. Currently in our research group, we have submitted some of these samples to collaborators studying DPP8/9. Based on the results of these assays, we can either optimize the structure to obtain broad-spectrum anti-cancer therapeutics (as was Talabostat[4]) or DPP-specific inhibitors. Either pursuit has potential for promising leads.

One other possibility involves POP in the parasite *Trypanosoma cruzi*. Although the parasitic POP has not been crystallized, the active site is believed to be slightly larger and more lipophilic than that of human POP, based on structures of active inhibitors.[5] We have already discussed with potential collaborators specializing in this parasite and provided samples of our most active POP inhibitors. Future endeavours in this project would involve optimization of the inhibitor structure to selectively target the parasitic POP over the native human POP.

7.2.2 Distant future

The findings presented in this dissertation have the potential to contribute to accelerated drug discovery and eventually to personalized medicine.

Many years of studying POP through computational modelling and biophysical characterizations led to synthetic endeavours giving nanomolar-potent inhibitors that penetrate cell membranes. We have thus become experts on this enzyme and have found the expert collaborators in biology and pharmacology to provide associated cellular assays and animal studies. We are now equipped to apply our skills to the accelerated discovery of potential POP therapeutics.

As discussed in Chapters 2 and 3, the POP active site is quite large and contains a sizeable lipophilic pocket, as well as residues of both positive and negative polarities. The binding pocket is therefore rather generous in terms of which types of compounds can be accommodated.

With our optimized and validated virtual screening method[6] (also see Chapter 6), we are able to conduct screenings of tens of thousands of compounds in just a couple of days, or in a few hours

with access to a supercomputer. With this, we could screen a library of drug candidates that failed due to inefficacy, i.e. failed Phase II or III but passed Phase I. Drugs that passed Phase I but failed II-III are proven to be safe but are not effective enough for approval and distribution. Re-purposing failed drugs is a much lower financial risk, as the compounds have already passed through pre-clinical and clinical toxicology studies and would only require efficacy studies.[7]

Nearly 80% of all drugs contain one or two aromatic rings.[8] The lipophilic pocket in the active site of POP conveniently accommodates relatively large aromatic drugs, as we saw in Chapters 2 and 3. It is therefore highly likely that at least a few failed candidates would be active against POP. This new application would consequently open doors for accelerated drug discovery in neurodegenerative diseases, epithelial cancers, and parasitic infections; the overall discovery, pre-clinical, and clinical investments would be much lower than for that of a novel drug candidate.[7]

While drug repurposing is already put into practice, many pharmaceutical endeavours involve high-throughput screening methods or large-scale computational approaches. A more efficient and lower-risk approach would involve more narrowly focused approaches, such as focusing on key biologically validated targets. Our own focus on POP could potentially generate valuable data for pharmaceutical companies and provide them with the necessary leads to pursue further developments.

While we are not yet fully equipped to apply these methods to FAP, as the enzyme is not as stable and is much more difficult to express and isolate, our lab hopes to, over the next few years, develop the necessary techniques to study this enzyme, as well as others, and discover and potentially re-purpose potent potential therapeutics.

7.3 References

(1) Copeland, R. A., The drug–target residence time model: a 10-year retrospective. *Nat Rev Drug Discov* **2016,** *15*, 87-95.

(2) Ahmed Laskar, A.; Younus, H., Aldehyde toxicity and metabolism: the role of aldehyde dehydrogenases in detoxification, drug resistance and carcinogenesis. *Drug Metab Rev* **2019,** *51* (1), 42-64.

(3) Pottel, J.; Moitessier, N., Customizable Generation of Synthetically Accessible, Local Chemical Subspaces. *J Chem Inf Model* **2017,** *57* (3), 454-467.

(4) Eager, R. M.; Cunningham, C. C.; Senzer, N.; Richards, D. A.; Raju, R. N.; Jones, B.; Uprichard, M.; Nemunaitis, J., Phase II trial of talabostat and docetaxel in advanced non-small cell lung cancer. *Clin Oncol (R Coll Radiol)* **2009,** *21* (6), 464-72.

(5) Bal, G.; Van der Veken, P.; Antonov, D.; Lambeir, A.-M.; Grellier, P.; Croft, S. L.; Augustyns, K.; Haemers, A., Prolylisoxazoles: potent inhibitors of prolyloligopeptidase with antitrypanosomal activity. *Bioorg Med Chem Lett* **2003,** *13* (17), 2875-2878.

(6) De Cesco, S.; Deslandes, S.; Therrien, E.; Levan, D.; Cueto, M.; Schmidt, R.; Cantin, L. D.; Mittermaier, A.; Juillerat-Jeanneret, L.; Moitessier, N., Virtual screening and computational optimization for the discovery of covalent prolyl oligopeptidase inhibitors with activity in human cells. *J Med Chem* **2012,** *55* (14), 6306-6315.

(7) Pushpakom, S.; Iorio, F.; Eyers, P. A.; Escott, K. J.; Hopper, S.; Wells, A.; Doig, A.; Guilliams, T.; Latimer, J.; McNamee, C.; Norris, A.; Sanseau, P.; Cavalla, D.; Pirmohamed, M., Drug repurposing: progress, challenges and recommendations. *Nat Rev Drug Discov* **2019,** *18* (1), 41-58.

(8) Mao, F.; Ni, W.; Xu, X.; Wang, H.; Wang, J.; Ji, M.; Li, J., Chemical Structure-Related Drug-Like Criteria of Global Approved Drugs. *Molecules* **2016,** *21* (75), 1-18.